

MEMBRANE BIOREACTOR PROCESS FOR REMOVING BIODEGRADABLE  
ORGANIC MATTER AND DISINFECTION BY-PRODUCT PRECURSORS FROM  
WATER: MODELING AND PROCESS EFFICIENCY

by

Mark D. Williams

---

A Dissertation Presented to the  
FACULTY OF THE GRADUATE SCHOOL  
UNIVERSITY OF SOUTHERN CALIFORNIA  
In Partial Fulfillment of the  
Requirements for the Degree  
DOCTOR OF PHILOSOPHY  
(ENVIRONMENTAL ENGINEERING)

August 2002

Copyright 2002

Mark D. Williams

UMI Number: 3094383

Copyright 2002 by  
Williams, Mark Dennis

All rights reserved.

UMI<sup>®</sup>

---

UMI Microform 3094383

Copyright 2003 by ProQuest Information and Learning Company.  
All rights reserved. This microform edition is protected against  
unauthorized copying under Title 17, United States Code.

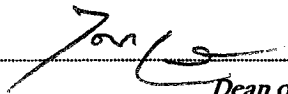
ProQuest Information and Learning Company  
300 North Zeeb Road  
P.O. Box 1346  
Ann Arbor, MI 48106-1346

UNIVERSITY OF SOUTHERN CALIFORNIA  
The Graduate School  
University Park  
LOS ANGELES, CALIFORNIA 90089-1695

*This dissertation, written by*

MARK WILLIAMS

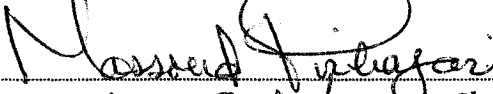
*Under the direction of his Dissertation  
Committee, and approved by all its members,  
has been presented to and accepted by The  
Graduate School, in partial fulfillment of  
requirements for the degree of  
DOCTOR OF PHILOSOPHY*



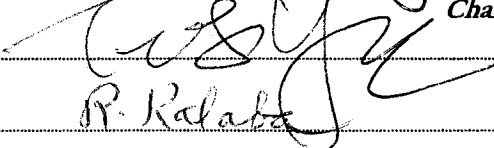
Dean of Graduate Studies

Date August 6, 2002

DISSERTATION COMMITTEE



Chairperson



R. Kalaba

## **DEDICATION**

This dissertation is dedicated to my father,

Dennis E. Williams

for his unconditional support, encouragement, and inspiration



## ACKNOWLEDGEMENTS

I could not have completed this work without the efforts of numerous people. First and foremost, I would like to thank my advisor, Dr. M. Pirbazari for his mentoring, patience, encouragement, financial support, and tireless persistence over my tenure at USC. I would also like to thank the members of my advisory committee for their time, effort, and insight.

A number of people made invaluable contributions to the experimental aspects of this research. First I would like to thank Nick Goodman and Cari Ishida for devoting all of their spare time to my research, over the 4-years they spent as undergraduates; and for never getting too frustrated with me when the research would lead us down dead ends. Additionally, I would like to thank Jeff Tsai for his substantial effort towards this research. I would also like to acknowledge the efforts of my fellow graduate students including Rajan Ravindran, Badri Badriyha, Walter Den, and Jesse Tu.

I would like to thank Brad Coffey of the Metropolitan Water District of Southern California for providing the pilot facilities and other resources, which were invaluable to the experimental aspect of this study. The staff at USC provided tremendous help over the years, and I wish to acknowledge Vanjie, Anna, Mary Kay, Irene, Leon, and all the

others in the Civil and Environmental Engineering staff as well as John and Kan in the Machine shop.

Finally, for all of their encouragement and support over the many years, I wish to thank my family, friends, and loved ones including: my mother and father, Dennis and Virginia Williams; my sister, Meridee; my uncle and aunt, Joe and Judy McCaron; the Burch family; and to my significant other, Tiffany, who was there during the good times and bad times. Without them, I could not have accomplished this.

## TABLE OF CONTENTS

DEDICATION .....	ii
ACKNOWLEDGEMENTS .....	iii
LIST OF TABLES .....	viii
LIST OF FIGURES.....	ix
LIST OF ACRYNOMS.....	xvi
LIST OF NOMENCLATURE .....	xvii
ABSTRACT .....	xviii
Chapter 1 - INTRODUCTION.....	1
Problem Statement .....	1
Research objectives and scope .....	3
Chapter 2 - BACKGROUND.....	6
Ozone .....	6
Background and Regulatory Impetus .....	6
Benefits of Ozone Oxidation .....	9
Ozone By-products .....	13
Biological Stability and Bacterial Regrowth .....	19
Measuring Biodegradability .....	21
Biological Filtration.....	23
Membrane Separation Processes.....	27
Hybrid Membrane Processes .....	28
MF/UF-PAC Processes.....	28
Membrane Bioreactors.....	30
Chapter 3 - MATERIALS AND METHODS .....	37
Source Water.....	37
Membranes.....	40
Activated Carbon .....	41
Experimental Methods .....	41
Methodology Development .....	41
Semi-batch Ozone Contactor .....	43
Pilot-scale Ozone Contactor .....	45
Biological Inocula.....	47
Bench-scale MBR.....	48

Mini-pilot-scale MBR.....	51
Adsorption Studies .....	53
Adsorption Isotherm Studies.....	54
Adsorption Rate Studies.....	54
Biokinetic Studies.....	56
Analytical Methods.....	58
pH and Alkalinity .....	58
UV Absorbance .....	59
Ozone Dose.....	59
Dissolved Ozone.....	60
TOC and DOC .....	61
AOC.....	61
BDOC .....	62
Aldehydes .....	64
Sample Chlorination and THM Analysis .....	65
Biomass Measurement.....	66
Activated Carbon Desorption Procedure.....	66
Heterotrophic Plate Counts .....	67
Direct microbial counts .....	67
SEM Analysis.....	68
Particle Counts.....	69
 Chapter 4 - EXPERIMENTAL RESULTS: BENCH- AND MINI-PILOT-SCALE STUDIES .....	 70
Objectives.....	70
Results and Discussion .....	71
Ozone Byproduct Formation .....	71
MBR Studies.....	77
Laboratory-Scale MBR Studies.....	77
Mini-pilot-scale MBR Studies .....	86
Reactor PAC Concentration.....	98
Summary and Conclusions .....	99
 Chapter 5 - MATHEMATICAL MODEL DEVELOPMENT .....	 102
Objectives.....	102
Model Conceptualization and Development.....	104
Review of Existing Models .....	104
MBR Model Conceptualization and Assumptions .....	109
Biodegradation.....	117
Biodegradation Models .....	117
Liquid-phase Mass Balance.....	119
Adsorption .....	121
Adsorption Models.....	121

Numerical Methods.....	128
Summary and Conclusions .....	138
 CHAPTER 6 - MODELING PARAMETER ESTIMATION: ADSORPTION AND BIOKINETIC STUDIES.....	 140
Objectives.....	140
Results and Discussion .....	141
Adsorption Isotherm Studies .....	141
Adsorption Rate Studies .....	148
Biokinetic Studies.....	151
Biokinetic Parameter Estimation Methods.....	152
Aldehyde Biokinetic Parameters .....	155
BDOC Biokinetic Parameters .....	159
AOC and THM Precursors .....	166
Summary and Conclusions .....	168
 Chapter 7 - MODEL VERIFICATION AND SENSITIVITY ANALYSIS .....	 172
Objectives.....	172
Results and Discussion .....	174
Prediction/Simulation of Total Aldehyde Removal .....	178
Prediction/Simulation of DOC and BDOC Removal .....	183
Prediction/Simulation of AOC Removal .....	190
Biomass Predictions .....	193
Summary and conclusions .....	194
 Chapter 8 - MBR MODEL SIMULATIONS.....	 199
Objectives.....	199
Results and Discussion .....	200
Effects of Inoperation and Shutdown .....	201
Changes in Substrate Concentration.....	205
Effects of Varying Hydraulic Residence Time.....	208
Summary and Conclusions .....	211
 Chapter 9 - SUMMARY, CONCLUSIONS, AND FUTURE WORK.....	 213
Summary and Conclusions .....	213
MBR Studies.....	214
MBR Model Development .....	216
Biokinetic and Adsorption Parameter Estimation .....	217
Model Verification and Sensitivity Analysis.....	220
MBR Model Simulations.....	222
Future Work .....	223
 REFERENCES.....	 226

## LIST OF TABLES

Table 1. Water quality for selected parameters in untreated SPW .....	38
Table 2. Characteristic ozone by-product levels formed in SPW .....	39
Table 3. Composition of mineral media added to supplement biodegradation.....	39
Table 4. MBR process variables and operating conditions .....	78
Table 5. Comparison of previous biodegradation and adsorption models .....	110
Table 6. MBR model input variables .....	129
Table 7. Overview of adsorption studies; all tests were conducted at 20°C and at ambient pH (8.0) .....	142
Table 8. Freundlich isotherm constants measured in the present study .....	148
Table 9. Experimental conditions used for biokinetic studies; all tests were conducted at 20°C.....	153
Table 10. Summary of biokinetic parameters measured in the current study .....	157
Table 11. Overview of model simulation conditions .....	176
Table 12. Calibration constants used for model verification and sensitivity analyses .....	177
Table 13. Operating parameters and initial conditions used for MBR model simulations .....	202

## LIST OF FIGURES

Figure 1. Overview of research objectives and scope for model development and calibration .....	4
Figure 2. Generalized reaction scheme for direct ozone oxidation and ozone-induced, free radical oxidation .....	14
Figure 3. Effect of ozone dose on fulvic acid size distribution. ....	16
Figure 4. Conceptual MBR process schematic illustrating two principal process configurations: (a) reactor contents are recirculated through hollow fiber or tubular membranes; or (b) membranes are immersed directly into the reactor and vacuum is applied to create TMP. ....	32
Figure 5. Apparent molecular weight size distribution for NOM in untreated SPW (Adapted from: Amy et al., 1991).....	38
Figure 6. SEM micrograph showing the ceramic membrane surface. ....	40
Figure 7. (a) Batch particle counts of a 10 mg/L PAC solution in ultra-pure water and in ozonated water, and (b) percentile distribution curve .....	42
Figure 8. Schematic illustration of the semi-batch ozonation reactor used for bench-scale studies .....	44
Figure 9. Schematic illustration of the pilot-scale ozone contactor .....	46
Figure 10. Schematic illustration of the bench-scale MBR .....	49
Figure 11. Schematic illustration of the mini-pilot-scale MBR.....	51
Figure 12. Batch reactor apparatus used for adsorption rate studies .....	55
Figure 13. Schematic illustration of the batch reactor setup used for biokinetic studies.....	57
Figure 14. Ozone <i>CT</i> exposure and mass transfer rate as a function of ozonation time for semi-batch ozone studies .....	73

Figure 15. Aldehyde formation as a function of ozone exposure in a semi-batch reactor .....	74
Figure 16. Disinfection by-product formation potential as a function of ozone exposure in a semi-batch reactor.....	75
Figure 17. Changes in AOC as a function of ozone exposure in a semi-batch reactor .....	76
Figure 18. Total aldehyde, DOC, and THM precursor removal in the laboratory-scale MBR where biomass and PAC were not added.....	80
Figure 19. DOC and total aldehyde removal in the laboratory-scale MBR when (a) 500 mg/L PAC (and no biomass) was added and (b) when biomass was added at startup.....	81
Figure 20. Effect of pre-ozonation on MF flux in a bench-scale MBR process .....	83
Figure 21. Specific membrane flux measured for different operating conditions in the laboratory-scale MBR; all tests were conducted at 20°C .....	84
Figure 22. SEM micrograph showing biologically-active PAC particles collected from the MBR.....	85
Figure 23. Effects of various operating strategies on DOC and THM precursor removal: region A, 0.3 percent PAC, acclimated biomass, and no reactor wasting; region B, continually wasting 7 percent (of the feed flow rate) of the reactor contents; region C, 5 mg/L PAC added and no reactor wasting; and region D, 5 mg/L PAC and 7 percent of the reactor contents were continually wasted.....	87
Figure 24. Effect of carbon addition on removal of total aldehydes in the mini-pilot-scale MBR process.....	90



Figure 25. Effects of nutrient addition, influent total aldehyde concentration, and pH on removal of DOC and total aldehydes: region A, mineral nutrients added to reactor feed; region B, ~400 µg/L total aldehydes added to the ozonated water feed (pH = ~8.0); region C, influent was pH lowered from ~8.0 to 6.4; region D, influent pH lowered from 6.4 to 4.2; and region E, influent pH raised to 6.0. (Note that nutrients were continuously added throughout the tests, and aldehydes were added from condition B onward; PAC was not continually added and reactor solids were not wasted).	91
Figure 26. Comparison of the effect of pH variation on removal of DOC and THM precursors: region C, influent pH lowered from ambient (~8.0) to 6.4; region D, influent pH lowered to 4.2; and region E, influent pH raised to 6.0. The MBR was operated without continuous carbon addition or reactor wasting. (Note that nutrients and aldehydes (~400 µg/L) were continuously added throughout testing; PAC was not continually added and reactor solids were not wasted).	93
Figure 27. Effect of various operating strategies on AOC removal: region A, 0.3 percent PAC, acclimated biomass, and no reactor wasting; region B, operating at a 7-percent reactor wasting rate; region C, 5 mg/L PAC added and operated without reactor wasting; and region D, 5 mg/L PAC and operated at a 7-percent reactor wasting rate.	94
Figure 28. Comparison of mini-pilot scale MBR permeate flux measured under various operating conditions; condition 1: 3000 mg/L PAC and ~50 mg/L biomass initially added at startup, no reactor solids wasting; condition 2: 7 percent wasting; condition 3: 7 percent wasting and 5 mg/L PAC continuously added	96
Figure 29. Theoretical PAC concentration in the reactor as a function of various operating strategies	98
Figure 30. Conceptual illustration of the proposed MBR model showing key process components and assumptions.	111
Figure 31. Realistic and idealized biologically-active PAC particle in a high-shear, low-substrate system.	112

Figure 32 - General illustration of the explicit finite difference method using a rectangular coordinate system.....	131
Figure 33. Idealized carbon particle showing method of grid determination and solution of the HSDM using an explicit finite difference method. ....	134
Figure 34. Adsorption equilibrium data and the Freundlich isotherm model for aldehydes in synthetic water and ozonated water. Total aldehydes represent the sum of formaldehyde, acetaldehyde, glyoxal, and methyl glyoxal. ....	143
Figure 35. Comparison of adsorption equilibrium data and the Freundlich isotherm model for DOC in ozonated and untreated water.....	144
Figure 36. Adsorption equilibrium data and the Freundlich isotherm model for BDOC in ozonated water.....	145
Figure 37. Adsorption equilibrium data and the Freundlich isotherm model for THM precursors in untreated and ozonated water.....	146
Figure 38. Adsorption equilibrium data and the Freundlich isotherm model for AOC in ozonated water .....	147
Figure 39. Adsorption rate data and HSDM profile for DOC in ozonated water .....	150
Figure 40. Adsorption rate data and HSDM profile for THM precursors in ozonated water.....	150
Figure 41. Aldehyde batch biokinetic data showing formaldehyde and acetaldehyde substrate depletion curves and biomass growth; experiment was conducted at 20°C in carbonate-buffered synthetic water containing mineral growth media .....	156
Figure 42. Determination of maximum growth rate coefficient ( $\mu_m$ ) for aldehydes.....	157
Figure 43. Determination of endogenous decay coefficient ( $k_d$ ) for aldehydes.....	158

Figure 44. Estimation of $K_S$ for total aldehydes using parameter-search technique showing measured substrate data and minimized-SSR model fit .....	159
Figure 45. Verification of $K_S$ for aldehydes showing measured biomass data for formaldehyde, acetaldehyde and model-predicted values.....	160
Figure 46. BDOC batch biokinetic data for high-BDOC water showing substrate depletion and biomass growth; experiment was run at 20°C in ozonated water containing mineral growth media where a DOC spike was initially added .....	161
Figure 47. BDOC batch biokinetic data for low-BDOC water showing substrate depletion curve along with biomass; experiment was run at 20°C in ozonated water with mineral growth media.....	162
Figure 48. Determination of maximum growth rate coefficient ( $\mu_m$ ) for BDOC.....	162
Figure 49. Determination of endogenous decay coefficient ( $k_d$ ) for BDOC .....	163
Figure 50. Estimation of $K_S$ for BDOC (using the parameter-search technique) showing measured substrate data for high-BDOC water, low-BDOC water, and the minimized-SSR model fit to each data set.....	164
Figure 51. Verification of $K_S$ for BDOC showing measured biomass data and model-predicted values.....	165
Figure 52. Biokinetic data for AOC , THM precursors (as measured by THMFP), and biomass; experiment was run at 20°C in ozonated water with mineral growth media .....	167
Figure 53. Experimental data and model-predicted profiles for total aldehyde removal when: (a) 1000 mg/L PAC was added (Condition 1, Table 11); (b) PAC was not added (Condition 2, Table 11); and (c) when total aldehyde feed concentration was increased (Condition 3, Table 11) .....	179

Figure 54. Sensitivity analysis for total aldehyde removal showing model sensitivity to: (a) the Monod maximum rate constant ( $\mu_m$ ), (b) the biomass yield coefficient ( $Y$ ), (c) and the Monod half velocity constant ( $K_S$ ).....	180
Figure 55. Sensitivity analysis for total aldehyde removal showing model sensitivity to: (a) the endogenous decay coefficient ( $k_d$ ), (b) initial biomass concentration ( $X_0$ ), (c) HRT ( $\theta$ ), and (d) solids wasting rate.....	182
Figure 56. DOC experimental data and model-predicted profiles for: (a) only biomass added (condition 4, Table 11), (b) biomass and 1000 mg/L PAC added at startup (condition 5), (c) biomass and 3000 mg/L PAC added at startup (condition 6), and (d) with continuous PAC addition (condition 7).....	184
Figure 57. Sensitivity analysis for BDOC removal (condition 4, Table 11) showing model sensitivity to: (a) the Monod maximum rate constant ( $\mu_m$ ), (b) the biomass yield coefficient ( $Y$ ), (c) and the Monod half velocity constant ( $K_S$ ) .....	187
Figure 58. Sensitivity analysis for BDOC removal (condition 4, Table 11) showing model sensitivity to: (a) the endogenous decay coefficient ( $k_d$ ), (b) initial biomass concentration ( $X_0$ ), (c) and HRT ( $\theta$ ) .....	188
Figure 59. Sensitivity analysis for DOC removal (condition 5, Table 11) showing model sensitivity to: (a) the Freundlich adsorption capacity constant ( $K_f$ ), (b) the Freundlich adsorption intensity coefficient ( $n$ ), and (c) the surface diffusion constant ( $D_s$ ).....	189
Figure 60. Model simulation of AOC removal showing experimental data and model-predicted profiles.....	191
Figure 61. Model sensitivity analysis for AOC removal (condition 8, Table 11) for: (a) the Monod maximum rate constant ( $\mu_m$ ), (b) the biomass yield coefficient ( $Y$ ), (c) and the Monod half velocity constant ( $K_S$ ).....	192

Figure 62. Effect of system shutdown on total aldehyde removal; reactor contents were not wasted during the 10-day shutdown period; model predictions assumed that only the organic substrate was limiting, and not mineral nutrients or oxygen .....	203
Figure 63. Effect of system shutdown on BDOC removal; reactor contents were not wasted during the 10-day shutdown period; model predictions assumed that only the organic substrate was limiting, and not mineral nutrients or oxygen .....	204
Figure 64. Biomass profile showing effects of process shutdown for a system that initially had low biomass concentrations; model predictions assumed that only the organic substrate was limiting, and not mineral nutrients or oxygen .....	204
Figure 65. Effect of increasing influent concentration on total aldehyde removal .....	206
Figure 66. Effect of increasing influent concentration on BDOC removal .....	207
Figure 67. Effect of increasing influent concentration on AOC removal .....	207
Figure 68. Effect of membrane cleaning on reactor HRT when operating at constant trans-membrane pressure .....	209
Figure 69. Effect of membrane cleaning and varying reactor HRT on total aldehyde removal .....	210
Figure 70. Effect of membrane cleaning and varying reactor HRT on BDOC removal .....	210

## LIST OF ACRONYMS

AOC – Assimilable organic carbon  
BDOC – Biodegradable dissolved organic carbon  
BOM – Biodegradable organic matter  
CFU – Colony forming unit  
CFV – Cross flow velocity  
DBPFP – Disinfection by-product formation potential  
D/DBP – Disinfectants/disinfection by-product  
DOC – Dissolved organic carbon  
DOM – Dissolved organic matter  
EBCT-Empty bed contact time  
HAAs – Haloacetic Acids  
HAAFP – Haloacetic acid formation potential  
HRT-Hydraulic retention time  
HSDM – Homogenous surface diffusion model  
MBR – Membrane bioreactor  
MF – Microfiltration  
NF - Nanofiltration  
NOM – Natural organic matter  
SEM – Scanning electron microscope  
SMPs – Soluble microbial products  
SRT – Solids retention time  
SPW – State project water  
SSR – Sum of squared residuals  
THMs - Trihalomethanes  
THMFP – Trihalomethane formation potential  
TMP-Trans-membrane pressure  
TOC – Total organic carbon  
TOX – Total organic halogen  
UF - Ultrafiltration

## LIST OF NOMENCLATURE

$C$  – Activated carbon concentration (g/L)  
 $D_f$  – Free liquid diffusion constant ( $\text{cm}^2/\text{s}$ )  
 $D_l$  – Free liquid diffusivity ( $\text{cm}^2/\text{sec}$ )  
 $D_s$  – Surface diffusion constant ( $\text{cm}^2/\text{s}$ )  
 $J, J_0$  – Normalized membrane flux (gal/day-ft<sup>2</sup>-psi)  
 $k_b$  – Biological uptake rate ( $\text{h}^{-1}$ )  
 $k_d$  – Monod endogenous decay constant ( $\text{h}^{-1}$ )  
 $k$  – Liquid film mass transfer coefficient ( $\text{cm}/\text{sec}$ )  
 $k_m$  – Monod maximum specific growth rate constant (CFU/mg substrate – h)  
 $K_c$  – Membrane fouling rate when cake resistance is flux limiting ( $\text{t}/\text{length}^2$ )  
 $K_s$  – Monod half saturation constant (mg/L)  
 $K_f$  – Freundlich isotherm equilibrium capacity constant (mg substrate/g carbon)  
 $L_l$  – Effective liquid film thickness (cm)  
 $1/n$  – Dimensionless Freundlich isotherm constant  
 $Q$  – Permeate flow rate (L/hr)  
 $q$  – Solid phase substrate concentration (mg adsorbate/g carbon)  
 $R$  – Mean diameter of activated carbon (cm)  
 $r$  – Internal coordinate of an idealized activated carbon particle (cm)  
 $Re$  = Reynolds number =  $r_s d_p v_s / \mu$   
 $S$  – Substrate concentration (mg/L)  
 $S_b$  – Bulk fluid substrate concentration (mg/L)  
 $S_s$  – Substrate concentration at the carbon surface (mg/L)  
 $S_0$  – Initial or influent substrate concentrations (mg/L)  
 $S_{\min}$  – Minimum substrate concentration (mg/L)  
 $Sc$  = Schmidt Number =  $\mu / (r_s D_l)$   
 $t$  – time  
 $V$  – Reactor volume (L)  
 $v_s$  – Superficial fluid velocity (cm/sec)  
 $X$  – Biomass concentration (mg/L)  
 $X_0$  – Initial biomass concentration (mg/L)  
 $Y$  – Monod yield constant (mg biomass/mg substrate)

### Greek Letters

$\delta_c$  – Membrane cake thickness (length)  
 $\rho_s$  – Activated carbon density ( $\text{g}/\text{cm}^3$ )  
 $\mu$  – Dynamic viscosity ( $\text{g}/\text{m}\cdot\text{s}$ )  
 $\mu_m$  – Monod maximum specific growth rate ( $\text{g}/\text{m}\cdot\text{s}$ )  
 $\theta$  – Mean hydraulic residence time  
 $\theta_c$  – Mean cell residence time

## ABSTRACT

The membrane bioreactor (MBR) process combines biodegradation and adsorption for removing dissolved constituents and microfiltration (MF) for removing suspended solids. The MBR process is a promising new technology for treating potable water sources having high disinfection by-product (DBP) formation or with high biodegradable organic matter (BOM) levels. This research evaluated an MBR process combined with pre-ozonation for removing BOM and lowering halogenated by-product formation in potable water. Additionally, a mathematical model was developed to predict MBR process efficiency.

Ozonation studies were first conducted to determine the magnitude of ozone by-product formation and to evaluate suitable BOM surrogates for mathematical modeling. A comprehensive series of tests were conducted using a bench-scale and mini-pilot-scale MBR process treating pre-ozonated water that exhibited high assimilable organic carbon (AOC) formation potential and high trihalomethane (THM) formation potential. These tests evaluated the MBR process efficiency for removing total aldehydes, dissolved organic carbon (DOC), biodegradable organic carbon (BDOC), AOC, and THM precursors at different powdered activated carbon (PAC) doses, varying hydraulic residence times (HRTs), and at different pH levels. A mathematical model was developed that predicted substrate removal in the MBR process. The combined



adsorption/biofilm model was calibrated using parameter constants measured in adsorption isotherm, adsorption rate, and biokinetic studies. The calibrated model was verified for predicting total aldehyde, DOC, BDOC, and AOC removal using data measured in MBR experiments. The calibrated model was then used to predict MBR process performance under a wide range of hypothetical large-scale operating conditions.

The major conclusions from MBR testing were that the MBR process could achieve very high removals of biodegradable organic carbon and ozone by-products (as measured by total aldehydes, BDOC, and AOC); PAC doses may be adjusted, as needed, to enhance THM precursor removal. When acclimated biomass was added to the MBR at startup, relatively low acclimation times were needed and steady-state operation was generally achieved within several days. Total aldehydes were found to be a good surrogate for BOM. Furthermore, aldehyde analysis is faster, and has a higher precision than bioassays (AOC and BDOC). Membrane fouling was highly dependent on operating conditions.

Adding activated carbon (doses tested = 1000 to 3000 mg PAC/L) to the MBR lowered flux-decline rates; however, when reactor solids were not wasted, fouling rates increased precipitously. When operated without PAC addition, the ceramic MF membrane rapidly fouled. Continuously adding low PAC doses (5 mg/L) combined with a low reactor

wasting rate drastically reduced fouling. Continuous PAC addition likely sequesters suspended solids, including biomass, that would otherwise foul the membranes. Finally, pre-ozonation enhanced membrane flux through either NOM oxidation or enhancing micro-flocculation.

A mathematical model of the MBR process was developed to predict process efficiency for total aldehyde, DOC, and AOC removal. Biodegradation was modeled using single-component Monod kinetics, and the Freundlich and HSDM adsorption models were coupled to describe PAC adsorption. A key assumption of the MBR model was that, due to the relatively high-energy environment and low substrate loading, a thin and discontinuous biofilm would establish on PAC added to the reactor. Additionally, sheared biomass would be retained within the system (as the MF membrane rejects it) and would be considered as part of the active biomass.

MBR model calibration constants were measured in a series of adsorption isotherm, adsorption rate, and biokinetic experiments. Constants were measured for total aldehydes, BDOC, AOC, and THM precursors. Comparison of bulk BOM parameters (AOC and BDOC) with specific BOM constituents (aldehydes) provided an indication of the suitability of aldehydes as a model surrogate for the bulk BOM. Batch adsorption isotherm tests were used to measure the Freundlich isotherm constants and data from adsorption rate studies were used to calculate the surface diffusivity constant.

Biodegradable fractions including total aldehydes, BDOC, and AOC were effectively non-adsorbable and Monod maximum growth rate constants were similar for the three substrates.

Model verification analyses were used to establish the efficacy of the MBR model for predicting substrate changes in a real system. The model was calibrated using constants measured in adsorption and biokinetic studies and verified using data from mini-pilot-scale testing. Model predictions and experimental data showed close agreement for total aldehyde and DOC removal over the wide range of conditions tested. Discrepancies between experimental data and model-predicted profiles were generally less than 10 percent. Model parameter sensitivity analyses, with respect to total aldehyde, BDOC, and AOC removal, showed that process efficiency was most highly influenced by changes in the Monod growth-rate parameters and to a much lesser extent by changes in adsorption parameters.

Hypothetical predictions were made using an MBR model calibrated to mini-pilot scale operating data. Predictions sought to assess the effects of likely real-world operating conditions. The model showed that sudden spikes in influent substrate concentration affected total aldehyde and AOC removal efficiency to a much greater extent than BDOC removal efficiency. Furthermore, total aldehyde removal efficiency was impacted to a much greater extent by HRT variations than BDOC.

In conclusion, the MBR process is a promising technology for treating potable water sources having high THM formation or with high BDOC levels. This study has demonstrated that operating strategy has a substantial impact on membrane flux and, ultimately, on process economics and viability. The scale of studies conducted in this work provided a proof of concept and a preliminary assessment of operating strategies to minimize membrane fouling and maximize BOM removal. Ultimately, economics will dictate the viability of MBRs for municipal water treatment. Additional research is needed at larger (pilot or demonstration) scales to thoroughly evaluate operating efficiencies and economics. Further testing is needed to evaluate effects of membrane type (i.e., polymeric vs. ceramic), membrane configuration (i.e., hollow fiber vs. tubular), and optimal strategies for in-situ membrane cleaning including frequent hydraulic back pulsing. Additional studies should also examine process efficiency at varying temperatures. The ranges of process recoveries and PAC addition strategies used in this work should be used as a baseline for further refinement in subsequent optimization studies.

## Chapter 1 - INTRODUCTION

### PROBLEM STATEMENT

The principal objective in potable water treatment is to provide water that is free of biological pathogens and that is chemically safe. Water utilities are faced with a delicate balance of these two treatment objectives to meet increasingly rigid regulatory requirements. Chlorine-based primary disinfectants are widely used in U.S. practice to provide biologically safe water, however, reactions between chlorine and naturally occurring organics in water can form a variety of disinfection by-products (DBPs)—containing both known and suspected carcinogens. Thus, increasing chlorine dose to improve microbial disinfection degrades the chemical quality by increasing DBP levels. As regulated DBP levels decrease, utilities are forced to change treatment practices by either lowering chlorine dosages, changing chlorine type (e.g., to chlorine dioxide) or to implement another primary disinfectant (e.g., ozone). Further complicating the issue are the likely future regulations requiring disinfection of *Cryptosporidium*—a naturally occurring pathogenic protozoa that cannot be inactivated by chlorine. Furthermore, systems treating surface water (using conventional processes) are also required to remove a certain percentage of the total organic carbon (TOC). Consequently, membrane processes and ozone oxidation have seen an increased use in U.S. practice.

Replacing chlorine with ozone as the primary oxidant has been shown to reduce DBP formation in a wide range of source waters. Ozone lowers DBP formation by oxidizing organic precursor material and when combined with biological filtration, DBP formation may be dramatically reduced. Ozone reacts with humic materials producing lower molecular weight, oxygenated end products including: carboxylic acids, alkanes, aliphatic ketones, aldehydes, and oxo-acids (Rice and Gomez-Taylor, 1986; Krasner et al., 1993a; Gracia et al., 1996). However ozonation alone does not substantially lower the TOC. A large fraction of ozone by-products are readily biodegradable and, if not removed through biological filtration, have the potential to promote bacterial re-growth in water distribution systems.

Alternately, membrane processes such as nanofiltration (NF) and reverse osmosis (RO) may be used to remove natural organics and DBP precursors. Additionally, membranes provide an absolute barrier to water-borne pathogens including bacteria, protozoa and viruses. However, in their current state of development, NF and RO processes are cost prohibitive for most utilities that treat otherwise unimpaired waters (i.e., not brackish or highly colored). Microfiltration (MF) and ultrafiltration (UF) operate at lower pressures and have been shown to be economically competitive with conventional processes for small systems (Adham et al., 1996b). MF and UF provide excellent particulate removal (including bacteria and protozoa), however, they cannot reliably remove DBP precursors or TOC.

The membrane bioreactor (MBR) has recently emerged as a viable technology for water and wastewater treatment (Ravindran et al., 1995; Pirbazari et al., 1996; Urbain et al., 1996; Cicek et al., 1998a). MBRs combine two basic processes: biodegradation for removing dissolved constituents and membrane separation for removing suspended solids. MBRs integrate a biological reactor and MF or UF into a single unit process and have the capability to reliably remove dissolved organics through biodegradation or adsorption onto system additives (e.g., powdered activated carbon [PAC]). Suspended solids (including bacteria) are completely retained within the system allowing exact control of biomass age and reactor solids concentration. MBRs have seen a substantial growth in wastewater processes, however, have not been widely used for treating potable water due to the relatively recent emergence of the technology.

## **RESEARCH OBJECTIVES AND SCOPE**

The principal research objectives are: (1) demonstrate the effectiveness of a combined ozonation and membrane-bioadsorption process for removing DBP precursors and TOC, and producing a biologically stable water; and (2) develop, calibrate, and validate a predictive mathematical model of the MBR process based on the fundamental phenomena of adsorption and biochemical oxidation. A general flow chart showing an overview of the research scope, with regard to model development and calibration, is shown in Figure 1 and summarized as follows:

1. Determine ozone by-product formation by conducting batch ozonation studies using a source water that has a high DBP and ozone by-product formation potential. These experiments will assess the effects of ozone dose on the formation of ozone by-products and on the formation of halogenated disinfection by-products.
2. Based on batch ozonation studies, select a group, or several groups, of specific ozone by-products that may be used as biodegradable organic matter (BOM) surrogates for mathematical modeling.

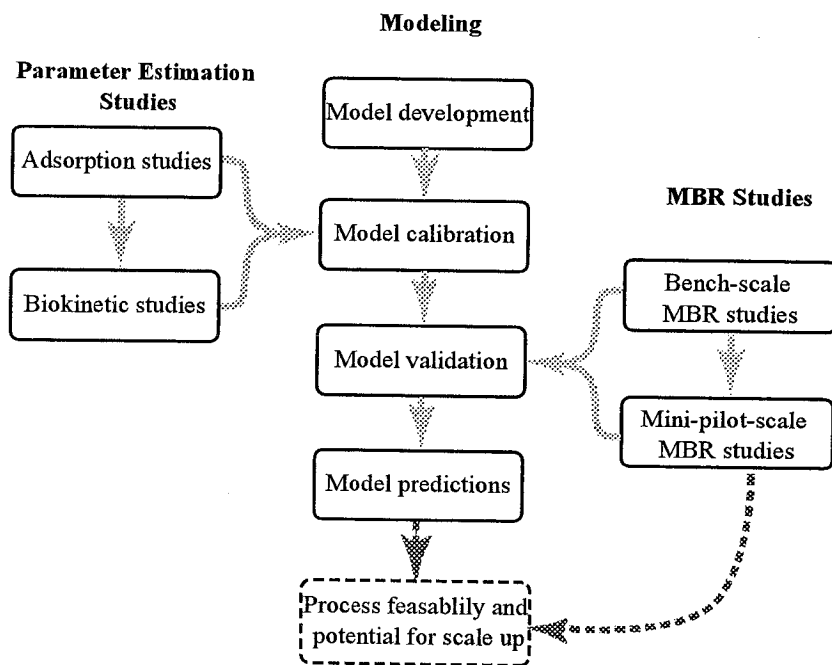


Figure 1. Overview of research objectives and scope for model development and calibration



3. Determine the adsorptive characteristics of surrogate model substrates by conducting batch adsorption equilibrium and adsorption rate studies.
4. Determine model substrate biodegradability through a series of biokinetic studies.  
Batch biokinetic studies will assess the biodegradability of the selected model substrates and determine biokinetic values necessary to mathematically model biodegradation.
5. Demonstrate the MBR process for removing DBP precursors and biodegradable organic carbon by conducting a series of experiments using a laboratory-scale, and mini-pilot-scale MBR. Studies will focus on optimizing BOM removal while minimizing membrane fouling. Process optimization will take into consideration:  
(a) membrane efficiency – as determined by permeate flux rates, (b) removal efficiency of the selected model substrates, and (c) removal efficiency of halogenated by-product precursors.
6. Develop a mathematical model for predicting process efficiency using the adsorption and biokinetic parameters determined in batch studies. Based on these parameters, as well as independent variables including reactor detention time and activated carbon concentration, predict substrate concentration, biomass concentration, and activated carbon lifespans.
7. Calibrate the mathematical model using adsorption and biokinetic constants for model substrates, and validate the model using data collected from mini-pilot-scale MBR experiments. Using the calibrated MBR model, predict process performance over a wide range of likely operating conditions and assess process scale up viability.

## **Chapter 2 - BACKGROUND**

### **OZONE**

#### **Background and Regulatory Impetus**

Ozone has been used for disinfecting water since the end of the 19<sup>th</sup> century. Ozone's efficacy for disinfecting water was first demonstrated in 1891 at a pilot plant constructed in Martinkkenfelde, Germany. Following this initial application of ozone, a full-scale plant employing ozone was built in the Netherlands in 1893 and by 1915, 49 treatment plants in Europe were using ozone (Langlais et al., 1991). In these early applications, ozone was used as a primary disinfectant; however, it was also observed that ozone was effective for treating taste, odor, color, iron, and manganese, producing an aesthetically acceptable finished water.

In the United States, ozone has seen less use in treatment practice due to the widespread use of chlorine as a primary disinfectant (Langlais et al., 1991). In 1990, there were approximately 40 plants in the United States using ozone compared to over 1000 plants in Europe (Glaze, 1987). This trend may be largely attributed to the relative abundance of good drinking water supplies in the U.S., the high costs of using ozone, and the willingness of U.S. consumers to tolerate the taste of chlorine in drinking water. However, many U.S. utilities are switching to ozone as a result of more stringent regulations for microbial disinfection as well as for chlorination by-

products, specifically trihalomethanes (THMs) and haloacetic acids [HAAs] (USEPA, 1998a).

Chlorine reacts with natural organic matter (NOM) forming a wide range of chlorinated by-products. Halogenated by-products resulting from the use of chlorine were first observed in the early 1970's (Rook, 1974) and subsequent research in the mid to late 70's showed THMs<sup>1</sup> to be a suspected carcinogen. Consequently, the USEPA began regulating THMs in 1979 at a 100-µg/L maximum contaminant level (MCL).

Subsequent amendments to the Disinfectants/Disinfection By-Products (D/DBP) rule have also added regulations for HAAs (USEPA, 1994), another common chlorination by-product formed by reactions between chlorine and NOM. Current U.S. regulations have lowered maximum allowable THM levels to 80 µg/L, and HAAs to 60 µg/L (USEPA, 1998a). Future versions of the D/DBP rule will lower THMs and HAAs to 60 µg/L and 40 µg/L, respectively (USEPA, 1998b).

Regulations currently require utilities treating surface water to remove *Giardia* and *Cryptosporidium*—two pathogenic protozoa commonly found in surface waters.

Utilities must achieve at least a 2-log (99-percent) removal of *Cryptosporidium* oocysts and 2-log removal of *Giardia* cysts. Regulations currently require physical removal

---

<sup>1</sup> Trihalomethanes consist of four chlorinated and brominated species: chloroform, bromodichloromethane, chlorodibromomethane, and bromoform.

and inactivation for *Giardia*, however, only physical removal is currently required for *Cryptosporidium* (USEPA, 1998c). Future regulations will likely require both physical removal and inactivation of *Cryptosporidium*, depending on source-water *Cryptosporidium* concentrations (USEPA, 1998b). Common water-treatment disinfectants such as chlorine and chloramines—even at high doses—will not inactivate *Cryptosporidium* (Oppenheimer, 2000). Ozone will inactivate *Cryptosporidium*, however higher ozone dosages are needed than currently used to meet existing *Giardia* disinfection requirements. Recent research has shown that inactivating *Cryptosporidium* will require an ozone *CT* (measured as the product of disinfectant residual and reaction time) ten times greater than needed to inactivate *Giardia* (Finch, 1994; Oppenheimer et al., 1997). Increasing oxidant concentration, increasing exposure time or a combination of both will increase *CT*.

As more toxicological data on halogenated by-products becomes available, and as regulations lower allowable levels of THMs and HAAs, ozone will likely see increased use in the U.S. (Coleman et al., 1992). Furthermore, future microbial disinfection requirements will require some utilities to switch primary oxidants from chlorine to ozone, as chlorine will not inactivate *Cryptosporidium*. However, chlorine cannot be completely eliminated from treatment processes, as U.S. regulations require disinfectant residuals throughout water distribution systems. Because ozone rapidly

decays (on the order of minutes to hours), a secondary, chlorine-based disinfectant<sup>2</sup> must be used.

### **Benefits of Ozone Oxidation**

Ozone oxidizes a variety of problematic inorganic and organic species in water including: THM precursors, the NOM fractions that impart natural color, reduced iron and manganese, and organics imparting unpleasant tastes and odors (Glaze, 1987). Furthermore, ozone has been shown to enhance particulate and NOM removal when applied prior to chemical coagulation and flocculation (Grasso and Weber, 1998).

Grasso and Weber (1998) studied ozone-induced particle destabilization of bentonite and silica colloids when ozonated in various matrices with commercial humic acid and NOM. When colloidal silica was used as the suspended-solid surrogate, particle destabilization did not occur over the range of ozone doses tested; however, bentonite suspensions were readily destabilized when ozonated. Polymerization of meta-stable organics and subsequent adsorption and inter-particle bridging was reportedly the most plausible mechanism for ozone induced destabilization. Furthermore, as in other adsorption phenomena, calcium concentration may substantially enhance particle destabilization after ozone oxidation. The authors concluded that the nature and

---

<sup>2</sup> Various forms of chlorine are used to maintain disinfectant residuals. Chloramines and free chlorine are most commonly used, however chlorine dioxide may also be used.

chemistry of both colloids and NOM play an important role in inducing particle destabilization when ozone is used (Grasso and Weber, 1998).

Using ozone alone has been reported to reduce chlorine by-product formation in some cases (Reckhow and Singer, 1984; Coleman et al., 1992; Siddiqui and Amy, 1993; Price et al., 1993; Speitel et al., 1993; Garside et al., 1996). Pre-ozonation followed by alum coagulation was investigated by Reckhow and Singer (1984) who found that, at low coagulant doses, ozone was effective in lowering trihalomethane formation potential and removing trichloroacetic acid (an HAA component), however, dichloroacetic acid formation increased after ozonation. Moreover, higher ozone doses lowered TOC by approximately 20 percent and  $UV_{254}$  absorbance by approximately 80 percent. At higher coagulant doses, pre-ozonation followed by alum coagulation did not decrease chlorinated DBPs, and in most cases, increased production of all (measured) halogenated by-products. In this case, although ozone generally decreased DBPs in untreated water, there was also a concomitant decrease in DBP precursor material removed during coagulation. Thus, at higher coagulant doses, DBP precursors were removed to a greater extent when ozone was not used.

Krasner (1996a) studied the effects of ozonation followed by chemical coagulation and biofiltration, on DBP formation. Ozonation did not lower TOC levels, however

specific ultraviolet absorbance (SUVA)<sup>3</sup> decreased from 3.0 L/m-mg to 1.7 L/m-mg, indicating a substantial shift in the humic composition. At the relatively low ozone doses used (1.3 mg/L), and after chemical coagulation (5 mg/L FeCl<sub>3</sub>), total THMs and HAA6 (a measure of the 6 most common HAAs) were lowered by approximately 20 percent and approximately 40 percent, respectively. Additionally, ozone enhanced particle destabilization and substantially lower filtered-water turbidities were observed. Source waters used in the study contained bromide (0.14 mg/L) and consequently, there was a marked increase in brominated DBPs, particularly bromoform, which increased greater than 200 percent over values measured in untreated water. An increase in brominated DBPs occurs from hypobromous acid (HOBr) formation when chlorine reacts with bromide. Subsequent reactions between hypobromous acid and NOM results in enhanced formation of some brominated DBPs (Krasner, 1996a). Brominated DBP chemistry is further influenced by pH; at higher pH, ozone reacts with bromide forming bromate, effectively sequestering bromine. At lower ozonation pH, bromate formation is suppressed and higher bromide levels are available for subsequent reactions with chlorine.

Speitel and coworkers (1993) reported similar results in a study of two surface waters. When used alone, ozone lowered THM formation potential (THMFP) by 5-20 percent.

---

3 SUVA is defined as:  $(UV_{254}/DOC) \times 100$ ; SUVA is a general indicator of humic content and roughly corresponds to NOM reactivity. Lower SUVA values will generally correspond to lower DBP formation (Krasner, 1996a).

HAA formation potential (HAAFP) was dependent on ozone dose; within a narrow dose range and at lower doses, ozone lowered HAAFP although at higher ozone doses an increase in HAAFP was seen. Other categories of chlorinated organics such total organic halogens (TOX) also decreased marginally after ozone oxidation (Speitel et al., 1993).

Ozone has been shown to enhance THM and HAA reduction when followed by biologically active filtration. Biologically active dual media filters are readily established by eliminating upstream chlorine residuals, allowing bacterial colonization of filter media by a natural consortium of microorganisms with metabolic capabilities to degrade DBP precursors.

Shukairy and Summers (1992) investigated pre-ozonation and biological filtration for removing organic halide precursors from Ohio River water and a synthetic ground water. Using a synthetic ground water spiked with humic acid, and a 2:1 applied ozone:TOC ratio, purgeable organic halide formation potential decreased by 40 percent when ozone was used alone and an 80-percent decrease was seen after biological filtration. Similarly, when ozonating Ohio River water at a 2:1 applied ozone:TOC ratio, a 28-percent reduction in purgeable organic halogen formation potential was seen and removal decreased by 47 percent when using ozone in conjunction with biological filtration.



Most researchers have reported similar results. Price and coworkers (1993) studied THMFP reduction at pilot scale and full scale. Using ozone alone, THMFP decreased by 20 percent, while biological filtration reduced THMFP by an additional 17 percent (Price et al., 1993). Speitel (1993) observed that biological filtration did not remove THM precursors when ozone was not used, however, biological filtration was effective in reducing HAAFP by 25-30 percent. When pre-ozonation was used (greater than 1 mg/mg TOC), biological filtration reduced THMFP up to 50 percent and HAAFP up to 70 percent. The authors reported that HAA precursors, such as acetic acid, were more amenable to biodegradation in dual-media filters than were THM precursors (Speitel et al., 1993). Krasner (1996a) reported a 20-percent reduction of total THMs by biodegradation, and chloroform levels were reduced by nearly 50 percent through biological filtration.

### **Ozone By-products**

Aqueous ozone reactions occur by two principal mechanisms; direct reaction with molecular ozone and indirect, free radical reactions initiated by ozone decomposition (Figure 2). Generally, direct-ozone oxidation occurs at lower pH (below 8), is more selective than free-radical reactions, and has a higher specificity for unsaturated sites within an organic molecule (Hoigne, 1998). At higher pH, ozone decay accelerates principally due to increased  $\text{OH}\cdot$  concentrations. Ozone decay forms short-lived secondary oxidants (e.g.,  $\text{OH}\cdot$ ) which have a lower substrate specificity and generally

higher reaction rate (Hoigne and Bader, 1976). Free radical species include hydroxyl, carbonate, superoxide, ozonide, and hydroperoxide. Hydroxyl radical reactions with NOM are much less selective than with molecular ozone and reaction rates may be orders of magnitude higher in some cases (Hoigne, 1984).

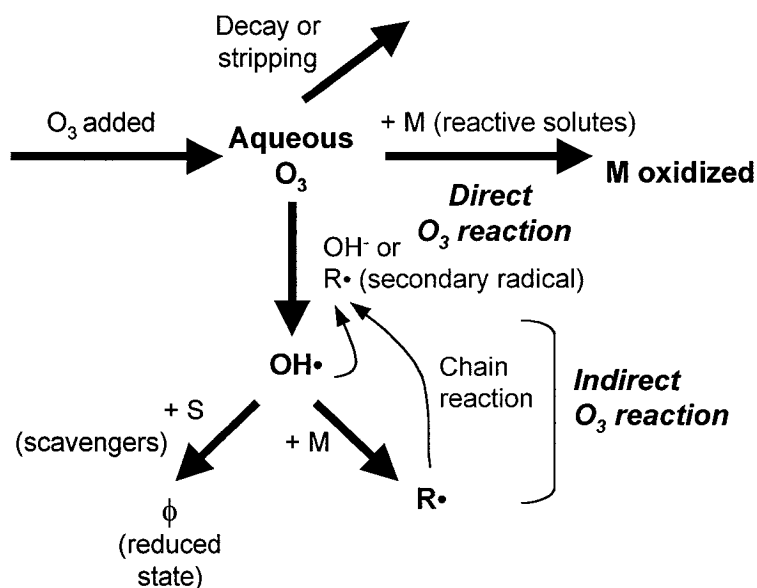


Figure 2. Generalized reaction scheme for direct ozone oxidation and ozone-induced, free radical oxidation

(Adapted from: Hoigné, 1984)

The ozone-induced free radical concentration is highly dependent on the presence of so-called inhibitor and promoter species, which may suppress and enhance, respectively, levels of secondary oxidants (Langlais et al., 1991). Furthermore, free-radical yield is dependent on ozone concentration whereas free radical concentration is dependent on ozone decay rates. In advanced oxidation processes, ozone decay is

accelerated by adding hydrogen peroxide; this increases free radical concentrations by condensing the time period for ozone decay (Hoigne, 1998).

Ozone reacts with NOM to produce a variety of oxidation byproducts (Watts, 1985; Anderson et al., 1986; Glaze, 1986; Cavanagh et al., 1992; Coleman et al., 1992; Andrews and Huck, 1994; Garcia-Araya et al., 1995; Gracia et al., 1996). Generally, ozone-NOM reactions are rapid and oxidize humic and fulvic NOM fractions to a wide range of low molecular weight, oxygenated by-products (Garcia-Araya et al., 1995). Ozone by-products measured in ozonated NOM solutions include: aromatics, aliphatics, alcohols and phenols, as well as other organics (Glaze, 1986; Killops, 1986; Coleman et al., 1992; Gracia et al., 1996).

However, in most natural waters, the aforementioned species are not formed ubiquitously and generally occur at trace levels when formed. Formation of oxygenated carbonyl compounds from ozonated NOM, however, is ubiquitous to most waters (Glaze, 1986; Killops, 1986). The most commonly formed species are carbonyls including: carboxylic acids, aldehydes, and aldoketo acids (Andrews, 1993; Schechter and Singer, 1995; Garcia-Araya et al., 1995; Krasner et al., 1996b). Single-carbon carboxylic acids (e.g., formate and acetate) may be produced from oxidation of mono-aldehydes (formaldehyde and acetaldehyde) and ketoacids (glyoxylic acid and pyruvic acid) form by oxidation of di-aldehydes (glyoxal and methyl glyoxal).

Glyoxylic acid forms as an intermediate species and may be further oxidized to oxalic acid—a prevalent ozonation by-product (Krasner et al., 1996b).

Ozone-NOM reactions are selective and the electrophillic ozone molecule preferentially reacts with unsaturated NOM sites (Andrews and Huck, 1994).

Researchers have generally not seen a substantial reduction in TOC after ozonation, only a shift from larger humic and fulvic NOM fractions to lower molecular weight oxygenated by-products (Gracia et al., 1996). In some waters, ozone may reduce TOC by producing volatile by-products that are then stripped by ozone gas sparging, or by completely oxidizing some NOM to mineral ( $\text{CO}_2$  and  $\text{H}_2\text{O}$ ) end products [Figure 3] (Anderson et al., 1986).

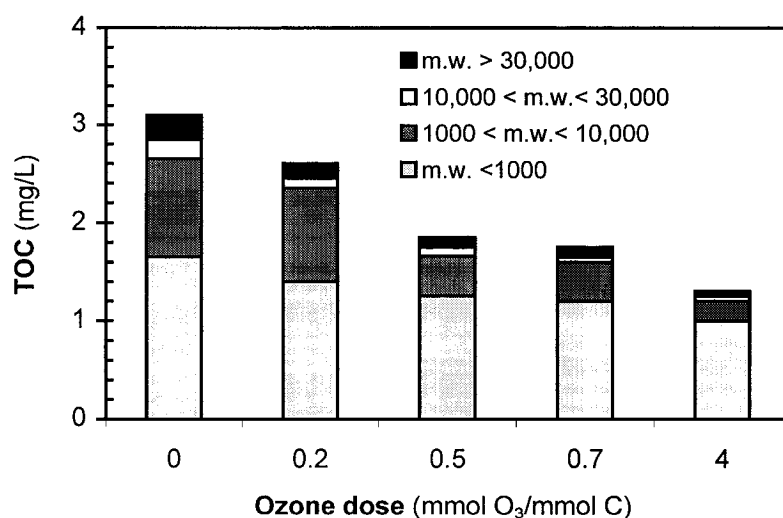


Figure 3. Effect of ozone dose on fulvic acid size distribution.  
(Adapted from: Anderson et al., 1986)

Schechter and Singer (1995) measured aldehyde formation in three different waters and found that aldehyde yield varied as a function of the hydrophobic NOM content. Four aldehydes were formed after ozonation: formaldehyde, acetaldehyde, glyoxal, and methyl glyoxal. Formaldehyde composed the largest fraction (60-80 percent) of the total aldehydes with yields ranging from 5.7  $\mu\text{g}/\text{mg}$  TOC to 36.4  $\mu\text{g}/\text{mg}$  TOC; yields of other aldehydes ranged from 0.9  $\mu\text{g}/\text{mg}$  TOC to 10.7  $\mu\text{g}/\text{mg}$  TOC. Ozone studies conducted on model waters (using re-constituted hydrophobic organic extracts) showed that aldehyde formation was proportional to the relative percentage of hydrophobic NOM. The authors concluded that at a constant ozone-to-TOC exposure, a doubling in hydrophobic TOC resulted in a doubling of aldehyde formation. Furthermore, ozonation at higher pH resulted in lower aldehyde production suggesting that direct ozone oxidation, and not free radical oxidation, was responsible for aldehyde formation (Schechter and Singer, 1995).

Garcia-Araya et al. (1995) studied glyoxylic acid, pyruvic acid, and ketomalonic acid formation in a variety of ozonated NOM extracts. At ozone:DOC ratios less than 2 mg/mg, glyoxylic acid was the major ketoacid formed, however, at higher ozone exposure, glyoxylic acid decreased and ketomalonic acid predominated. Comparison of the humic, fulvic, and hydrophilic NOM fractions showed that humic and hydrophilic fractions produced the highest yields. The authors concluded that ketoacid

formation was dependent on ozone dose, pH, and hydrogen peroxide concentrations, and that both glyoxylic acid and pyruvic acid could be oxidized by free-radical attack.

Watts (1985) analyzed ozone by-products in two surface water sources whose total organic fraction was composed of 90 percent humic and fulvic acids. Humic and fulvic acids were separately extracted and then ozonated. Ozone by-products included aliphatic hydroxy acids, aldehydes, ketones, and alcohols. Ozonated fulvic acid produced hydroxy acids, aldehydes, and various alkanes. When solutions containing both humic and fulvic acid fractions were ozonated, the majority of by-products consisted of aldehydes, ketones, aliphatic carboxylic acids, and benzoic acid (Watts, 1985).

Gracia and coworkers (1996) studied the catalytic ozonation of a synthetic humic acid solution and found that the principal by-products formed included aromatics, carboxylic acids, alcohols, phenols, aldehydes, ketones, furans, and phthalates. Aldehydes included formaldehyde, acetaldehyde, glyoxal, and methylglyoxal. Production of these compounds was measured as a function of ozonation time and it was observed that formaldehyde and glyoxal were formed to a much greater extent than glyoxal and methylglyoxal. In another study, Krasner et al. (1996) measured ozone by-product levels in California aqueduct water. Three categories of by-products were measured: aldehydes, ketoacids, and carboxylic acids. Carboxylic acid production accounted for 24 percent of the biodegradable carbon fraction, whereas ketoacids and

aldehydes accounted for 7 percent and 4 percent, respectively, of the biodegradable carbon fraction.

Andrews (1993) measured a variety of ozone by-products in Canadian surface waters including: aldehydes, ketones, ketoacids, carboxylic acids, bromate, chloral hydrate, cyanogen chloride, THMFP, and HAAFP. Two surface water sources were studied using fractionated fulvic acid (at pH 6 and 8) and using two different ozone:DOC ratios (1:1 and 3:1). In both source waters, aldehydes and carboxylic acids formed the majority of by-products, with the production of oxoacids such as glyoxylic acid, ketomalonic acid, and pyruvic acid totaling 15 percent of aldehyde production. Andrews suggested that fulvic acids were oxidized to aldehydes and further oxidized forming carboxylic acids, however, some of the aldehydes were first converted to oxoaldehydes and oxoacids, and then subsequently oxidized to carboxylic acids (Andrews and Huck, 1994).

### **Biological Stability and Bacterial Regrowth**

Biological stability is a measure of biodegradability and the capacity to promote bacterial regrowth in water distribution systems (van der Kooij, 1992). Bacterial regrowth is a phenomenon where microorganisms colonize and form sustainable communities inside water distribution networks. A typical drinking water distribution system consists of vast pipeline networks that may facilitate attachment and growth of

potentially pathogenic microorganisms such as *Klebsiella* sp., *Escherichia coli*, and *Enterobacter cloacae* (LeChevallier, 1990). Occurrence of such pathogens in public drinking water supplies has been linked to episodes of bacterial regrowth where communities of microorganisms proliferate in distribution systems. Bacterial regrowth is usually associated with a lack of disinfectant residual and high BOM concentration (LeChevallier et al., 1988; LeChevallier, 1990; LeChevallier et al., 1996). Once microbial communities establish within a distribution system, they are difficult to eliminate and may be exceptionally resistant to chlorine disinfection.

Bacterial regrowth may occur through a combination of three principal routes (Rittmann and Wooschlager, 1996). The first route involves growth of heterotrophic microorganisms through the assimilation of organic substrates. Organic substrates may naturally occur in source water or may be created by oxidizing NOM to biodegradable end products. A second route involves growth of autotrophic microorganisms in waters containing a suitable electron donor. Electron donors in surface water sources are most commonly ammonia, however, may also include reduced sulfur species. Usually, autotrophic regrowth occurs in conditions where chloramines are used; ammonia sequestered in the chloramine molecule is released after chlorine decay (Rittmann and Wooschlager, 1996).

A third type of regrowth involves both autotrophic and heterotrophic bacteria. In this instance, regrowth is initiated first by proliferation of autotrophic microorganisms—



forming biofilm communities. As autotrophic biofilms begin to mature, biogenic compounds (generically referred to as soluble microbial products [SMPs]) are released which may serve as a substrate source for heterotrophic microorganisms, and may significantly contribute to biofilm activity (Gagnon et al., 2000).

### **Measuring Biodegradability**

The total BOM fraction in most waters cannot be completely measured by direct chemical analysis due to its heterogeneous composition and generally low levels. Consequently, bioassay procedures have been developed to quantify BOM in water (van der Kooij et al., 1982a; Huck, 1990). The assimilable organic carbon (AOC) assay was the first method developed to assess bacterial re-growth potential.

Assimilable organic carbon measures the growth of two bacteria species (*Pseudomonas fluorescens* strain P17 and *Aquaspirillum* strain NOX) which were originally isolated from biologically active filters in the Netherlands (van der Kooij, 1979; van der Kooij et al., 1982a; van der Kooij et al., 1982b). The AOC assay involves first sterilizing a sample by membrane-filtration and subsequently inoculating known numbers of P-17 and NOX. Organisms are then enumerated using a spread plate technique and AOC is determined based on standard yields of P17 and NOX strains on acetate and oxalate, respectively. Organisms used in the AOC assay have different metabolic capabilities; P-17 is not capable of metabolizing some major ozonation by-products including carboxylic acids (oxalate and formate) and aldoketo acids (glyoxylate) whereas NOX

does not utilize aromatic acids, alcohols, and carbohydrates, which are lesser ozonation by-products (van der Kooij et al., 1989).

In some instances, the limited metabolic capabilities of P-17 and NOX may underestimate the total level of biodegradable carbon present, consequently, the biodegradable dissolved organic carbon (BDOC) bioassay was subsequently developed (Huck, 1990). BDOC and AOC measurements are fundamentally different; BDOC measures the DOC fraction that is mineralized via biochemical oxidation, and AOC measures the DOC fraction that can be converted to biomass. Thus, the BDOC method directly measures changes in substrate concentration while the AOC method measures biomass growth and then relates biomass levels to substrate concentration. Frías et al. (1995) compared different BDOC methods to the AOC method and concluded that AOC generally gave lower results (expressed as carbon equivalents) than the various BDOC methods tested, and that the coefficient of variation was higher for AOC data than for BDOC data. Furthermore, the different BDOC methods tested gave statistically similar results in a range of waters (Frias et al., 1995).

Although BDOC may provide a more rapid method for determining BOM, and is arguably more accurate than AOC, analytical error for biological assay procedures, in general, is much higher than for direct chemical measurements. Furthermore, substantial effort must be invested in maintaining a viable, active culture. For this

reason, researchers have investigated BOM surrogates that can be measured by direct chemical analysis. In most ozonated waters, formation of carboxylic acids, aldehydes, and aldoketo acids has been reported (Glaze, 1987; Andrews and Huck, 1994; Schechter and Singer, 1995; Krasner et al., 1996b). Although these carbonyl compounds do not compose the whole BOM fraction (Krasner et al., 1996b), they can be used as a primary growth substrate and can be measured more precisely than bulk BOM in a bioassay technique. Thus, these constituents may be used as a surrogate for filter-removable BOM.

### **Biological Filtration**

Biologically active filtration has been demonstrated as a robust technology for removing BOM and producing biologically stable water. In Europe, biological filtration has been extensively implemented into water processes due to the widespread use of ozone (Urfer et al., 1997). Biological filtration is a more recent occurrence in the United States due to less widespread advanced oxidation use and a generally higher source water quality. Recently, with the increased use of ozone in the U.S., biological filtration has seen a substantial application in pilot-and demonstration-scale projects, and in some full-scale applications. Biological filters utilize fixed-biofilms on conventional dual-media filters or on GAC columns. Incorporation of biological filtration into conventional processes principally entails eliminating disinfectants within the treatment process. The lack of oxidant residual promotes biofilm formation

on filter media by a natural consortium of microorganisms (van der Kooij et al., 1989; Servais et al., 1991; LeChevallier et al., 1992).

LeChevallier et al. (1992) evaluated pre-ozonation followed by biological filtration under pilot-conditions. Several different biological filter configurations were tested including a granular activated carbon (GAC)-sand filter, anthracite-sand filter, and a deep-bed GAC filter. After ozonation, a 230 percent increase in AOC was seen. Even though biological filtration reduced AOC levels below 100 µg/L (using a 5-10 min empty bed contact time [EBCT]), AOC in the biologically filtered effluent was always higher than in the raw water. Increasing EBCTs enhanced both AOC and TOC removal, however, this required relatively long detention times (~20 min) that may not be feasible in some full-scale processes. A correlation was also observed between TOC removal and decreases in THMFP. Over a one-year operating period, average THMFP removals were ~50 percent in biologically active GAC-sand filters when operating at a 10 min EBCT. However, this average reflects enhanced removal due to adsorption over the first several months of operation and THMFP removal from adsorption and biodegradation were not differentiated in this case (LeChevallier et al., 1992).

Miltner et al. (1992) conducted bench-scale biotreatment studies on ozonated Ohio River water using a batch reactor containing acclimated biomass supported on sand. Over the range of ozone doses tested (0.5-3 mg O<sub>3</sub>:mg TOC) aldehyde, AOC, and

BDOC concentrations increased as a function of ozone dose. Aldehyde removal ranged from 40-100 percent and DOC removal ranged from 10-23 percent. A 75-percent reduction in HAAFP and a 50-percent reduction in THMFP were reported after ozonation and biological treatment. However, the testing scale used for this study and the long detention times used has limited applicability to a continuous process.

Huck et al. (1991) measured BOM removal in biologically active, sand/anthracite filters followed by GAC adsorption. Raw water was first treated by coagulation, flocculation, and sedimentation, and was subsequently ozonated and biologically filtered. Ozonation generally increased AOC, however, AOC increase was not directly dependent on ozone dose, and a statistically significant relationship between the two could not be established. AOC removal in the dual media filters was generally high, however, varied operationally as a function of loading rate and ozone dose, and varied seasonally as a function of water temperature. AOC Removal criterion ( $<20 \mu\text{g/L}$ ) could not be met during the spring and summer months but could be met roughly 50 percent of the time during the winter and fall months. The authors also observed that  $\text{AOC}_{\text{NOX}}$  was removable by GAC adsorption to some extent whereas  $\text{AOC}_{\text{P-17}}$  was not.

Coffey and et al. (1995) studied pertinent biofilter operating variables including the effects of filter media, acclimation times after start-up and biofilm perturbation after filter backwashing. Following plant start-up, AOC removal began after operating for 10-15 days, and reached steady state after 40 days. During the initial two weeks following start-up, AOC removal was less than 5 percent and after operating for 40 days, AOC removal varied from 75 percent to nearly 90 percent. Tests were conducted where chlorine was added for 24- and 48-hour periods prior to biological filtration to observe biological filter upset. Adding chlorine for a 24-hour period, and after operating for 93 days, decreased AOC removal by over 50 percent. After chlorination, filter biofilms took 10-15 days to re-establish. Subsequent chlorination at later time periods showed a similar trend, however, did not decrease AOC removal to the same extent.

In a study on similar source water, Krasner and coworkers (1993b) tested biologically active filters for removing aldehydes, and specifically, the effects of contact time and filter media. Krasner concluded that replacing conventional anthracite with activated carbon resulted in a denser biofilm, which needed shorter acclimation times and was less prone to fluctuation and upset. Formaldehyde and glyoxal data were reported to provide surrogate parameters for removal of readily biodegradable and recalcitrant ozone by-products, respectively. Total aldehyde removal followed trends similar to those observed for AOC removal.

## MEMBRANE SEPARATION PROCESSES

As regulations for chemical and biological contaminants in water have become more stringent, membrane processes including NF, UF, and MF have been utilized as treatment alternatives. NF has been used in place of conventional processes (employing chemical coagulation for removing dissolved species and filtration for removing suspended species) due to its ability to reject divalent metal ions (e.g., calcium and magnesium) as well as NOM and DBP precursors (AWWARF, 1996). NF membranes typically reject dissolved species having molecular weights of 200 daltons and larger. Molecular weights of natural organic matter species typically range from 5000 daltons for fulvic acid species, to upwards of 100,000 daltons for some humic acids. The first NF applications were for softening and more recently NF has been used to remove NOM and DBP precursors (Amy et al., 1990a). As of 1996, there were approximately 150 plants worldwide using nanofiltration, with a total treatment capacity of 150 million gallons per day (AWWARF, 1996). Nanofiltration operations typically operate using trans-membrane pressures between 72 to 220 psi.

UF has been used to remove suspended solids, in particular, pathogenic organisms, which include bacteria, protozoa, and viruses. UF membranes may reject larger NOM fractions on the order of 20,000 daltons and larger. Ultrafiltration will reject dissolved humic species to a limited extent, however, is substantially less effective than nanofilter membranes for this application. As of 1996, there were 34 ultrafiltration

plants in operation or under construction (worldwide), having a total capacity of 34 million gallons per day (Adham et al., 1996). Ultrafiltration membranes typically operate using pressures from 7 to 70 psi.

MF has been used in water treatment for removing suspended solids (larger than approximately 0.1  $\mu\text{m}$ ). MF has been used by water utilities in place of conventional process, where treatment objectives are suspended solids control microbial removal. MF can not achieve a reliable degree of dissolved organics control. Studies on the cost effectiveness of microfiltration vs. conventional treatment have shown that for small utilities treating in the range of 3 million gallons per day, microfiltration is economically competitive with conventional treatment (Adham et al., 1996). As of 1996, there were 40 plants using MF, having a combined capacity of 12 mgd. Operating pressures for MF are low and in the same general range as UF.

## **HYBRID MEMBRANE PROCESSES**

### **MF/UF-PAC Processes**

Hybrid membrane processes have been developed that incorporate adsorption for dissolved organics removal with MF or UF filtration (Pirbazari et al., 1992; Adham et al., 1993; Jack and Clark, 1998). PAC is added to the process to sequester dissolved species that would otherwise pass through the relatively permeable MF/UF membranes.



Furthermore, PAC has been shown to enhance membrane flux by forming a permeable, non-compressible filtration cake on membrane surfaces (Pirbazari et al., 1992). Membranes are used for particulate rejection and to completely retain PAC within the process. Hybrid membrane/adsorption processes have been used for removing NOM and DPB precursors as well as for removing trace contaminants such as TCE.

Pirbazari et al. (1992) used MF-PAC to remove TCE from surface water spiked with NOM. With a 200- $\mu\text{g/L}$  initial TCE level and continuously feeding 50 mg/L PAC, permeate TCE levels were reduced to below detection limits ( $<0.5 \mu\text{g/L}$ ). Extensive evaluations were conducted that examined the effect of PAC concentrations on permeate flux and the effect of various operating variables including trans membrane pressure (TMP) and hydraulic cross flow velocity (CFV) within the tubular MF membrane. Increasing PAC dose was reported to increase permeate flux from 130 gal/ft<sup>2</sup>-day, when operating without carbon, to 310 gal/ft<sup>2</sup>-day when 3000 mg/L PAC was added to the reactor. A linear relationship was observed between TMP and permeate flux rates indicating that the PAC cake deposited on the membrane was relatively incompressible.

UF-PAC was tested at pilot scale and full scale for removing NOM from ground water and surface water (Adham et al., 1993). A continuous PAC dose (42 mg/L) was used

in pilot scale tests and a consistent TOC removal was seen (~80 percent). In another study (Jack and Clark, 1998), UF-PAC was used to remove DOC and pesticides (atrazine and cyanazine). Using a 10-mg/L PAC dose, DOC was marginally reduced (15-25 percent), however, cyanazine and atrazine levels were reduced to a greater extent. Due to operational difficulties, however, only 85 percent recovery was achieved and reported membrane flux ranged from 4 gal/day-ft<sup>2</sup>-psi to 12 gal/day-ft<sup>2</sup>-psi.

Chang et al. (1998) used a bench-scale hybrid adsorption-UF process for removing DOC and THM precursors from several different surface waters. Adsorbents used in the process consisted of 0.5-50 µm iron oxide particles prepared by neutralizing, and then heating a ferric nitrate solution. Iron oxide particles were added to a recirculation loop that was filtered through a cellulose acetate hollow fiber membrane. Reported DOC removals were between 25 percent to 80 percent and were directly dependent on iron oxide dose. A linear relationship was observed between TOC removal and THM precursor removal where THM precursors were generally removed at the same percentages as TOC.

### **Membrane Bioreactors**

The membrane bioreactor (MBR) has recently emerged as a viable technology for water and wastewater treatment. MBRs combine two basic processes: biodegradation

for removing dissolved organic and inorganic constituents and membrane separation for removing suspended solids (Figure 4). In a recirculation-type MBR (Figure 4a), reactor contents are recirculated (under pressure) through the lumen of an MF or UF membrane and the rejected solids are subsequently recycled back into the reactor. Due to the high solids content and abrasion incurred from high cross flow velocities, tubular inorganic (e.g., ceramic) membranes are often used (Pirbazari et al., 1996; Cicek et al., 1998a). In the submerged type MBR (Figure 4b), membranes are directly immersed into the biological reactor and TMP is provided by operating under a vacuum. Hollow-fiber membranes are typically used in immersed type MBRs due to the lower energy environment and the need to minimize space requirements as existing basins are often retrofitted.

A key advantage of MBRs over other bioreactor types is their ability to completely retain biomass within the system, allowing explicit control of biomass age and reactor solids (AWWARF, 1996). Additionally, PAC or other additives may be used to enhance membrane flux, sequester dissolved species, and provide a high-surface-area support for microorganism attachment and biofilm growth (Pirbazari et al., 1996).

MBRs have seen a substantial growth in wastewater processes, however, have not been widely used for treating potable water.

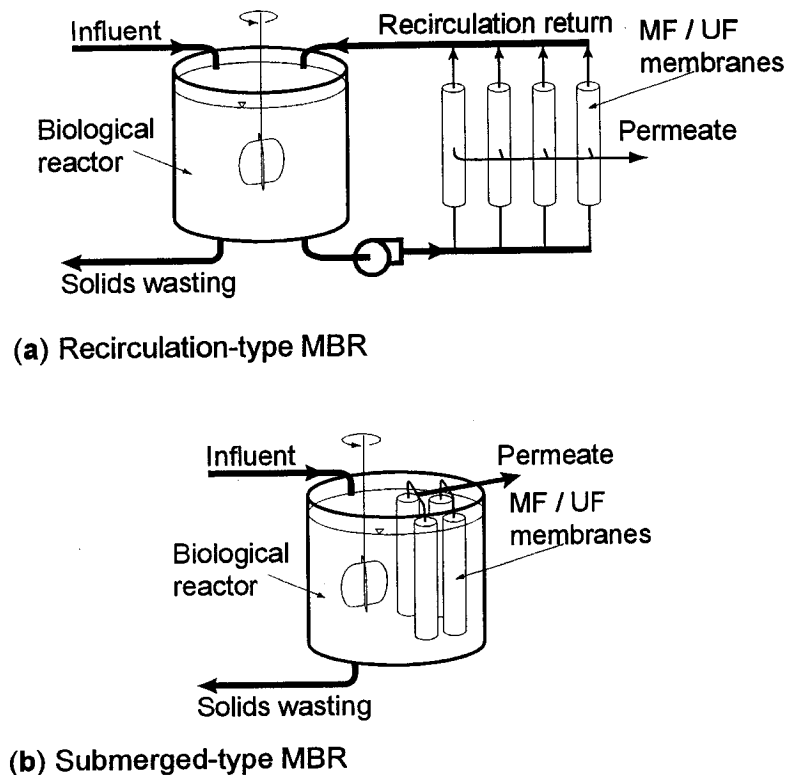


Figure 4. Conceptual MBR process schematic illustrating two principal process configurations: (a) reactor contents are recirculated through hollow fiber or tubular membranes; or (b) membranes are immersed directly into the reactor and vacuum is applied to create TMP.

Pirbazari et al. (1996) used an MBR to treat high-TOC landfill leachate containing a wide variety of volatile and non-volatile organics. The process was operated with a high PAC dose (1- percent w/w) added at startup and without subsequent PAC addition during operation. Untreated leachate had high TOC (900-960 mg/L), biochemical oxygen demand (1500-1700 mg/L), and substantial levels of acetone (12-15 mg/L) and 1,2-dichloroethane (approximately 2 mg/L). Over a 30-hour operating period after startup, TOC removals were consistently high (>98 percent). As the treatment

objective was to maximize TOC removal, long (3 day) hydraulic retention times (HRTs) were used and increasing HRT beyond 3 days had no measurable effect on process efficiency. Membrane fouling was minimized by the high reactor PAC concentrations. After operating for 100 hours, flux declined by approximately 70 percent when 1 percent PAC was initially added and when leachate was pre-treated for suspended solids removal, flux loss was minimized; declining by approximately 15 percent after operating for 25 hours (Pirbazari et al., 1996).

In another study, Ravindran and co-workers (1995) used a membrane-bioreactor for removing gasoline from water. A multi-component mixture containing aromatic and aliphatic hydrocarbons was treated using biologically active adsorption in conjunction with MF. Aromatic hydrocarbon removals were on the order of 90-95 percent. PAC addition reduced membrane fouling, and also removed adsorbable hydrocarbon species, particularly during start-up when biodegradation was low. Different PAC addition strategies were tested including adding high doses at startup and continuous addition at low doses. Without continuous PAC addition, hydrocarbon removal was consistently high suggesting that activated carbon is biologically regenerated (Ravindran et al., 1995).

MBRs have been extensively used in municipal wastewater processes (Beaubien et al., 1996; Choo and Lee, 1996; Cicek et al., 1998a; Cicek et al., 1998b; Rosenbeger et al.,

2000; Xing et al., 2000). In a pilot-scale study, Cicek and co-workers (1998) demonstrated that consistently low TOC and chemical oxygen demand (COD) levels could be achieved when treating simulated municipal wastewater using an MBR. The pilot-scale MBR consisted of a completely mixed and continually aerated reactor, and a tubular ceramic UF membrane. Solids retention times were on the order of 30 days and TMP was varied to maintain a constant permeate flow rate and HRT. Average effluent TOC and COD removals over the 500-day testing period were 97 percent and 99 percent, respectively, however, after membrane regeneration, DOC removal dropped for the first 12 hours of the filtration cycle. The authors concluded that following membrane cleaning, removal decreased due to the lack of a filtration cake on the membrane surface and that once established, the filtration cake enhanced process efficiency. The relationship between membrane cake layer and processes efficiency has also been reported by others (Choo and Lee, 1996).

In another study, Xing and co-workers (2000) used a pilot-scale MBR to treat municipal wastewater with COD values ranging from 200 mg/L to 800 mg/L, and with a high total suspended solids content (~350 mg/L). Tubular ceramic membranes were used as they provided a higher resistance to chemical and physical deterioration. Over an extended operating period (162 days), COD removal averaged 97 percent (HRT = 5 h). A sequential increase in solids retention time (SRT) from 5 days to

30 days had little effect on COD removal, while both flux and HRT were maintained at consistent levels.

Heesu et al. (1999) studied the effects of PAC addition on MBR process efficiency. Studies were conducted using a high-strength, synthetic wastewater (COD = 27,000 mg/L) and used a bench-scale MBR apparatus operating in a batch-feed mode. Specific cake resistances measured for biomass alone were roughly four orders of magnitude higher than measured for mixtures of PAC and biomass. PAC was reported to provide a rigid, relatively incompressible filtration cake that interfered with formation of the dense filtration cakes formed by biosolids. Adding 0.1 percent PAC enhanced flux to a moderate extent over a 10-day testing period; however, PAC addition appeared to minimize flux decay only during startup as the long-term flux decline rate was comparable when PAC was not added. Particle distribution analysis showed that adding PAC increased mean particle sizes from 7.5  $\mu\text{m}$  to 22  $\mu\text{m}$  after operating for 5 hours. The authors conclude that PAC enhances flux by sorbing and coagulating organics and fine colloids, effectively changing the particle distribution and sequestering finer suspended fractions that would otherwise form dense filtration cakes and subsequently foul the membrane.

MBRs have seen a very limited application in municipal water treatment. Urbain and co-workers (1996) used an MBR to remove pesticides, THM precursors, and nitrate

from a contaminated ground water source. Pilot- and full-scale processes were tested using a biological culture in conjunction with powdered activated carbon and ultrafiltration. The biological culture was used in addition with an electron donor (ethanol) to biologically reduce nitrate to nitrogen gas. Activated carbon was used for removing NOM and pesticides. Consistent biological nitrate removal (averaging 80 percent) was achieved. Removal of THM precursors was also reported, which was likely a result of activated carbon adsorption, in conjunction with rejection of hydrophobic (humic) NOM species by the ultrafiltration membrane.



## **Chapter 3 - MATERIALS AND METHODS**

### **SOURCE WATER**

Real water and synthetic water were used for this research; surface water from the California State water project (SPW) was used for most tests while synthetic water was used in some tests to eliminate background NOM. SPW was chosen because it is a major potable water source for Southern California and has been extensively characterized (Coffey et al., 1995). Moreover, SPW may have high THM formation potential (depending on chlorine exposure) and generally yields relatively high BDOC and AOC concentrations when ozonated. Table 1 shows the average and range of raw water quality measured over the testing period, Table 2 shows typical ozone by-product formation at a 3-mg/L-ozone dose, and Figure 5 shows the apparent NOM molecular weight distribution. Note that data shown in Table 2 and Figure 5 were measured in previous studies and represent typical values for SPW.

Synthetic water was obtained from an ultra-pure water process that used deionization, RO-filtration, and GAC adsorption. Background organic matter levels in ultrapure water were less than the TOC method detection limit (MDL) of 0.1 mg/L TOC. Synthetic water was buffered with 1.4 mmol  $\text{NaHCO}_3$  to provide an alkalinity of 70 mg/L as  $\text{CaCO}_3$ . For biokinetic tests using synthetic water, mineral nutrients were added to ensure carbon was limiting (Table 3).

Table 1. Water quality for selected parameters in untreated SPW

Parameter	Units	Average Value	Range
pH	–	8.1	8.0 - 8.4
Temperature	°C	16	10 - 25
Turbidity	NTU	3.6	1.9 - 12
Total alkalinity	mg/L as CaCO <sub>3</sub>	72	63 - 79
TDS	mg/L	229	176 - 279
TOC	mg/L	4.0	2.9 – 5.0
Ca <sup>++</sup>	mg/L	19	16 - 22
Mg <sup>++</sup>	mg/L	12	10 - 14
Na <sup>+</sup>	mg/L	42	31 - 57
SO <sub>4</sub> <sup>2-</sup>	mg/L	32	22 - 41
NO <sub>3</sub> <sup>-</sup>	mg/L	2.4	0.9 – 5

(Source: Metropolitan Water District of Southern California; monthly water quality reports)

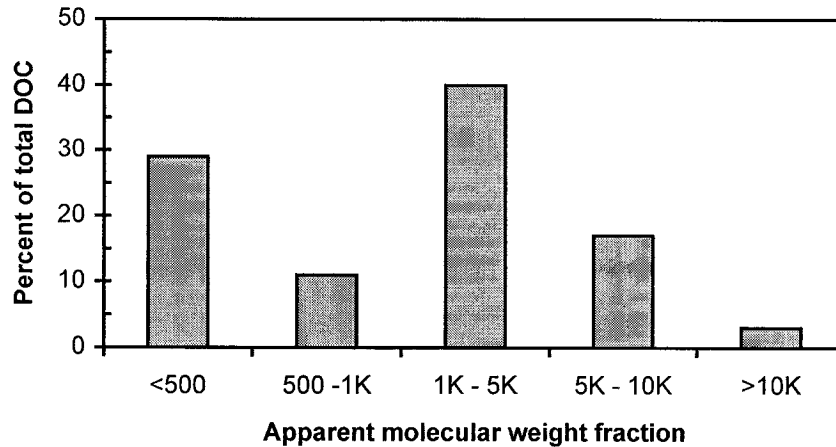


Figure 5. Apparent molecular weight size distribution for NOM in untreated SPW (Adapted from: Amy et al., 1991)

Table 2. Characteristic ozone by-product levels formed in SPW

Parameter	Units	Value
<b>Carboxylic acids</b>		
Formate	µg/L	86
Acetate	µg/L	47
Oxylate	µg/L	139
<b>Aldoketo acids</b>		
glyoxylic acid	µg/L	29
Pyruvic acid	µg/L	15
Ketomalonic acid	µg/L	34
<b>Aldehydes</b>		
Formaldehyde	µg/L	12
Acetaldehyde	µg/L	5
Glyoxal	µg/L	7
Methyl Glyoxal	µg/L	5
AOC	µg C/L	445
DOC	mg/L	2.8
BDOC	mg/L	0.76

Source: (Krasner et al., 1996b)

Table 3. Composition of mineral media added to supplement biodegradation

Mineral	Molar ratio added (M salt:M formaldehyde)	Final Concentration (mg/L)
KH <sub>2</sub> PO <sub>4</sub>	2	9.1
NH <sub>4</sub> Cl	2	3.6
KNO <sub>3</sub>	2	6.7

## MEMBRANES

Bench- and mini-pilot-scale MBR testing used tubular ceramic membranes (Membralox® T1-70; U.S. Filter Corp.; Redmond, WA.) composed of a cast ceramic sol-gel membrane on a ceramic support. Each ceramic tube had a 1-cm internal diameter and a 63 cm<sup>2</sup> membrane surface area; membranes provided a 0.2-μm nominal rejection. Figure 6 shows a scanning electron microscope (SEM) micrograph of a virgin ceramic membrane surface. A single ceramic tube was used for bench-scale testing, and a 6-tube module was used for mini-pilot tests. To restore permeate flux, membranes were mechanically cleaned using a surfactant solution and small-diameter brush. Membranes were also chemically cleaned by soaking in base (1N NaOH) and acid (1N H<sub>2</sub>SO<sub>4</sub>) solutions for approximately 1 hour. During most tests, chemical cleaning was performed less frequently than mechanical cleaning.

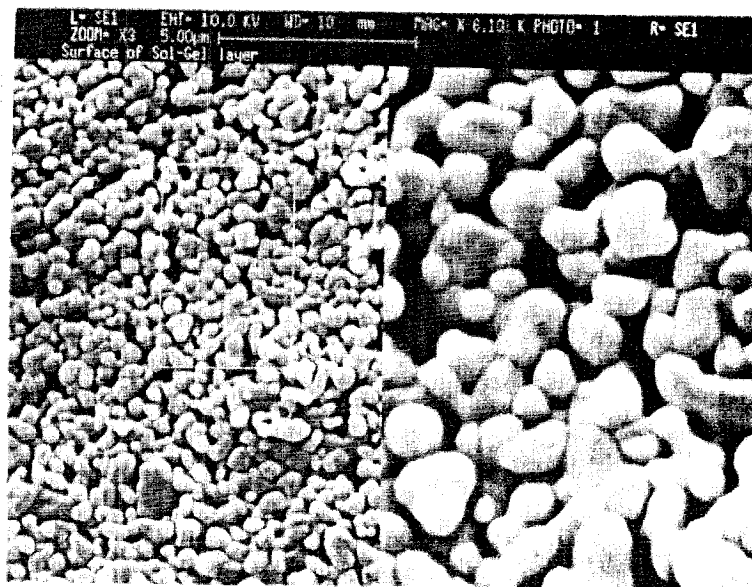


Figure 6. SEM micrograph showing the ceramic membrane surface.

## **ACTIVATED CARBON**

Commercially available powdered activated carbon (Type WPH pulverized; Calgon Corp.; Pittsburgh, PA.) was used as supplied by the manufacturer without subsequent washing (for fines separation) or mechanical sieving. Particle counts were conducted on dilute PAC solutions to establish the mean PAC particle diameter for mathematical modeling. Methods used for particle counts are discussed in a subsequent section (Particle counts) in the current chapter. Figure 6 (a) shows batch particle count data for 10 mg/L virgin PAC in ultra-pure water and ozonated water; Figure 6 (b) shows a percentile rank indicating the mean PAC size (9  $\mu\text{m}$ ).

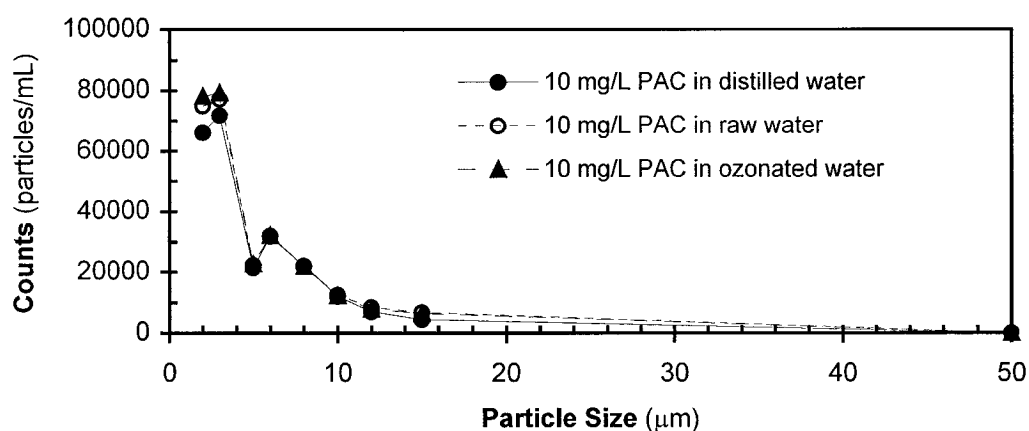
## **EXPERIMENTAL METHODS**

### **Methodology Development**

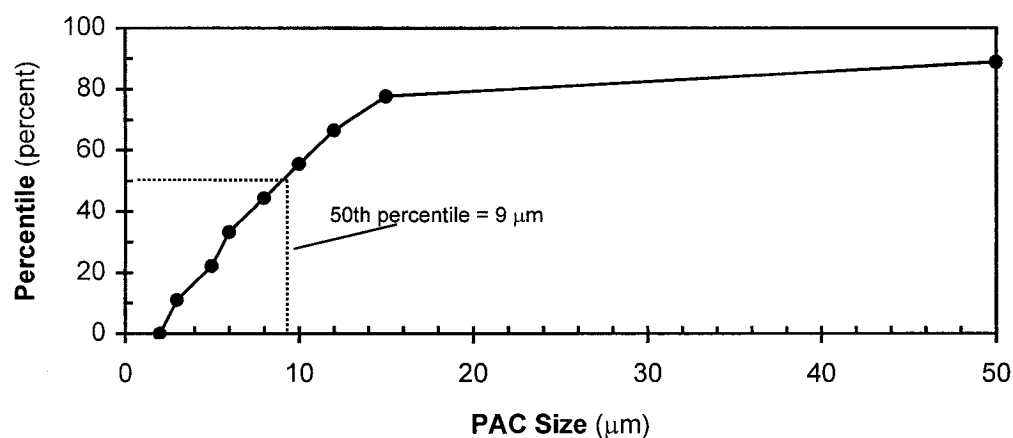
A number of challenges were faced in developing the research methodology due to the inherent complexity of both the physical apparatus as well as the process chemistry.

One of the challenges was maintaining control under laboratory conditions. It was determined in initial laboratory tests, for example, that it was not possible to accurately measure changes in formaldehyde concentrations in ozonated water exposed to the lab air due to liquid absorption of gas-phase formaldehyde and acetaldehyde. When exposed to air, the low levels of aldehydes in ozonated water would increase

substantially over time. Another challenge was maintaining ozonated water batches while minimizing biological growth in the feed. Once contaminated, BDOC in the ozonated feed water would rapidly deplete and the experiment had to be stopped.



(a)



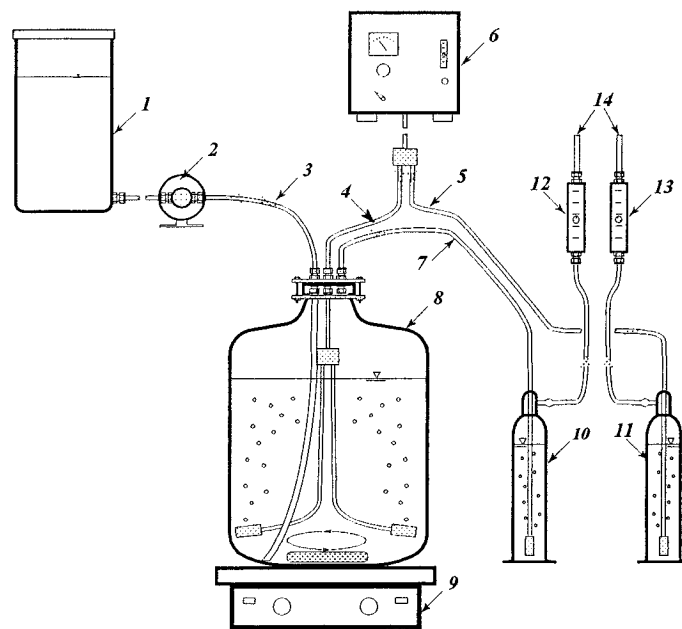
(b)

Figure 7. (a) Batch particle counts of a 10 mg/L PAC solution in ultra-pure water and in ozonated water, and (b) percentile distribution curve

Other challenges faced included developing a strategy for sampling in biokinetic studies which required continuous sample collection at 4-8 hour intervals for over a week. Although samples were easily collected using sampling pumps set on automatic timers, the bio-oxidation of substrates had to be essentially quenched at the time of sampling or the data would be meaningless. For adsorption rate tests, large sample volumes (0.5 L) were needed within short time intervals, due to the rapid rate of PAC adsorption. A methodology was needed to rapidly (within approximately 30 sec) collect and filter PAC from a batch reactor while maintaining a closed system to prevent gas-phase contaminant absorption.

### **Semi-batch Ozone Contactor**

Figure 8 shows an illustration of the semi-batch ozone reactor used for bench-scale tests. The reactor was constructed of Pyrex<sup>®</sup> glass and had a 40-L effective capacity. Porous glass frits near the bottom of the reactor were used to diffuse ozone gas into solution and mixing was accomplished using a magnetic stirrer. Ozone feed gas was controlled using a stainless steel needle valve downstream of a rotameter used to measure gas flow rate. Typical gas flow rates were 150 - 250 mL/min (at 14 psig gas feed pressure). Reactor off-gas was collected in the headspace and could be diverted either directly to a fume hood or through a KI trap to measure the applied and transferred ozone dose.



#### Explanation

- |   |  |
|---|--|
| 1 - Raw water feed and ozonated water storage       | 8 - 40 L Pyrex batch ozone reactor                     |
| 2 - Feed Pump                                       | 9 - Magnetic stirrer                                   |
| 3 - Water drain/fill line                           | 10 - Reactor off-gas gas wash bottle filled with 2% KI |
| 4 - Ozone gas feed to reactor                       | 11 - Ozone control gas wash bottle filled with 2% KI   |
| 5 - Ozone gas feed to control gas wash bottle       | 12 - Gas flow meter - reactor                          |
| 6 - Ozone generator                                 | 13 - Gas flow meter - control                          |
| 7 - Off-gas from reactor to reactor gas wash bottle | 14 - Off gas vented to hood                            |

Figure 8. Schematic illustration of the semi-batch ozonation reactor used for bench-scale studies

Ozone gas was generated using a bench-top ozone generator (Griffin Technics Corp.; Lodi, NJ) using a pure-oxygen feed gas. Ozone concentrations typically ranged from 4 percent to 6 percent leaving the generator. Ozone-enriched gas from the generator was split into two streams of equal flow rate. The first stream was supplied to the reactor, and the second stream flowed directly to a 500-mL gas washing bottle containing a 2-percent KI solution. Applied and transferred ozone dose was calculated



using the ozone mass measured in the control and off-gas traps. Applied ozone dose was calculated by dividing ozone mass in the control trap by the reactor fluid volume. Transferred ozone dose was calculated by first subtracting the ozone mass measured in the reactor-off-gas trap from the control, and then dividing by volume.

Water batches were ozonated by first pumping the desired sample volume into the reactor. Second, the batch was exposed to ozone gas for a time period that depended on the desired dose. Exposure time was determined by first determining percent ozone in the feed gas stream and, once the needed gas flow rates were determined, an exposure time was then calculated based on the desired applied dose. After water was ozonated, dissolved ozone was allowed to decay for several hours, and the sample was pumped into a polypropylene storage container.

### **Pilot-scale Ozone Contactor**

The pilot-scale ozone column used during mini-pilot MBR experiments is shown in Figure 9. The contactor was constructed from 3-in PVC pipe in a U-tube configuration. The first 20-ft leg was used as a counter-current chamber for ozone gas transfer and the second 20-ft leg was used as a reaction column. Ozone gas was added at the base of the first column using a porous ceramic frit. A 1.5-gpm raw water stream (HRT = 13 min) was supplied by gravity flow. Ozone gas was generated using an ozone generator with a compressed air feed (Model Labo-76; Trailgaz Ozone of

America; Jenkintown, PA), and accurately regulated and measured using a rotameter upstream from a needle valve. A gas-phase ozone monitor (Model H1; In USA; Needham, MA) was connected to a side-stream from the generator to measure feed gas ozone concentration. Ozone gas flow rates were calculated based on the gas-phase ozone concentration, pressure, and the desired ozone dose.

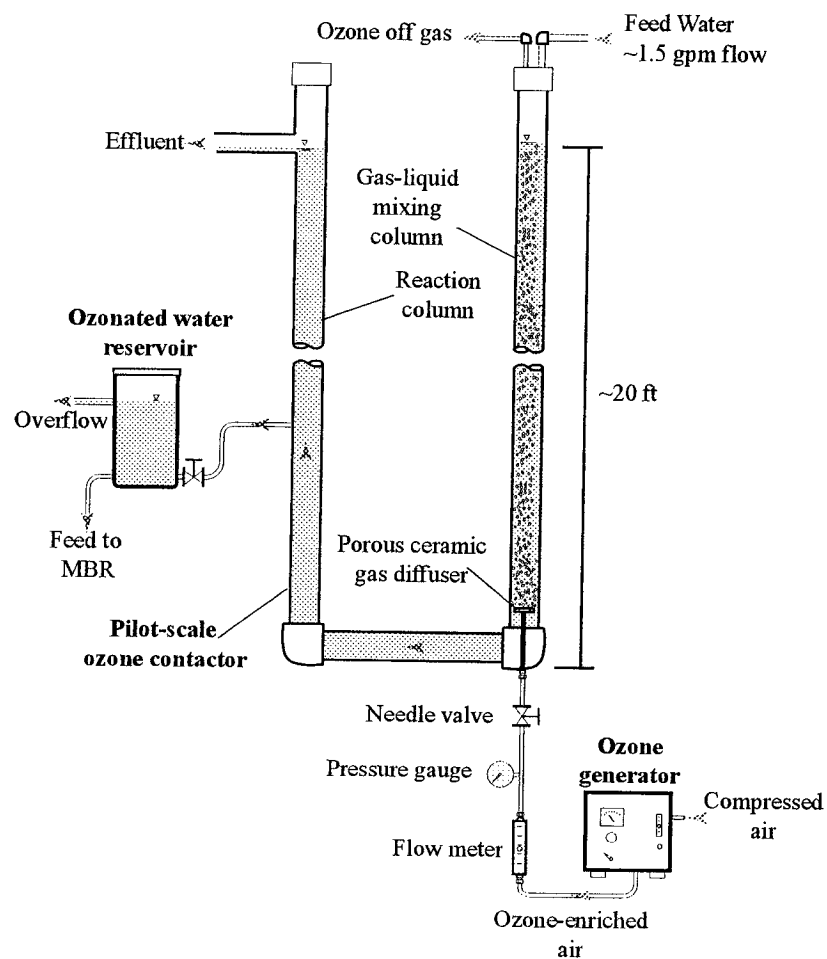


Figure 9. Schematic illustration of the pilot-scale ozone contactor

## **Biological Inocula**

An indigenous consortium of organisms was used for seeding in both MBR tests and biokinetic tests. Biomass was grown in fixed-bed columns continually supplied with ozonated water (average ozone dose = 5 mg/L). Ozonated water was collected from the pilot-scale ozone contactor where it first flowed into a storage tank with a 90-min (average) detention time to allow complete ozone residual decay.

Water was then fed using a variable speed peristaltic pump (Masterflex® L/S; Cole-Parmer; Vernon Hills, IL) through a series of two chromatography-type columns (Cat. # 5820; Ace Glass; Vineland, NJ) each containing a 3-6 in. deep bed of porous biological support media (Siran®; Schott Engineering; Mainz, Germany). A 30-mL/min feed rate was used to achieve an average 17-min EBCT and 8-min EBCT in the first and second columns, respectively.

The BDOC-depleted feed from the first column was supplemented with 700 µg/L total aldehydes (consisting of: 400-µg/L formaldehyde, 100-µg/L acetaldehyde, and 200-µg/L methyl glyoxal) before it was fed to the second column. A second peristaltic pump was used to feed aldehydes from a 70-mg/L stock solution into the second column. The stock solution reservoir and connecting tubing was periodically autoclaved to prevent biomass growth in the aldehyde feed reservoir. This setup was used to establish biomass acclimated to both ambient BDOC (in the first column) and

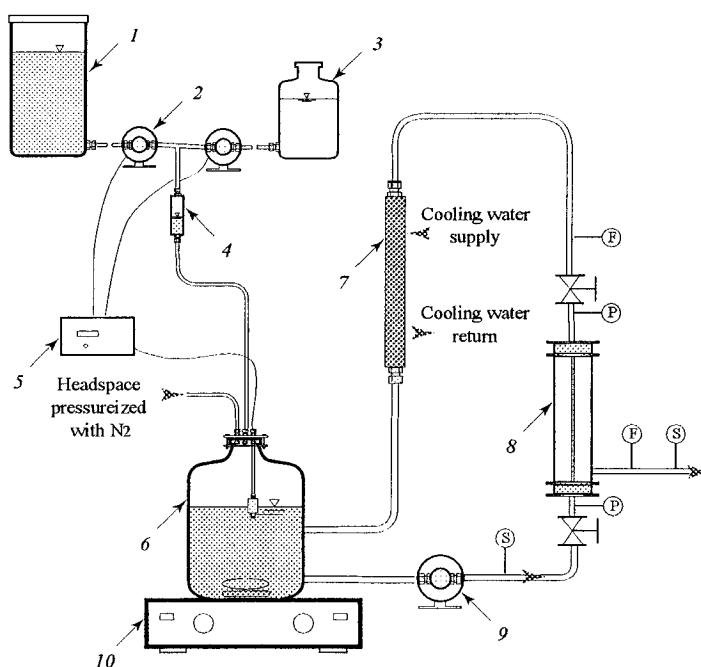
to high aldehyde levels (in the second column). Most MBR tests, and some of the biokinetic tests, used organisms that were acclimated to ambient BDOC levels. However, two of the biokinetic tests were conducted in synthetic water using only total aldehydes at relatively high concentrations (300 µg/L). Cultures from the aldehyde-enriched column were used for inoculating aldehyde biokinetic tests.

Columns were acclimated for approximately 60 days before biomass was first harvested. Biomass was harvested by removing the columns and agitating the packed bed by repeatedly inverting the column for several minutes. This sheared off a substantial amount of the thick biomass, which was subsequently collected from the bulk fluid within the column (as the packing only filled ~25 percent of the column depth). The clumped biomass was homogenized by continued, high-intensity vortex mixing using a 50-mL, conical-bottom vial. Biomass was then enumerated by plate counting and used for tests. Biomass was stored at 4°C for no longer than a week before being used.

### **Bench-scale MBR**

A bench-scale MBR was constructed for preliminary MBR tests under controlled laboratory conditions. The apparatus was operated in a continuous mode and consisted of a 4-L reactor, a single-element membrane module, a recirculation pump, and an automatic level controller (Figure 10). Reactor contents were completely mixed using

a magnetic stirrer and pumped through the tubular membrane using a low-lift recirculation pump at flow rates ranging from 1-4 L/min. The ceramic tubular membrane had a 1-cm internal diameter and 63 -cm<sup>2</sup> total surface area and was operated in a tangential flow mode where generally less than 5 percent of the feed flow was recovered as permeate. The remaining concentrate, including biomass and PAC, was re-circulated back to the reactor.



#### Explanation

- |   |                                 |
|---|---------------------------------|
| 1 - Ozonated water feed tank              | 9 - Low-lift recirculation pump |
| 2 - Diaphragm metering pump               | 10 - Magnetic stirrer           |
| 3 - Aldehyde feed reservoir               | ⓕ - Flow measurement            |
| 4 - Aseptic air-gap                       | Ⓟ - Pressure measurement        |
| 5 - Flow and level controller             | Ⓢ - Sample measurement          |
| 6 - 4-L reactor                           |                                 |
| 7 - In-line, tube-in-shell heat exchanger |                                 |
| 8 - Single element membrane module        |                                 |

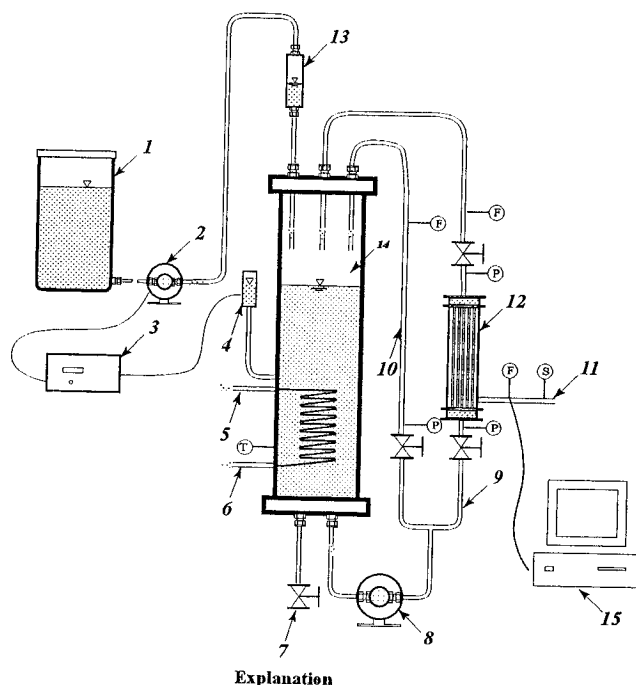
Figure 10. Schematic illustration of the bench-scale MBR

Reactor samples were collected from a sample tap in the membrane-recirculation loop, and permeate samples were collected from a permeate sample tap. An in-line, tube-in-shell heat exchanger was used to control temperature and all tests were conducted at 20°C.

Driving pressure for membrane filtration was accomplished by pressurizing the reactor headspace using compressed air. Typical trans-membrane pressures ranged from 10 to 20 psi. A consistent reactor volume was maintained using an automatic level controller that sensed reactor levels using a magnetic float switch, and modulated a diaphragm feed pump (LMI Milton Roy; Acton, MA). Feed water was stored in a 30-gal polypropylene tank usually in 20-30 gallon batches. Before each test, the feed reservoir was thoroughly cleaned with laboratory detergent and rinsed repeatedly with distilled water, and the MBR apparatus was autoclaved to prevent biofilm growth in the reactor tubing. Feed water was not kept for more than 3-5 days, as biodegradation of ozonated feed water would generally begin within 5-7 days. Some tests used aldehydes in a synthetic water matrix; for these tests, sterile synthetic water was fed from the reservoir, and aldehydes were directly added to the MBR from a separate, sterile feed reservoir. Between tests, the membrane was cleaned using a small brush followed by immersion in a strong acid (1 N  $\text{H}_2\text{SO}_4$ ) and base (1 N NaOH).

## Mini-pilot-scale MBR

A schematic illustration of the mini-pilot-scale MBR is shown in Figure 11. The essential components of this apparatus are a reactor, membrane module, and a centrifugal pump to re-circulate reactor contents and provide driving pressure. The reactor had a variable volume (5 to 20 L) and was constructed from acrylic with a conical bottom to eliminate PAC accumulation in dead-zones.



- |                                  |                                 |
|----------------------------------|---------------------------------|
| 1 - Ozonated water Storage       | 8 - Reactor Re-circulation Pump |
| 2 - Feed Pump                    | 9 - Membrane Feed Loop          |
| 3 - Reactor Level Controller     | 10 - By-pass Loop               |
| 4 - Reactor Level Switch         | 11 - Permeate Effluent          |
| 5 - Reactor Cooling Water Feed   | 12 - Membrane Module            |
| 6 - Reactor Cooling Water Return | 13 - Influent Trap              |
| 7 - Sludge Wasting Line          | 14 - Bioreactor                 |
| (F) - Flow Measurement           | 15 - Data acquisition system+   |
| (P) - Pressure Measurement       |                                 |
| (T) - Temperature Measurement    |                                 |
| (S) - Sample Measurement         |                                 |

Figure 11. Schematic illustration of the mini-pilot-scale MBR

Reactor contents were pumped through the MF membrane lumen using a centrifugal pump where a small percentage of the feed was recovered as permeate and the concentrate was recycled back to the reactor. Re-circulation rates provided a 1.4-m/sec tangential velocity within the membrane tubes. A multi-tube membrane module was constructed so that membrane area could be increased by adding additional membrane tubes (Membralox<sup>®</sup> T1-70; U.S. Filter Corp.; Redmond, WA.). Trans-membrane pressure (TMP) was adjustable and most tests were operated at 20 psi TMP.

Ozonated feed water was pumped into the MBR from a 30-gal polypropylene reservoir that was continuously supplied with a side-stream from the pilot-scale ozone contactor. Hydraulic retention time in the feed reservoir was on the order of several hours, allowing complete ozone residual decay. The feed reservoir was cleaned frequently as biomass would rapidly colonize the tank. Ozonated water was pumped into the MBR reactor through an in-line trap that maintained an air-gap between the feed stream and the reactor, preventing contamination (and subsequent degradation) of the feed solution by microorganisms in the reactor. The reactor volume (and average HRT) could be changed by using a set of liquid level switches mounted in an external, variable-height liquid cell that was hydraulically connected to the reactor. Level switches were attached to a controller, which cycled the MBR feed pump as needed. During some tests, reactor contents were bled using a peristaltic pump that would cycle with the feed pump, wasting a small percentage of the reactor volume.



Prior to each test the entire apparatus was drained and cleaned to remove PAC and or biomass from the previous test. Tubular membranes were mechanically cleaned between and during tests using a small-diameter flask brush. For most tests, PAC and biomass were initially added to the reactor at startup. In some tests, PAC was continuously added by feeding high-concentration PAC slurry from a 4-L reservoir. The metering pump would cycle with the MBR feed pump, and flow rate was set based on feed concentration and desired dose. In other tests, the same method was used to add aldehydes and to lower influent pH by adding reagents from a high-concentration stock solution. Permeate flow rates and temperature were measured using on-line instruments and data were recorded using a computer with analog data acquisition software (Labtech Notebook; Labtech; Andover, MA). Since permeate flow would sometimes vary more than the flow meter turndown capacity, both a high- and low-range flow meter were used.

### **Adsorption Studies**

Two types of adsorption experiments were conducted: equilibrium experiments and rate experiments. Equilibrium studies measured the equilibrium liquid phase adsorbate concentrations, and rate studies measured liquid phase adsorbate concentrations as a function of time.

### *Adsorption Isotherm Studies*

Adsorption isotherm studies measured PAC adsorption capacity by measuring the liquid-phase concentrations at different PAC doses after equilibration. PAC was first dried at 105°C overnight and then accurately weighed using a precision balance. The weighed carbon was then added to 1000-mL borosilicate bottles with Teflon-lined septa, and 1 L of sample was accurately measured and added to each bottle.

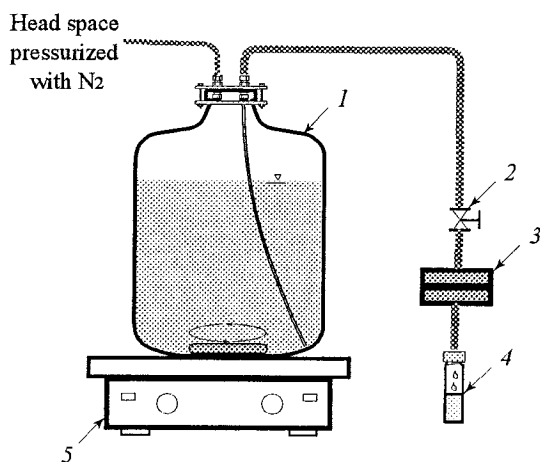
Additionally, a control (to measure  $C_0$ ) was used for each isotherm test, where carbon was not added. Samples were allowed to equilibrate by tumbling for 24 hours at 20°C.

After equilibration, PAC was removed from solution using a quartz-fiber filter (Grade QM-A; Whatman; Maidstone, England), and the filtrate was collected and analyzed.

The adsorbed mass was calculated from the decrease in liquid phase adsorbate concentration for the different PAC doses.

### *Adsorption Rate Studies*

Adsorption rate studies were conducted using the apparatus shown Figure 12. The apparatus consisted of a 20-L Pyrex<sup>®</sup> reactor with an airtight fitting that sealed the reactor headspace while allowing sample collection. Sealing the headspace served two functions: to maintain a closed system and eliminate absorption of gas-phase aldehydes, and to provide a means to rapidly collect and filter samples.



### Explanation

- 1 - 20-L Pyrex reactor
- 2 - Plug valve
- 3 - 47 mm, in-line membrane housing with quick disconnect fittings
- 4 - 500 mL sample collection bottle
- 5- Magnetic stirrer

Figure 12. Batch reactor apparatus used for adsorption rate studies

The reactor headspace was pressurized (~3-5 psi) using bottled nitrogen gas. Once the headspace was pressurized, samples were collected by opening a valve connected to a Teflon sampling tube. Care was taken to ensure the headspace could not be mistakenly pressured at higher pressure (> 5 psi), which would pose a danger. High-pressure, stainless steel inline filter housing (Millipore; Bedford, MA) with a glass-fiber filter (Grade QM-A; Whatman; Maidstone, England) was used to filter PAC from samples. Pressure within the reactor headspace provided the driving force for sample filtration. Using this method, a 500-mL sample could be simultaneously collected and filtered within 20 to 30 seconds. Glass-fiber filters were changed between samples. Having

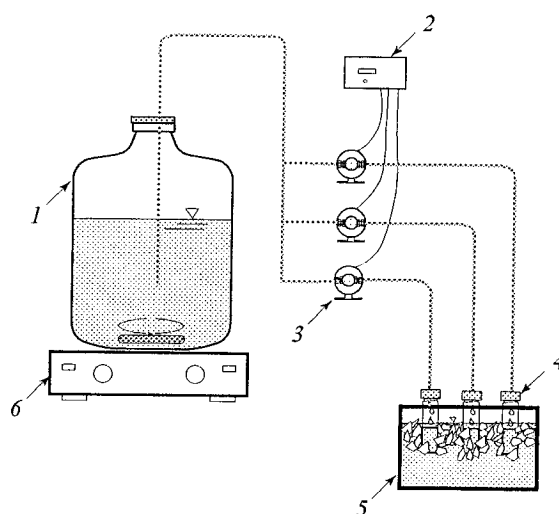
the ability to rapidly collect and filter samples was crucial because PAC adsorption kinetics were rapid and greater than 80 percent of the equilibrium concentration was reached within the first 5 minutes.

All tests were conducted at 20°C, and care was taken to insulate the reactor from heat generated from the magnetic stirrer. A 3-in cylindrical stirring bar (having a minimal surface area in contact with the glass reactor) was used at a low mixing rpm (approximately 100-rpm) to minimize PAC pulverization that may occurred during stirring. Moreover, the 20-L glass reactor had a convex bottom that further reduced the potential for PAC pulverization by minimizing the contact area between the stir bar and reactor bottom. During tests, the reactor was first filled with 20 L of sample and completely mixed for several minutes. The desired PAC mass was weighed using a precision balance and then hydrated with a small volume (100 mL) of distilled water to facilitate rapidly adding PAC to the 20-L batch. Prior to adding PAC, a control sample was first collected; PAC slurry was then added to the stirred reactor. Samples were collected at varying intervals with more frequent sampling towards the beginning of the test. Tests were typically run for 2 hours.

### **Biokinetic Studies**

Batch biokinetic studies were conducted using the reactor setup shown in Figure 13. A batch reactor setup was used rather than a continuous-flow chemostat reactor for

several reasons: first, biomass concentrations were substantially lower than typically seen for wastewater, and consequently, maintaining a low-biomass concentration in a suspended-growth reactor chemostat would not be feasible, and second, because BDOC and AOC are comprised of complex, heterogeneous mixtures, increasing AOC or BDOC concentration would not be practical.



#### Explanation

- 1 - 20-L Pyrex reactor
- 2 - Programmable timer/pump controller
- 3 - Peristaltic sample collection pump
- 4 - 125 mL sample collection bottle
- 5 - Ice bath
- 6 - Magnetic stirrer

Figure 13. Schematic illustration of the batch reactor setup used for biokinetic studies

The apparatus consisted of a 10-L Pyrex<sup>®</sup> reactor that was completely mixed using a magnetic stirrer. Tests required continuous sample collection every 6 hours over a 7-day period. To accomplish this, timer-controlled sampling pumps (Masterflex<sup>®</sup> L/S;

Cole-Parmer; Vernon Hills, IL) were used to collect some samples. Sample bottles used for collecting unattended samples (from automatic sampling pumps) were immersed in an ice-bath to halt reaction kinetics and prevent continued degradation. All water quality samples were subsequently filtered using a 0.2  $\mu\text{m}$  nylon membrane (Type WNYL; Whatman; Maidstone, England) prior to analysis and biomass samples were immediately plated after collection.

Prior to each test, the entire apparatus was sterilized using an autoclave to eliminate biomass carry over from previous tests. The reactor was filled with 10 L of either ozonated water or synthetic water spiked with aldehydes. For both types of water, mineral nutrients were added to ensure that carbon was growth limiting (Table 3). Synthetic water was sparged with pure oxygen for approximately 30 minutes to ensure sufficient oxygen was available throughout the test. Tests were initiated by adding 500 CFU/mL of acclimated biomass, and run at 20°C until substrate was depleted and the biomass was well into the endogenous decay phase.

## **ANALYTICAL METHODS**

### **pH and Alkalinity**

pH was measured using a bench-top pH meter and combination glass electrode. The instrument was calibrated using standard (pH 4, 7, and 10) pre-prepared buffer solutions. Alkalinity was measured using the titration technique as described in

Standard Method 2320 B (APHA, 1998) where a 50-mL sample is collected and titrated against 0.02N hydrochloric acid to pH 4.5.

### **UV Absorbance**

UV absorbance at 254 nm ( $UV_{254}$ ) was measured by first filtering samples through a 0.45- $\mu$ m nylon membrane (Type WNYL; Whatman; Maidstone, England) to remove turbidity and then absorbance was measured with a UV-Vis. Spectrophotometer (Model Lambda 4A; Perkin-Elmer Corporation; Norwalk, CT) using a 1-cm quartz cuvette.

### **Ozone Dose**

Applied ozone dose and transferred ozone dose used in bench-scale tests were measured using the semi-batch technique as described in Method 2350 E (APHA, 1998). Ozone mass in both the reactor feed and off-gas was measured by first absorbing gas-phase ozone into a 2-percent potassium iodide solution, and then titrating the oxidized iodine back to iodide using 0.01 N sodium thiosulfate. Ozone gas streams were directed to the 500-mL potassium iodide traps or to vent using a 3-way valve.

During pilot-scale tests, ozone dose was calculated using gas flow rate, liquid flow rate, column pressure, and ozone concentration in the feed gas. Gas and liquid flow rates

were measured using a variable-area flow meter, pressure was measured using an analog gauge, and gas-phase ozone was measured using a high-range ozone monitor (Model H1; In USA; Needham, MA). Along with temperature, these variables were input into a spreadsheet program, and ozone dose was calculated using known mass transfer efficiencies.

### **Dissolved Ozone**

Dissolved (aqueous-phase) ozone was measured using the indigo colorimetric method (Method 4500 B; (APHA, 1998). Aqueous ozone rapidly reacts with indigotrisulfonate in acidic solution, decolorizing the indigo. Measuring the subsequent decrease in absorbance at 600 nm provides a linear relationship with aqueous ozone residual ( $0.42 \text{ cm}^{-1}/\text{mg/L}$  ozone) (Bader and Hoigne, 1981). A 1-mmol indigo solution was prepared using 85 percent pure, reagent-grade indigotrisulfonate (Sigma-Aldrich; St. Louis, MO). A known volume of indigo reagent and sample were added to a 125-mL flask and mixed by swirling. Absorbance of the sample and indigo blank were then measured at 600 nm using a UV-Vis. Spectrophotometer (Model Lambda 4A; Perkin-Elmer Corporation, Norwalk, CT) and dissolved ozone was calculated as per Standard Method 4500 B (APHA, 1998).



## TOC and DOC

Organic carbon was measured as per Standard Method 5310 B (APHA, 1998). A combustion-type TOC analyzer with a non-dispersive infrared detector (Model TOC-5000; Shimadzu Scientific Instruments; Columbia, MD) was used. Total organic carbon was calculated by first measuring total carbon measured in the combustion furnace and then subtracting inorganic carbon (IC) measured in a separate IC channel. In most natural waters, IC is substantially higher than TOC and may severely interfere with accurate TOC measurement. To eliminate IC interference, 125 mL TOC samples were first acidified with 100  $\mu$ L of concentrated phosphoric acid and then purged with nitrogen gas for 20 minutes. This lowered IC levels to near detection limits and eliminated interference. DOC samples were first filtered through a 0.45  $\mu$ m pre-washed nylon membrane (Type WNYL; Whatman; Maidstone, England) and then analyzed for TOC. DOC samples were also acidified and purged to remove IC.

## AOC

AOC was measured using Standard Method 9217 B using both *Pseudomonas fluorescens* Strain P-17 and *Aquaspirillum* Strain NOX (APHA, 1998). Water samples were initially filter sterilized using a 0.2- $\mu$ m nylon membrane. Prior to filtration, the membrane was washed with 500 mL of ultra-pure water to eliminate leachable organics. After filtration, 40 mL of sterilized sample was transferred to a 45 mL borosilicate glass vial with a Teflon-lined cap. Samples were then inoculated with 500 colony forming units (CFU)/mL from each of the previously prepared *P. fluorescens*

and *Aquasprillum* stock solutions. *P. fluorescens* strain P-17 and *Aquasprillum* strain NOX stock were obtained from the American Type Culture Collection (ATCC, Manassas, VA) in freeze-dried form and were subsequently hydrated using a glycerol-water mixture and stored at  $-70^{\circ}\text{C}$  for subsequent use. Note that both organisms were inoculated simultaneously, this is in contrast to other method variations where organisms are added sequentially (i.e. NOX is added after P-17 reaches steady growth) (van der Kooij et al., 1989). Samples were incubated until colony counts reached a maximum (this was typically after 7 days) and then enumerated using a spread-plate technique on agar (Difco R2A; Becton Dickinson; Sparks, MD). AOC was calculated based on the maximum number of organisms multiplied by the standard carbon yield as outlined in Standard Method 9217 B (APHA, 1998).

## **BDOC**

Several approaches exist for measuring BDOC, however, most methods may be categorized as either batch analysis or dynamic (rapid BDOC) analysis. In both methods an indigenous consortium of organisms is used and BDOC values are subsequently calculated based on the difference in DOC concentrations before and after incubation. Indigenous bacteria have been shown to possess a wider metabolic diversity than those used for the AOC assay, consequently, DOC uptake is typically higher (Frias et al., 1995). In the batch BDOC assay, either suspended or fixed biomass may be added where fixed biomass are usually grown on an inorganic support

(silica sand or Siran<sup>®</sup>) and must be continually acclimated in a biological filter. Typical incubation times for batch BDOC tests range from 5 days to 21 days, depending on the method used.

Dynamic, or rapid-BDOC methods use a pre-acclimated, fixed-bed biological reactor which is continually supplied with the sample stream. However, some modifications exist where a batch is used and recirculated through the column (Prevost, 1996). In the rapid BDOC method, BDOC is calculated from the difference between influent and effluent DOC. The rapid BDOC method was developed to provide full-scale processes a means to rapidly assess BDOC without the long incubation times that are required for batch methods. This method usually requires a large sample volume.

A modification of the batch BDOC method described by Block (1992) was used for this work. Approximately 100 mL of sample was added to a 125-mL amber borosilicate glass bottle with a Teflon-lined closure. The sample was subsequently inoculated with acclimated biomass (500 CFU/mL) harvested from columns according to procedures described in Chapter 3 (Biological inocula). After incubating for 7 days at 20°C, samples were filtered using a 0.2- $\mu$ m Nylon membrane. Samples were then analyzed for DOC, and BDOC was calculated from the difference in DOC before and after incubation.

## Aldehydes

Aldehydes were measured using derivatization with *O*-(2,3,4,5,6-pentafluorobenzyl) hydroxylamine hydrochloride (PFBHA) followed by gas chromatography/electron capture detection (GC/ECD) as described in Standard Method 6252 B (APHA, 1998). The method was first described by Yamada and Somiya (1989) and later modified by Krasner et al. (1993b). Samples were derivatized by adding 1 mL of a 10-mg/mL PFBHA derivatizing agent (Sigma-Aldrich; St. Louis, MO) to 20 mL of sample in a 45-mL borosilicate glass vial with Teflon-lined closures. Samples were buffered to pH 6.0 using a potassium hydrogen phthalate buffer. Samples were then derivatized in a 45°C water bath for 2 hours. After cooling, concentrated sulfuric acid (250 µL) and 3-mL high purity hexane (Fisher Scientific; Pittsburgh, PA) were added and samples were shaken vigorously for 15 min using a wrist-action shaker. Following extraction, the organic layer was transferred (using a hexane-washed Pasteur pipette) to a 5-mL borosilicate glass vial containing 3-mL of sulfuric acid (0.2 N) and shaken for 2 min. Approximately 1 mL of the hexane layer was removed with a Pasteur pipette and placed in a 2-mL borosilicate glass vial containing approximately 50 mg of oven-baked 12/60 mesh sodium sulfate (J.T. Baker Chemical Co.; Phillipsburg, NJ).

Extracts were analyzed using GC/ECD (Model 5790A; Hewlett Packard Co., Palo Alto, CA) and a SPB-5 capillary column (Supelco, Inc.; Bellefonte, PA) 15 m in length x 0.53 mm in diameter. The initial column temperature was 90°C, which was

subsequently increased linearly to 250°C at a rate of 3°C /min. Injector and detector temperatures were set at 250°C and 300°C, respectively. Data was collected using an integrator (Hewlett Packard Co.; Palo Alto, CA) that measured both peak area and height. Standard curves were prepared from certified aldehyde standard solutions (Chem Service Inc.; West Chester, PA) to establish both retention times and peak area for a given constituent. The four aldehydes measured were: formaldehyde, acetaldehyde, glyoxal, and methyl glyoxal.

### **Sample Chlorination and THM Analysis**

Samples were chlorinated to simulate secondary disinfection and to measure effects of treatment on THM formation. Based on changes in trihalomethane formation potential (THMFP) after treatment, inferences were made with regards to THM precursor removal. THMFP is defined as the THM levels formed in a 7-day chlorine exposure period when chlorine is added in excess. However, in this study a 24-hour chlorine exposure was used for most samples, as the research objectives were to compare process changes while maintaining other variables. Shorter chlorine exposure times were used to lower sampling processing times.

Sample chlorination followed procedures described in Standard Method 5710 B (APHA, 1998). Samples were collected in duplicate 125 mL amber borosilicate glass bottles with Teflon septa screw caps and were first buffered at pH 7.0 using a

phosphate buffer (0.01 M final concentration). A 5-mg/mL sodium hypochlorite solution was used for dosing chlorine at a 3:1 chlorine:TOC ratio. This translated to a 10-mg/L free chlorine dose. Samples were then stored in a dark, temperature-controlled room (20°C) for 24 hours. After the 24-hour reaction period, the remaining chlorine was quenched with 0.1 mL of a 10-percent sodium sulfite solution to stop the reaction. Samples were stored at 4°C for no longer than 7 days before extraction and analysis.

Trihalomethanes were measured using liquid-liquid extraction followed by GC/ECD analysis according to Standard Method 6232 D (APHA, 1998). THM-grade pentane (Fisher Scientific; Pittsburgh, PA) was used as the extraction solvent. The pentane extract was then analyzed using a Hewlett Packard model 5790A GC (Hewlett Packard Co.; Palo Alto, CA) equipped with an ECD detector. The column was operated under isothermal conditions (50°C); the injector was set at 225°C and the detector at 300°C.

## **Biomass Measurement**

### *Activated Carbon Desorption Procedure*

Biomass attached to PAC was quantified by first using procedures to detach bacteria. The method described by Camper et al. (1985) was used with several modifications. PAC-biomass samples were diluted 50:1 to a 20-mL final volume using a desorption buffer consisting of the following: 0.1 mL of 10 µM Zwittergent (Calbiochem-Behring

Corp.; La Jolla, CA), 1.0 mL of 1.0 M Tris (pH = 7.5), 1.0 mL of EGTA (pH = 8.0), and 0.1 g peptone added to 1 L sterile water. Samples were then agitated for 5 min at a 50 –percent setting using a Vertishear Tissue Homogenizer (Virtishear; Virtis Co.; Gardiner, NY). De-sorbed bacteria were enumerated using spread plate techniques or examined microscopically.

#### *Heterotrophic Plate Counts*

Biomass was quantified using the spread plate method for heterotrophic plate counts according to Standard Method 9215 C (APHA, 1998). Briefly, 1 mL of sample was diluted in a decimal dilution sequence using sterilized water. Samples were then plated on agar (Difco R2A; Becton Dickinson; Sparks, MD) and subsequently incubated for 3-7 days or until the small, slowly growing colonies could be seen. Plates containing 20-200 colonies were counted. Biomass was subsequently reported (as colony forming units [CFU]/mL) after correcting for dilution. Samples were plated in triplicate and reported biomass values reflect the average of the replicate samples.

#### *Direct microbial counts*

Biomass was quantified in some samples by direct observation using epifluorescence microscopy (Standard Method 9216 B; Standard Methods, 1998). Prior to counting, biomass was first detached from PAC using the activated carbon desorption procedure described in Chapter 3. If samples were not counted immediately, a preservative

(5 percent w/v gluteraldehyde) was added and samples were stored (4°C) for no longer than 14 days before counting. Biomass was counted at 1000 times magnification (in oil immersion) using an optical microscope (Model CHS; Olympus Corporation; Lake Success, NY) equipped with an epifluorescence light source.

### **SEM Analysis**

Biological samples were prepared for SEM analysis by fixation and subsequent dehydration. Sample fixation involved a pre-fixation for 1 hour in a modified Karnovsky fixative (2.5 percent gluteraldehyde, 2 percent p-paraformaldehyde, 0.04 percent calcium chloride, 0.1M cacodylate buffer), followed by three rinses in a 0.2-M cacodylate buffer and post-fixation (30 min) in 1-percent osmium tetroxide. Fixed samples were subsequently dehydrated using a graded ethanol series (30 percent-100 percent). Dehydrated samples were further dried in hexamethyldisilazane overnight. Dried samples were then mounted to aluminum specimen stubs in their proper orientation using colloidal graphite and Au/Pt sputter coated for 5 min.

Samples were analyzed using a scanning electron microscope (Model S360; Cambridge Scientific Instruments; England) equipped with an energy dispersive spectrometer and lanthiumhexaboride filament. SEM analysis was conducted using a 10-kV beam acceleration voltage.



## **Particle Counts**

Particle counts were conducted on virgin PAC samples using a batch-fed particle counter using a laser optic light source (Model LS-200 Liquilaz; Particle Measuring Systems Inc.; Boulder, CO). Particles were counted in 10 size ranges from 2-100  $\mu\text{m}$  and were reported as a function of discrete sizes. Prior to analysis, ultra-pure water was analyzed to zero the instrument and flush residual particulates from the sampling lines. The instrument sampled in a batch mode and reported values based on replicate samplings of a single batch.

## **Chapter 4 - EXPERIMENTAL RESULTS: BENCH- AND MINI-PILOT-SCALE STUDIES**

### **OBJECTIVES**

This chapter presents results from bench- and mini-pilot-scale MBR studies and semi-batch ozonation studies. Objectives of the MBR studies were to conduct bench-scale and mini-pilot-scale MBR tests and evaluate process efficiency for removing DOC, THM precursors, AOC, and total aldehydes from pre-ozonated water. Additionally, using data from semi-batch ozone tests and MBR studies, evaluate appropriate surrogate BOM parameters for subsequent modeling. Specific objectives are summarized as follows:

1. Conduct semi-batch ozonation experiments to establish the nature and concentrations of products formed during ozonation and assess the variability of byproduct formation and sensitivity to ozone dose. Data will be subsequently used, along with biokinetic data, to select surrogate parameters for modeling organic carbon removal and biological stability of treated water.
2. Perform preliminary tests under laboratory conditions using a bench-scale MBR process to evaluate the range of process variables to be used for subsequent mini-pilot tests. Specifically, evaluate HRT, suitable PAC doses, and the expected rates

of flux decline from membrane fouling. Based on the results, establish design criteria for a mini-pilot-scale process.

3. Demonstrate a mini-pilot MBR process under field conditions for removing organic carbon from pre-ozonated source water, while minimizing biological and particulate membrane fouling. Establish the effect of the following process operating variables: HRT, PAC concentration, influent substrate concentration, and process recovery rates on removal of total aldehydes, DOC, BDOC, THM precursors, and AOC. Some of the data sets generated in these studies will later be used to validate the MBR model by comparing measured data to predictions from the calibrated model.
4. Establish the effects of operating strategy and PAC dose on membrane fouling rates and determine which operating strategy maximized BOM removal while minimizing membrane fouling.

## **RESULTS AND DISCUSSION**

### **Ozone Byproduct Formation**

Semi-batch tests were conducted to evaluate the effect of ozone oxidation on organic constituents, and to assess the magnitude of ozone byproduct formation. These data were used with MBR results and biokinetic data to determine appropriate surrogates for modeling adsorption and biodegradation in the MBR process. These tests measured

ozone byproduct formation as a function of ozone exposure. Constituents measured included: total aldehydes, THMFP, BDOC, DOC, and AOC. Samples were collected from the semi-batch reactor after various ozone exposure times, and dissolved ozone was subsequently quenched with  $\text{Na}_2\text{S}_2\text{O}_3$  to stop further reaction. Tests were conducted at ambient pH (7.8) and at 20°C.

In water treatment practice, ozone exposure is typically expressed as either an applied or transferred dose, or as the product of the integrated ozone concentration multiplied by time—expressed as a *CT* value (Langlais et al., 1991). Ozone exposure is typically expressed as a dose when oxidation is the treatment objective, and as a *CT* value when disinfection is the treatment objective. Ozone is generated in the gas phase and is subsequently transferred into water using a gas/liquid contactor. Ozone mass transfer from gas to liquid is dependent on a number of variables which include: water temperature, pH, the presence of (aqueous) free radical promoters and inhibitors, gas bubble size, gaseous and dissolved ozone concentration, and ozone contactor geometry. Furthermore, once dissolved in water, ozone decays rapidly (first order half-lives generally range from several minutes to less than an hour). Consequently, *CT* values cannot be directly determined from the applied or transferred dose. Rather, ozone *CT* must be determined by measuring dissolved ozone within the reactor. Figure 14 shows *CT* values and ozone mass transfer rates for the semi-batch reactor. These values

represent a range of what would typically be used in a full-scale process (Williams et al., 2000).

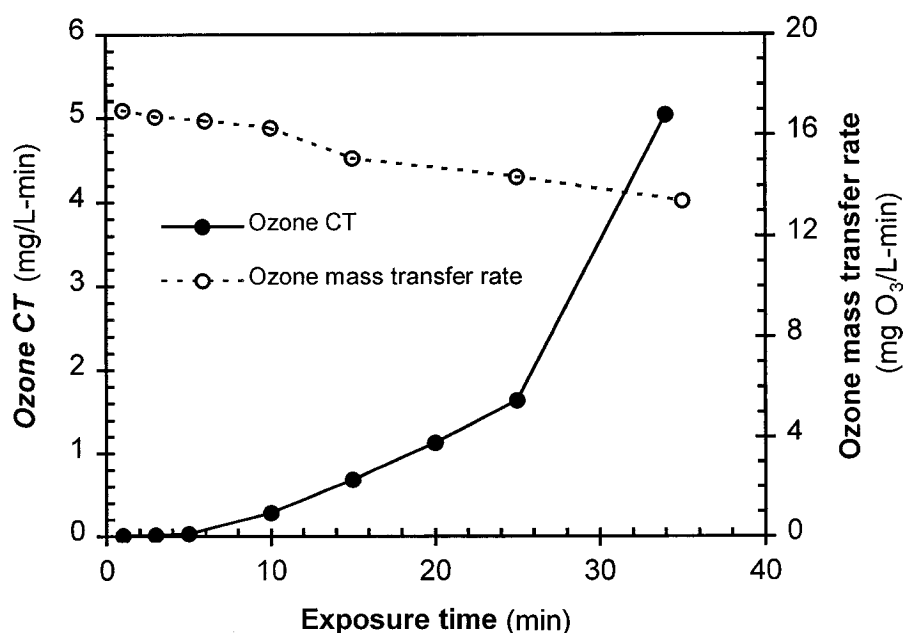


Figure 14. Ozone *CT* exposure and mass transfer rate as a function of ozonation time for semi-batch ozone studies

Figure 15 shows aldehyde production over a range of *CT* values. Formaldehyde and glyoxal production increased as a function of ozone concentration, although formaldehyde yields were substantially greater than glyoxal yields. Acetaldehyde and methylglyoxal exhibited similar results; however, their yields were lower. Weinberg et al. (1993) surveyed 11 ozone plants and reported total aldehyde yields between 4.9 to 20  $\mu\text{g}$  per mg TOC and formaldehyde yields between 1.1 and 13  $\mu\text{g}$  per

mg TOC. Over the *CT* range used in the current study, total aldehyde yields ranged from 3.5 to 18  $\mu\text{g}$  per mg TOC, and formaldehyde yields ranged from 2 to 5.3  $\mu\text{g}$  per mg TOC.

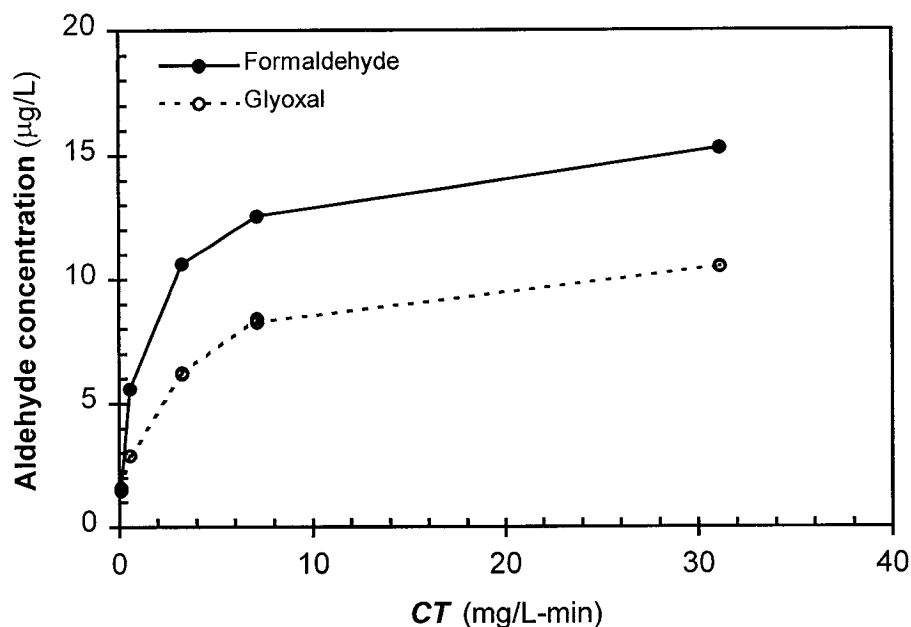


Figure 15. Aldehyde formation as a function of ozone exposure in a semi-batch reactor

Samples collected from semi-batch ozone studies were analyzed for THM formation potential using a 7-day chlorine exposure (Figure 16), which is considered an estimate of the maximum THM yield. Measured THM constituents included chloroform, bromoform, bromodichloromethane and dibromochloromethane. Of these, chloroform was produced in the greatest yields, and bromoform in the lowest. These results suggest that ozone exposure at *CT* values greater than 1  $\text{mg/L-min}$  will reduce chloroform in post-chlorinated water by approximately 20 percent, while other THM

constituents showed smaller changes. Reduction in chloroform with increasing ozone dose was also observed by Coleman et al. (1992) who reported that a 3:1 ozone-to-DOC ratio reduced chloroform by 59 percent in ozonated, and post-chlorinated humic acid solutions. Others have reported similar results for chloroform formation in ozonated NOM solutions (Kusakabe et al., 1990), and for total THMFP reduction in natural waters (Speitel et al., 1993).

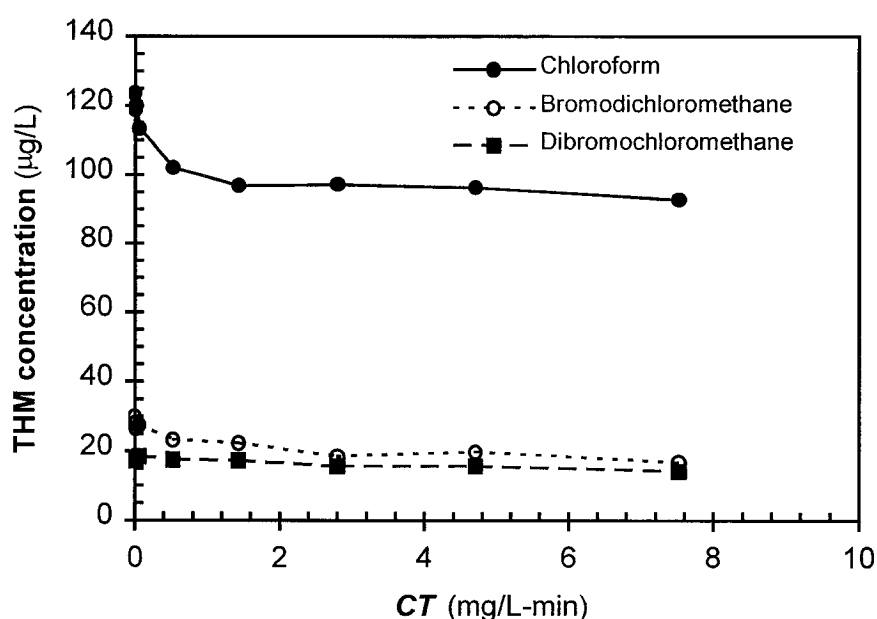


Figure 16. Disinfection by-product formation potential as a function of ozone exposure in a semi-batch reactor

AOC production was measured over a range of *CT* values (Figure 17). Sample replicates are shown in Figure 17 to illustrate the method precision. Each point represents the average of nine separate platings (triplicate platings of triplicate samples). Due to inherently low precision of biological assays, a large number of

sample replicates was needed. Substantial data scattering is apparent and there is not a well-defined trend between AOC formation and ozone dose.

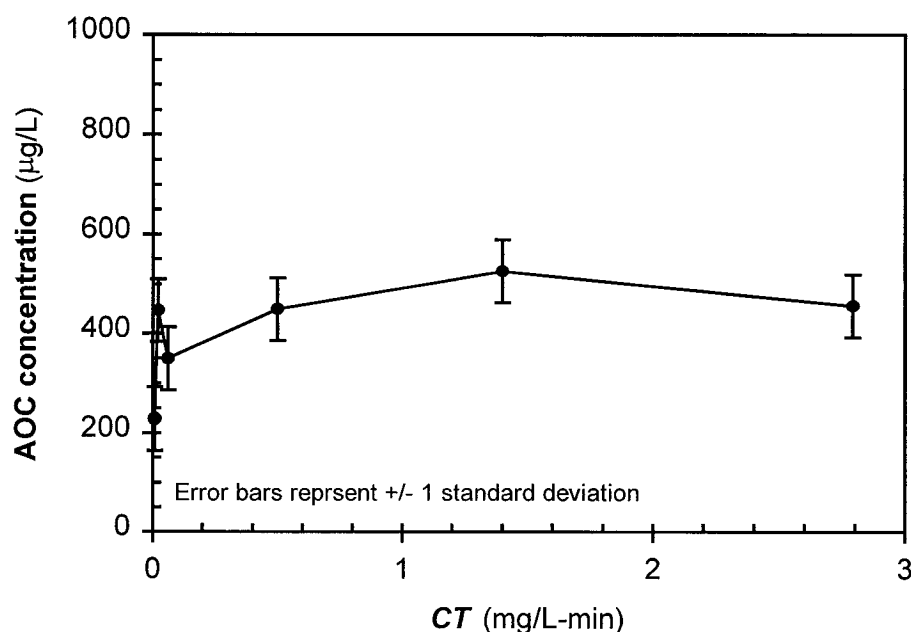


Figure 17. Changes in AOC as a function of ozone exposure in a semi-batch reactor

Hacker et al. (1994) studied AOC formation as a function of ozone dose in SPW and did not find a consistent dose-dependent relationship between ozone and AOC production. These investigators concluded that AOC production was usually maximized at ozone doses below 4 mg/L and higher ozone doses began to mineralize the TOC, consequently, lowering AOC in some cases. Observations from the relatively limited data in this work are consistent with the findings by Hacker et al. (1994). Although AOC may be a widely used surrogate for quantifying biological stability of



drinking water, the method precision, its analytical complexity, and subjectiveness of the AOC method make it a less desirable choice for modeling BOM removal.

## **MBR Studies**

### *Laboratory-Scale MBR Studies*

Prior to the present study, MBRs had not been applied for removing BOM from water; consequently, criteria needed for process design were not available. Thus, studies were required to determine initial estimates of pertinent process design parameters, which would subsequently be used as a baseline for mini-pilot-scale studies. To achieve this objective, a bench-scale MBR apparatus was constructed that provided the flexibility to evaluate process operating variables over a wide range. The bench-scale MBR apparatus provided a high-level of experimental control because feed flow rates were relatively low (less than 50 mL/min on average) and a single, homogenous, source water batch could be used for the experiments, which minimized variation in source water BOM levels. Moreover, the apparatus was constructed so it could be easily setup in a 20°C cold room and autoclave sterilized between tests, providing additional experimental control.

Temperature and raw-water BOM levels were maintained at consistent levels during testing. The independent variables assessed were hydraulic residence time and initial biomass concentration. Organic carbon removal and membrane flux were then

measured as dependant variables. Table 4 lists the values (or range of values) used during bench-scale MBR tests.

Table 4. MBR process variables and operating conditions

Parameter	Units	Value	
		Bench scale	Mini pilot scale
Reactor type		completely mixed	completely mixed
Reactor volume	L	0.5 – 3.5	5 - 20
Membrane type		0.2 $\mu$ m tubular ceramic, 1 cm o.d.	0.2 $\mu$ m tubular ceramic, 1 cm o.d.
Membrane area	m <sup>2</sup> (ft <sup>2</sup> )	0.006 (0.06)	0.04 (0.4)
Trans-membrane pressure	kPa (psi)	55-138 (8-20)	138 (20)
Cross-flow velocity	m/sec (ft/sec)	1.3 (4.1)	1.3 (4.1)
Recirculation rate	L/min (gal/min)	3 (0.8)	20 (5.3)

### *Control Studies*

Dissolved organic removal in an MBR may occur by (1) physical removal by the MF membrane, (2) adsorptive removal from PAC added to the process, and (3) biodegradation by the active biomass within the reactor. A control study was run to establish MF membrane rejection of DOC, THM precursors, and aldehydes in ozonated water where PAC and biomass were not added. An experimental challenge was to suppress biodegradation that would naturally occur in the feed tank and within the MBR reactor. Biological inhibitors were not added because organic inhibitors (e.g.,

benzalkonium chloride) would interfere with DOC analysis and inorganic inhibitors (e.g., mercuric chloride) would be too toxic for sanitary sewer disposal.

To minimize biodegradation, the bench-scale MBR reactor and appurtenant plumbing were initially sterilized by autoclaving (15 min at 121°C). Furthermore, the experimental run was relatively short (24 hours) as biodegradation would have occurred over extended testing.

Figure 18 shows changes in DOC, THMFP, and AOC measured in a system where neither biomass nor PAC was added. Rejection of all constituents measured was less than 10 percent over the first 23 hours. DOC rejection was highest at startup (approximately 20 percent); however, removal declined 2 hours after startup to levels below 10 percent. MF membrane fouling from DOC has been shown to occur through either adsorption or through gel layer formation on the membrane surface (Carroll et al., 2000; Schafer et al., 2000). DOC rejection is dependent on a variety of variables including pH, membrane chemistry, and NOM charge and size. Carroll (2000) reported no difference in MF fouling rates from hydrophobic and charged hydrophilic DOC fractions isolated from natural waters, but observed higher fouling rates when neutral DOC fractions were used. In the present study, the ozonated DOC consisted of lower molecular weight hydrophilic fractions (Amy et al., 1991), thus, DOC rejection, through either adsorption or gel layer formation, was negligible as evidenced by the lack of consistent rejection.

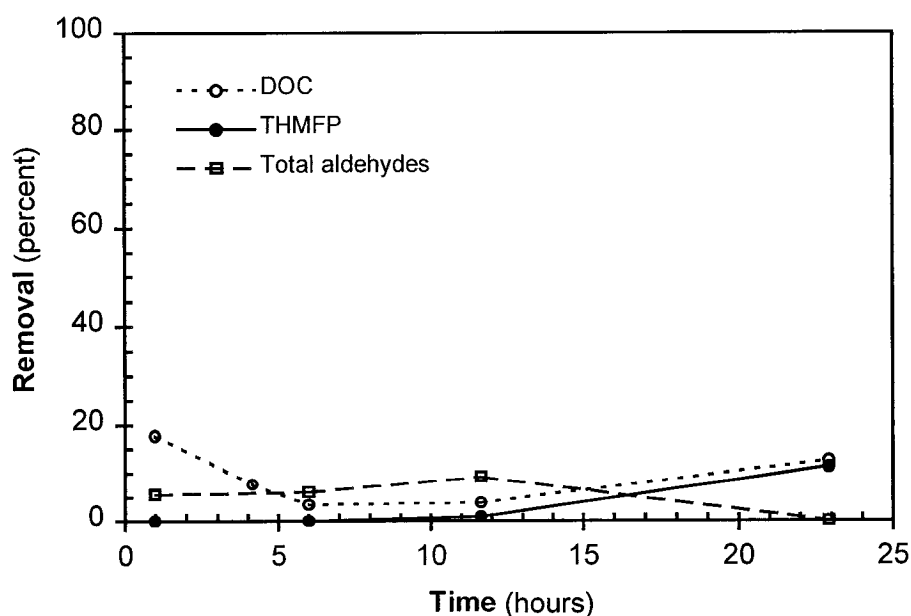
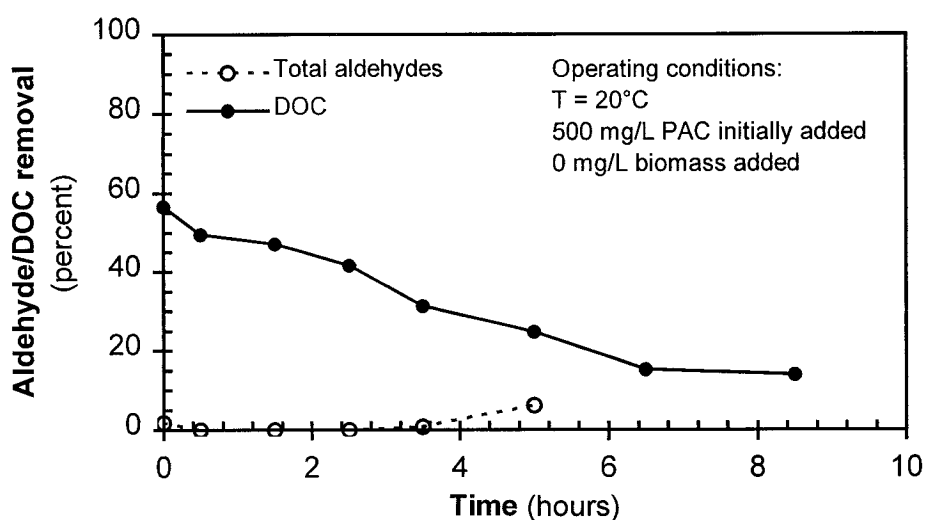


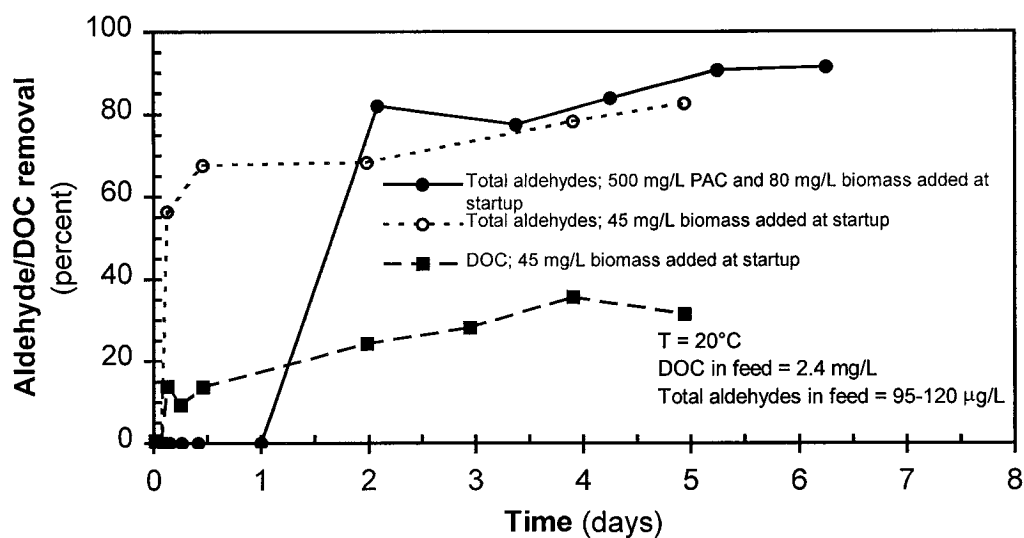
Figure 18. Total aldehyde, DOC, and THM precursor removal in the laboratory-scale MBR where biomass and PAC were not added

#### *Aldehyde and DOC removal studies*

Dissolved organic carbon and total aldehyde removal was measured in a series of tests designed to evaluate effects of the initial biomass and PAC concentrations on transient and steady-state organic carbon removal, as well as on membrane flux. Figure 19 (a) shows the transient DOC and total aldehyde removal in an adsorbing, non-biologically-active MBR where 500 mg/L PAC was added at startup. Figure 19 (a) shows that DOC was weakly adsorbed while total aldehydes were not adsorbed at all. After operating for 8 hours (mean HRT = 70 min), DOC removal decreased from 57 percent to 14 percent.



(a)



(b)

Figure 19. DOC and total aldehyde removal in the laboratory-scale MBR when (a) 500 mg/L PAC (and no biomass) was added and (b) when biomass was added at startup

Figure 19 (b) shows total aldehyde and DOC removal profiles for a biologically active MBR where PAC was not added. Additionally, this figure shows the total aldehyde removal profile for a biologically active process where 500 mg/L PAC was added at startup. Once acclimated, biological metabolism of total aldehydes was rapid. Acclimation times for aldehyde removal ranged from several hours to a day and steady-state total aldehyde removal varied from approximately 80 to 90 percent. DOC removal in a biologically active process, when PAC was not added, followed a similar trend to total aldehyde removal where nearly 50 percent of the steady-state DOC removal was achieved within 2 hours after startup.

Because a constant TMP was used during testing, HRTs inadvertently varied as a function of time due to flux loss from membrane fouling. Note that HRT varied from 40 min to 600 min during tests where only biomass was added, and from 50 min to 190 min during tests where PAC and biomass were added. Because membranes were cleaned before each test but not during testing, HRTs were low during the initial phase of testing and as testing progressed, there was a concomitant increase in HRT due to membrane fouling. Although HRTs were not intentionally varied, steady state removal profiles shown in Figure 19 (b) show that total aldehydes, and most of the biodegradable DOC, may be removed at HRTs on the order of 1 hour. Moreover, higher HRTs provided little benefit in terms of higher BOM removal. Testing lower HRTs was not practical under the laboratory-scale conditions used because of the large volumes of ozonated water that would have been needed.

### *Membrane Fouling*

The effect of pre-ozonating water on membrane flux loss is shown in Figure 20. The flux profiles shown in Figure 20 were measured in a control study where neither biomass nor PAC was added to the reactor. Although the steady-state flux of both waters approached a similar level, pre-ozonation substantially lowered the initial flux decline and increased cleaning intervals. It appears that ozone pre-oxidation increased membrane flux by oxidizing NOM fractions which may otherwise foul the MF membrane through adsorption or gel layer formation. Ozonated water also likely promoted colloid microflocculation, which enhanced colloid destabilization and settling within the ozonated water feed reservoir, a phenomena previously described by Grasso and Weber (1998) and Hashino et al. (2000).

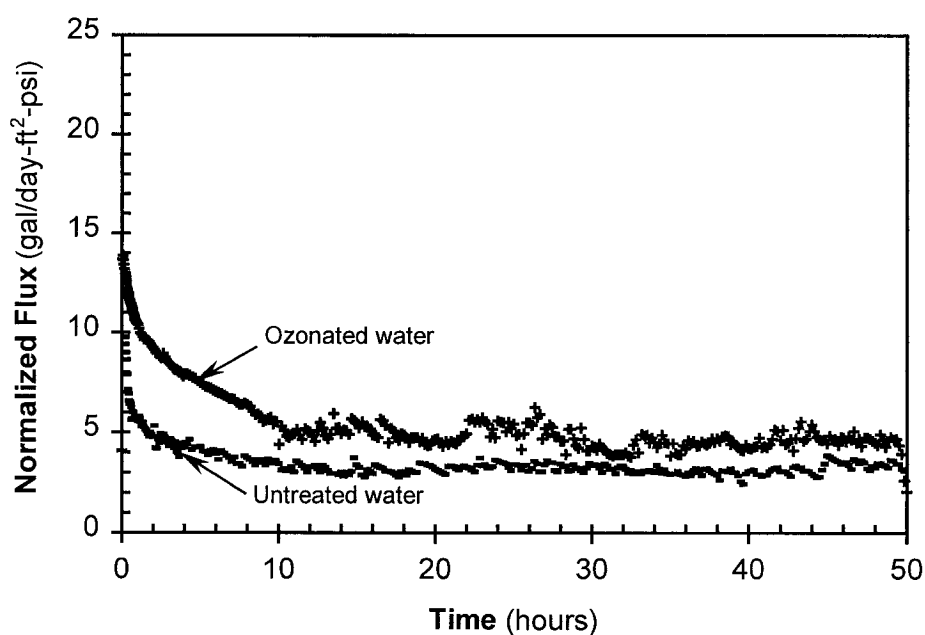


Figure 20. Effect of pre-ozonation on MF flux in a bench-scale MBR process

Membrane flux was measured for the three different bench-scale operating conditions: (1) a control where only pre-ozonated water was used, (2) when biomass (45 mg/L) was initially added to the reactor, and (3) when biomass (80 mg/L) and PAC were initially added to the reactor. Figure 21 shows specific flux profiles (normalized as a function of membrane area and TMP) for the three conditions tested. Note that membranes were not cleaned during each test, however, they were cleaned between tests using the procedures described in Chapter 3 (Membranes).

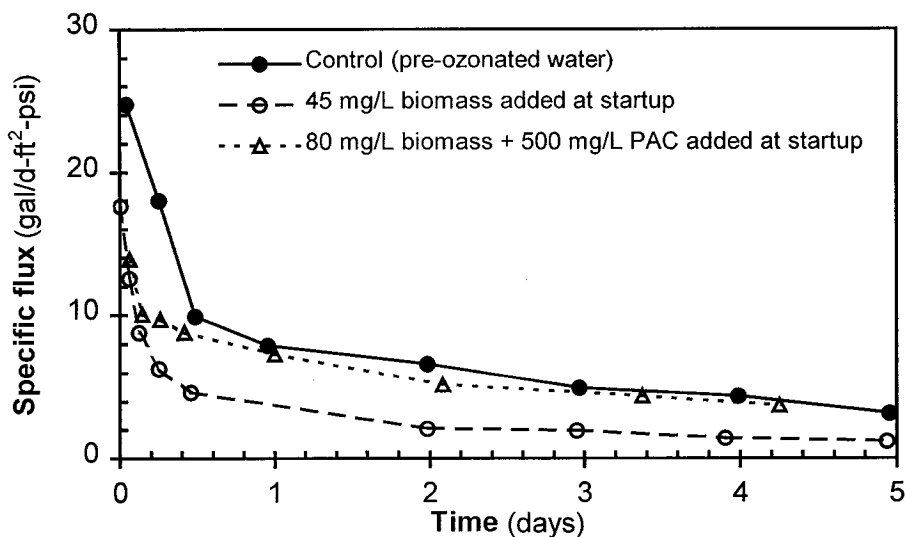


Figure 21. Specific membrane flux measured for different operating conditions in the laboratory-scale MBR; all tests were conducted at 20°C

Pre-ozonated water without biomass or PAC showed the highest initial flux (25 gal/d-ft²-psi), however, flux rates rapidly declined to values similar to test 3 (biomass and PAC added). When only biomass was added, flux rates were substantially lower (approximately 70 percent after 4 days). Thus, adding biomass without PAC resulted



in an increased flux loss rate and a lower steady state flux. When PAC and biomass were added flux was comparable to the control (ozonated water only) demonstrating that adding PAC to a biologically active system reduces membrane fouling.

Figure 22 shows an SEM micrograph of biologically active PAC particles collected from the MBR. Figure 22 shows patchy biomass growth on the PAC particles. This figure illustrates the benefits of adding PAC to the MBR process: (1) PAC serves a high surface area support for biomass attachment and (2) biologically-active PAC forms a relatively permeable and incompressible layer when deposited on the membrane surface. Without PAC addition, biomass would deposit directly on the membrane surface, substantially reducing membrane flux.

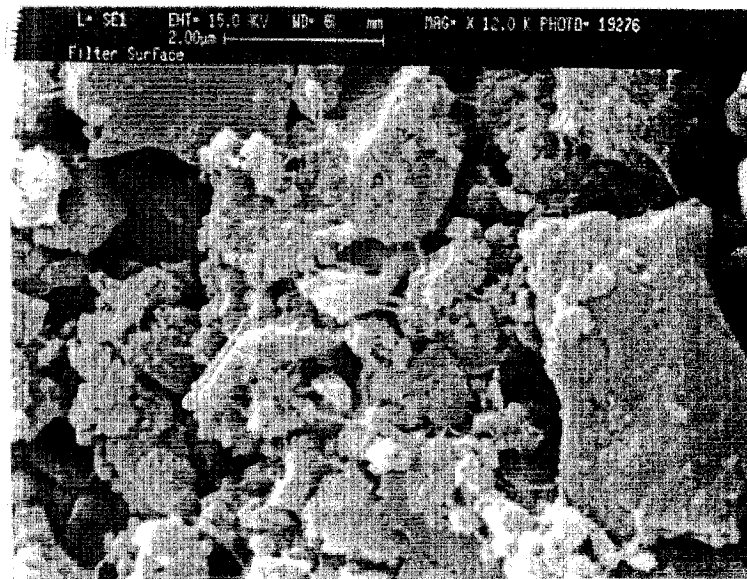


Figure 22. SEM micrograph showing biologically-active PAC particles collected from the MBR.

### *Mini-pilot-scale MBR Studies*

Extensive mini-pilot-scale testing was conducted to evaluate effects of pertinent MBR operating variables including: the effect of PAC on substrate removal and membrane flux, effects of HRT, process sensitivity to influent substrate concentration, and effects of reactor wasting and solids retention time (SRT). The mini-pilot-scale MBR was designed and constructed based on the preliminary results from laboratory-scale MBR studies. Laboratory-scale studies bracketed an upper bound for an appropriate HRT; however, experimental constraints did not permit determination of HRTs below 50 min. Consequently, the mini-pilot-scale MBR was designed to operate at a minimum 20-min HRT to evaluate process performance at lower HRTs. Table 4 (page 78) lists the range of process design values used.

Tests were conducted over an 8-month period using the Metropolitan Water District of Southern California's pilot plant in LaVerne, CA. The pilot plant had an uninterrupted source water supply which was first pre-ozonated using a pilot-scale ozone contactor. A single source water and applied ozone dose were used throughout testing. Although mini-pilot-scale tests evaluated a wider range of variables over longer periods, temporal variations in source water quality and applied ozone doses did introduce an added degree of experimental variation not present in bench-scale tests.

### *DOC and THM precursor removal*

The effects of reactor wasting and different PAC addition strategies on DOC and THM precursor removal are shown in Figure 23. In region A (Figure 23), 3000 mg/L PAC

and biological inocula were added at startup; the system was subsequently operated without wasting or subsequent PAC addition for approximately 10 days. The process was then operated (region B) with a 7-percent (of the feed flow rate) wasting stream (mean SRT = 1-4 days) from the reactor without adding PAC. In region C, PAC (5 mg/L) was continuously added and the process was operated without solids wasting; in region D, the 5-mg/L PAC dose was maintained and the process was operated with a 7-percent reactor wasting stream.

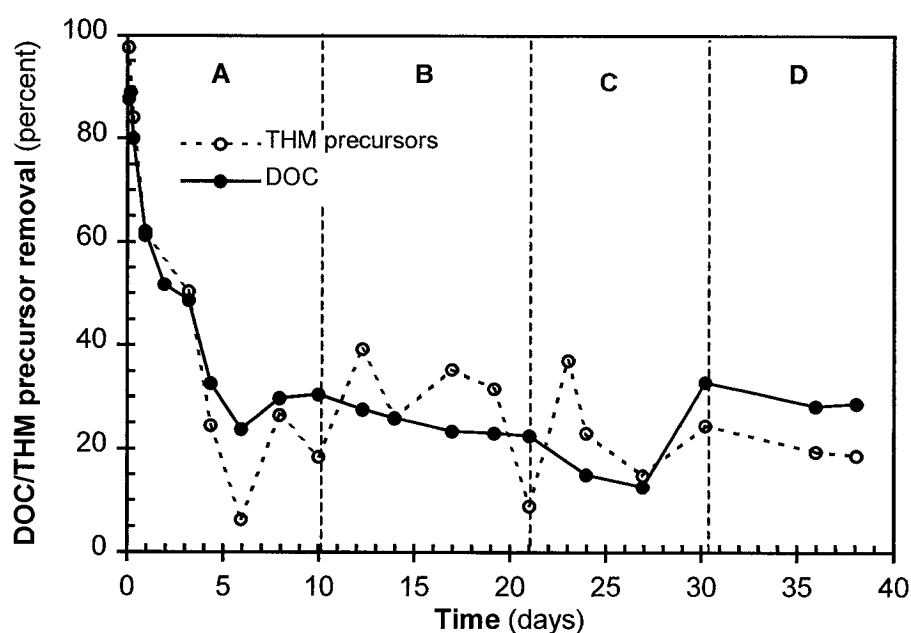


Figure 23. Effects of various operating strategies on DOC and THM precursor removal: region A, 0.3 percent PAC, acclimated biomass, and no reactor wasting; region B, continually wasting 7 percent (of the feed flow rate) of the reactor contents; region C, 5 mg/L PAC added and no reactor wasting; and region D, 5 mg/L PAC and 7 percent of the reactor contents were continually wasted

Generally, DOC and THMFP removal exhibited similar trends although THMFP removal fluctuated to a greater extent than DOC. This concomitant increase in THM

precursor removal with DOC has also been reported by others (Speitel et al., 1993). Initially, due to the high PAC dose (region A), DOC and THM precursor removal was high, however, due to the relatively low carbon adsorption capacity for both DOC and THM, removal substantially declined since carbon was not continually added. In region B, DOC removal marginally decreased as biomass and carbon were wasted from the system. When 5-mg/L PAC was continually added (region C) removal trends varied, however, after operating for 10 days under these conditions, DOC and THMFP removal had marginally increased. In region D (7 percent reactor solids wasting and continuous PAC addition) provided the best optimization for lowering DOC and THMFP while maximizing membrane flux.

Fluctuation in THMFP removal (relative to DOC removal) likely occurred from experimental variation including temporal changes in the effective ozone dose (i.e. ozone:DOC ratio) and source water DOC fluctuations. Moreover, THMFP precursors were measured using a constant chlorine dose (chlorine:DOC = 3:1 based on raw water DOC) throughout testing and as THM precursor levels were reduced, through either adsorption or biodegradation, the THM yield may have been higher due to the increased chlorine:THM precursor ratio.

### *Aldehyde Removal*

Figure 24 shows a comparison of total aldehyde removal in a biologically active process when 0.75 percent PAC was initially added and when carbon was not added. PAC was not wasted or added after startup. The data in Figure 24 illustrate two key points: (1) aldehydes were metabolized nearly completely within a relatively short acclimation period (several days) and (2) aldehydes were not adsorbed as evidenced by their low removal at startup (when a high PAC dose was initially added). When carbon was not added, acclimation was rapid and within a day, total aldehydes were nearly completely removed. In both cases, within 30 hours of startup, aldehyde removal increased to greater than 98 percent (within detection limits). Once steady state was reached, lowering HRT from 240 minutes to 100-minutes (average HRT) did not substantially reduce aldehyde removal.

### *MBR process efficiency at high substrate loading and at low pH*

BOM concentration in ozonated water usually depends on both DOC character and concentration, and ozone dose. Thus, waters with high BOM formation potential may experience a wide variation in BOM levels if ozone dose is changes. Furthermore, some full-scale ozone processes must operate at lower pH to control bromate formation. Operating at pH 6-7 has been shown to suppress bromate formation when ozonating waters containing bromide (Krasner et al., 1993a).

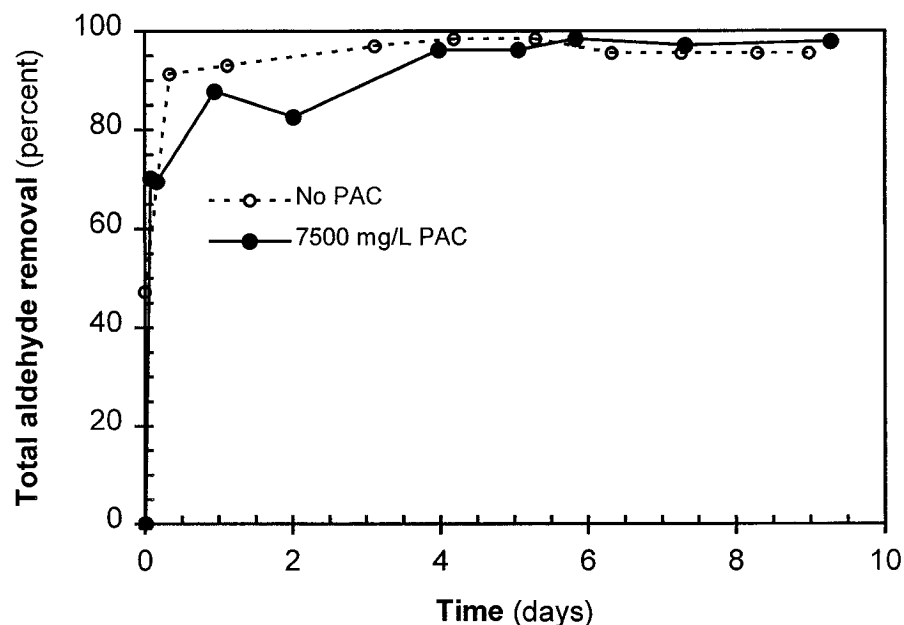


Figure 24. Effect of carbon addition on removal of total aldehydes in the mini-pilot-scale MBR process

Tests were conducted to evaluate MBR performance at elevated BOM levels and at lower pH. The tests evaluated process robustness by first introducing a high-BOM spike and measuring process response. Once the process had reached steady state, pH was then lowered to determine process sensitivity to pH change. Figure 25 shows a comparison of total aldehyde and DOC removal at high BOM loading and under varying pH conditions. High BOM loading conditions were simulated by adding formaldehyde, acetaldehyde, and methyl glyoxal into the ozonated water feed to raise total aldehydes from ambient levels (50  $\mu\text{g/L}$  average) to approximately 400  $\mu\text{g/L}$  (Figure 25); pH was lowered by adding HCl. Note that PAC (3000 mg/L) was added to

the MBR at startup, however the process had been operating for 40 days prior to testing. Thus, tests began from steady-state conditions. Over the course of tests shown in Figure 25, PAC was not continually added and the MBR was operated without solids wasting.

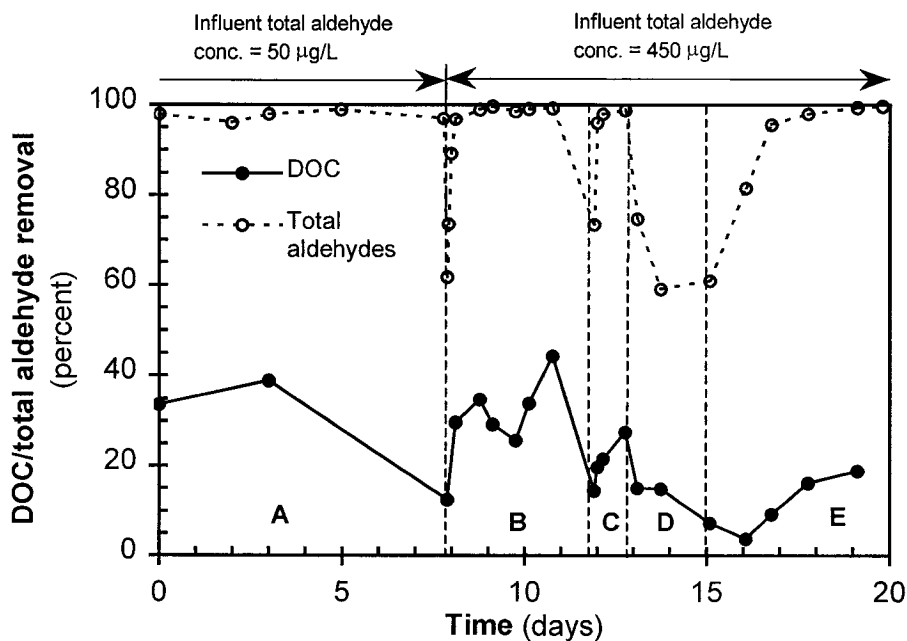


Figure 25. Effects of nutrient addition, influent total aldehyde concentration, and pH on removal of DOC and total aldehydes: region A, mineral nutrients added to reactor feed; region B,  $\sim 400 \mu\text{g/L}$  total aldehydes added to the ozonated water feed ( $\text{pH} \sim 8.0$ ); region C, influent was pH lowered from  $\sim 8.0$  to 6.4; region D, influent pH lowered from 6.4 to 4.2; and region E, influent pH raised to 6.0. (Note that nutrients were continuously added throughout the tests, and aldehydes were added from condition B onward; PAC was not continually added and reactor solids were not wasted).

In region A (Figure 25), total aldehyde concentration in the MBR influent was at the ambient level (approximately  $50 \mu\text{g/L}$ ), however, mineral nutrients were added to observe the effects of nutrient addition on DOC removal and to establish a baseline

condition. To ensure that organic carbon was limiting, mineral nutrients including nitrogen and phosphorous were supplemented in the MBR feed (Table 3, page 39). Increased aldehyde loading (region B; Figure 25) initially lowered total aldehyde removal to approximately 60 percent, and within 24 hours removal increased to greater than 95 percent. Lowering pH to 6.4 (region C; Figure 25) did not effect removal although at pH 4.2 (region D; Figure 25) both aldehyde and DOC removal substantially decreased. When pH was again raised to 6.0 (region E; Figure 25), removal increased. This result verifies that organic carbon removal (under the conditions used) is from biodegradation. When pH was lowered to 4.2, the enzymatic pathways used for carbon metabolism were effectively blocked and degradation ceased (Atlas and Bartha, 1993).

Figure 26 compares DOC and THM precursor removal when operating the MBR at lower pH. In region C, pH was lowered from 8.0 to 6.4; pH was lowered to 4.2 in region D and then raised back to 6.0 in region E. Note that the operating conditions shown in Figure 26 (specifically, regions C, D, and E) correspond with those shown in Figure 25 (i.e. aldehydes were also spiked and mineral nutrients were added). DOC and THM precursor removal did not substantially change when pH was lowered from 8.0 to 6.4. THM precursor removal was completely suppressed by lowering pH to 4.2 and subsequently resumed after raising pH to 6.0. The lack of THM precursor removal at pH 4.2 shows that THM precursor removal occurs through biodegradation, however, the exact pathway (e.g., metabolic or catabolic) is unclear.



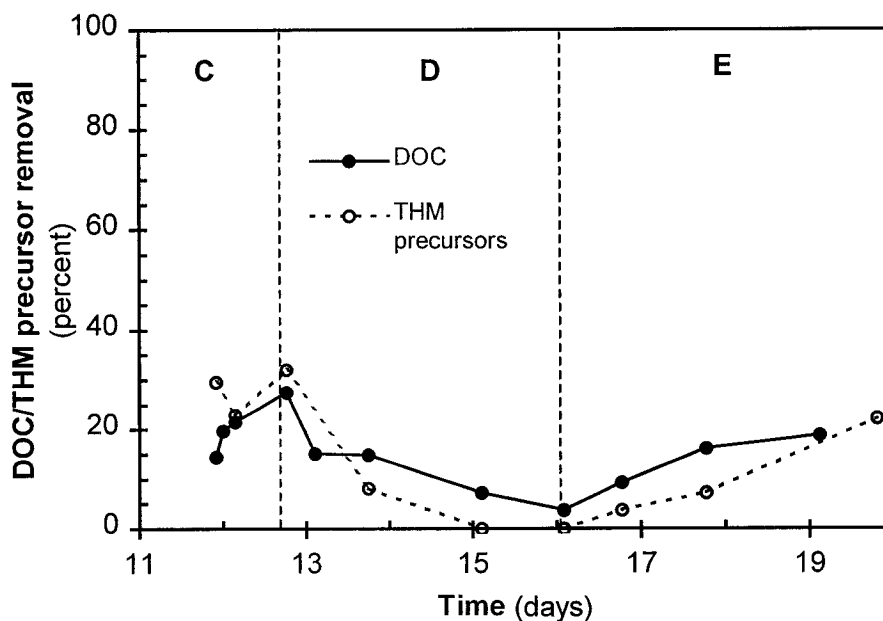


Figure 26. Comparison of the effect of pH variation on removal of DOC and THM precursors: region C, influent pH lowered from ambient ( $\sim 8.0$ ) to 6.4; region D, influent pH lowered to 4.2; and region E, influent pH raised to 6.0. The MBR was operated without continuous carbon addition or reactor wasting. (Note that nutrients and aldehydes ( $\sim 400 \mu\text{g/L}$ ) were continuously added throughout testing; PAC was not continually added and reactor solids were not wasted).

### *AOC removal*

The effects of reactor wasting and different PAC addition strategies on AOC removal are shown in Figure 27. In region A, 3000 mg/L PAC and biological inocula were added at startup; the process was then operated (region B) with a 7-percent (of the feed flow rate) wasting stream (mean SRT = 1-4 days) from the reactor without adding PAC; in region C, PAC (5 mg/L) was continuously added and the process was operated

without solids wasting; in region D, the 5-mg/L PAC dose was maintained and the process was operated with a 7-percent reactor wasting stream.

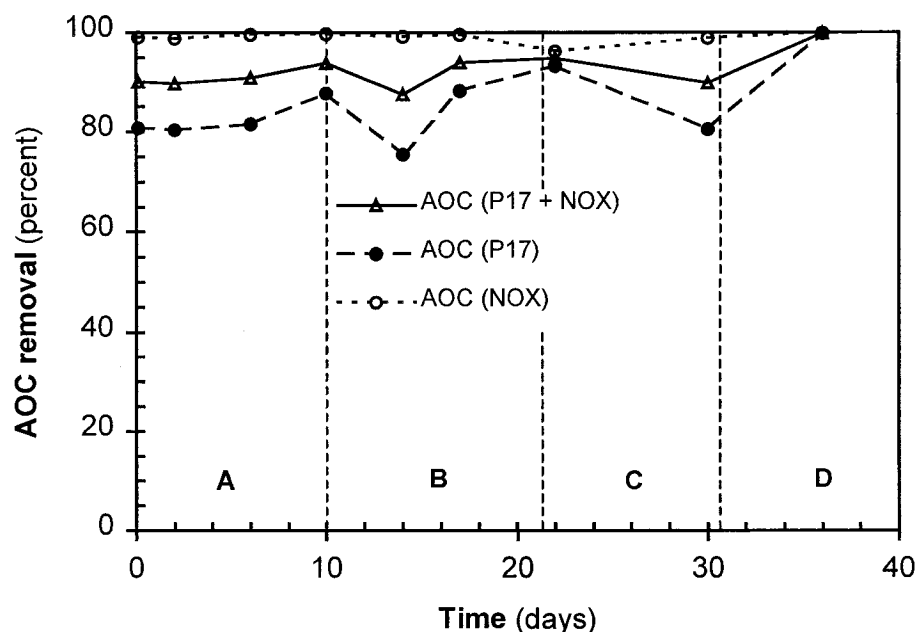


Figure 27. Effect of various operating strategies on AOC removal: region A, 0.3 percent PAC, acclimated biomass, and no reactor wasting; region B, operating at a 7-percent reactor wasting rate; region C, 5 mg/L PAC added and operated without reactor wasting; and region D, 5 mg/L PAC and operated at a 7-percent reactor wasting rate.

At the relatively high ozone dose used (5 mg/L), AOC concentrations increased to approximately 600  $\mu\text{g C/L}$  in the ozonated feed water. The MBR was operated at a constant TMP and, consequently, hydraulic residence times varied as a function of permeate flow rates. Average detention times ranged from 30 to 60 minutes after membrane cleaning, to a maximum of 4 hours at the end of a cleaning cycle. There was consistently high AOC removal over the entire 35-day testing period. Within

several hours of startup (region A; Figure 27), removal efficiencies for total AOC, AOC<sub>NOX</sub>, and AOC<sub>P-17</sub> were 90, 98, and 80 percent, respectively. When operating at a 7-percent reactor wasting rate and without adding carbon (region B; Figure 27), AOC<sub>P-17</sub> removal decreased slightly (approximately 10 percent). A 5-mg/L continuous PAC dose, in conjunction with a 7-percent reactor-wasting rate, resulted in the highest AOC removal (region D; Figure 27).

Higher AOC<sub>NOX</sub> removal in pre-ozonated, biologically filtered water was also reported by van der Kooij (1989). According to van der Kooij et al. (1989), lower AOC removal is due to the inability of *Pseudomonas fluorescens* strain P-17 to utilize the major ozone by-products: formic acid, glyoxylic acid, and oxalic acid; while *Aquaspirillum* strain NOX has the metabolic capabilities to use these compounds.

#### *Effect of solids wasting and PAC addition strategy on membrane flux*

Studies were conducted to determine the effects of continuous PAC addition and solids wasting on membrane flux rates. Tests were conducted by first changing the MBR operating condition, allowing the process to reach steady state (with respect to both substrate removal and membrane flux), and then measuring flux profiles immediately after membrane cleaning. Figure 28 compares normalized permeate flux measured under three different operating conditions: (1) 0.3 percent PAC and biomass (~50 mg/L) added at startup, (2) 7 percent continuous solids wasting, and (3) 7 percent

continuous solids wasting and 5 mg/L continuous PAC addition. It is important to note that tests were run sequentially without discharging reactor contents from the previous condition. Each condition was run for approximately 10 days and the MF membrane was cleaned when flux dropped below 1 gpd/ft<sup>2</sup>.

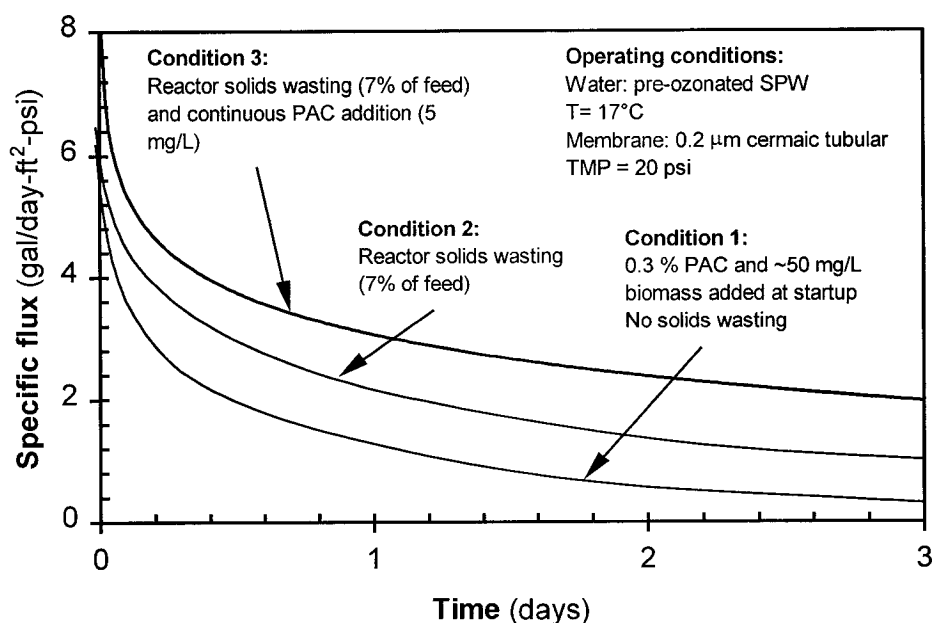


Figure 28. Comparison of mini-pilot scale MBR permeate flux measured under various operating conditions; condition 1: 3000 mg/L PAC and ~50 mg/L biomass initially added at startup, no reactor solids wasting; condition 2: 7 percent wasting; condition 3: 7 percent wasting and 5 mg/L PAC continuously added

Adding 0.3 percent PAC and acclimated biomass at startup, and operating without wasting solids (Figure 28; condition 1) resulted in a relatively high flux loss rate decreasing from 6 gpd/ft<sup>2</sup>-psi to less than 1 gpd/ft<sup>2</sup> in 18 hours. Flux loss rates (measured immediately after membrane cleaning) increased over time as reactor solids

were not wasted. Consequently, long-term MBR operation without wasting reactor solids is not a viable operating strategy. Although a high SRT may minimize active biomass levels, solids continually accumulate in the MBR from colloidal material in the feed (average feed suspended solids = 1 mg/L, high = 15 mg/L, and low = 0.1 mg/L) which is rejected by the MF membrane and retained within the reactor.

When operating at a 7-percent wasting rate (Figure 28; condition 2), mean SRTs ranged between 1 to 4 days, depending on flux rate. When operating with a 7-percent wasting rate, membrane-fouling rates were reduced and the time between cleaning cycles increased from less than 2 days to 3-10 days. When operating at a 7-percent wasting rate and continually adding 5 mg/L PAC (Figure 28; condition 3), a decrease in the flux decline rate and increase in the steady-state flux was observed. Continually adding PAC when operating with reactor wasting is essential for optimizing both membrane and substrate removal flux as it maintains carbon within the system, functioning as a support for microorganisms as well as a high-permeability filter aid. Continuously adding PAC (in low doses) may also facilitate sequestration of other low-permeability suspended solids, including biomass, and subsequently reduce flux loss rate—a phenomenon also observed by Heesu et al. (1999).

### *Reactor PAC Concentration*

Maintaining PAC within the reactor while wasting solids is crucial for efficient MBR operation. Figure 29 shows the theoretical reactor PAC concentration under the various operating strategies tested. If PAC is added to the MBR only at startup (initial concentration = 1000 mg/L), and the MBR is then operated at a 7-percent (of the feed flow rate) reactor-wasting rate, then PAC would be completely flushed from the reactor within 65 detention times. Adding a continuous PAC dose (5 mg/L) while operating at a 7-percent wasting rate will result in a 100-mg/L steady-state concentration (in the MBR reactor) after 60 detention times. Similarly, adding 50 mg/L PAC continuously will result in a 750-mg/L steady-state concentration after 20 detention times.

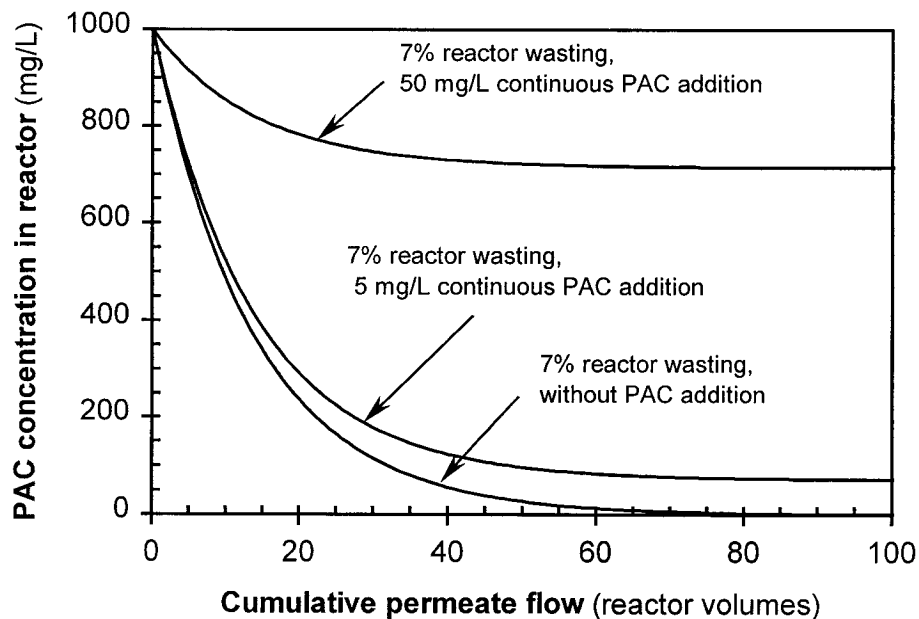


Figure 29. Theoretical PAC concentration in the reactor as a function of various operating strategies

This research has shown that to optimize both organic carbon removal and membrane flux, PAC must be added when the process is operated with reactor wasting. Carbon functions in several capacities in the MBR, one of which is providing a high-surface-area support for biomass, and wasting all reactor carbon would be detrimental to both organic carbon removal and membrane flux. Thus, PAC must be maintained within the MBR to achieve a sustained membrane flux and removal of biodegradable substrates.

## **SUMMARY AND CONCLUSIONS**

The principal findings of this Chapter are:

1. Organic carbon is removed through biodegradation and adsorption in the MBR process. Because hydraulic detention time, PAC concentration, and biomass residence times can be controlled within this process, a high DOC removal can be achieved using biologically active PAC. Although adsorption of some species occurred initially, the primary mode of removal was through biodegradation. DOC removal from adsorption was dependant on the PAC addition strategy; when a high PAC dose (e.g., 3000 mg/L) was added at startup, DOC removal was high (greater than 80 percent) for the first several hours of operating, however removal declined rapidly.
2. High removal of total aldehydes (>95 percent) was achieved within several hours of startup. Adding PAC did not measurably enhance total aldehyde removal.

Aldehyde removal was not sensitive to the reactor wasting rates and detention times used in this study, and was consistently high during all conditions tested.

3. AOC removal was consistently high over the range of operating conditions tested. AOC in this source water was weakly adsorbable and adding carbon did not have a measurable influence on AOC removal.
4. Reduction in THMFP occurred through both adsorption and biodegradation of THM precursors. At high initial carbon doses (0.3 percent by weight) THMFP was lowered by greater than 98 percent, however, without continuous addition, the carbon was rapidly exhausted and removal decreased. Biological degradation of THM precursors can result in as high as 65 percent removal, however, removal was variable and these high removal rates were not sustained.
5. When total aldehydes were increased from 50 mg/L to 400 mg/L, removal initially dropped, however, within 1 day removal had increased to greater than 95 percent. Lowering pH is essential for controlling bromate when ozonating waters containing bromide. Ozonating at pH 6-7 has been shown to suppress bromate formation in a wide range of waters. Lowering pH from 8.0 to 6.4 had little effect on organic carbon removal, although at lower pH (4.2) biodegradation effectively ceased; though rapidly recovered when pH was raised back to 6.0.
6. Pre-ozonation enhanced permeate flux through either NOM oxidation or enhancing micro-flocculation and settling.
7. Adding activated carbon serves as a high-surface area support for microorganisms and enhances membrane permeate flux under appropriate operating conditions.



When operated without intermittent or continuous PAC addition and reactor wasting, membrane flux rapidly declined. Continuous addition of PAC at low doses (5 mg/L) combined with a low (3-7 percent) reactor solids wasting rate resulted in the highest sustained flux.

## **Chapter 5 - MATHEMATICAL MODEL DEVELOPMENT**

### **OBJECTIVES**

One of the most cost-effective means to evaluate a new or unproven process, or to rapidly assess a wide range of operation conditions, is by mathematical simulation. Although modeling cannot be used as a substitute for pilot- or demonstration-scale studies, it provides a preliminary means to evaluate process performance, using a limited data set. Modeling dynamics in complex processes, such as adsorption or biological filtration, presents a number of challenges to the modeler due to the inherent heterogeneity of the system, and the difficulties that arise in simulating dynamics of complex mixtures which often have varying properties. While empirical models can be used to describe most phenomena, they do not offer a long-range, predictive capability. Predictive models build on a fundamental understanding of phenomena, and, ideally, provide a tool which can be calibrated using an independent data set, and then used to predict process performance under different operating conditions.

The general objective of this chapter is to develop a predictive mathematical model of the MBR process that will describe both biodegradation and adsorption phenomena.

The specific objectives of mathematical modeling in the current work are:

1. Evaluate existing biofilm, adsorption, and integrated biofilm-adsorption models and establish a conceptual paradigm for modeling combined adsorption-biodegradation phenomena in an MBR.
2. Select the fundamental dynamic and equilibrium models describing the various process phenomena including adsorption and biodegradation.
3. Determine the assumptions necessary for modeling the MBR processes, specifically: (1) the mode of biofilm growth and modeling assumptions for biomass attached to the carbon surface and sheared biomass in the bulk solution and (2) estimate the major mass-transfer resistance(s). Determine, based on similar data, which of these may potentially be rate limiting.
4. Once modeling assumptions have been made, develop mathematical expressions for biodegradation, adsorption, and other phenomena specific to the MBR process.
5. Develop a computer-based, numerical model of the MBR process by solving the family of equations describing process phenomena using finite-difference-modeling techniques. Verify that the model converges over a reasonable range of input parameters.

## MODEL CONCEPTUALIZATION AND DEVELOPMENT

### Review of Existing Models

A substantial amount of research on modeling biologically active adsorption can be found in the literature (Ying, 1978; Rittmann and McCarty, 1980b; Andrews and Tien, 1981; Chang and Rittmann, 1987a; Speitel et al., 1987b; Kim and Pirbazari, 1989). Ying (1978) modeled bioactive adsorption in fixed-bed (plug flow) reactors and completely-mixed reactors using a variety of biodegradable and adsorbable model parameters including glucose and sucrose. Model constants were established using bench-scale adsorption and biokinetic studies, and predictions generally compared well to measured data. Substrate concentrations were high (~100 mg/L as TOC) and, consequently, mass-transport limitations through the biofilm layer became an issue. Subsequent bio-adsorber models have addressed the mass-transfer resistance imparted by thick biofilms by incorporating a biofilm diffusion constant (Kim, 1987).

Several models have been developed for predicting BOM removal in ozonated water (Huck et al., 1994; Zhang and Huck, 1996; Hozalski, 1996), however these models have only considered biodegradation and not adsorption. Zhang and Huck (1996) developed a steady-state biofilm model to predict AOC removal in biological filters. The model was calibrated from pilot-scale data using a multi-parameter search routine, however the model was not verified against an independent data set. Drawbacks of this

approach were the relatively low precision of pilot-scale data used for parameter estimation and the multi-variant-curve-fitting method used to simultaneously determine multiple calibration constants. Consequently some of the reported biokinetic parameters were several orders of magnitude greater than would be expected.

Hozalski (1996) modeled TOC removal in ozonated water and the effects of filter backwashing on biofilm shearing. Model calibration used acetate biokinetic data from batch biokinetic studies as well as previously reported AOC values (Zhang and Huck, 1996). When bench-scale column results were verified against model predictions using the AOC calibration data, poor agreement between measured values and model-predicted values was seen, however, when the acetate calibration data were used, a much better qualitative approximation was reported.

Adsorption models have been developed for UF-PAC processes (Adham et al., 1993); however, none for ozone-byproduct or BOM removal. Adham and colleagues (1993) developed a steady-state model predicting TOC removal in a UF-PAC process where TOC was added. Adsorption was modeled using an analytical solution for steady state diffusion in a sphere, first developed by Crank (1956). Reactor hydraulics were modeled using a plug-flow model for the membrane recycle loop, and a completely-mixed model for the PAC feed tank. A constant residence time was also assumed. Independent isotherm tests were conducted to establish the adsorption equilibrium and

kinetic parameters needed, and pilot-scale verification data were used with generally good agreement between measured and model-predicted data.

Most biofilm models idealize the bio-active particles as a spherical support covered by a uniformly distributed biofilm. The support may either be inert (e.g., anthracite or silica), or an adsorbent to provide additional substrate removal (e.g., activated carbon).

Concentration gradients between the bulk solution and bioactive particles drive diffusion through the liquid boundary layer and into the biofilm, where biochemical reaction occurs. If there is sufficient chemical gradient at the base of the biofilm, diffusion continues into the activated carbon particle and a partition between solid and liquid then occurs (Ying and Weber, 1979; Chang and Rittmann, 1987a; Kim and Pirbazari, 1989).

Modeling biomass growth on activated carbon has been approached in several different ways. Peel and Benedek (1976) assumed a constant biofilm thickness in modeling bioactive adsorption for wastewater treatment. Peel concluded that although biofilm thickness was difficult to estimate, its influence on modeling results was relatively minor. Others (Ying, 1978; Kim, 1987; Chang and Rittmann, 1987a) have modeled biofilm by first establishing biomass concentration and then by relating biomass to volume, thereby establishing a biofilm thickness. Consequently, biofilm thickness increases as biomass concentration changes. The model is then solved as a moving-

boundary system where the biomass is continually re-discretized as the biofilm/liquid boundary changes over time.

Biofilm loss from shearing or sloughing is an important consideration when modeling biofilm processes, and especially at low-substrate concentrations as biochemical oxidation depends on biomass concentration (Rittmann, 1982). Mechanisms for biofilm loss include erosion, sloughing, abrasion, and predation from other microorganisms (Rittmann, 1989). Some researchers have modeled biofilm loss from shearing and sloughing by incorporating an additional decay term that effectively models the different biofilm loss mechanisms using a single apparent rate constant (Rittmann, 1982; Speitel and DiGiano, 1987a). Others have developed more complex shearing models. Hozalski (1996) developed a biomass detachment model for biologically active dual-media filters taking into account biomass detachment during filter backwash, where bed fluidization and air scouring can substantially increase biomass shearing (Hozalski, 1996).

In conventional dual-media biological filters, biomass sheared from the particle surface detaches into the bulk solution and is then transported out of the bioreactor along with other suspended and dissolved constituents (Rittmann, 1989). While the sheared biofilm is a component of active biomass, its contribution for substrate removal is relatively negligible due to comparatively low shear rates (when compared to biofilm

growth rates), and the short HRTs (2-10 min) typically used in biological water treatment processes (Rittmann, 1982). Hozalski (1996) estimated only 4.6 percent of the total acetate degraded in a biological filter resulted from the sheared, suspended growth.

However, these assumptions are not valid in an MBR process because sheared biomass (suspended in the bulk fluid) is retained within the system, and HRTs are longer than used in conventional biofiltration (Urbain et al., 1996). Moreover, higher shearing would be expected in an MBR due the pressure-driven nature of the process, where, depending on the membrane configuration, a pump would be required to establish TMP. Alternately, vacuum-driven membranes could be used that would provide less shearing as water is not pressurized using a pump. In any case, the sheared biomass component cannot be neglected when modeling an MBR.

The rate of biomass shearing corresponds with the rate of biomass growth and hydrodynamic conditions (Speitel and DiGiano, 1987a). Models of biomass shearing in fixed-bed bioadsorbers have indicated the shear loss rate is roughly equal to 0.3 to 0.65 x biomass growth rate (Speitel and DiGiano, 1987a; Hozalski, 1996). The biomass shear rate was reported to be roughly proportional to the square root of the superficial fluid velocity. Consequently, increasing velocity will increase shearing. Generally, velocities within an MBR are substantially greater than those in a fixed-bed



reactor<sup>4</sup>. The higher likely rate of biomass shearing in the MBR, coupled with the high surface area available for microbial colonization and growth (when PAC is added to the process) suggests that biofilm on the carbon surface will generally be low due to both the high surface areas available for growth and the high-shear environment.

Table 5 compares previously published biodegradation and adsorption models along with their key assumptions.

### **MBR Model Conceptualization and Assumptions**

The proposed MBR model builds on previous biofilm/adsorption models, incorporating unique aspects of the MBR process. Figure 30 shows a conceptual illustration of the model, with a schematic of the MBR process, key modeling components, and key assumptions. The model considers both adsorption, from PAC added to the system, and biodegradation. The MF membrane rejects suspended solids while passing dissolved constituents. Consequently, suspended solids, including PAC and biomass, are conserved in the reactor and can only be discharged by wasting the reactor contents.

---

4. Tangential fluid velocity in the membrane lumen is high to promote shearing of membrane fouling layers. The range of cross-flow velocities used for MBRs is on the order of 1-4 m/sec (Urbain et al., 1996; Cicek et al., 1998b).

Category	Ying and Weber, 1979	Kim and Pirbazari, 1987	Chang and Rittman, 1987	Speitel and DiGiano, 1987	Adham, Snoeyink, and Clark, 1993	Zhang and Huck, 1995	Current MBR model
External mass transfer	Liquid Film	Liquid film & biofilm	Liquid film & biofilm	Liquid film & biofilm	Liquid film	Liquid & biofilm - steady state	Liquid film
Biofilm thickness	Thin-Variable	Variable	Variable	Variable	None	Fixed	Thin-variable
Biofilm coverage	Incomplete	Complete	Complete	Complete	None	Variable-fixed	Incomplete
Biofilm shear loss	Boundary condition	Boundary condition	First Order loss term	Loss term	None	Fixed	Loss term
Adsorbent type	GAC	GAC	Bead shaped GAC	GAC	PAC	GAC	PAC
Surface or pore diffusion	Surface diffusion	Surface diffusion	Surface diffusion	Surface diffusion	Surface	None	Surface diffusion
Adsorption equilibrium model	Freundlich	Freundlich	Freundlich	Freundlich	Freundlich	None	Freundlich
Substrate tested	Glucose, sucrose	Glucose, sucrose, wastewater	Phenol	Phenol and paranitrophenol	Trichlorophenol and NOM	AOC	Total carboxylic acids
Substrate concentration	High ~600 mg/L	High	~3 mg/L	23 µg/L and 65 mg/L, respectively.	1.9 - 3.2 mg/L	~400 µg/L as acetate	~500 µg/L
Reactor type(s)	Fixed bed-plug flow and completely mixed solid phase	Fixed bed and fluidized bed	Completely mixed and fixed bed with recycle	Fixed bed	Completely mixed coupled with a plug flow recirculation loop	Fixed Bed	Completely mixed membrane bioreactor
Biokinetic model	Monod	Monod	Monod	Monod	None	Monod	Monod
Biokinetic limitation	Substrate	Substrate	Substrate	Substrate	None	Substrate	Substrate
Biokinetic parameter determination	Biokinetic studies	Biokinetic studies	Biokinetic studies	Biokinetic studies	None	Estimated	Biokinetic studies
Numerical method(s)	Finite difference-explicit and implicit methods	Finite difference - orthogonal collocation	Finite difference - orthogonal collocation	Finite difference - orthogonal collocation	Crank's analytical solution for the HSDM	Analytical solution of S. S. biofilm model-Saez and Rittman, 1988	Finite difference

Table 5. Comparison of previous biodegradation and adsorption models

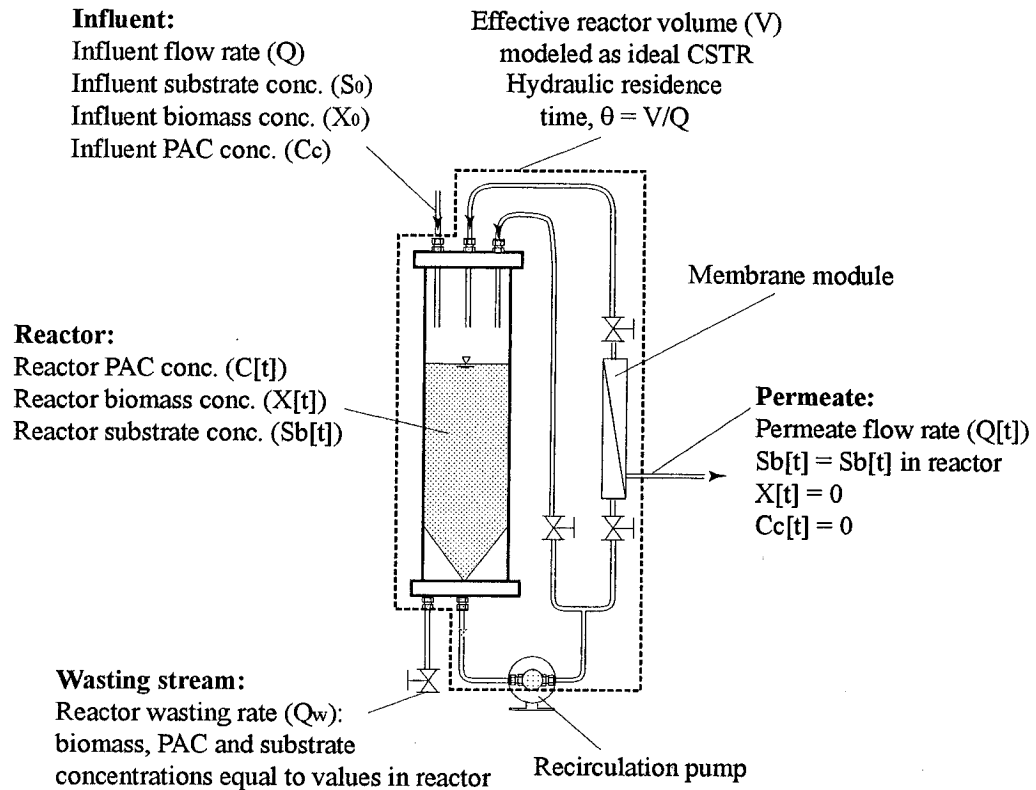


Figure 30. Conceptual illustration of the proposed MBR model showing key process components and assumptions.

Reactor hydraulics are modeled as an ideal completely stirred tank reactor (CSTR).

The effective volume includes both the reactor volume as well as fluid contained within the membrane recycle loop. Although previous models have modeled the membrane recycle loop as a plug flow reactor (PFR) (Adham et al., 1993), the relative percentage of the total volume in the recycle loop is comparatively small and flow is in a turbulent regime, creating a substantial amount of dispersion. A strict model would incorporate PFR with dispersion or a CSTR-in-series model for this re-circulation loop, however this introduces a substantial amount of complexity into an already complex model. For

this reason, the recycle loop in the current MBR model is modeled as part of a single CSTR.

Both attached and sheared biofilm is considered as part of the active biomass (Figure 31). One of the simplifying assumptions used for the current model is that biofilm on carbon surfaces is thin and discontinuous; consequently, biofilm thickness is small. Substrate diffusion through the biofilm is assumed not to be rate limiting (i.e., substrate concentrations do not approach 0 in the biofilm) under typical operating conditions and substrate loadings. Given this assumption, determining a substrate gradient through the biofilm is not needed and therefore a model-calculated biofilm thickness is not essential.

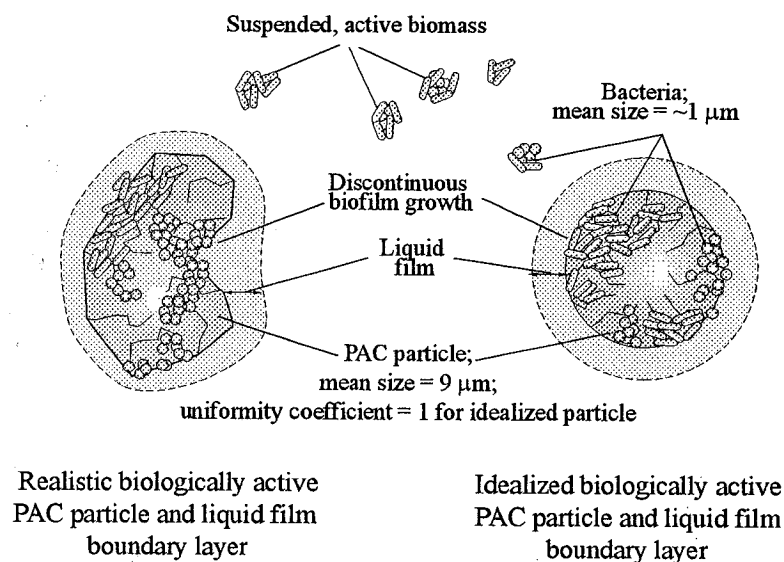


Figure 31. Realistic and idealized biologically-active PAC particle in a high-shear, low-substrate system.

The principal model assumptions are summarized as follows:

1. Diffusion of absorbable substrates in activated carbon occurs according to surface diffusion.
2. Biofilms that develop on activated carbon are relatively thin, presenting a negligible mass transport (diffusive) resistance.
3. Activated carbon is homogenous, and may be effectively modeled assuming a spherical particle.
4. Substrates are biodegradable and reversibly adsorbed.
5. Adsorbate equilibrium at the carbon surface may be modeled by the Freundlich equation.
6. Permeate flow rates and reactor detention times are constant.
7. Activated carbon and biomass are conserved within the system.
8. Substrate concentrations in the recycle return stream are equal to bulk fluid substrate concentrations in the reactor
9. Membranes function to reject only particulates in the system and not dissolved species (substrates).
10. Substrate utilization is biochemically and not diffusionally limited (i.e. diffusion does not present a mass transport limitation in the biofilm).

In biological filters with low substrate loading (typical for water treatment processes) biomass yields are low (Speitel et al., 1987b; Speitel and Zhu, 1990). Single-substrate studies at low concentrations (0.1 mg/L) have shown yield factors that are relatively

low (approximately 0.3 mg biomass/mg substrate) as compared to processes using higher substrate loadings (e.g., wastewater = approximately 0.6 mg biomass/mg substrate). Due to the low substrate concentrations and likely biomass yields, two key model assumptions are made: (a) biomass forms a thin, discontinuous layer on activated carbon surfaces and (b) substrate diffusion through biofilms on activated carbon does not present a significant mass transport resistance. Assumptions that substrate uptake is biochemically limited have been made based on a comparison of biochemical utilization rates vs. liquid film mass transfer rates. Assuming the validity of Monod kinetics for substrate utilization, a substrate utilization rate characteristic of an oligotrophic system may be described by Equation 5-1.

$$k_b = \frac{k_m S}{X} \quad (5-1)$$

Assuming typical values for  $k_m$ ,  $S$ , and  $X$  of  $4.4 \cdot 10^{-5}$  mg cells/mg substrate-sec, 100 mg/L, and 100 mg/L (Speitel et al., 1989), respectively, biological uptake rates ( $k_b$ ) are on the order of  $4.4 \cdot 10^{-10}$ /sec. Comparing this with a liquid film mass transfer coefficient ( $k_m$ ) for mass transfer across a liquid film layer in a high energy environment ( $k_f = 0.04$  cm/sec; film depth = 10  $\mu$ m), there is approximately an eight order of magnitude difference. Assumptions that biomass as well as activated carbon are conserved in a membrane bioreactor are well founded, based solely on the size rejection (mean pore size = 0.2  $\mu$ m) of membranes used in the process. Assumptions

that sheared biomass remains viable in the system as well as the assumption that biofilms on carbon particles consistently remain thin, negate the necessity for a shear loss term in this model due to the fact that sheared biomass remains as a component of the viable and active biomass.

A final key assumption is that permeate flux rates and system residence times are constant. Depending on the operating times of a system and the percent flux decline allowed before membranes are back-flushed, variation in hydraulic residence times, and the corresponding degree of substrate utilization, may be substantial. Although this assumption may prove problematic in some conditions, it will serve to establish an initial membrane-bioreactor model. Implementation of a term describing a transient membrane flux may prove worthwhile during a later refinement of the current model. These proposed assumptions most likely restrict the application of this model to conditions whereby substrate loading is relatively low. Oligotrophic microorganisms (typically found in biological water treatment processes) are characterized by their ability to exist in environments where organic substrate concentrations are low. The defining characteristics of oligotrophic microorganisms includes their ability to degrade a wide range of substrates as well as their ability to produce substrate transport enzymes with a high affinity for catabolic substrates, and inducible synthesis of catabolic pathways (transport enzymes). From a biokinetic modeling perspective, oligotrophic bacteria typically exhibit lower maximum specific growth rates (with

correspondingly lower half velocity constants), as well as relatively low respiration rates, and low minimum specific growth rates (Rittmann and McCarty, 1980a; Rittmann and McCarty, 1980b). Biokinetic models of oligotrophic systems have sometimes considered the parameter,  $S_{min}$ , which is defined as the minimum substrate concentration at which a biofilm may exist. This parameter may be defined by Equation 5-2, which is a function of  $Y$  (yield),  $K_s$  (half velocity constant),  $k_m$  (maximum specific growth rate), and  $k_d$  (endogenous decay constant).

$$S_{min} = K_s \frac{k_d}{Yk_m - k_d} \quad (5-2)$$

From this expression, it is obvious that strategies adopted by oligotrophic bacteria, namely, lower  $K_s$  and  $k_d$  values, contribute to an overall lower minimum substrate concentration at which a biofilm community may exist.  $S_{min}$  has been proposed as a lower boundary condition for substrate concentrations, with the argument that at substrate concentrations below  $S_{min}$ , a biofilm would decay due to the predominance of endogenous decay as well as the lack of new biomass development as (Rittmann et al., 1986). It is arguable, however, given the adaptability of oligotrophic bacteria, that at concentrations below  $S_{min}$  substrate utilization will not occur.

Substrate concentrations typical of a biologically unstable drinking water are on the order of 0.1 to several milligrams per liter. These substrates are comprised of a number



of different types of compounds having different rates of biodegradation. Different biodegradable fractions in heterogeneous mixtures are sometimes generally categorized as rapidly degradable and slowly degradable (Carlson et al., 1996). Biochemical bases for such classifications are rooted in the substrate characteristic, and more importantly, to its metabolic pathway. However, in general, rapidly degradable compounds may be directly assimilated by a microorganism as compared to the extra-cellular enzymatic catabolic pathways involved in the uptake of “slowly” biodegradable compounds. It is the former (rapidly degradable) class of substrates that are predominantly utilized in the relatively short detention times (hours as compared to days or weeks) in biological treatment processes.

## **Biodegradation**

### *Biodegradation Models*

The Monod model describes substrate utilization as a function of microbial biomass concentration and time (Monod, 1949). Although the model was originally developed for pure culture, it has been applied by many researchers to describe the biokinetics of heterogeneous systems—both with respect to the microbial population and substrate (Ying and Weber, 1979; Robinson, 1985; Chang and Rittmann, 1987b; Kim and Pirbazari, 1989; Zhang and Huck, 1996). A general form of the Monod equation is given in Equation 5-3.

$$\mu = \mu_m \frac{S}{K_s + S} \quad (5-3)$$

Where:

$\mu$  = specific growth rate ( $t^{-1}$ )

$\mu_m$  = maximum specific growth rate ( $t^{-1}$ )

$S$  = concentration of growth-limiting substrate in solution (mass/volume)

$K_s$  = half velocity constant defined as the substrate concentration at one half the maximum growth rate (mass/volume)

The general form of the Monod model may be expanded to describe substrate utilization as a function of biomass concentration by coupling Equation 5-3 with Equation 5-4, which describes bacterial growth rate ( $r_g$ ), substrate utilization rate ( $r_{su}$ ), and the yield coefficient ( $Y$ ):

$$r_g = -Yr_{su} \quad (5-4)$$

This results in the following general expression relating substrate utilization rate to biomass concentration:

$$r_{su} = \frac{\mu_m XS}{Y(K_s + S)} \quad (5-5)$$

Zhang and Huck (1996) used Monod kinetics to model steady-state AOC removal in fixed-bed bioreactors. A general agreement was seen between observed and model-predicted values, however, high variability in the AOC method and field testing conditions resulted in some discrepancy between measured and predicted values.

#### *Liquid-phase Mass Balance*

The liquid-phase substrate mass balance in the MBR process may be generally expressed as follows:

$$\text{Mass Accumulation} = \text{Mass Inflow} - \text{Mass Outflow} - \text{Adsorption} - \text{Biodegradation}$$

A mathematical formulation of the preceding expression for a CSTR is given in Equation 5-6.

$$V \frac{dS_b}{dt} = QS_0 - QS_b - V \frac{k_m XS_b}{K_s + S_b} - QqC \quad (5-6)$$

Where:

$V$  = Reactor volume (L)

$S_b$  = Reactor bulk fluid substrate concentration (mg/L)

$S_0$  = Substrate feed concentration (mg/L)

$k_m$  = maximum specific substrate utilization rate ( $\text{hr}^{-1}$ )

$X$  = Biomass concentration (mg/L)

$K_s$  = Half saturation constant (mg/L)

$Q$  = Permeate flow rate

$q$  = Solid phase substrate concentration (mg adsorbate/g of carbon)

$C$  = Activated carbon concentration (mg/L)

In the preceding transient expression, a net accumulation of substrate may occur in the system due to adsorption on activated carbon. However, an underlying model assumption considers all absorbable substrates to be physically (reversibly) adsorbed and a steric factor for desorption is not included. Given this assumption, bio-regeneration of activated carbon may occur. The rate term in the preceding expression considers a total substrate flux diffusing into the biofilm and subtracts substrate utilized in biochemical reactions. Substrate, which is not biodegraded, is adsorbed on the underlying activated carbon, resulting in a net accumulation of substrate.

A biomass mass balance in a CSTR may be represented by:

$$V \frac{dX}{dt} = V \frac{1}{Y} \frac{k_m S_b}{K_s + S_b} X - V k_d X \quad (5-7)$$

Where:

$Y$  = Yield coefficient (mg biomass/mg substrate)

$k_d$  = Endogenous decay coefficient ( $\text{day}^{-1}$ )

Equation 5-6 and Equation 5-7 comprise the principal substrate and biomass mass balances, respectively, describing transient changes in substrate and biomass concentrations as a function of time. One of the key simplifying assumptions in this model is that biofilms which develop on activated carbon are thin and discontinuous. Consequently, mass transport resistances, although finite, are considered to be negligible. With this simplifying assumption, only two mass transfer resistances are considered: (a) mass transfer across the liquid film layer, and (b) surface diffusion inside the activated carbon adsorbent.

## **Adsorption**

### *Adsorption Models*

The Freundlich model assumes a distribution of site energies which is more consistent with the heterogeneity of carbon adsorption sites as well as adsorbates in multi-component systems (Crittenden, 1976). In the Freundlich isotherm model ( $q_e = K_f C_e^n$ ),  $q_e$  is the equilibrium adsorbate concentration on the solid phase,  $K_f$  is a general indicator of sorption capacity,  $n$  represents a magnitude and distribution of adsorption energies for a given reaction, and  $C_e$  is the equilibrium liquid-phase adsorbate concentration.

A single-solute Freundlich model will be used in the current work as it has been successfully demonstrated in several previous studies for modeling NOM adsorption.

McGuire and coworkers (1989) compared single- and multi-solute competitive adsorption modes for predicting TOC adsorption in SPW. TOC was modeled by first establishing the adsorbable and non-adsorbable TOC fractions. The adsorbable fraction was then modeled using a range from one to five fictive components, each having a different adsorbability. Multiple-solute, competitive adsorption was modeled using the Ideal Adsorbed Solution Theory (IAST), which, for a single-component system, reduces to the Freundlich model. While a five-component model more accurately predicted TOC adsorption, a single component model was found to be accurate over a narrower range of initial TOC concentrations. The study concluded that, over a wide range, varying TOC concentration resulted in a concomitant variation in the carbon adsorption capacity.

While adsorption models such as the Freundlich model describe adsorption equilibrium under a specific set of conditions, it cannot be used to describe transient behavior. Modeling adsorption dynamics in activated carbon has been studied extensively (Peel and Benedek, 1976; Ying, 1978; Crittenden et al., 1985; Smith and Weber, 1988; Speitel et al., 1989; Pirbazari et al., 1996), and the homogenous surface diffusion model (HSDM) has been widely used for this application. The HSDM is a simplified form of the material balance for mass transport within a differential volume of an adsorbent particle, and the formal mathematical derivation is described elsewhere (Ying, 1978). The HSDM describes dynamic adsorption in a framework where physically adsorbed substrates are transported along the surface of porous structures of an activated carbon particle. Initially, liquid-phase adsorbate will adsorb at the carbon

particle surface. Adsorbates condensed on the carbon surface are subsequently transported through the inner carbon pores by surface diffusion whereby adsorbates are driven by a concentration gradient to lower concentrations of the inner surfaces of a carbon particle. In an evaluation of both surface- and pore-diffusion models for a variety of low molecular weight model compounds, Ying (1978) concluded that the dominant mode of intra-particle mass transport is surface diffusion, however, pore diffusion was reported to become more important as intra-particle concentrations increased. Similarly, Crittenden and et al. (1980) used surface diffusion to model adsorption of low concentrations of para-nitrophenol onto activated carbon.

The general form of the surface diffusion equation (in spherical coordinates) may be expressed as (Weber and DiGiano, 1996):

$$\frac{\partial q}{\partial t}(r,t) = \frac{D_s}{r^2} \frac{\partial}{\partial r} \left[ r^2 \frac{\partial q}{\partial r} \right] \quad (5-8)$$

Where:

$q$  = Adsorbed substrate concentration (mg substrate/g carbon)

$r$  = Inner coordinate of activated carbon particle (cm)

$D_s$  = Surface diffusion coefficient (cm<sup>2</sup>/s)

One initial condition and two boundary conditions are necessary to solve the HSDM. The first boundary condition (Equation 5-9) is based on the assumption that activated carbon is assumed to be homogenous with respect to adsorptive capacity and is spherical in dimension. The first boundary condition is then used to mirror the concentration profile in the center of a carbon particle where changes in adsorbate concentration as a function of particle radius are equal to zero. The second boundary condition (Equation 5-10) is applied at the outer particle surface and assumes that the substrate flux entering the carbon particle is equal to the difference between mass transport across the liquid film boundary layer, and biochemical oxidation on the carbon surface. Equation 5-11 (the initial condition) sets adsorbate concentrations equal to 0 inside the carbon particle at  $t=0$ .

$$\frac{\partial q}{\partial r}(0,t) = 0 \quad (5-9)$$

$$\frac{3kC}{\rho_s R} (S_b - S_s) = \frac{\rho_s}{R^2} \frac{\partial}{\partial t} \int_0^R q(r,t) r^2 dr \quad (5-10)$$

Where:

$k$  = Liquid film mass transfer coefficient (cm/sec)

$\rho_s$  = Activated carbon density (g/cm<sup>3</sup>)

$R$  = Mean carbon particle radius (cm)



$$q(r,0) = 0 \quad (5-11)$$

A local equilibrium exists at the activated carbon surface where adsorbates are distributed between solid and liquid. This distribution is described by the Freundlich adsorption model:

$$q(R,t) = K_f S_s^{\frac{1}{n}} \quad (5-12)$$

Where:

$K_f$  = Freundlich isotherm constant (mg substrate/g carbon)

$1/n$  = Dimensionless Freundlich isotherm constant

$S_s$  = Substrate concentration at carbon surface

A fundamental assumption of this model draws from previous work in which a mass transport resistance is imparted across a continuous liquid film covering suspended activated carbon/biofilm particles. Mass transport resistance may be expressed in terms of a liquid film transfer coefficient, previously defined as  $k$ . Although, as previously discussed,  $k$  is not rate limiting, it is nonetheless included in this model. This coefficient is a function of free liquid diffusivity and hydraulic regime (i.e., degree of mixing and turbulence). This liquid film transfer coefficient is inversely related to the

liquid film thickness as well as the free liquid diffusivity according to the following relationship:

$$L_l = \frac{D_l}{k} \quad (5-13)$$

Where:

$L_l$  = Effective liquid film thickness (cm)

$D_l$  = Free liquid diffusivity (cm<sup>2</sup>/sec)

$k$  = Liquid film transfer coefficient (cm/sec)

The liquid film transfer coefficient may be determined directly from the Sherwood correlation (Equation 5-14) or by determining the effective liquid layer thickness (Equation 5-15) and then substituting into Equation 5-13 (Chang and Rittmann, 1987b; Heath et al., 1990).

$$k = 2.4v_s (\text{Re})^{-0.66} (\text{Sc})^{-0.58} \quad (5-14)$$

$$L_l = \frac{D_l (\text{Re})^{0.75} (\text{Sc})^{0.67}}{5.7v} \quad (5-15)$$

Where:

$Re$  = Reynolds number =  $r_s d_p v_s / \mu$

$Sc$  = Schmidt Number =  $\mu / (r_s D_l)$

$v$  = Superficial fluid velocity (cm/sec)

$D_l$  = Free liquid diffusivity (cm<sup>2</sup>/sec)

$\mu$  = Dynamic viscosity (g/m-s)

$\rho_s$  = Activated carbon density (g/cm<sup>3</sup>)

The preceding equations describing biochemical oxidation and adsorption are more readily solved numerically using dimensionless variables (Kim, 1987). Dimensionless variables used in this model are defined as follows:

$$\bar{q} = \frac{q}{q_0}, \quad \bar{S}_s = \frac{S_s}{S_0}, \quad \bar{S}_b = \frac{S_b}{S_0}, \quad \bar{K}_s = \frac{K_s}{S_0}, \quad \bar{X} = \frac{X}{X_i}, \quad \bar{r} = \frac{r}{R} \quad (5-16)$$

Substituting dimensionless variables into Equations 5-6 and 5-7 yields Equation 5-17 and 5-18, respectively.

$$V \frac{d\bar{S}_b}{dt} = Q S_0 - V \frac{k_m X \bar{S}_b}{\bar{K}_s + \bar{S}_b} - Q \bar{q} C - Q \bar{S}_b \quad (5-17)$$

$$V \frac{d\bar{X}}{dt} = V \frac{1}{Y} \frac{k_m \bar{S}_b}{\bar{K}_s + \bar{S}_b} \bar{X} - V k_d \bar{X} \quad (5-18)$$

The dimensionless form of the surface diffusion equation in radial coordinates may be expressed by:

$$\frac{\partial \bar{q}}{\partial t}(\bar{r}, t) = \frac{D_s}{\bar{r}^2} \frac{\partial}{\partial r} \left[ \bar{r}^2 \frac{\partial \bar{q}}{\partial \bar{r}} \right] \quad (5-19)$$

The dimensionless Freundlich equation that couples the solid and liquid phase may be expressed by:

$$\bar{q}(R, t) = K_f S_s^{\frac{1}{n}} \quad (5-20)$$

The initial conditions that must be specified for model simulations are:

$$S_b(0) = S_0, \quad S_s(0) = 0, \quad q(0) = q_0, \quad X(0) = X_i, \quad q(r, 0) = 0 \quad (5-21)$$

Table 6 lists the input variables required for the current MBR model, as well as methods used for determining variables.

## NUMERICAL METHODS

A solution for the combined set of substrate mass balance governing equations was achieved using finite difference techniques for partial differential equations, and one-step (Euler) methods for ordinary differential equations.

Table 6. MBR model input variables

Variable	Description	Units	Method of Determining
<b>Initial Conditions</b>			
$C_c$	Initial PAC dose added at startup	g/L	Specified
$C_d$	PAC dose continually added	g/L	Specified
$X_0$	Initial biomass concentration added at startup	CFU/mL	Specified
<b>Hydraulics</b>			
$V_r$	Effective reactor volume including membrane re-circulation loop	L	Specified
$\theta$	Mean hydraulic residence time	min	Specified
$\theta_c$	Mean solids residence time based on reactor bleed rate	min	Specified
<b>Adsorption</b>			
$K_f$	Freundlich adsorption capacity constant	mg adsorbate/ g PAC	Batch isotherm tests
$1/n$	Freundlich adsorption intensity coefficient	dimensionless	Batch isotherm tests
$D_s$	Surface diffusion coefficient	cm <sup>2</sup> /sec	Batch adsorption rate tests
$R$	Mean PAC particle radius	cm	Particle counts
<b>Mass transfer</b>			
$k$	Liquid boundary layer mass transfer coefficient	cm/sec	calculated
$D_l$	Free liquid diffusivity	cm <sup>2</sup> /sec	calculated
<b>Biodegradation</b>			
$\mu_m$	Maximum growth rate constant	h <sup>-1</sup>	Batch biokinetic tests
$Y$	Yield coefficient	CFU/mg substrate	Batch biokinetic tests
$K_s$	Half saturation constant	mg/L	Batch biokinetic tests
$k_d$	Endogenous decay constant	h <sup>-1</sup>	Batch biokinetic tests
<b>Numerical method</b>			
$T$	Global time	sec	Specified
$\delta t$	Incremental time step	sec	Specified
$\delta r$	Incremental radius step	cm	Specified

An explicit finite difference method was used to initially solve the HSDM, using a central divided difference scheme with respect to position. Solutions to the HSDM have been approached by considering an activated carbon particle (either PAC or GAC) as a perfect sphere with a radius equal to the mean particle radius. A second assumption is made concerning distributions of adsorbate between the solid and liquid phases. This assumption assumes that the Freundlich isotherm constants ( $K_f$  and  $1/n$ ) which have been measured under equilibrium conditions, will accurately describe partitioning of solute at the outer surface of the carbon particle. Using these isotherm constants, an adsorbed phase concentration may be initially calculated at the carbon surface. The HSDM assumes that surfaces of activated carbon are in equilibrium with the surrounding bulk fluid.

Once an adsorbed phase concentration has been calculated for the surface of a carbon particle, transport of the adsorbate within the carbon particle is calculated using a form of Fick's second law, which has been transformed into spherical coordinates (Equation 5-8). Before this equation can be implemented, several other assumptions must first be made. These assumptions state that the coefficient of diffusion within the carbon particle is constant, the slope of the diffusion gradient = 0 in the center of the carbon particle, and that adsorption is completely reversible.

Numerical methods used for solving the HSDM include finite element and finite difference methods. In both of these approaches, an adsorbate profile is calculated at internal points within the carbon particle. In the case of finite difference methods,

solutions are obtained by considering values of a dependant variable at the current and previous time steps, which afford an estimate at subsequent time steps.

Figure 32 graphically illustrates a general approach using the explicit finite difference method. This method uses a central divided difference with respect to position and a forward divided difference with respect to time. In the preceding illustration,  $i$  is used as a reference to position within the carbon particle (as a function of  $r$ ) and  $j$  is used as a time reference.

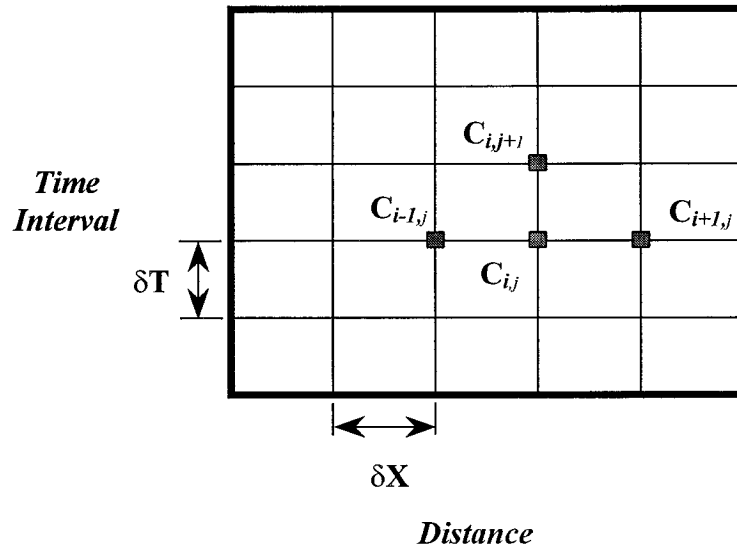


Figure 32 - General illustration of the explicit finite difference method using a rectangular coordinate system

The explicit method may be derived using a Taylor series expansion as follows:

$$C_{i,j+1} = C_{i,j} + \delta T \left( \frac{\partial c}{\partial T} \right)_{i,j} + \frac{1}{2} (\delta T)^2 \left( \frac{\partial^2 c}{\partial T^2} \right)_{i,j} + \dots, \dots (a)$$

where :

$$\left( \frac{\partial c}{\partial T} \right)_{i,j} = \frac{C_{i,j+1} - C_{i,j}}{\delta T} + O(\delta T) \dots (b)$$
(5-22)

Similarly, using a Taylor series expansion, a generic expression for concentration change as a function of position may be derived as follows:

$$C_{i,j+1} = C_{i,j} + \delta X \left( \frac{\partial c}{\partial X} \right)_{i,j} + \frac{1}{2} (\delta X)^2 \left( \frac{\partial^2 c}{\partial X^2} \right)_{i,j} + \dots, (a)$$

$$C_{i-1,j} = C_{i,j} - \delta X \left( \frac{\partial c}{\partial X} \right)_{i,j} + \frac{1}{2} (\delta X)^2 \left( \frac{\partial^2 c}{\partial X^2} \right)_{i,j} - \dots, (b)$$

where :

$$\left( \frac{\partial^2 c}{\partial X^2} \right)_{i,j} = C_{i,j} + \frac{(C_{i+1,j} - 2C_{i,j} + C_{i-1,j}))}{(\delta X)^2} + O(\delta X)^2 (c)$$
(5-23)

Combining the previous expressions, which relate concentration changes to time and position, respectively, a general numerical expression for the explicit method may be expressed as:

$$C_{i,j+1} = C_{i,j} + \lambda (C_{i-1,j} - 2C_{i,j} + C_{i+1,j})$$
(5-24)



Where:

$$\lambda = D_s \delta t / \delta x^2$$

Equation 5-24 represents a general solution for diffusion in a 2 dimensional rectangular coordinate system. By inspecting the error terms in Equation 5-22 (b) and Equation 5-23 (c), it is apparent that this method is accurate to the first order with respect to time and second order with respect to position within the carbon particle. Having a first order accuracy, with respect to time, implies that decreasing time steps by half will result in a decrease in error to the order of 1. In other words, doubling  $\delta T$  will double error. Second order accuracy in position (radius) implies that decreasing the distance step half (doubling the number of internal points inside the carbon), will yield an error  $1/4^{\text{th}}$  as large. Similarly, tripling the number of internal points will result in an error  $1/8^{\text{th}}$  as large.

Based on this general derivation of the explicit finite difference method for rectangular coordinates, an explicit finite difference relationship was developed for one-dimensional diffusion in spherical coordinates, relating concentration as a function of radius and time. Figure 33 illustrates the conceptual approach in implementing the explicit finite difference method for a spherical coordinate system. In applying this method, several fundamental assumptions are made: first, PAC particles are a uniform size (size distribution = 1); second, a homogenous density is assumed throughout the particle as well as a single diffusion coefficient; and finally, the adsorbate profile inside

the carbon particle is assumed to be symmetrical, with a slope equal to zero in the center point..

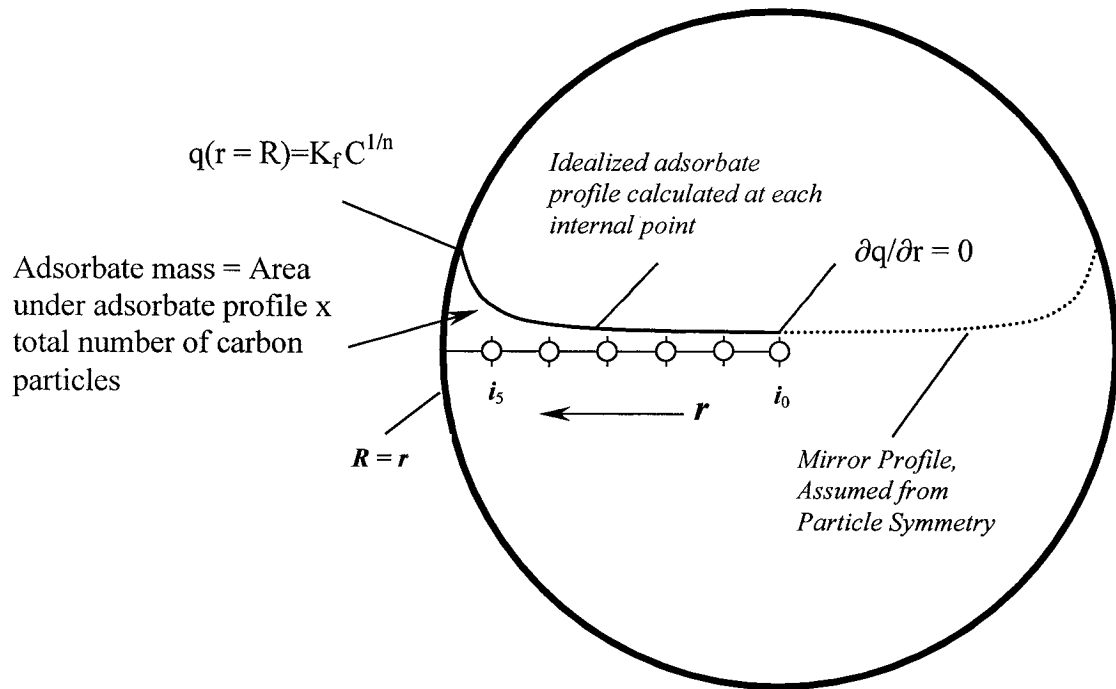


Figure 33. Idealized carbon particle showing method of grid determination and solution of the HSDM using an explicit finite difference method.

To implement the general form of the explicit finite difference method for diffusion in a spherical system, Equation 5-22 (b) and Equation 5-23 (c) are combined with the HSDM (Equation 5-8) as follows:

$$\frac{\partial q}{\partial t}(r,t) = \frac{D_s}{r^2} \frac{\partial}{\partial r} \left[ r^2 \frac{\partial q}{\partial r} \right] = \frac{\partial^2 q}{\partial r^2} + \frac{2}{r} \frac{\partial q}{\partial r} \quad (a)$$

*Substituting :*

$$\frac{\partial^2 q}{\partial r^2} = \frac{q_{i+1,j} - 2q_{i,j} + q_{i-1,j}}{(\delta r)^2} \quad (b)$$

*and,*

$$\frac{\partial q}{\partial t} = \frac{q_{i+1,j} - q_{i-1,j}}{2\delta r} \quad (c)$$

*After collection of terms :*

$$\frac{\partial q}{\partial t}(r,t) = \frac{D_s}{i(\delta r)^2} \{ (i+1)q_{i+1,j} - 2iq_{i,j} + (i-1)q_{i-1,j} \}, \dots \text{ for } i \neq 0 \quad (d)$$

$$\frac{\partial q}{\partial t}(r,t) = \frac{\lambda}{i} \{ (i+1)q_{i+1,j} - 2iq_{i,j} + (i-1)q_{i-1,j} \}, \dots \text{ for } i \neq 0 \quad (e)$$

(5-25)

$$\frac{\partial q}{\partial t}(r,t) = 6\lambda(q_{1,j} - q_{0,j}), \dots \text{ for } i = 0 \quad (f)$$

Equation 5-25 (e) and (f) were used to solve for diffusion within, and in the center, respectively, of an idealized carbon particle. Constants for surface diffusion, time, and distance steps ( $D_s \delta t / \delta r^2$ ) were substituted by the constant  $\lambda$ . Once adsorbate concentration was determined at each of the internal points within the carbon particle, adsorbate mass was calculated by integrating the area underneath the adsorbate profile.

Initial attempts at integrating this curve utilized a trapezoidal approach for integration, which effectively, summed up two points and took the mean of this sum as an area.

However, the method proved problematic, particularly in instances during the initial stages of a model simulation. Problems arose from the severity in adsorbate gradients, which occurred when the PAC surface was assumed to (always) be in equilibrium with the bulk solution. During the initial stages of a model simulation this high external adsorbate concentration (when averaged with internal adsorbate concentrations which were effectively zero) yielded an unrealistically large adsorbate mass during the first few seconds of a model simulation.

To overcome this problem, a polynomial was fitted to the internal points, having an order of  $m+1$  (where  $m$  is equal to the number of internal points). To calculate an adsorbate mass, this interpolating function was integrated over intervals of  $\delta r$ , beginning in the center of the particle. Once an average adsorbate concentration was determined over a particular interval, a weighting function was applied. This function calculated a volume equal to  $(r+\delta r) - r$ , and then divided this volume by the total volume of an idealized carbon particle. This percentage was subsequently multiplied by the average adsorbate concentration within a particular spherical shell. Summing up the individual weighted adsorbate concentrations resulted in an adsorbate concentration for an idealized carbon particle, which was multiplied by the total number of idealized carbon particles in the system to yield a total adsorbate mass.

A one-step (Euler's) method was used to solve Equation 5-17 (change in bulk fluid substrate) and Equation 5-18 (change in biomass). Using this method, an estimate of the dependant variable is made at time step  $t + \delta t$  by determining a slope based on the value at the current time step. A one step solution may be generally expressed as:

$$C_{t+1} = C_t + f(C_t, X_t)\delta t \quad (5-26)$$

Applied specifically to Equation 5-17 and Equation 5-18, the one-step solution may be expressed as:

$$\bar{X}_{(t+\delta t)} = \bar{X}_{(t)} + \left[ \frac{1}{Y} \frac{k_m \bar{S}_{b(t)}}{\bar{K}_s + \bar{S}_{b(t)}} \bar{X}_{(t)} - k_d \bar{X}_{(t)} \right] dt \dots (24 a) \quad (5-27)$$

$$\bar{S}_{b(t+\delta t)} = \bar{S}_{b(t)} + \left[ \theta S_0 - \frac{k_m X_{(t)} \bar{S}_{b(t)}}{\bar{K}_s + \bar{S}_{b(t)}} - \theta q_{mass(t)} C - \theta \bar{S}_{b(t)} \right] dt \dots (24 b)$$

Equation 5-27 (a) is a solution of the dimensionless biomass equation (Equation 5-18), and Equation 5-27 (b), a solution of reactor substrate balance (Equation 5-17). Each of these equations relies on values at the current time step to estimate values at subsequent time steps. Once a bulk fluid substrate concentration has been calculated for a subsequent time step (from Equation 5-27 b), a new carbon surface concentration ( $S_s$ ) may be calculated. This value is calculated from the boundary condition in Equation 5-

10. This boundary condition computes a new value of  $S_s$  based on the mass of adsorbate that has adsorbed or de-sorbed. The boundary condition listed in Equation 5-10 may be solved analytically for  $S_s$  according to the following equation:

$$S_{s(t+\delta t)} = S_{b(t)} - \alpha \left[ \frac{q_{mass(t)} - q_{mass(t-\delta t)}}{\delta t} \right] \quad (5-28)$$

Where:

$$\alpha = 3 \times 10^3 C_c V_r (R + L_l)^2 / R^3 \rho$$

$q_{mass}$  = Mass of adsorbate in activated carbon at time t

$C_c$  = PAC concentration

$V_r$  = Reactor volume

$R$  = Carbon particle radius

$L_l$  = Effective liquid film depth

$\rho$  = Mean PAC density

## SUMMARY AND CONCLUSIONS

A mathematical model of the MBR process was developed that predicted both adsorption and biodegradation. The model expanded on previously published models of biodegradation in fixed-bed adsorbers. Process hydraulics, including the membrane-recycle loop, were modeled as an ideal CSTR, and the MF membrane was assumed to

completely retain suspended solids within the process, including biomass and PAC.

Biodegradation was modeled using single-component Monod kinetics, and the Freundlich and HSDM models were coupled to describe adsorption onto PAC. A series of governing equations was developed and solved using finite-difference numerical methods. A model code was implemented using Mathematica<sup>®</sup> software. The major conclusions of the model development section were:

- Previously developed biofilm/adsorption models can accurately describe adsorption and biodegradation phenomena using surface diffusion coupled with the Freundlich equation to describe phase partitioning; bio-oxidation can be predicted using Monod kinetic expressions.
- Substrate loading in this process was several orders of magnitude lower than in domestic wastewater processes and, consequently, biomass production would be low. The concept of  $S_{min}$ , or the minimum substrate concentration, is often used to model biofilm processes in low-substrate waters however would not likely limit biodegradation in an MBR.
- Due to the relatively high-energy environment, biofilm shear rates would be high, and coupled with low biomass levels, bacteria growth on PAC would likely be thin and discontinuous. Additionally, sheared biomass is retained within the system and is considered as part of the active biomass. Based on this, mass transport is limited by biokinetic reaction and surface diffusion within PAC, and not by diffusion through biofilms. With this assumption, biomass may be distributed in any proportion on the PAC and in the bulk fluid.

## **CHAPTER 6 - MODELING PARAMETER ESTIMATION: ADSORPTION AND BIOKINETIC STUDIES**

### **OBJECTIVES**

The validity of mathematical model predictions is dependent on accurate and representative calibration data. Although previously published calibration data may be used in some cases, variations in water matrices as well as differences in BDOC composition between source waters require measuring calibration data for each source water tested. This chapter presents the results from adsorption and biokinetic studies, which were used to determine adsorption rate constants, adsorption kinetic constants, and biokinetic constants for total-aldehydes, DOC, THM precursors, and AOC. The specific chapter objectives are summarized as follows:

1. Conduct batch isotherm experiments using PAC and determine the Freundlich adsorption coefficients ( $K_f$  and  $n$ ) for the four groups of monitoring parameters (aldehydes, DOC, AOC, and THM precursors).
2. Determine if the Freundlich model accurately describes (heterogeneous NOM) adsorption and verify that adsorption may be modeled using a single-component model.
3. Conduct adsorption rate experiments and determine the surface diffusivity coefficient ( $D_s$ ) using adsorption rate data.



4. Conduct batch biokinetic experiments and determine the Monod biokinetic constants ( $\mu_m$ ,  $K_s$ ,  $k_d$ , and  $Y$ ) for the various model substrates.

## RESULTS AND DISCUSSION

### Adsorption Isotherm Studies

Adsorption isotherms were conducted using the batch isotherm procedures discussed in Chapter 3 (Adsorption isotherms). Isotherm data were then used to determine the Freundlich adsorption constants ( $K_f$  and  $n$ ) for the various modeling parameters (aldehydes, DOC, BDOC, AOC, and THM precursors). The Freundlich constants were determined by first linearizing batch adsorption data and then fitting a least-squares regression through the data. A linearized form of the Freundlich equation may be expressed by:

$$\log q_e = \frac{1}{n} \log C_e + \log K_f \quad (6-1)$$

If adsorption follows the Freundlich model then plotting  $\log C_e$  vs.  $\log q_e$  will result in a straight line with a slope equal to the exponential factor ( $1/n$ ), and an intercept equal to  $K_f$ .

Aldehyde adsorption was measured in both pre-ozonated natural water and carbonate-buffered synthetic water, while all other components were measured in either untreated or ozonated water. Relatively high ozone doses were applied to maximize ozone by-product production. All isotherms were conducted at ambient pH and at 20°C. Table 7 outlines the experimental conditions used for adsorption isotherm studies and adsorption rate studies.

Table 7. Overview of adsorption studies; all tests were conducted at 20°C and at ambient pH (8.0)

Exp. no.	Experiment type	Analyte	Initial concentration	Water source and treatment	PAC dose (mg/L)	Fig.
1	Isotherm	total aldehydes	200 µg/L	CO <sub>3</sub> <sup>2-</sup> buffered synthetic water	0 - 400	34
2	Isotherm	total aldehydes	65 µg/L	Ozonated SPW	0 - 200	34
3	Isotherm	DOC	3.2 mg/L	Untreated SPW	0 - 2000	35
4	Isotherm	DOC	2.7 mg/L	Ozonated SPW	0 - 2000	35
5	Isotherm	BDOC	0.6 mg/L	Ozonated SPW	0 - 2000	36
6	Isotherm	THM precursors	290 µg/L	Untreated SPW	0 - 2000	37
7	Isotherm	THM precursors	120 µg/L	Ozonated SPW	0 - 2000	37
8	Isotherm	AOC	818 µg C/L	Ozonated SPW	0 - 2000	38
9	Rate	DOC	2.2 mg/L	Ozonated SPW	200	39
10	Rate	THM precursors	120 µg/L	Ozonated SPW	200	40

Figure 34 shows adsorption equilibrium data and the Freundlich isotherm model for total aldehyde adsorption in ozonated SPW and synthetic water. The synthetic (carbonate buffered) water isotherm was run as a control to assess aldehyde adsorbitivity in the absence of NOM. In both waters, aldehydes do not appear to have adsorption affinity for carbon, as demonstrated by  $K_f$  values ranging from  $7 \times 10^{-4}$  mg total aldehydes/g PAC to  $\sim 0$  mg total aldehydes/g PAC for synthetic and ozonated water, respectively. At high carbon doses, the synthetic water isotherm (Figure 34) exhibited a non-linear tailing caused by weakly adsorbing di-aldehydes. Weak adsorption of di-aldehydes was not seen in the ozonated water isotherm due to the presence of more strongly adsorbing DOC in the natural water matrix.

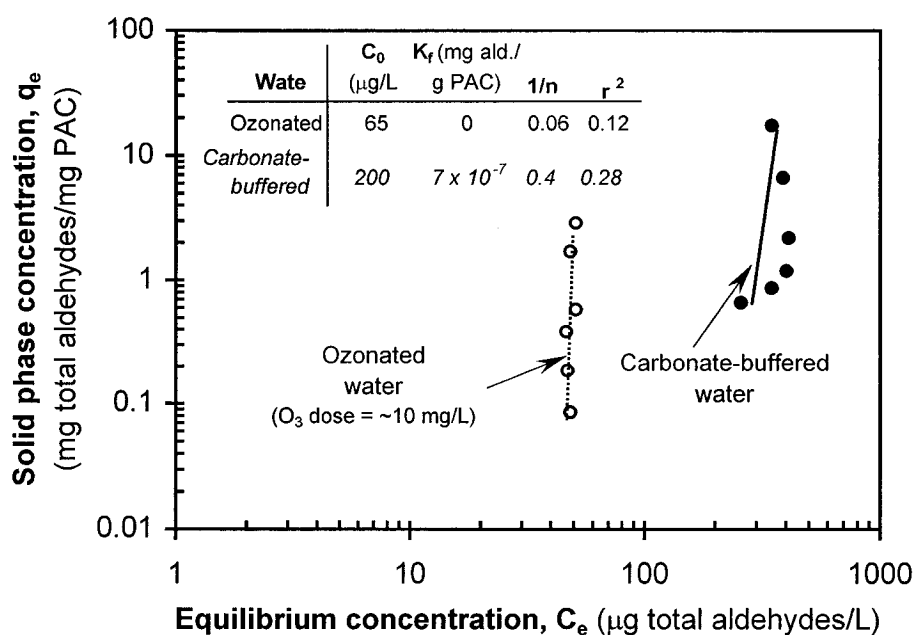


Figure 34. Adsorption equilibrium data and the Freundlich isotherm model for aldehydes in synthetic water and ozonated water. Total aldehydes represent the sum of formaldehyde, acetaldehyde, glyoxal, and methyl glyoxal.

Dissolved organic carbon adsorption equilibrium data and the Freundlich isotherm model are shown for untreated water and ozonated water in Figure 35. Isotherm results indicate that DOC adsorbability is higher in untreated water. This result is expected since ozone oxidizes DOC to lower molecular weight, hydrophilic end products (Andrews, 1993; Krasner et al., 1996b), consequently decreasing adsorbability. After pre-ozonation at relatively high ozone doses (10 mg/L),  $K_f$  values were roughly half of those measured in untreated water (4.5 mg DOC/g carbon versus 8.8 mg DOC/g carbon for ozonated and untreated water, respectively). Freundlich exponential constants ( $n$ ) were also lower in ozonated water (0.28 and 0.78 in ozonated and untreated water, respectively).

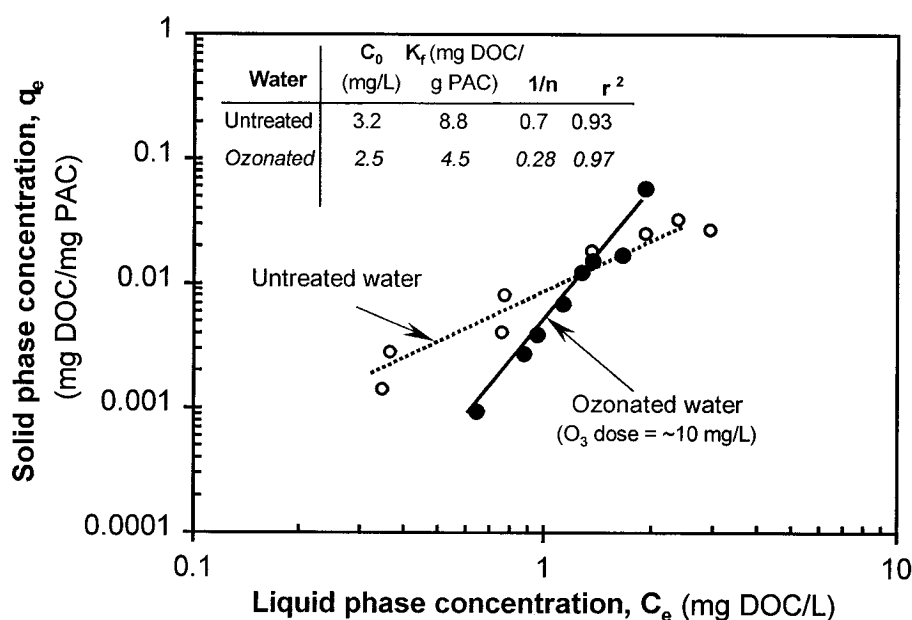


Figure 35. Comparison of adsorption equilibrium data and the Freundlich isotherm model for DOC in ozonated and untreated water

Figure 36 shows BDOC adsorption equilibrium data and the Freundlich model in an ozonated water matrix. The adsorbable BDOC fraction was measured by (1) conducting an isotherm at varying PAC doses and (2) after equilibration, filtering PAC and conducting a BDOC analysis on the sample filtrate. Figure 36 shows that BDOC is not adsorbable. This result is expected as the major BODC fractions consist of hydrophilic species including carboxylic acids, aldehydes, and aldoketo acids (Andrews, 1993; Krasner et al., 1996b).

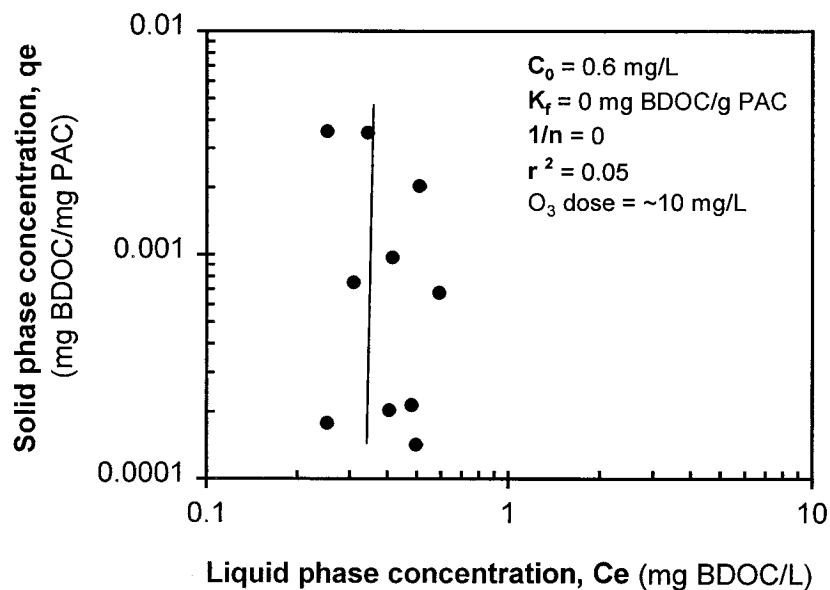


Figure 36. Adsorption equilibrium data and the Freundlich isotherm model for BDOC in ozonated water

THM precursor adsorption equilibrium data and the Freundlich isotherm model are shown for untreated and ozonated water in Figure 37. Adsorption equilibrium data shown in this figure were measured by conducting a batch isotherm using either

untreated or ozonated water ( $O_3$  dose = 10 mg/L) and a varying PAC dose. After equilibration, PAC was separated by filtration, and total THMs were measured in filtrate aliquots after first chlorinating samples. Results show that ozone oxidation substantially reduced THM precursor adsorbability, although ozone oxidation may lower total THMs to some extent by oxidizing THM precursors. Ozone oxidation lowered  $K_f$  from 63 mg/g PAC in untreated water to 1.4 mg/g PAC in ozone-treated water. It must be noted that shifts in THM speciation after ozonation resulted in lower levels of chloroform and increased levels of brominated THMs, particularly bromoform. Similar results have been reported by other investigators (Krasner, 1996a).

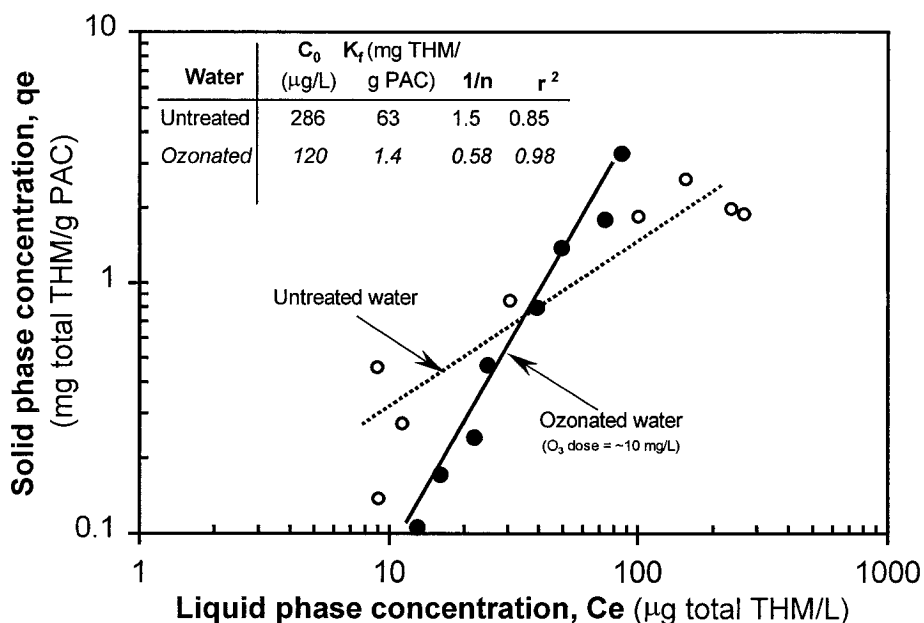


Figure 37. Adsorption equilibrium data and the Freundlich isotherm model for THM precursors in untreated and ozonated water

AOC adsorption equilibrium was conducted using ozone-treated water and different PAC doses. Once samples reached equilibrium, PAC was separated and AOC was measured in the filtrate. Figure 38 shows AOC equilibrium data fitted to the Freundlich isotherm model. The Freundlich isotherm calculated for AOC (Figure 38) show that it is effectively non-adsorbable. Zhang and Huck (1996) modeled AOC removal (in another source water) in biologically-active GAC filters and reported that AOC removal was not influenced by adsorption. The Freundlich adsorption constants measured in this study are listed in Table 8.

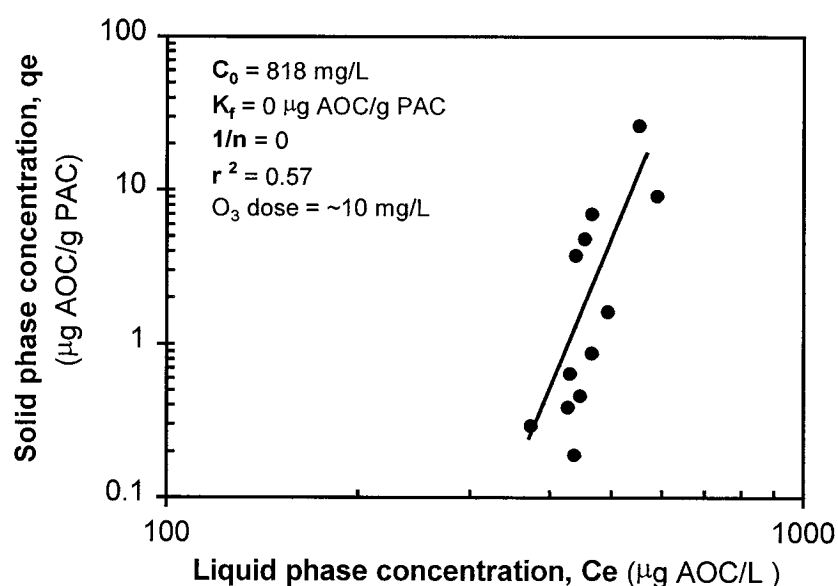


Figure 38. Adsorption equilibrium data and the Freundlich isotherm model for AOC in ozonated water

Table 8. Freundlich isotherm constants measured in the present study

Model Parameter	$K_f$ (value)	$K_f$ (units)	$1/n$	Fig.
Total aldehydes in ozonated water	~0	(mg total aldehydes/g PAC)	-	34
Total aldehydes in synthetic (carbonate-buffered) water	$7 \times 10^{-7}$	(mg total aldehydes/g PAC)	0.4	34
DOC (untreated water)	8.8	(mg DOC/g PAC)	0.72	35
DOC (ozone-treated water)	4.5	(mg DOC/g PAC)	0.28	35
BDOC (ozone-treated water)	~0	(mg DOC/g PAC)	-	36
THMFP (untreated water)	63	(mg THMFP/g PAC)	1.5	37
THMFP (ozone-treated water)	1.4	(mg THMFP/g PAC)	0.58	37
AOC	~0	(mg AOC/g PAC)	-	38

### Adsorption Rate Studies

Batch adsorption rate experiments were conducted to determine the surface diffusion coefficient ( $D_s$ ) using the experimental methods described in Chapter 3 (Adsorption rate studies) and the experimental conditions listed in Table 7. An adsorption kinetic model, which used the HSDM (discussed in Chapter 5) to model adsorption kinetics and the Freundlich model to describe solid/liquid partitioning, was used to determine  $D_s$  from batch adsorption rate measurements. Using the Freundlich constants measured in equilibrium studies (Table 7), the surface diffusion coefficient was then determined by fitting model-predicted values to observed data. A parameter search routine was used that minimized the objective function (Equation 6-2) by incrementally varying  $D_s$  from an initial estimate.



$$f(t) = \sum_{i=1}^n \frac{(C_{obs} - C_{pred})^2}{n} \quad (6-2)$$

Using Equation 6-2, measured concentrations ( $C_{obs}$ ) were compared with model-predicted concentrations ( $C_{pred}$ ) for each of the  $n$  data points. A preliminary estimate of  $D_s$  ( $1 \times 10^{-11}$  cm<sup>2</sup>/sec) was used and the routine incrementally changed the value until the sum of squared residuals (SSR) calculated by Equation 6-2 was minimized within a certain tolerance.

Experimental absorption rate data and the corresponding model profiles are shown in Figure 39 and Figure 40 for DOC and THM precursors, respectively. Total aldehyde and AOC concentrations were also measured during adsorption rate studies, however, are not included herein, as they are virtually non-adsorbable. A similar value for  $D_s$  ( $D_s = 2 \times 10^{-10}$  cm<sup>2</sup>/sec) was estimated for both the DOC and THM precursor data sets.

McGuire et al. (1989) reported  $D_s$  values ranging from  $1.2 \times 10^{-10}$  cm<sup>2</sup>/sec to  $1.5 \times 10^{-11}$  cm<sup>2</sup>/sec for GAC adsorption of TOC from untreated water. The authors concluded that  $D_s$  values were influenced by the adsorbent particle size where  $D_s$  generally increased as particle size decreased. Thus, the  $D_s$  values measured in the current study are consistent with the findings of McGuire et al. (1989) given that PAC has a smaller mean particle size (average = 9  $\mu$ m). In another study, using different source water, Adham et al. (1993) reported a  $D_s$  value of  $0.5 \times 10^{-11}$  cm<sup>2</sup>/sec for TOC adsorption from ground water onto PAC, which is substantially lower than values measured in this work.

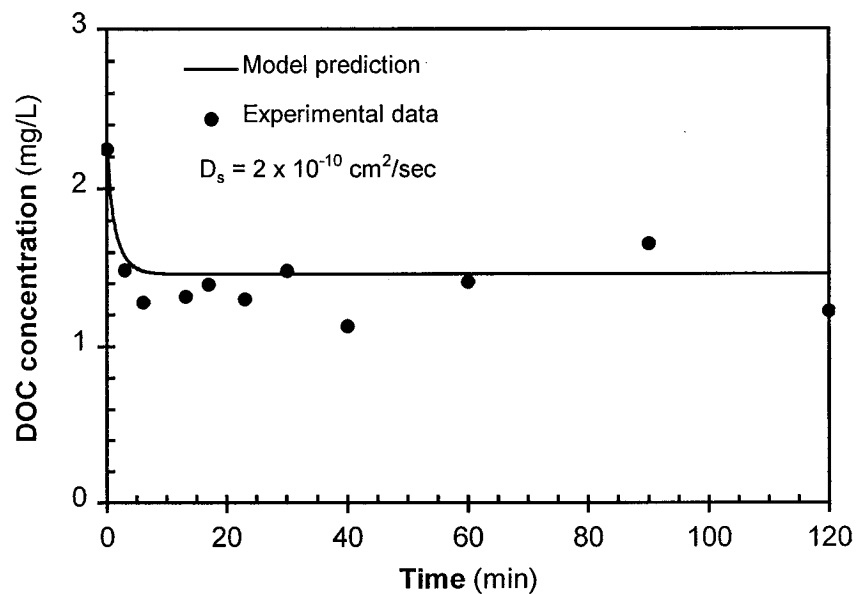


Figure 39. Adsorption rate data and HSDM profile for DOC in ozonated water

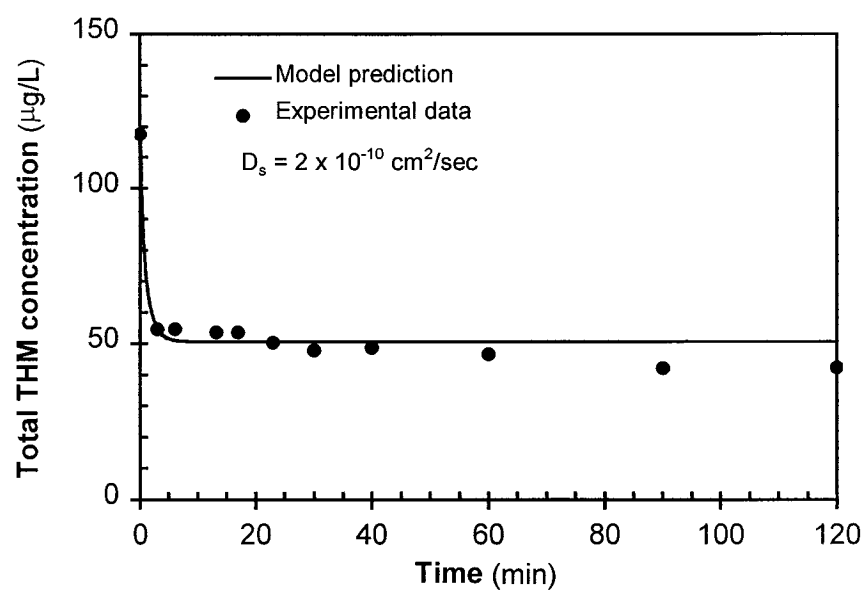


Figure 40. Adsorption rate data and HSDM profile for THM precursors in ozonated water

## Biokinetic Studies

Batch biokinetic studies were conducted to determine the Monod kinetic parameters:  $\mu_m$  (maximum growth rate constant),  $k_d$  (endogenous decay constant),  $K_s$  (half saturation constant), and  $Y$  (yield coefficient) using the experimental procedures described in Chapter 3 (Biokinetic studies). Replicate biokinetic experiments were run to determine biokinetic constants for total aldehydes, BDOC, AOC, and THM precursors. Table 9 lists the experimental conditions and monitoring parameters measured in biokinetic tests.

Replicate tests measuring BDOC degradation were run using high- and low-DOC waters to determine the effects of concentration on biokinetic parameters. The low-DOC water consisted of an undiluted SPW sample and high-DOC water was synthesized by spiking SPW with a high-DOC spike (45 mg/L) collected from an agricultural drain feeding into SPW source waters. High-DOC agricultural runoff has been reported to be a representative surrogate for SPW organics (Amy et al., 1990). Samples were ozonated at a high dose (10 mg/L) and then stored for several hours to allow dissolved ozone to decay. Nutrients were also added to ensure carbon, and not phosphorous or nitrogen, was limiting. Additionally, since carbonate has been reported to influence the metabolic rate of oligotrophic organisms (Fransolet et al., 1988) carbonate was added to synthetic water to achieve a total alkalinity = 80 mg/L as  $\text{CaCO}_3$ . Mineral nutrient constituents and concentrations used for biokinetic tests are listed in Table 3 (page 39).

Biokinetic tests measuring total aldehyde degradation were conducted using synthetic water to more precisely establish the Monod biokinetic constants. Composition of the synthetic water matrix is described in Chapter 3 (Source water). Although measuring aldehyde degradation in ozone-treated natural water would provide a more representative water matrix, it is not possible to measure the active aldehyde-degrading biomass when a variety of other carbon substrates are present. Aldehyde biokinetic data measured in an ozonated water matrix would provide an accurate measure of substrate depletion; however, maximum growth rate, yield, and endogenous decay rates would reflect those of BDOC, and not necessarily aldehydes. Aldehyde concentrations in biokinetic tests were higher than those typically measured in ozonated water (300  $\mu\text{g/L}$  in these tests compared to 50-75  $\mu\text{g/L}$  in ozonated water). Using a higher substrate concentration provides a larger response in biomass growth as well as minimized error associated with measuring aldehydes at low levels.

#### *Biokinetic Parameter Estimation Methods*

Batch biokinetic data were analyzed by first determining  $\mu_m$ ,  $Y$ , and  $k_d$ , from biomass and substrate depletion data, and then determining  $K_s$  using the measured  $\mu_m$ ,  $Y$ , and  $k_d$ , values. The general form of the Monod equation describing batch biomass growth may be expressed as:

$$\frac{dX}{dt} = \frac{\mu_m SX}{K_s + S} - k_d X \quad (6-3)$$

Table 9. Experimental conditions used for biokinetic studies; all tests were conducted at 20°C

Test	Water	Monitoring parameters	C <sub>0</sub> (mg/L)	X <sub>0</sub> (CFU/mL)	Duration (days)
1	High-DOC SPW	DOC / BDOC	4.1 / 2.6	8.5 x 10 <sup>2</sup>	9
2	Low-DOC SPW	DOC / BDOC	2.1 / 0.7	2.8 x 10 <sup>3</sup>	13
		THM precursors	0.11	2.8 x 10 <sup>3</sup>	13
		AOC	0.68	2.8 x 10 <sup>3</sup>	13
3	Synthetic (carbonate buffered)	Aldehydes	0.3	1.6 x 10 <sup>2</sup>	8
4	Synthetic (carbonate buffered)	Aldehydes	0.36	6.6 x 10 <sup>3</sup>	7

A typical batch growth curve will exhibit four characteristic regions: (1) an initial lag phase; (2) a log-growth phase characterized by essentially unlimited substrate and nutrients; (3) a stationary phase where substrate becomes limiting and growth stops; and (4) an endogenous decay phase where substrate is depleted and cells die. During the log-growth phase substrate is effectively unlimited; consequently  $S$  is much larger than  $K_s$  and Equation 6-3 reduces to:

$$\frac{dX}{dt} = \mu_m X \quad (6-4)$$

Equation 6-4 may be linearized by plotting  $\log (X_t/X_0)$  versus time, where  $\mu_m$  defines the slope of the resulting line. Conversely, when substrate has been depleted and endogenous decay predominates, Equation 6-3 may be reduced to:

$$\frac{dX}{dt} = -k_d X \quad (6-5)$$

Equation 6-5 may be linearized in the same way as Equation 6-4 where a plot of  $\log (X_t/X_0)$  versus time will result in a straight line with a slope equal to  $k_d$ . The biomass yield coefficient ( $Y$ ) was determined according to the following relationship:

$$Y = \frac{\Delta X}{\Delta S} \quad (6-6)$$

The yield coefficient was calculated by dividing the increase in biomass by the corresponding substrate decrease. Data from the experimental log-growth phase were used to estimate biomass yield.

Different methods exist for determining  $K_S$  from batch biokinetic data. Some researchers have used a linearization technique (Robert, 1992; Kornaros et al., 1996) while others have used parameter searching and fitting methods (Hozalski, 1996). The parameter search method was chosen for this work as it permitted the use of previously

developed parameter searching routines. Monod kinetic expressions for biomass growth in a batch reactor is described as follows:

$$\frac{dS}{dt} = \frac{\mu_m SX}{Y(K_s + S)} \quad (6-7)$$

Equation 6-7 and Equation 6-3 were solved using finite difference methods to predict substrate depletion and biomass growth using values for  $\mu_m$ ,  $Y$ ,  $k_d$ ,  $S_0$ , and  $X_0$  measured in each test. A parameter estimation routine (based on Equation 6-2) was used to search for the  $K_s$  value that minimized the SSR between measured data and model-predicted values.

#### *Aldehyde Biokinetic Parameters*

Figure 41 shows biomass growth and aldehyde depletion data measured in Test 4 (Table 9). In both of the replicate aldehyde biokinetic tests there was a clear trend in the substrate utilization sequence, where acetaldehyde was first metabolized followed by formaldehyde. An intermediate stationary growth phase can be seen as acetaldehyde is depleted and metabolism shifts to utilize formaldehyde. Although glyoxal and methyl glyoxal were measured in these tests, they were not included in rate determinations since methyl-glyoxal degradation began after biomass had reached a stationary-growth phase, and continued into the endogenous-decay phase. Consequently, calculating maximum growth rates for these slowly degraded substrates would only be possible in a single-component system. This indicates that di-aldehydes

(glyoxal and methyl glyoxal) may be used as a surrogate for slowly degradable BOM as suggested by others (Krasner et al., 1993b).

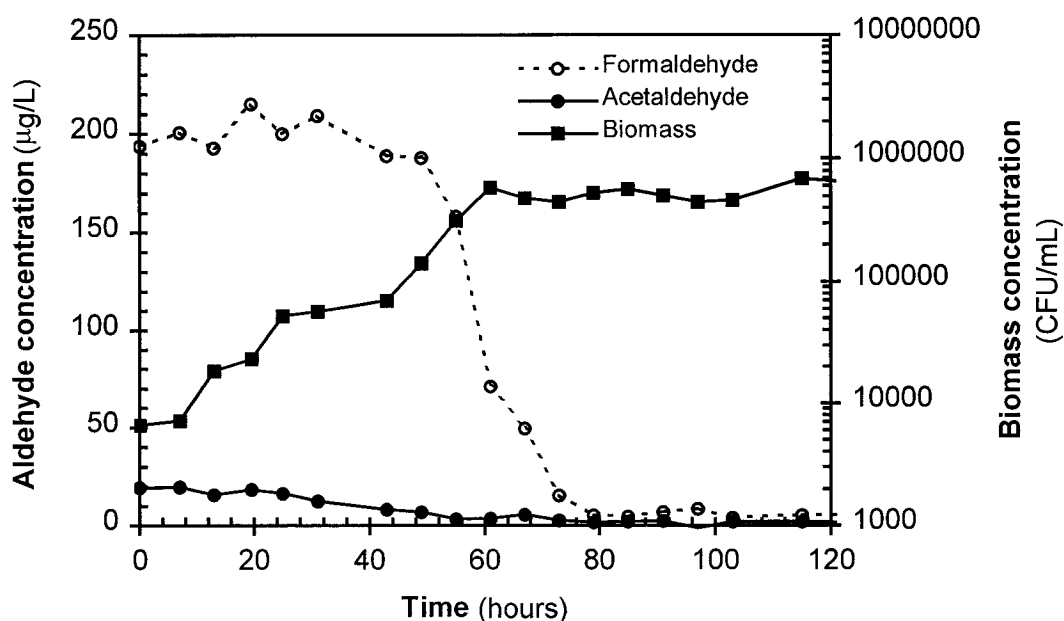


Figure 41. Aldehyde batch biokinetic data showing formaldehyde and acetaldehyde substrate depletion curves and biomass growth; experiment was conducted at 20°C in carbonate-buffered synthetic water containing mineral growth media

Using biomass data measured in the respective log-growth phases, maximum growth rates ( $\mu_m$ ) were determined for individual aldehyde components and averaged to estimate a total aldehyde substrate utilization rate. Figure 42 shows characteristic  $\mu_m$  data for formaldehyde and acetaldehyde. Maximum growth rates ranged from 0.10 h<sup>-1</sup> to 0.18 h<sup>-1</sup> with an average 0.12 h<sup>-1</sup> total aldehyde growth rate. Average biomass yields for growth on formaldehyde and acetaldehyde were 2.4 x 10<sup>3</sup> CFU/µg and 6.6 x 10<sup>3</sup> CFU/µg, respectively, and average yields for total aldehydes were



$2.6 \times 10^3$  CFU/ $\mu\text{g}$ . Total aldehyde biokinetic constants measured in the current study are summarized in Table 10.

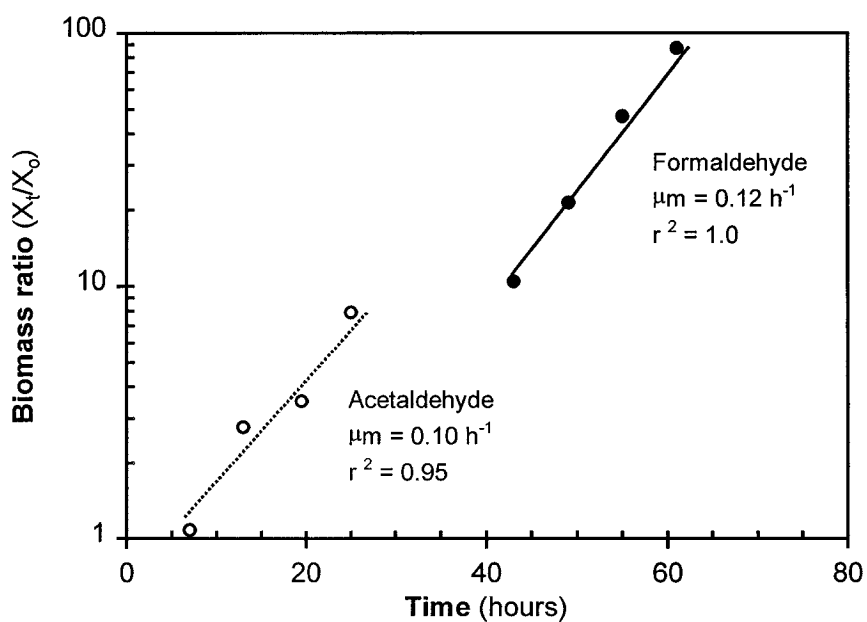


Figure 42. Determination of maximum growth rate coefficient ( $\mu_m$ ) for aldehydes

Table 10. Summary of biokinetic parameters measured in the current study

Substrate	Parameter	Units	Value
Total aldehydes	$\mu_m$	$\text{h}^{-1}$	0.12
	$Y$	CFU/ $\mu\text{g}$	$2.6 \times 10^3$
	$K_s$	$\mu\text{g/L}$	90 (0.4% of $S_0$ )
	$k_d$	$\text{h}^{-1}$	$1.5 \times 10^{-2}$
BDOC	$\mu_m$	$\text{h}^{-1}$	0.28
	$Y$	CFU/ $\mu\text{g}$	$3.8 \times 10^4$
	$K_s$	mg/L	0.15 (0.23% of $S_0$ )
	$k_d$	$\text{h}^{-1}$	$7.7 \times 10^{-3}$
AOC	$\mu_m$	$\text{h}^{-1}$	0.28
	$Y$	CFU/ $\mu\text{g}$	$4.6 \times 10^4$
	$K_s$	$\mu\text{g/L}$	300 (0.45% of $S_0$ )
	$k_d$	$\text{h}^{-1}$	$7.7 \times 10^{-3}$

Figure 43 shows  $k_d$  determination using biomass data collected after substrates were essentially depleted. Some researchers have determined  $k_d$  by using substrate-free water where only mineral media and biomass are added, however the approach followed in this study does not consider culture age and SMP recycling (Rittmann and Woolschlager, 1996). The average  $k_d$  value measured for total aldehydes was  $1.5 \times 10^{-2} \text{ h}^{-1}$ . Hozalski (1996) reported similar values ( $1.54 \times 10^{-2} \text{ h}^{-1}$ ) for decay of *P. aeruginosa* in mineral-nutrient-fortified, buffered water.

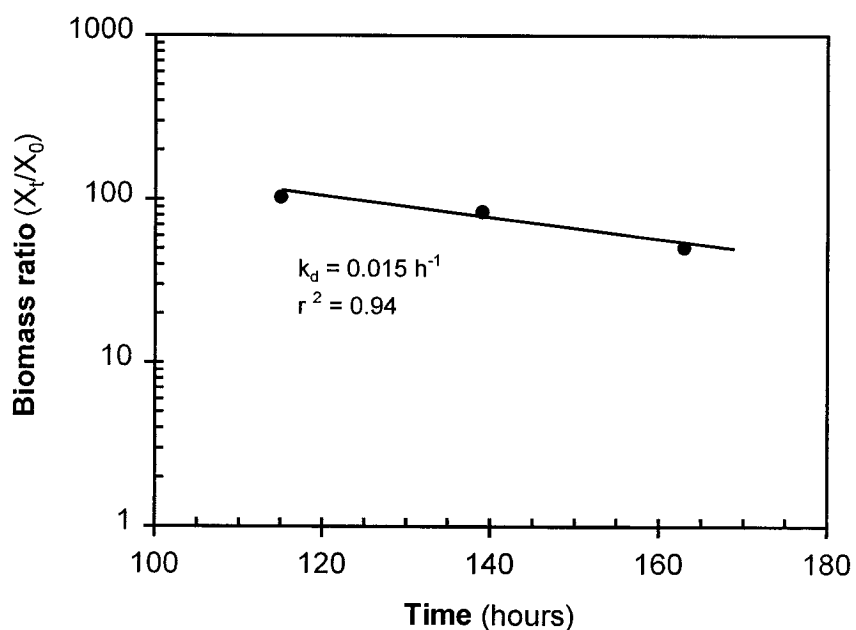


Figure 43. Determination of endogenous decay coefficient ( $k_d$ ) for aldehydes

The Monod half saturation constant ( $K_S$ ) was determined using a parameter search routine (SSR algorithm, Equation 6-2) which minimized the error between model-predicted substrate profiles and measured data (Figure 44). When expressed as a

percentage of the initial substrate concentration,  $K_S$  values ranged from 10 percent to 60 percent of the initial substrate concentration, with an average of 40 percent. Figure 45 shows the experimental data and the model profiles for biomass growth utilizing formaldehyde and acetaldehyde. Model profiles were generated using the average values determined for  $\mu_m$ ,  $Y$ ,  $k_d$ , and  $K_S$ .

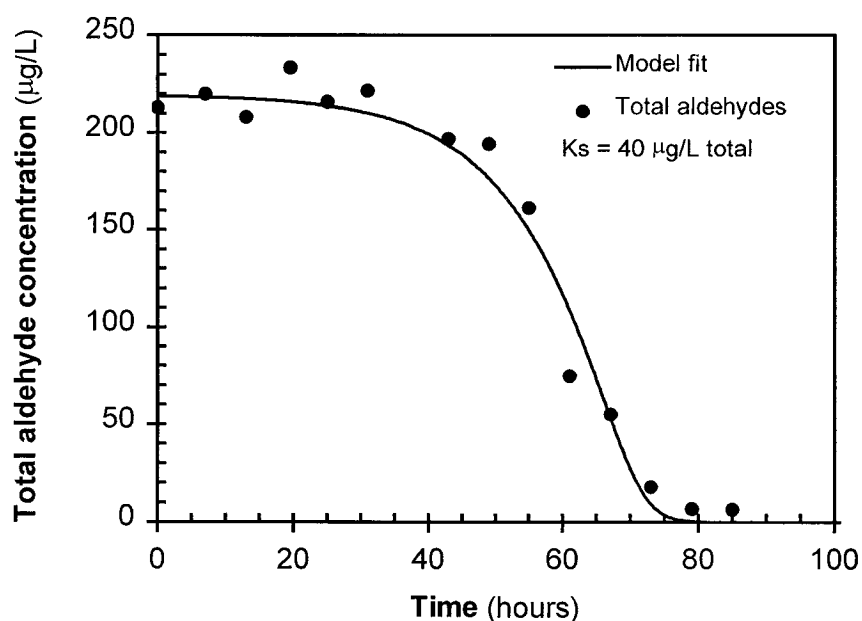


Figure 44. Estimation of  $K_S$  for total aldehydes using parameter-search technique showing measured substrate data and minimized-SSR model fit

#### *BDOC Biokinetic Parameters*

Two BDOC biokinetic tests were conducted using water with high (2.6 mg/L) and comparatively low (0.7 mg/L) BDOC (Table 9). The biomass growth and substrate utilization profiles are shown in Figure 46 and Figure 47 for high- and low-BDOC waters, respectively. In both tests, substrate was depleted within 70 hours and the two

waters were similar with respect to growth and decay rates; however, biomass yield was greater in the low-DOC test.

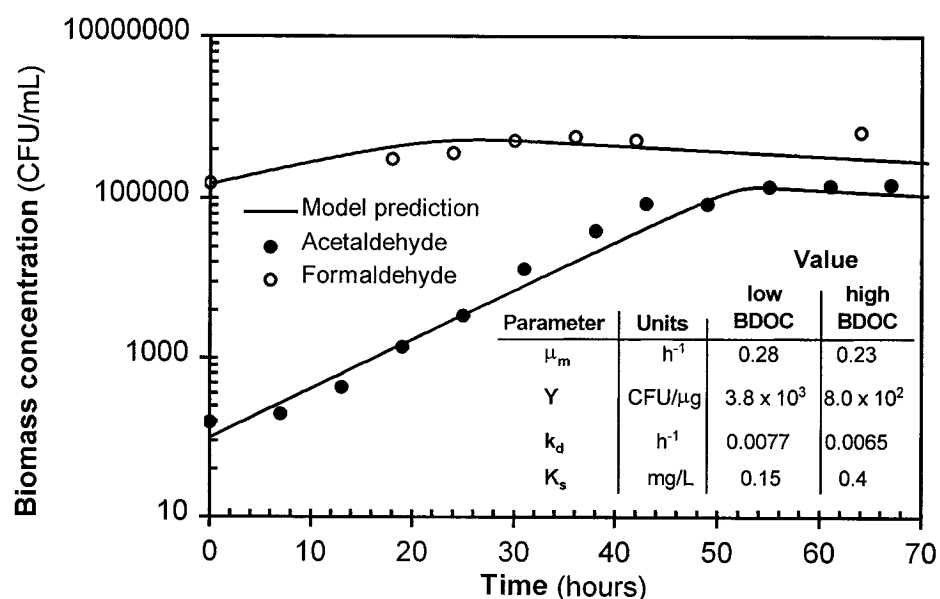


Figure 45. Verification of  $K_s$  for aldehydes showing measured biomass data for formaldehyde, acetaldehyde and model-predicted values

The maximum growth rates ( $\mu_m$ ) were determined for BDOC data by first plotting log of the biomass ratio ( $X_t/X_0$ ) versus time and then fitting a liner regression through the data; the resulting slope is equal to  $\mu_m$ . Maximum growth rates were nearly identical in the two tests ranging from  $0.23 h^{-1}$  to  $0.28 h^{-1}$  in high- and low-BDOC water, respectively (Figure 48). BDOC biokinetic constants are summarized in Table 10.

Endogenous decay constants ( $k_d$ ) were determined using methods as used to determine  $\mu_m$ . Measured endogenous decay constants showed close agreement in the two tests

with values ranging from  $6.5 \times 10^{-3} \text{ h}^{-1}$  to  $7.7 \times 10^{-3} \text{ h}^{-1}$  for low- and high-BDOC waters, respectively (Figure 49). Note that these values are over an order of magnitude lower than the  $k_d$  value measured for total aldehydes. This was likely due to the higher biomass levels in the BDOC tests and subsequent nutrient recycling once the endogenous decay phase began. Biomass yield ( $Y$ ) was substantially lower in the high-BDOC test ( $8.1 \times 10^5 \text{ CFU/mg BDOC}$  vs.  $3.8 \times 10^7 \text{ CFU/mg BDOC}$  in low-BDOC water), again suggesting a difference in BDOC composition.

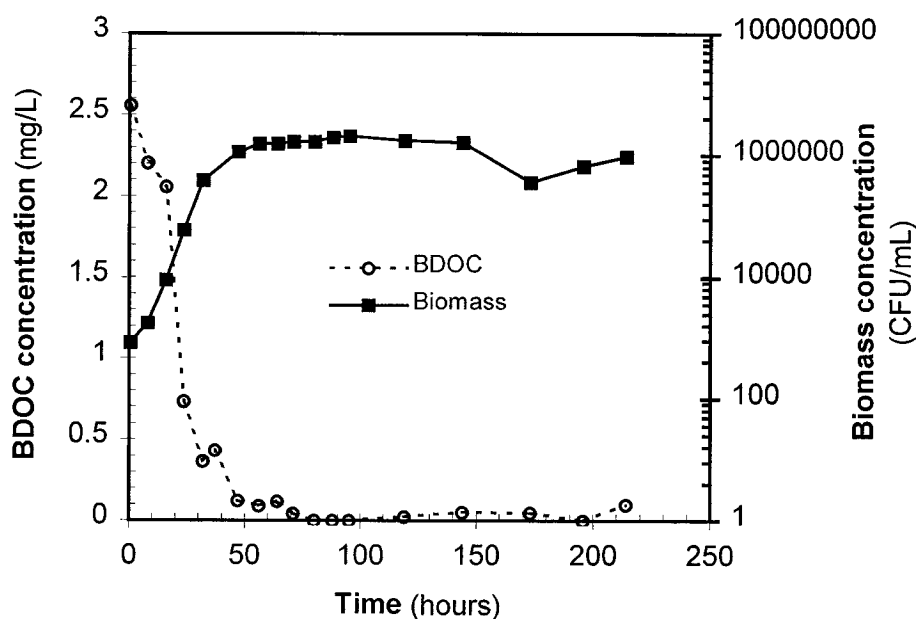


Figure 46. BDOC batch biokinetic data for high-BDOC water showing substrate depletion and biomass growth; experiment was run at 20°C in ozonated water containing mineral growth media where a DOC spike was initially added

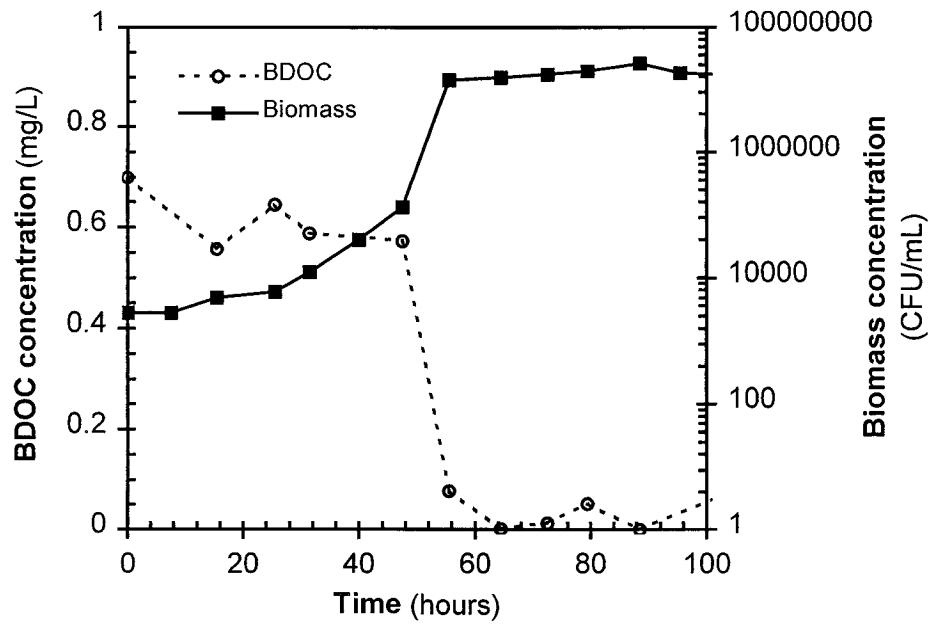


Figure 47. BDOC batch biokinetic data for low-BDOC water showing substrate depletion curve along with biomass; experiment was run at 20°C in ozonated water with mineral growth media

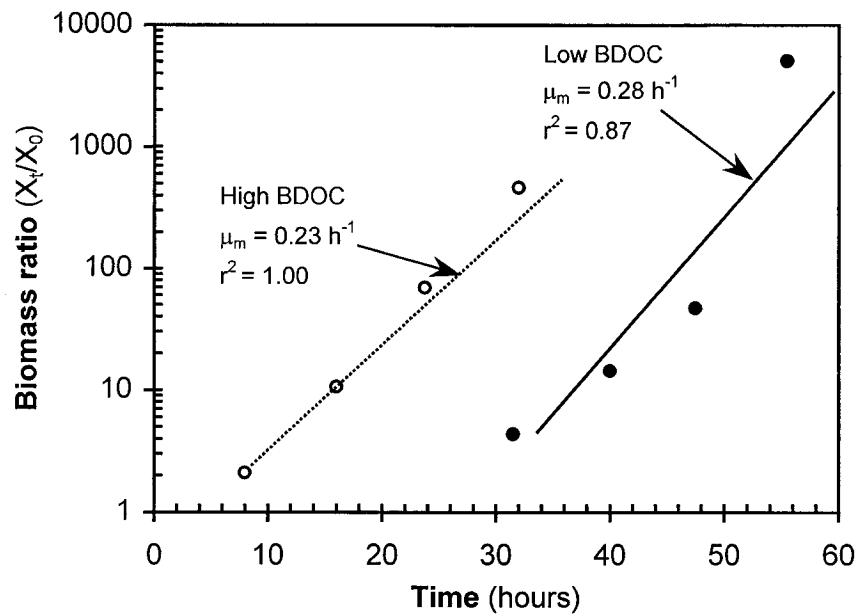


Figure 48. Determination of maximum growth rate coefficient ( $\mu_m$ ) for BDOC

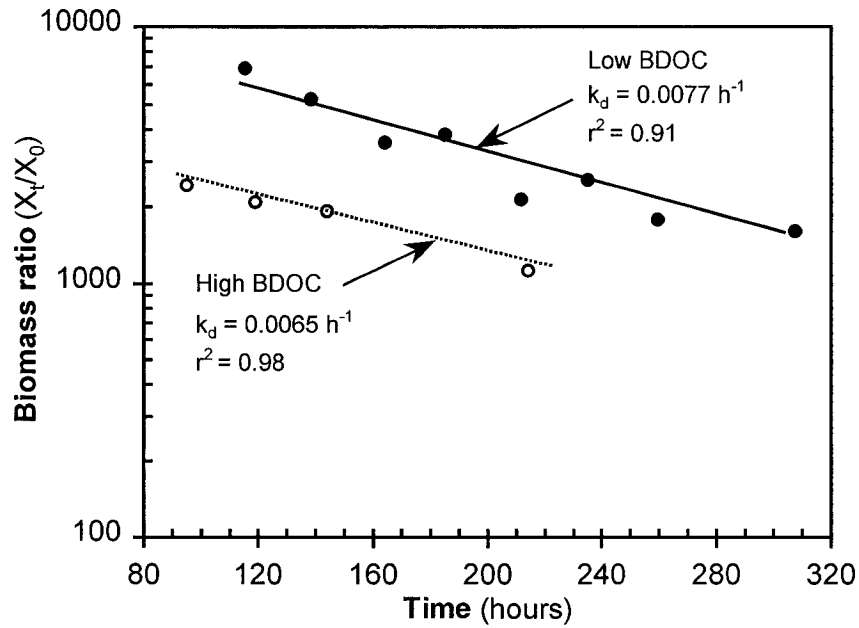


Figure 49. Determination of endogenous decay coefficient ( $k_d$ ) for BDOC

The Monod half saturation constant ( $K_S$ ) was determined for high- and low-BDOC waters using the SSR parameter search routine which determined a best-fit  $K_S$  value based on the sum of squared residuals between calculated and measured values. Figure 50 shows model profiles, generated using the best-fit  $K_S$  values, and measured data for high- and low-BDOC waters. Calculated  $K_S$  values for high- and low-BDOC waters were 0.4 mg/L and 0.15 mg/L, respectively. These values are similar when expressed as an initial substrate percentage (16 percent and 23 percent for high and low BDOC, respectively).

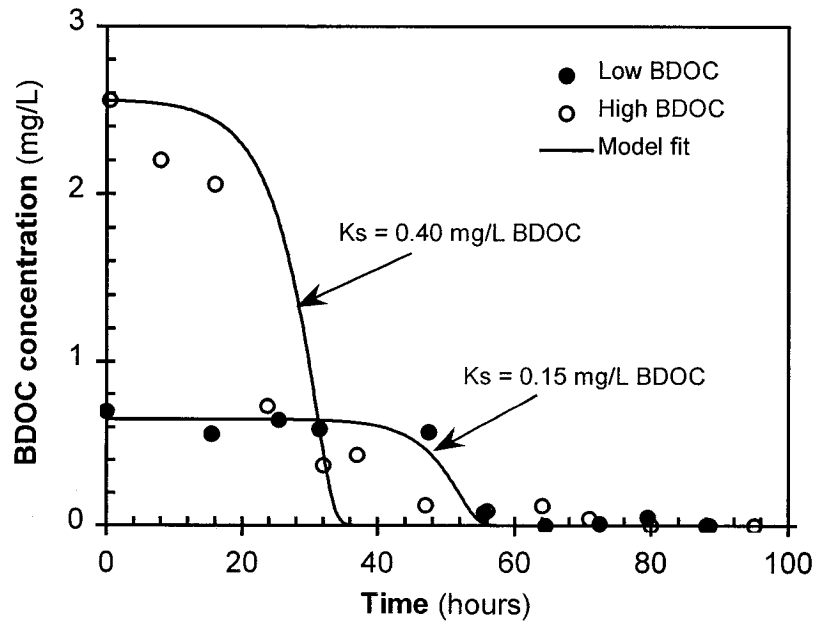


Figure 50. Estimation of  $K_s$  for BDOC (using the parameter-search technique) showing measured substrate data for high-BDOC water, low-BDOC water, and the minimized-SSR model fit to each data set

Figure 51 shows a verification of the calculated  $\mu_m$ ,  $k_d$ ,  $Y$ , and  $K_s$  against the measured biomass data. Agreement between low-BDOC biomass data and model predictions is poor during the growth phase; however, the stationary and endogenous decay phases show better agreement. In the low-BDOC biomass profile, there is an apparent lag phase, which was not seen in the high-BDOC biokinetic test. Furthermore, stationary-phase biomass concentrations were lower in the high-BDOC test even though BDOC levels were four times higher. Differences between the two waters are likely attributable to the difference in ozone byproducts; by-products formed from the high-DOC spike resulted in lower biomass yield. In comparison, with the exception of the



yield coefficient, biokinetic parameters measured in the high- and low-BDOC waters were similar.

Multi-parameter biokinetic models have been developed for predicting phenomena such as biological denitrification (Kornaros et al., 1996); however, this would require determination of kinetic constants for individual substrates. The possibility of an increase in accuracy that a multiple-substrate model would provide does not justify the large investment in analytical work and model complexity required for a multi-parameter biokinetic model.

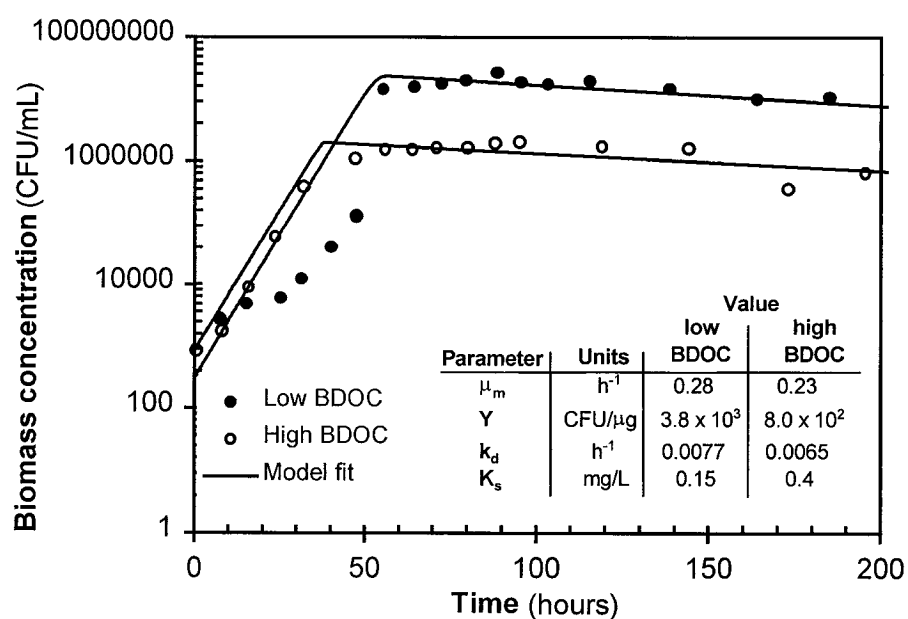


Figure 51. Verification of  $K_s$  for BDOC showing measured biomass data and model-predicted values

### *AOC and THM Precursors*

AOC and THM precursor degradation rates were measured in Test no. 2 (Table 9).

Both AOC and THM precursors are comprised of heterogeneous organic mixtures, however, it is important to note that AOC is (by definition) completely biodegradable and is a constituent of the total BDOC, while the THM precursors are generally considered recalcitrant (Miltner et al., 1992; Carlson et al., 1996). Other researchers studying the relative composition of ozone by-products in this source water (Krasner et al., 1996b) have reported that filter-removable constituents, which include aldehydes, aldoketo acids, and carboxylic acids, comprise roughly 40 percent of the total AOC; and AOC levels (expressed as carbon equivalents) were reported to be roughly 60 percent of the total BDOC. Other researchers report AOC composing nearly the entire BDOC fraction, suggesting AOC is a suitable surrogate for BDOC in some cases (Zhang and Huck, 1996). In this work, AOC levels (as carbon equivalents) were roughly equivalent to BDOC levels, and consequently, AOC composed a large fraction of the total BDOC.

Results of biokinetic tests measuring AOC and THM precursor degradation are shown in Figure 52 and measured biokinetic constants are listed in Table 10. Over an 80-hour period, AOC was reduced from 680  $\mu\text{g/L}$  to less than 100  $\mu\text{g/L}$  after 60 hours. As expected, given the high AOC/BDOC ratio, substrate depletion profiles for AOC closely followed BDOC substrate utilization (Figure 47). The values for maximum

growth rate ( $\mu_m$ ) and endogenous decay ( $k_d$ ) for AOC were  $0.28 \text{ h}^{-1}$  and  $7.7 \times 10^{-3} \text{ h}^{-1}$ , respectively ( $\mu_m$  and  $k_d$  were determined using the procedures described in the previous section (BDOC biokinetic parameters). Note that the  $\mu_m$  and  $k_d$  values measured for AOC are identical to those measured for BDOC as there is no means to fractionate biomass into BDOC-degrading and AOC-degrading. The  $Y$  and  $K_S$  values for AOC were of  $4.6 \times 10^4 \text{ CFU}/\mu\text{g AOC}$  and  $300 \mu\text{g/L}$  (or 45 percent of  $S_0$ ), respectively. The biomass yield constant for AOC was comparable to that of BDOC (BDOC biomass yield =  $3.8 \times 10^4 \text{ CFU}/\mu\text{g BDOC}$ ), however, the Monod half velocity constant ( $K_S$ ) showed a higher percentage of initial substrate concentration (45 percent for AOC and 23 percent for BDOC in the same test).

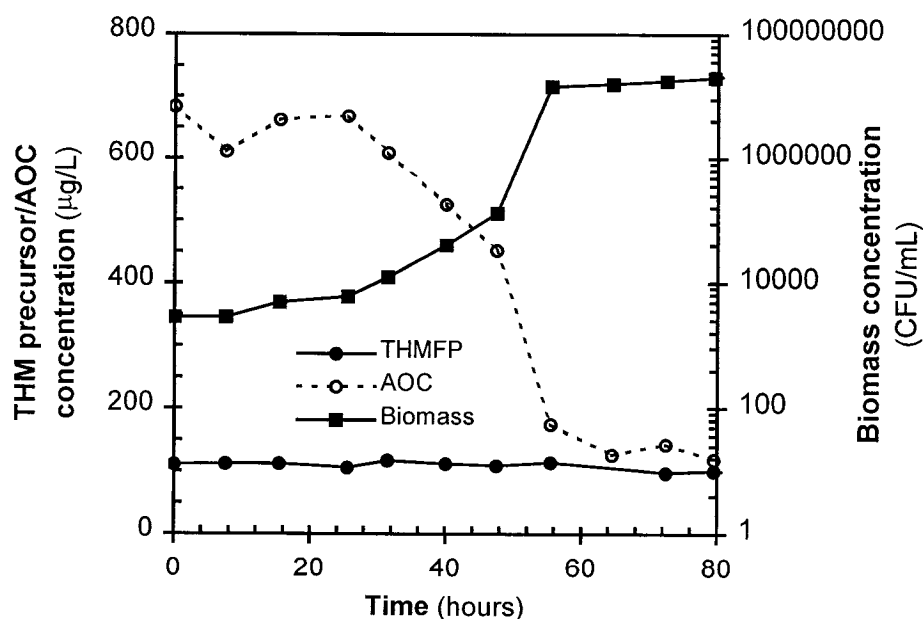


Figure 52. Biokinetic data for AOC , THM precursors (as measured by THMFP), and biomass; experiment was run at 20°C in ozonated water with mineral growth media

THM precursors showed a minimal change during the biokinetic test (Figure 52).

THMFP decreased by approximately 10 percent after 80 hours of testing. It is arguable that the small decrease in THM precursors is significant since the analytical precision of the THM method is on the order of 10 percent. Note that the biomass inocula used for this test was taken from a column that had been acclimated for several months using ozonated water and would have presumably contained a metabolically-diverse biomass.

Based on this result, it can be postulated that THM precursors are not used as a primary substrate. Consequently, THM precursor degradation cannot be reliably modeled using the current approach.

## **SUMMARY AND CONCLUSIONS**

MBR model calibration constants were measured in a series of adsorption isotherm, adsorption rate, and biokinetic experiments. Constants were measured for total aldehydes, BDOC, AOC, and THM precursors (as measured by THMFP). Comparison of bulk BOM parameters (AOC and BDOC) with specific BOM constituents (aldehydes) provided an indication of the suitability of aldehydes as a model surrogate for the bulk BOM. Batch adsorption isotherm tests were used to measure the Freundlich isotherm constants ( $K_f$  and  $n$ ) and data from adsorption rate studies were used to calculate the surface diffusivity constant ( $D_s$ ). Adsorption isotherms used a natural water matrix (untreated and ozonated) as well as limited tests in carbonate-

buffered synthetic water. Isotherms using synthetic water served as a comparison to evaluate effects of competitive adsorption in the multi-component mixtures (in natural water) used. Batch biokinetic studies measured Monod kinetic parameters ( $\mu_m$ ,  $K_s$ ,  $Y$ , and  $k_d$ ) for single- and multi-component substrates in natural water and synthetic water. Based on a careful consideration of these data, the following findings are presented:

1. The high ozone dose used in these tests substantially lowered adsorbitivity of both DOC and THM precursors when compared to untreated water. At a 3:1 ozone:DOC ratio, measured  $K_f$  values decreased by 48 percent and 97 percent for DOC and THM precursors, respectively. Ozone oxidation lowered NOM adsorbitivity by oxidizing organics to lower molecular weight, hydrophilic end products. When modeling adsorbitivity of non-specific parameters such as DOC, THM precursors, and AOC, the effect of ozone dose on adsorbitivity must be considered. Also, in a treatment process, changes in ozone dose and NOM character may affect adsorption constants. Thus, depending on the modeling objective, a single data set for adsorption parameters should not be relied upon for long-range predictions.
2. Formaldehyde and acetaldehyde had no adsorption affinity for the PAC used, whereas glyoxal and methyl glyoxal showed weak adsorbability when measured in pure solution and at high concentration. However, total aldehyde adsorption

isotherms measured in ozonated water using ambient concentrations ( $\sim 50 \mu\text{g/L}$ ) showed no adsorption. Under these conditions, glyoxal and methyl glyoxal did not adsorb to PAC.

3. Over the wide range of PAC doses used, neither AOC nor BDOC (in an ozonated water matrix) were adsorbable. This result simplifies DOC modeling, as the BDOC fraction can then be modeled separately from the adsorbable DOC fraction. Modeling DOC, with an adsorbable BDOC fraction, would require a multi-component adsorption model to distinguish the adsorbable DOC fraction, which is also biodegraded.
4. Adsorption rate experiments yielded similar  $D_S$  values ( $2 \times 10^{-10} \text{ cm}^2/\text{sec}$ ) for both DOC and THM precursors. Adsorption onto PAC was rapid and 90 percent of the equilibrium value was generally reached within approximately 5 min.
5. Using heterotrophic plate counts to measure biomass provided an accurate method to measure biomass growth in low-substrate waters. Replicate biokinetic tests measured in different waters showed reproducibility for most BDOC biokinetic constants (similar values were measured for  $\mu_m$  and  $k_d$  in replicate tests), however microbial yields measured in low-DOC water were higher than high-DOC water. AOC levels were nearly as high as BDOC levels in the waters tested and microbial yields for AOC and BDOC were similar.
6. In batch biokinetic studies on aldehyde mixtures, acetaldehyde was consumed first followed by formaldehyde. Methyl glyoxal was utilized once other aldehydes were

depleted. According to this study, formaldehyde and acetaldehyde may be considered as representative surrogates for rapidly-degradable BOM, while glyoxal and methyl glyoxal are less preferred (metabolically) and have slower degradation rates and may be an appropriate surrogate for slowly-degradable BOM. Biomass maximum growth rates and yields were lower for aldehydes as compared to those for BDOC.

7. THM precursors in ozonated solutions are degraded in biofilm processes (Miltner et al., 1992; Speitel et al., 1993). In the present study, THM precursors were not significantly degraded during the batch biokinetic studies. Thus, it was not possible to model THM precursor degradation using the batch biokinetic data. It is important to note that a mature biofilm community in a full-scale biofilter contains a more robust metabolic capability and a portion of the biomass directly metabolizes THM precursors. Alternately, degradation could occur through indirect enzymatic reaction within the dense biofilm communities. Degradation of THM precursors during biological filtration is crucial for many utilities to meet strict regulations. As a result, additional effort should be invested in this area to accurately model and predict this phenomena.

## **Chapter 7 - MODEL VERIFICATION AND SENSITIVITY ANALYSIS**

### **OBJECTIVES**

The objective of this chapter is to verify the calibrated MBR model using data measured in the mini-pilot-scale studies (Chapter 4). Model verification evaluates data used for model calibration as well as the validity of the initial model governing assumptions. Ultimately, it is the model validation that determines the accuracy of the model for describing a given process. Precise determination of calibration variables is generally essential in developing an accurate, predictive model. However, for some variables, precise parameter estimation may not be essential for model accuracy, and either approximate or even previously reported values may be used instead of investing in time-intensive parameter estimation studies (e.g., biokinetic studies). A parameter sensitivity analysis can provide an estimation how much a given parameter influences model predictions. Consequently, an informed decision can then be made regarding the data precision needed for parameter estimation.

The intended use of modeling data is also important in determining the needed level of parameter precision. If the process engineer is only interested in evaluating long-term, steady state performance, then accurate estimation of parameters that only influence transient behavior is not essential. Finally, the variability of the system must be taken into account. While the biokinetic constants measured for specific parameters (e.g.



formaldehyde or oxalate degradation) will not likely change in different waters, biokinetic and adsorption constants measured for non-specific parameters (e.g. DOC and AOC degradability) are likely to be source-water specific.

Three organic substrates have been chosen for modeling: total aldehydes, DOC, and AOC. Calibration studies were also conducted for THMFP, however, due to the inability to accurately model THM precursor biodegradation, this parameter is not included. The objective of this chapter is to verify the MBR model by comparing MBR experimental data to model-predicted values and to determine the sensitivity of MBR model predictions to variations in model constants. Using these data, an attempt is made to establish which parameters would require more-precise measurement as well as which parameters may be source-water specific. A co-objective is to assess the suitability of the monitoring parameters to the chosen modeling approach (i.e. modeling heterogeneous mixtures as a single substrate or adsorbate) and to establish if heterogeneous and variable mixtures, such as AOC and DOC, are amenable to predictive modeling using these methods. Specific objectives of this chapter are summarized as follows:

1. Calibrate the MBR model using biokinetic and adsorption constants measured in Chapter 6 and compare model predictions to MBR mini-pilot data for total aldehydes, DOC, BDOC, and AOC

2. Verify model accuracy for predicting total aldehyde, DOC, and AOC removal in adsorbing and non-adsorbing processes
3. Evaluate the efficacy of modeling DOC and AOC using a single-solute modeling approach
4. Evaluate model assumptions governing the mode of biomass growth and compare model-predicted biomass data to observations
5. Establish model sensitivity to the biodegradation ( $\mu_m$ ,  $Y$ ,  $K_s$ , and  $k_d$ ) and adsorption ( $K_f$ ,  $n$ , and  $D_s$ ) calibration constants
6. Determine process sensitivity to HRT and process recovery rate
7. Establish which parameters influence transient and steady-state process performance, and the magnitude of this influence

## RESULTS AND DISCUSSION

Total aldehyde, DOC, AOC, and biomass data measured in MBR mini-pilot tests were compared to model-predicted values. The operating variables assessed included: PAC dose, detention time, effect of continuous carbon addition, and the effect of increasing substrate concentration. Conditions used for model validation are listed in Table 11. With the exception of condition 3, each of the MBR tests began by adding acclimated biomass and carbon (when applicable) to the reactor. In condition 3, high concentrations of formaldehyde, acetaldehyde, glyoxal, and methyl glyoxal were added to the feed once the system had reached steady state. Ozonated water (SPW) was used

for all MBR experiments and, although ozone doses were kept constant (average = 5 mg/L), variations in influent water quality did occur over the testing period. Mean HRT and influent concentrations for each condition (Table 11) represent average values, however, both parameters varied during MBR experimental runs—HRT varied to a larger extent than influent substrate concentration.

Calibration constants (determined from experimental batch studies) for modeling total aldehydes, BDOC, and AOC are listed in Table 12. Model calibration values (Table 12) determined from adsorption and biokinetic studies (Chapter 6) were used as the baseline condition for parameter sensitivity analyses. Each parameter was varied independently over a +/- 50-percent range and, in some cases, the parameter was varied by an order of magnitude.

In most conditions, accurate measurement of initial biomass concentration was not possible, consequently, initial biomass concentrations were estimated from model calibration of transient profiles<sup>5</sup>. Several interferences prevented accurate measurement of initial biomass concentration. Inocula used for reactor seeding was first harvested from biomass growing in acclimation columns and measured by plate counts prior to inoculation, however, microorganisms could not be completely dissociated from biofilm clusters (i.e., bacteria remained attached in biofilm fragments). Consequently,

---

5 Steady-state model predictions were independent of initial biomass concentration, however, transient profiles were sensitive, within a certain range, to initial biomass levels.

plate counts underestimated inocula biomass levels. Additionally, some of the conditions used for model verification involved modeling a steady state process where only operating conditions were changed; in these conditions, the active biomass was already established within the reactor and interferences in measuring reactor biomass levels prevented accurate biomass quantitation (an issue which is further discussed in the “Biomass predictions” section of the current chapter).

Table 11. Overview of model simulation conditions

Simulation condition	Reactor volume (L)	Mean HRT (min)	Initial PAC dose (mg/L)	Initial biomass (CFU/mL) *	Substrate	Average influent conc.	Fig .
1	12	200	1000	$1 \times 10^6$	Total aldehydes	40 $\mu$ g/L	53 (a)
2	12	240	0	$4 \times 10^5$	Total aldehydes	40 $\mu$ g/L	53 (b)
3	6	100	3000	$7.5 \times 10^6$	Total aldehydes	310 $\mu$ g/L	53 (c)
4	12	120	0	$4 \times 10^5$	DOC BDOC	3.6 mg/L 0.70 mg/L	56 (a)
5	12	200	1000	$1 \times 10^5$	DOC BDOC	2.8 mg/L 0.85 mg/L	56 (b)
6	6	100	3000	$1 \times 10^5$	DOC BDOC	3.3 mg/L 0.65 mg/L	56 (c)
7	6	100	3000 initially; 50 mg/L	$1 \times 10^5$	DOC BDOC	2.7 mg/L 0.60 mg/L	56 (d)
8	6	120	3000	$1 \times 10^5$	AOC	590 $\mu$ g/L	60

\* Note that initial biomass was estimated to provide the best model fit

Table 12. Calibration constants used for model verification and sensitivity analyses

Parameter	Total aldehydes		DOC and BDOC		AOC	
	value	units	value	units	value	units
<b>Initial conditions</b>						
Influent substrate ( $S_0$ )	100	$\mu\text{g/L}$	1	$\text{mg/L}$	500	$\mu\text{g/L}$
Initial biomass ( $X_0$ )	$1 \times 10^6$	CFU/mL	$1 \times 10^7$	CFU/mL	$5 \times 10^6$	CFU/mL
Mean HRT ( $\theta$ )	120	min	120	min	120	min
Initial PAC dose	0	$\text{mg/L}$	0, 1000	$\text{mg/L}$	0	$\text{mg/L}$
<b>Adsorption constants</b>						
$K_f$	0	-	4.5	$\text{mg DOC/g carbon}$	0	-
$n$	0	-	0.28	-	0	-
$D_s$	0	-	$2 \times 10^{-10}$	$\text{cm}^2/\text{sec}$	0	-
$R$	$9 \times 10^{-4}$	cm	$9 \times 10^{-4}$	cm	$9 \times 10^{-4}$	cm
<b>Mass transfer constants</b>						
$k$	$4 \times 10^{-3}$	$\text{cm/sec}$	$4 \times 10^{-3}$	$\text{cm/sec}$	$4 \times 10^{-3}$	$\text{cm/sec}$
$D_l$	$1 \times 10^{-6}$	$\text{cm}^2/\text{sec}$	$1 \times 10^{-6}$	$\text{cm}^2/\text{sec}$	$1 \times 10^{-6}$	$\text{cm}^2/\text{sec}$
<b>Biokinetic constants</b>						
$\mu_m$	0.12	$\text{h}^{-1}$	0.28	$\text{h}^{-1}$	0.28	$\text{h}^{-1}$
$Y$	$2.6 \times 10^3$	CFU/ $\mu\text{g}$ total aldehydes	$3.8 \times 10^4$	CFU/ $\mu\text{g}$ BDOC	$4.6 \times 10^4$	CFU/ $\mu\text{g}$ AOC
$K_s$	28	$\mu\text{g/L}$	300	$\mu\text{g/L}$	225	$\mu\text{g/L}$
$k_d$	$1.5 \times 10^{-2}$	$\text{h}^{-1}$	$7.7 \times 10^{-3}$	$\text{h}^{-1}$	$7.7 \times 10^{-3}$	$\text{h}^{-1}$

## Prediction/Simulation of Total Aldehyde Removal

The MBR model was tested for predicting total aldehyde removal under different operating conditions using the calibration constants listed in Table 12. Activated carbon dose and influent substrate concentration were varied in the three different conditions modeled. Figure 53 shows experimental data and model predictions for total aldehyde removal in the MBR when: (a) PAC and biomass are initially added (condition 1, Table 11), (b) only biomass is added (condition 2, Table 11), and (c) influent total aldehyde concentration was increased (condition 3, Table 11). In the three conditions modeled, total aldehydes were rapidly degraded to near-detection-limit levels and model fit to observed data was good in both the initial (transient) stages as well as at steady state.

While increasing the maximum growth rate ( $\mu_m$ ) by 50 percent had a minor effect on transient profiles, lowering  $\mu_m$  by 50 percent effected both transient and steady-state total aldehyde removal (Figure 54 [a]); lowering  $\mu_m$  increased the transient period by a factor of 3 and lowered steady state removal efficiency by 5 percent. Changing the yield coefficient ( $Y$ ) influenced transient profiles; however, steady-state removal efficiency was not affected (Figure 54 [b]). Transitory periods increased by 110 percent when the Monod half-velocity constant ( $K_s$ ) was increased from baseline values, and steady state removals were 5 percent lower (Figure 54 [c]). Decreasing  $K_s$  by 50 percent lowered the transitory time by 20 percent. Varying  $k_d$  by +/- 50 percent minimally influenced steady-state removal (Figure 55 [a]) where total aldehyde removal marginally decreased when  $k_d$  was increased by 50 percent.

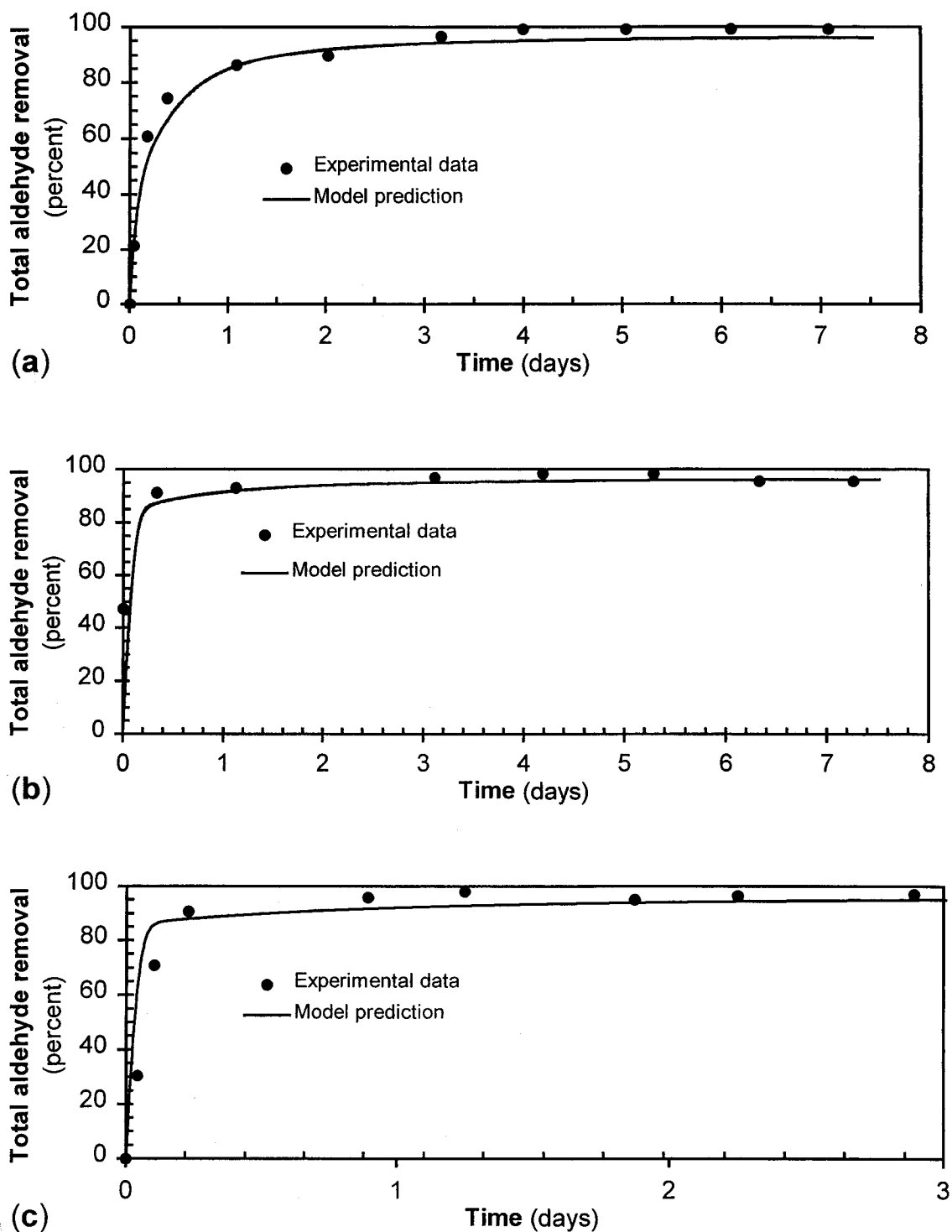


Figure 53. Experimental data and model-predicted profiles for total aldehyde removal when: (a) 1000 mg/L PAC was added (Condition 1, Table 11); (b) PAC was not added (Condition 2, Table 11); and (c) when total aldehyde feed concentration was increased (Condition 3, Table 11)

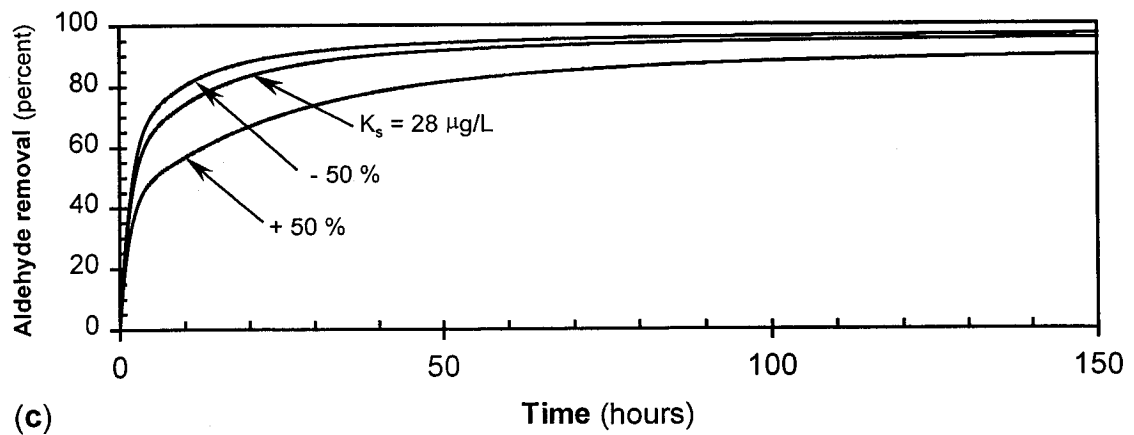
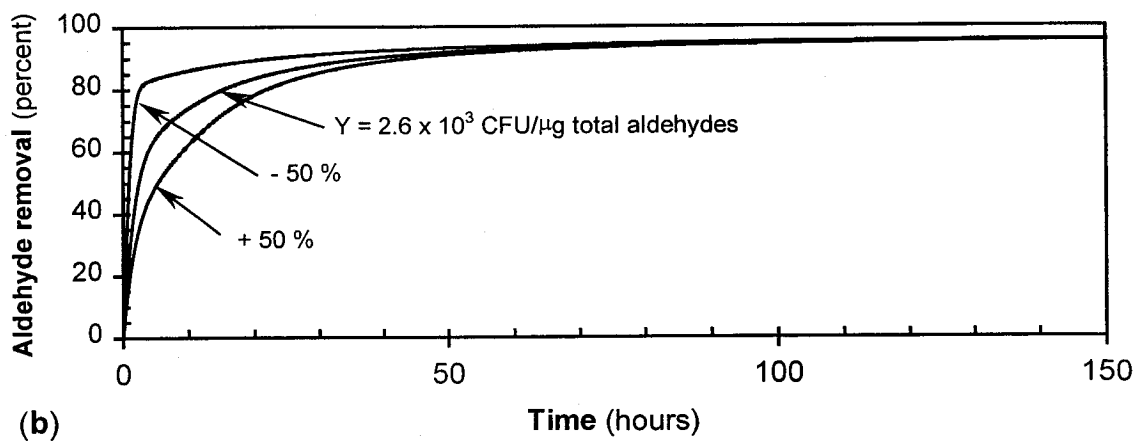
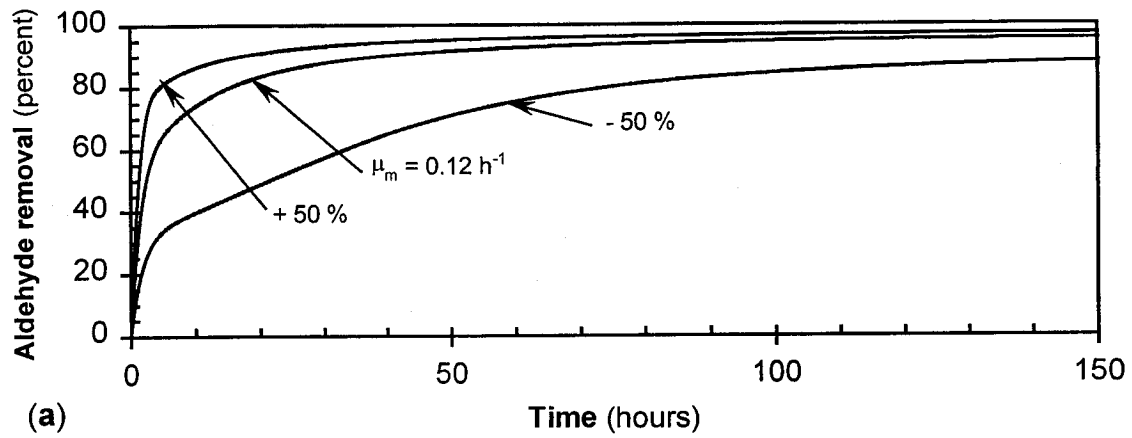


Figure 54. Sensitivity analysis for total aldehyde removal showing model sensitivity to: (a) the Monod maximum rate constant ( $\mu_m$ ), (b) the biomass yield coefficient ( $Y$ ), (c) and the Monod half velocity constant ( $K_s$ )



Model sensitivity analysis showed that the initial active biomass concentration ( $X_0$ ) greatly influenced startup acclimation periods but did not affect substrate removal at steady state. Figure 55 (b) shows that varying  $X_0$  by an order of magnitude influenced the acclimation period, however, when  $X_0$  was increased to levels greater than  $1 \times 10^7$  CFU/mL, the transitory period was minimally influenced. Thus, above certain threshold values, changes in the initial biomass concentration will not affect substrate removal profiles. Varying HRT influenced transient profiles (Figure 55[c]) while a 3 percent and 5 percent reactor solids wasting rate lowered the steady-state total aldehyde removal by 5 percent and 10 percent, respectively (Figure 55[d]).

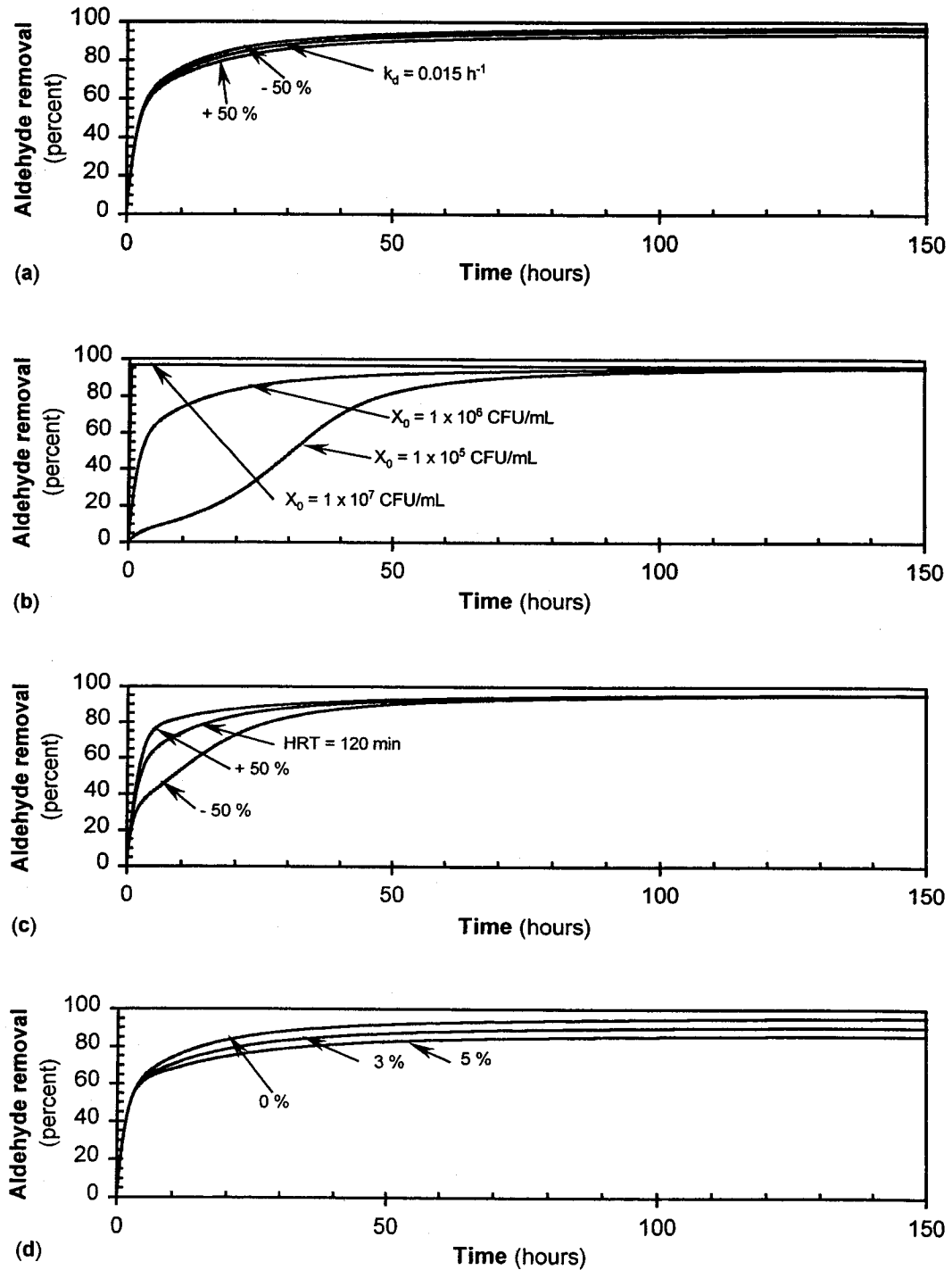


Figure 55. Sensitivity analysis for total aldehyde removal showing model sensitivity to: (a) the endogenous decay coefficient ( $k_d$ ), (b) initial biomass concentration ( $X_0$ ), (c) HRT ( $\theta$ ), and (d) solids wasting rate

## **Prediction/Simulation of DOC and BDOC Removal**

Model-predicted DOC and BDOC profiles were compared to mini-pilot-scale MBR experimental data, over a limited range of operating conditions, where carbon dose and HRT were varied (Table 11). DOC and BDOC removal was modeled using the parameter values listed in Table 12. The modeling assumptions for DOC were: (1) ozonated DOC consisted of a biodegradable and non-biodegradable fraction; (2) the biodegradable fraction was not adsorbable; and (3) the DOC/BDOC ratio was constant over the course of testing.

Experimental data and model-predicted profiles are shown for simulation conditions 4 through 7 (Table 11) in Figure 56. Model predictions and experimental data showed close agreement over the wide range of conditions tested; discrepancies between experimental data and model-predicted profiles were generally less than 10 percent.

Experimental data and model profiles showed close agreement (Figure 56 [a]) when the MBR was operated in a biologically active mode without PAC addition (condition 4, Table 11). Adding 1000 mg/L PAC and acclimated biomass at startup (condition 5, Table 11) resulted in initially higher DOC removal due to adsorption (Figure 56 [b]). However, because PAC had a relatively low capacity for ozonated DOC, PAC was rapidly exhausted and removal decreased to steady state values that were roughly equal to the BDOC fraction (approximately 30 percent). Experimental data and model predictions showed that steady-state values were reached within 1 day. Note that an increased sampling frequency was used during the transitory period when substrate levels were rapidly changing.

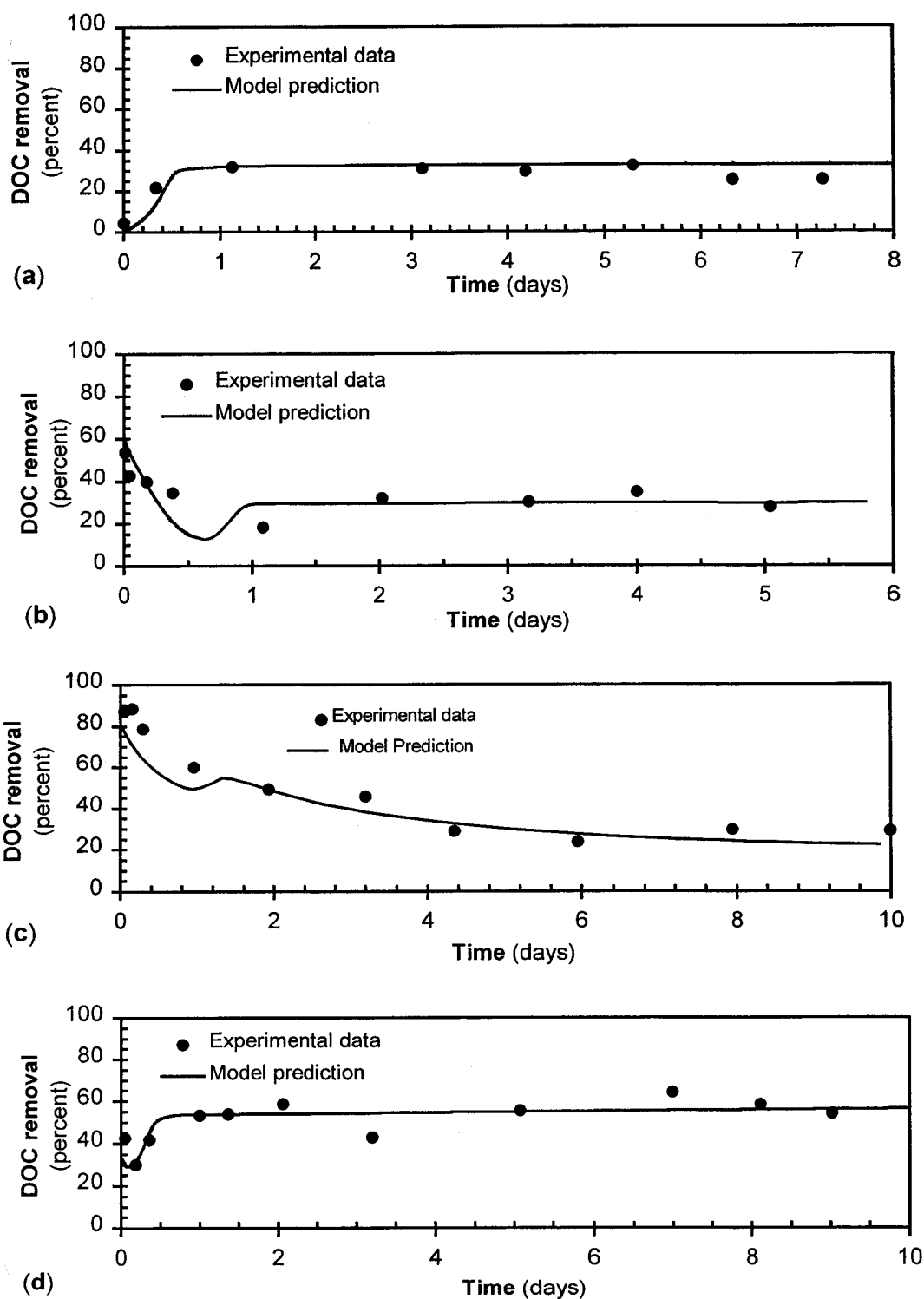


Figure 56. DOC experimental data and model-predicted profiles for: (a) only biomass added (condition 4, Table 11), (b) biomass and 1000 mg/L PAC added at startup (condition 5), (c) biomass and 3000 mg/L PAC added at startup (condition 6), and (d) with continuous PAC addition (condition 7)

Lowering detention time and increasing the initial PAC dose to 3000 mg/L (condition 6, Table 11) showed higher initial removal, as expected, and reached steady-state values within 6-8 days (Figure 56 [c]). Model predictions and experimental data generally showed similar trends, however, there were some discrepancies, most notably in the initial transient period. Model predictions showed a lower initial removal and also predicted a slight peak in the profile after approximately 24 hours. The lower model-predicted DOC removal was likely due to changes in DOC adsorbitivity between the ozonated water used for MBR tests and for isotherm tests. Source water batches used for DOC isotherm analyses were collected roughly 8 months apart and a lower ozone dose was used for MBR testing.

Experimental data and the model profile for a biologically active system, where 3000 mg/L was initially added at startup and 50 mg/L PAC was continually added (condition 7, Table 11), are shown in Figure 56 (d). In this case, model-predictions and MBR data show closer agreement during transient stages while steady-state values show some discrepancy. However, given that measured DOC data are subject to experimental error (e.g., variation in source water quality, ozone dose, and PAC feed rates) as well as analytical error (DOC method precision limit =  $\pm 0.1$  mg/L), model predictions show very good agreement with measured data.

A sensitivity analysis was conducted for BDOC biokinetic parameters (condition 4, Table 11) and for DOC adsorption parameters (condition 5, Table 11). Increasing  $\mu_m$  by 50 percent (Figure 57 [a]), minimally decreased transitory periods and lowering  $\mu_m$  by 50 percent substantially increased the transitory period. Steady-state substrate removal percentages were not affected by variations in  $\mu_m$ . Varying the biomass yield coefficient ( $Y$ ) by +/- 50 percent minimally affected substrate removal. Figure 57 (b) shows that lower  $Y$  values had a greater effect on the transitory region than higher values and steady-state removal was not affected. A similar result was seen for  $K_s$ , (Figure 57 [c]). Varying  $k_d$  by +/- 50 percent had a negligible effect on model profiles (Figure 58 [a]). Changing the initial biomass concentration by an order of magnitude influenced the lag time at startup; however, steady-state profiles were not influenced (Figure 58 [b]). The range of HRTs tested (60 – 180 min) showed a minor effect on BDOC removal (Figure 58 [c]), and there was a negligible change in model profiles when reactor wasting was increased (from a 0-percent baseline) to 5 percent.

Figure 59 shows MBR model sensitivity to variations in the Freundlich adsorption constants ( $K_f$  and  $n$ ) and the surface diffusion coefficient ( $D_s$ ). Note that the profiles shown in Figure 59 are for a bioactive system with PAC and reflect both absorbable and biodegradable DOC removal. The model shows low sensitivity to the changes in all adsorption parameters. Varying  $K_f$  has some effect on DOC removal at startup, however, once the process reached steady state,  $K_f$  did not influence substrate removal.

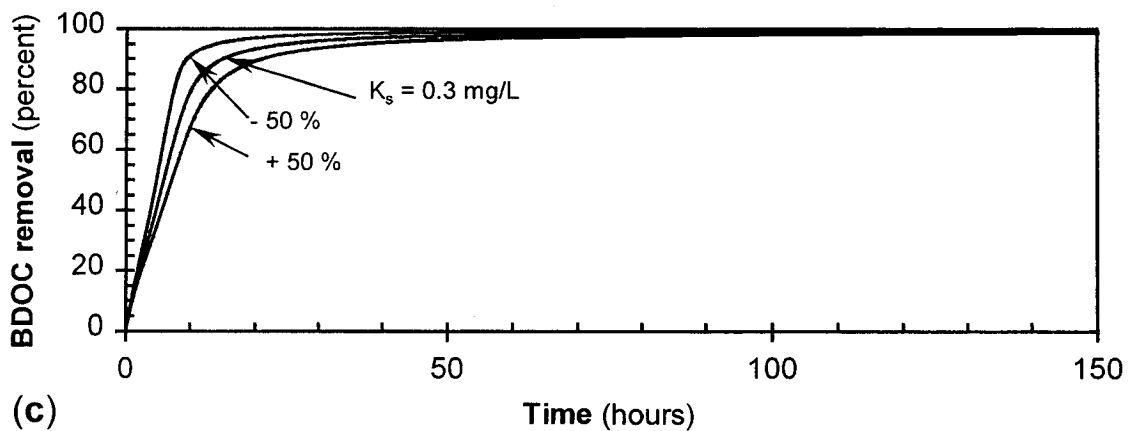
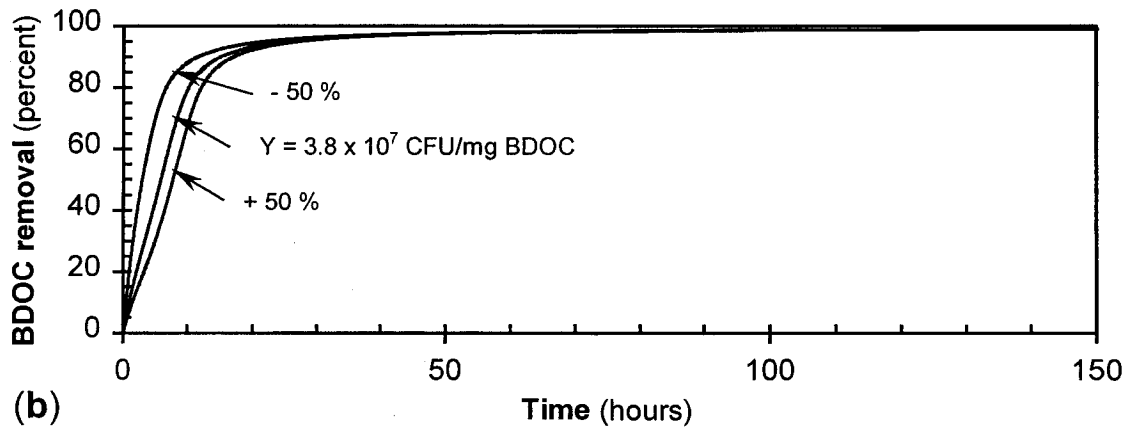
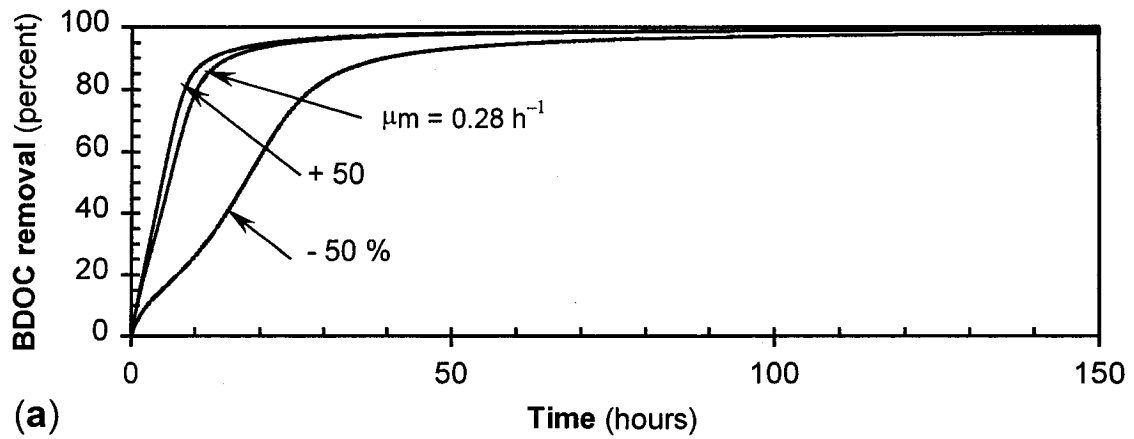


Figure 57. Sensitivity analysis for BDOC removal (condition 4, Table 11) showing model sensitivity to: (a) the Monod maximum rate constant ( $\mu_m$ ), (b) the biomass yield coefficient ( $Y$ ), (c) and the Monod half velocity constant ( $K_s$ )

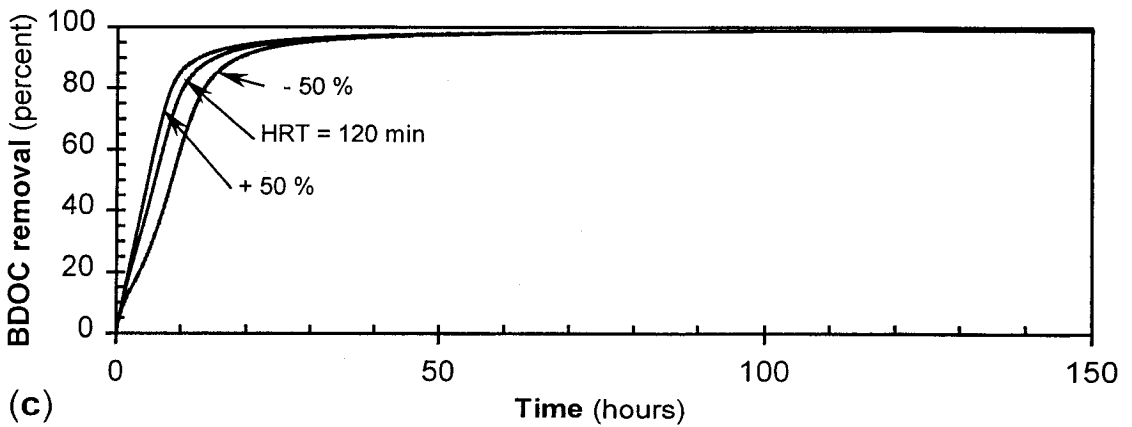
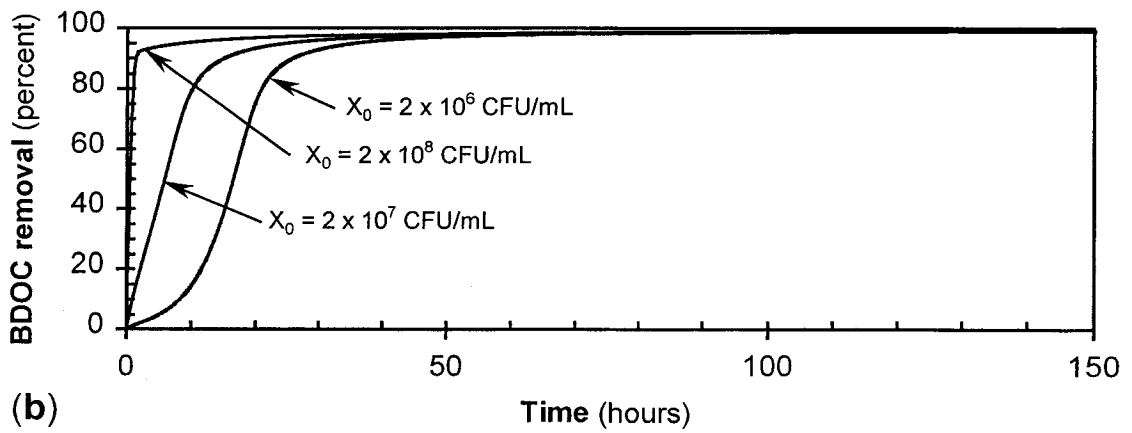
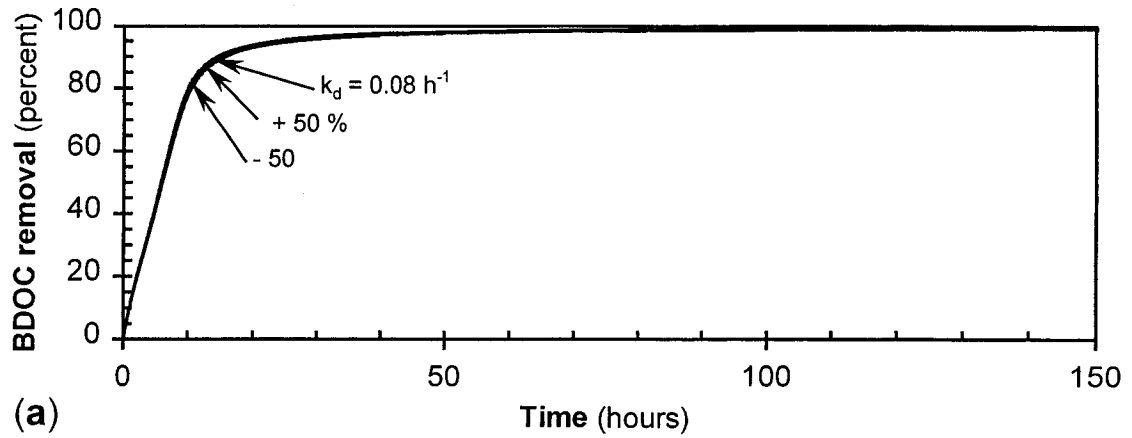
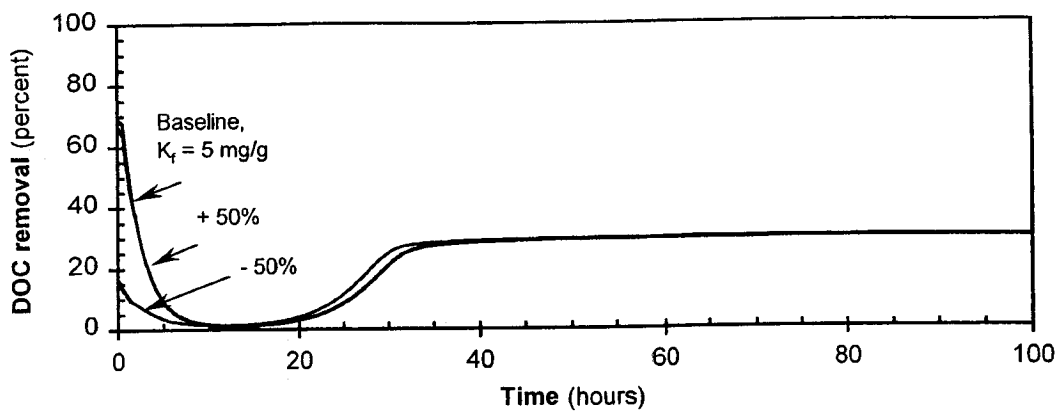
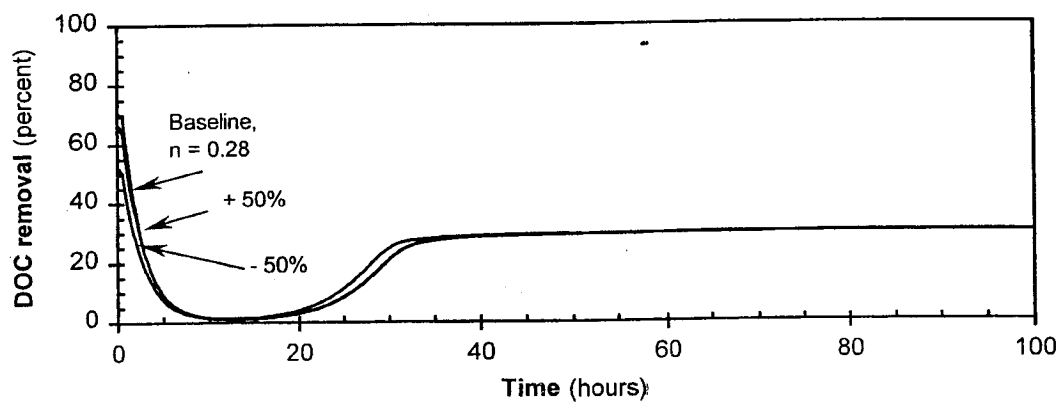


Figure 58. Sensitivity analysis for BDOC removal (condition 4, Table 11) showing model sensitivity to: (a) the endogenous decay coefficient ( $k_d$ ), (b) initial biomass concentration ( $X_0$ ), (c) and HRT ( $\theta$ )

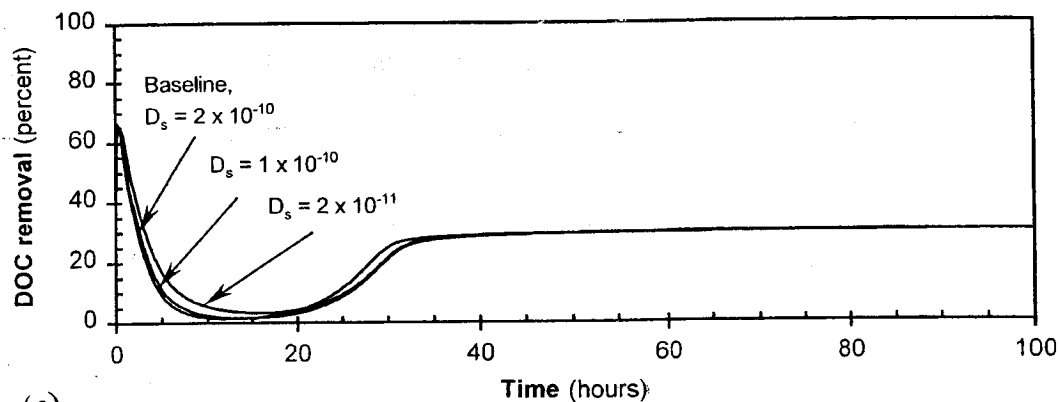




(a)



(b)



(c)

Figure 59. Sensitivity analysis for DOC removal (condition 5, Table 11) showing model sensitivity to: (a) the Freundlich adsorption capacity constant ( $K_f$ ), (b) the Freundlich adsorption intensity coefficient ( $n$ ), and (c) the surface diffusion constant ( $D_s$ )

## Prediction/Simulation of AOC Removal

A single condition was assessed for AOC (condition 8, Table 11) where acclimated biomass and 3000 mg/L PAC were added at startup. Figure 60 shows experimental AOC data along with the model-predicted profile. Measured AOC removal was generally lower than model-predicted values, however, the model-predicted rapid initial uptake and sustained AOC removal trends agreed well with the experimental data. Because a large percentage of the AOC in this water is rapidly degradable<sup>6</sup>, biokinetic constants determined from batch studies reflected the higher degradation rates of the more rapidly degraded fractions. The lower measured AOC values likely reflected the presence of recalcitrant (slowly degradable) AOC that is not completely degraded within the MBR. Furthermore, the relatively low precision of the AOC assay (average AOC precision =  $\pm 30 \mu\text{g/L}$ ) may account for some of the difference in measured data and model predictions.

Figure 61 shows the model sensitivity to variation in AOC biokinetic parameters. Generally, AOC biokinetic parameters showed a moderate to minimal sensitivity to a

---

6. Rapidly-degradable DOC or AOC is loosely defined as the fraction that is removed in the relatively low detention times of a dual-media filter used for conventional biological water treatment. This fraction is sometimes referred to as filter-removable (Carlson et al., 1996). Because a large percentage of the AOC was removed within a relatively short detention time (~2 hours), an operational definition of “rapidly degradable” may be applied to the AOC.

+/- 50 percent variation in the values listed in Table 12. Lowering the Monod maximum growth rate constant ( $\mu_m$ ) by 50 percent (Figure 61 [a]) influenced the transitory period, however, steady state removal was minimally affected. Increasing  $\mu_m$  had a less pronounced effect. Variations in the biomass yield coefficient ( $Y$ ) and Monod half velocity constant ( $K_S$ ) influenced transient profiles, however, minimally influenced steady state removal profiles. Thus, when determining AOC biokinetic constants, higher priority should be given to accurately determining the maximum growth rate constant.

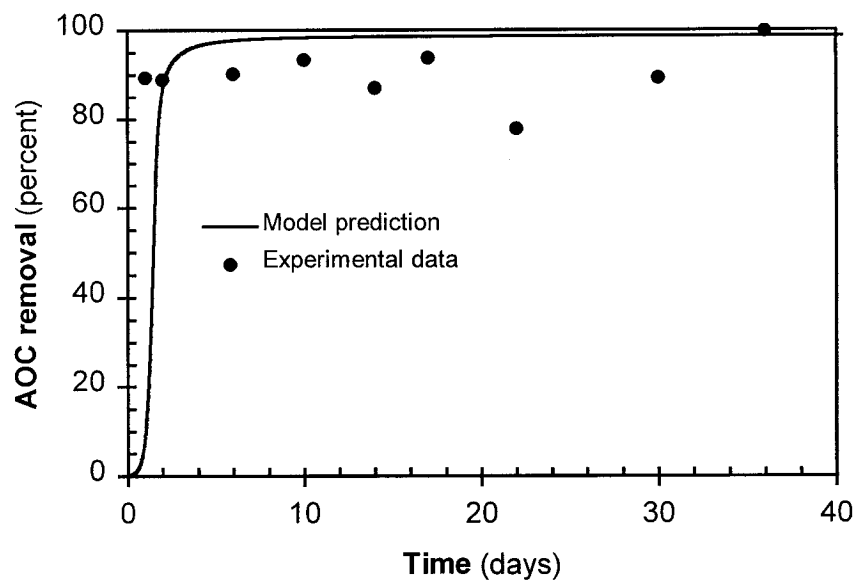


Figure 60. Model simulation of AOC removal showing experimental data and model-predicted profiles

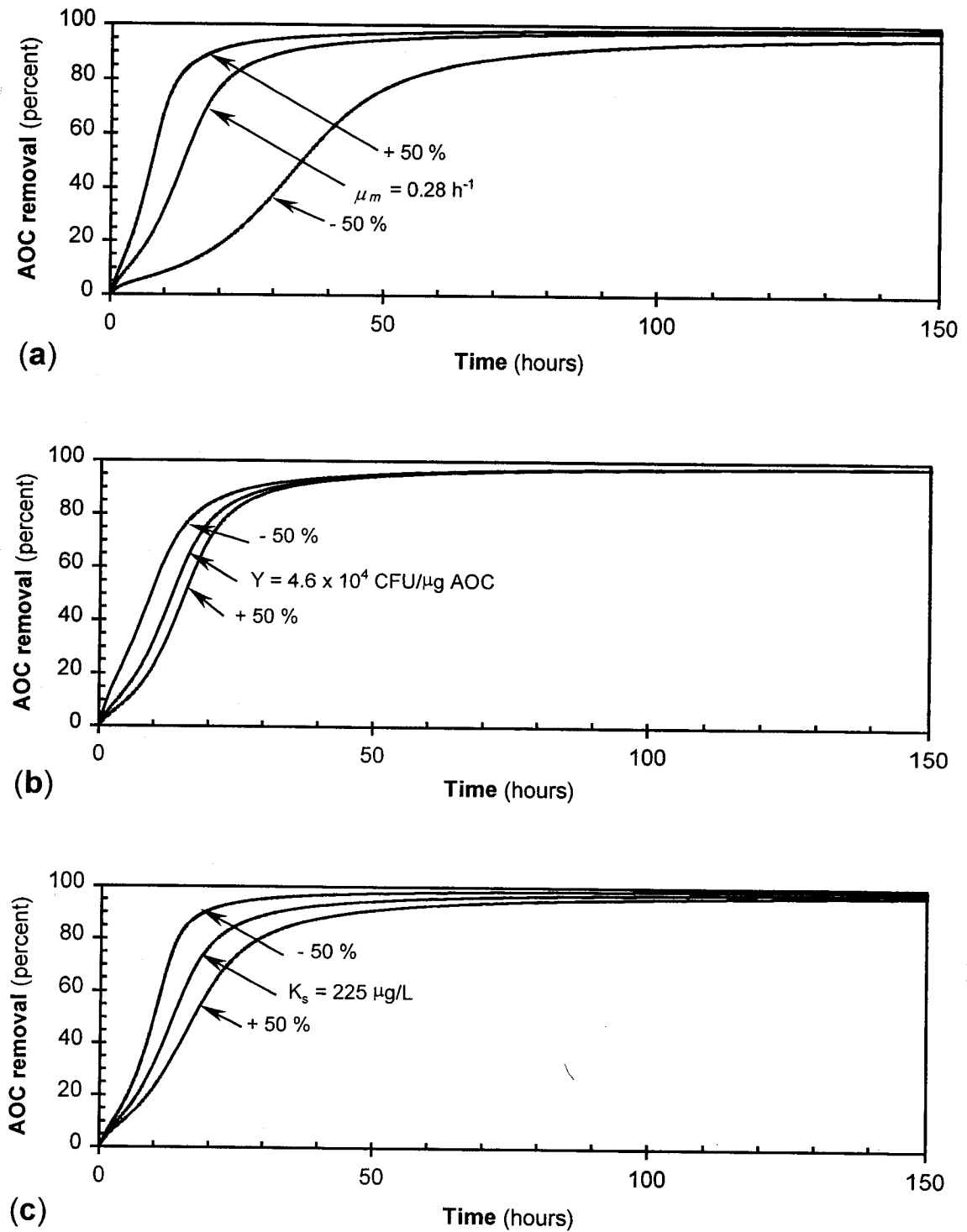


Figure 61. Model sensitivity analysis for AOC removal (condition 8, Table 11) for: (a) the Monod maximum rate constant ( $\mu_m$ ), (b) the biomass yield coefficient ( $Y$ ), (c) and the Monod half velocity constant ( $K_s$ )

## **Biomass Predictions**

An experiment was conducted to provide biomass concentration data for model validation. A biomass inoculum ( $1.6 \times 10^5$  CFU/mL) was added at startup and the process was operated without PAC for 10 days. During the test, samples were collected from the MBR reactor and biomass was enumerated using heterotrophic plate counts. PAC was not added during the test in an attempt to eliminate interferences associated with de-sorbing biomass from PAC. A detachment method (Chapter 3) was used to enumerate biomass growing on PAC. However, subsequent observation using epifluorescence microscopy showed that there was substantial biomass remaining on the PAC after the detachment procedure. Consequently, the direct-count method used for biomass quantitation generally underestimated system biomass when PAC was added. Thus, in the biomass verification study, PAC was not added.

Initially, within the first 6 hours of operation, measured values agreed with model predictions (biomass concentration was predicted using the BDOC calibration constants listed in Table 12). However, as the test progressed, model predictions were substantially higher (two orders of magnitude at steady state) than measured data. While some of the biomass was suspended in solution, an active biofilm was also observed on most other surfaces within the system; in particular on tubing and reactor surfaces which, in relatively small apparatus used for this work, has a higher surface to volume ratio than a larger-scale process. Not adding PAC to the system likely enhanced this phenomenon, as there was less surface area within the bulk fluid for

bacterial attachment. In either case, biofilm attached to reactor and tubing surfaces likely represented a substantial fraction of active biomass in the system and was the reason that measured biomass levels were substantially lower than model predictions.

The phospholipid analysis has been successfully used for quantifying microbial biofilm populations in attached-growth processes (Moll and Summers, 1996). In future studies, although analytically more complex and time consuming, this method may be used as a surrogate for total biomass provided that a suitable calibration for direct counts can be established. However, regardless of the method used, when measuring biomass levels in a bench- or pilot-scale unit, an accurate biomass determination must account for biomass growing on reactor and tubing surfaces.

## **SUMMARY AND CONCLUSIONS**

Model verification analyses were used to establish the efficacy of the MBR model for predicting substrate changes in a real system. Model sensitivity analyses demonstrated the required precision needed when determining model calibration constants.

Additionally, by identifying which parameters had the greatest influence on substrate removal, the model parameter sensitivity analysis provides insight into strategies for MBR process optimization. Model predictions were conducted for total aldehydes, DOC, AOC, and biomass using data measured in the mini-pilot MBR and model calibration constants determined in batch adsorption and biokinetic studies. Based on this analysis, the following conclusions are offered:

1. In the three conditions modeled for total aldehyde removal, MBR model predictions closely agreed with measured data. In all conditions, changes in concentration during the transient stage were high, and steady-state values were rapidly approached. The model accurately predicted both transient and steady state removal (within 5-10 percent of observed values) for all conditions tested, indicating the validity of the batch biokinetic parameters measured. While values for the Monod parameters  $\mu_m$ ,  $K_s$ ,  $Y$ , and  $k_d$  (determined from biokinetic studies) were not varied, values for initial biomass ( $X_0$ ) were adjusted to better fit transient profiles. Accurate measurement of the initial, active biomass is essential to accurately predict transient behavior.
2. In the four conditions modeled for DOC removal, the ozonated DOC was modeled by first establishing the biodegradable fraction, or BDOC. The simplifying assumption was made that BDOC is not adsorbable and this is supported by BDOC batch isotherm data. Although BDOC was considered non-adsorbing for purposes of this model, adsorption most likely does play a role in this system, where adsorption of higher molecular weight BDOC may be masked by its low concentration.
3. Although DOC in ozonated water showed substantially lower adsorptivities than in non-ozonated water, adsorption could not be neglected. Model-predicted DOC removal showed good agreement with experimental data. Because adsorption constants are dependent on ozone dose (and possibly seasonal DOC changes), they

are accurate only under a certain range of operating conditions. This must be taken into account when modeling DOC removal in processes which operate over a wide ozone dose range.

4. Total AOC was modeled as a non-adsorbing substrate. Model simulation results qualitatively predicted the rapid initial uptake although experimental steady-state values were generally lower than model predictions.
5. Model parameter sensitivity analyses, with respect to total aldehyde, BDOC, and AOC removal, showed that process efficiency was most highly influenced by changes in the Monod growth-rate parameters  $\mu_m$  and  $K_s$ , and to a much lesser extent by changes in  $k_d$  and  $Y$ . Total aldehydes showed greater sensitivity to changes in biokinetic constants than BDOC or AOC. Because MBR process efficiency is principally limited by  $\mu_m$ , the process may be optimized by using a more efficient reactor (i.e. plug flow) or by possibly seeding with biomass having a higher  $\mu_m$  value. Furthermore, temperature will likely have a substantial impact on MBR process efficiency because kinetics are controlled by  $\mu_m$ . A single temperature (20°C) was used in the current study; however, future studies should investigate MBR process efficiency at other temperatures.
6. Initial biomass concentration ( $X_0$ ) influenced lag-times at startup; however, changing  $X_0$  did not influence steady-state efficiency. The model showed higher sensitivity to lowering  $X_0$  below baseline values. Higher values did not influence removal to the same extent suggesting that there is an initial biomass threshold,



beyond which there is no effect on model predictions. This is pertinent when modeling processes that have high initial biomass, suggesting that an accurate initial biomass measurement may not be critical for accurate predictions when initial biomass exceeds a certain threshold value. From a practical perspective, it is also important to note that biomass seeding has a limited influence on the transitory period required to reach steady-state and that seeding will not influence the ultimate steady-state removal efficiency.

7. Under the conditions tested, model-predicted DOC removal showed a small response to changes in adsorption constants. Only slight changes were seen when  $K_f$  was increased, and variation in  $n$  and  $D_s$  had a small effect on process efficiency. Adsorption influenced DOC removal only at startup, and due to weak DOC adsorbability, this influence was relatively small. It should be noted that the Freundlich constants,  $K_f$  and  $n$ , are source water specific and, consequently, seasonal water quality changes coupled with process variability (e.g. changes in oxidant dose) may have a significantly greater effect on them. Thus, when modeling DOC adsorption, changes in DOC adsorbability should be given proper consideration in addition to accurate parameter estimation.
8. Analytical methods for measuring total aldehydes are generally more precise than methods for measuring AOC or BDOC. Moreover, adsorption and biokinetic parameters are not influenced by ozone dose or by seasonal water quality changes.

Consequently, total aldehydes are good surrogate for modeling MBR process performance.

9. Measured biomass was substantially lower than model-predicted values due to interference from prolific biofilm growth in the system. Biomass growth was observed on tubing surfaces and reactor walls, and consequently, bulk biomass concentrations were lower than predicted (model assumptions assumed all biomass was in the bulk fluid; either attached to PAC or suspended). Measuring biomass in biofilms is prone to underestimation when using plate-counting methods. Plate counts showed excellent accuracy and sensitivity for measuring suspended organisms, however substantially underestimated biofilm populations, even when bacteria were desorbed from carbon surfaces. Subsequent work should investigate other methods such as phospholipid analysis to more accurately determine the active biomass.

## **Chapter 8 - MBR MODEL SIMULATIONS**

### **OBJECTIVES**

In many cases when a new or unproven process is evaluated, mathematical modeling is used to project large-scale performance based on bench- or pilot-scale operating data.

Modeling provides an inexpensive means to answer questions regarding process efficiency and the impacts of different operating conditions, which otherwise would require testing. However, model-prediction validity is contingent on accurate calibration and an understanding of the pertinent differences between the bench-, pilot-, and full-scale processes. In this chapter, the calibrated MBR model was used to evaluate various operating conditions with respect to total aldehyde, BDOC, and AOC removal efficiency. Model predictions provided an a-priori evaluation of various full-scale operating scenarios. The specific objectives are as follows:

1. Evaluate the effect of startup where high concentrations of active biomass are not initially added to the reactor, and determine the effects of process shutdown for extended periods.
2. Simulate variations in influent substrate level, and evaluate process efficiency.
3. Assess different likely conditions where HRT varies as a function of membrane cleaning cycles, and predict how this effects process efficiency.

## RESULTS AND DISCUSSION

Before representative large-scale simulations can be made using this mini-pilot-scale model, appropriate consideration must first be given to differences between pilot-scale and full-scale conditions. Significant differences may include reactor type and other issues such as mixing energy and mass transfer. The following key issues were considered:

1. Biokinetic and adsorption phenomena (at a fundamental level) are independent of scale, consequently, biokinetic and adsorption constants measured in batch studies are applicable to a full-scale process.
2. Free liquid diffusivity values are not dependent on scale, however, mass transfer rates are. The film transfer rate used from this work ( $k = 0.004 \text{ cm/sec}$ ) is a function of hydraulic energy, which may be quantified using the Reynolds number. Reynolds numbers in a larger-scale process would likely be lower than conditions used in this study. Mixing in the mini-pilot MBR was high ( $Re =$  approximately 10,000; completely turbulent flow), as reactor contents were completely re-circulated less than once per minute. Mixing energies in a demonstration- or full-scale process would likely be substantially lower, and so will the film transfer rate. However, for purposes of this generic evaluation, it was assumed that liquid film mass transfer would not be rate limiting.

3. One of the assumptions of this model is that biofilm thickness on PAC is small and consequently, is not rate limiting. This was verified in experimental work where only sparse biomass was seen growing on PAC (Chapter 4, MBR studies). This assumption provides a great deal of flexibility in modeling because then biomass can be distributed in any ratio between the PAC surface and in bulk solution (from shearing). However this assumption only applies to a completely mixed system. If a substantial fixed-film biomass were to establish (such as in biofilters), active biofilm thickness may increase to the point where diffusion within the biofilm becomes rate limiting. In this instance, model assumptions may no longer be valid and should be re-examined.

MBR process efficiency was predicted for total aldehyde, BDOC, and AOC removal under a range of operating conditions including: taking the process off-line for extended periods, large fluctuations in influent substrate concentration, and large fluctuations in HRT due to membrane cleaning. Model simulations were run using the kinetic constants listed in Table 12 and the initial conditions and operating parameters listed in Table 13.

### **Effects of Inoperation and Shutdown**

A likely scenario for any system is the event of routine or unforeseen maintenance that will require the process to be taken out of service for a period of time. Biological processes are much more sensitive to upset than chemical or physical processes.

Taking a biological filter off-line disrupts the biofilm by eliminating the substrate source. Additionally, long ripening periods (30 to 80 days) are sometimes needed to re-establish biofilters if biofilm is completely lost through long shutdown periods or filter media replacement (Coffey et al., 1995). Although an MBR is not prone to the same upsets as a conventional fixed bed biological filter (e.g. sloughing or exposure to oxidants in filter backwash water), changes in the biofilm metabolic state during process shutdown may be similar in both instances.

Table 13. Operating parameters and initial conditions used for MBR model simulations

Parameter	Units	Value
Initial substrate ( $S_0$ )	$\mu\text{g/L}$	25 (total aldehydes) 500 (BDOC) 300 (AOC)
Initial biomass ( $X_0$ )	CFU/mL	10,000
HRT	min	120
Solids wasting rate	%	0

With the mean HRT = 120 min, and with a low initial biomass concentration ( $1 \times 10^4$  CFU/mL), steady-state conditions would be reached generally within 5-10 days for total aldehyde removal, and less than 5 days for BDOC removal (Figure 62 and Figure 63). After a 10-day shutdown, and while retaining the reactor contents, model-predictions show that the process will re-establish itself within 1 to 3 days. Note that

this scenario assumes substrate-limiting conditions where the culture would be maintained in an aerobic environment to prevent a shift to anaerobic metabolism. After shutdown, model-predictions showed a logarithmic biomass decrease; however, biomass maintained a relatively high concentration ( $1.5 \times 10^7$  CFU/mL) after the 10-day shutdown (Figure 64).

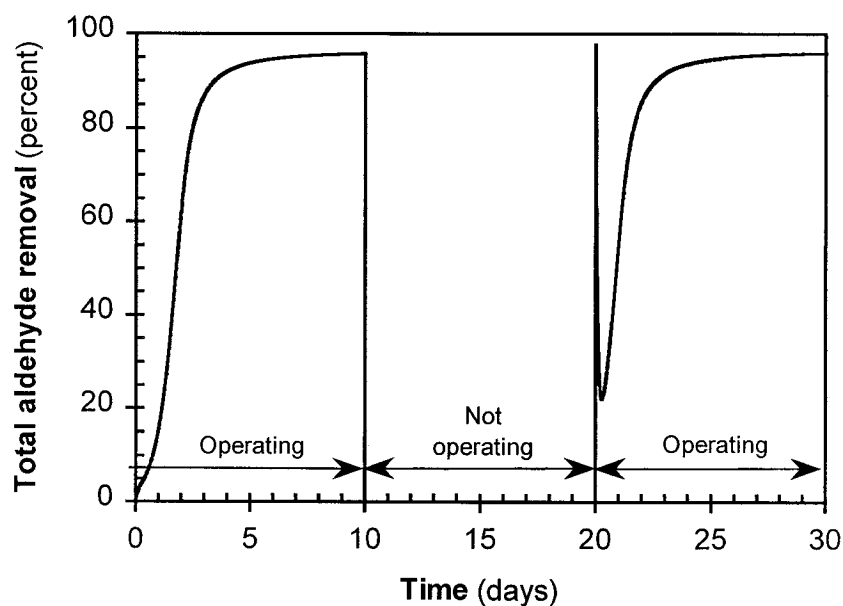


Figure 62. Effect of system shutdown on total aldehyde removal; reactor contents were not wasted during the 10-day shutdown period; model predictions assumed that only the organic substrate was limiting, and not mineral nutrients or oxygen

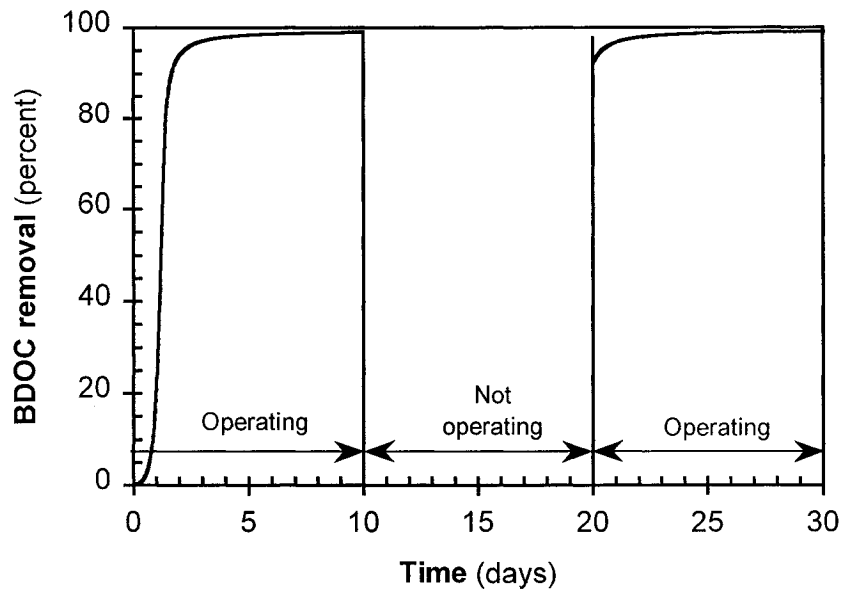


Figure 63. Effect of system shutdown on BDOC removal; reactor contents were not wasted during the 10-day shutdown period; model predictions assumed that only the organic substrate was limiting, and not mineral nutrients or oxygen

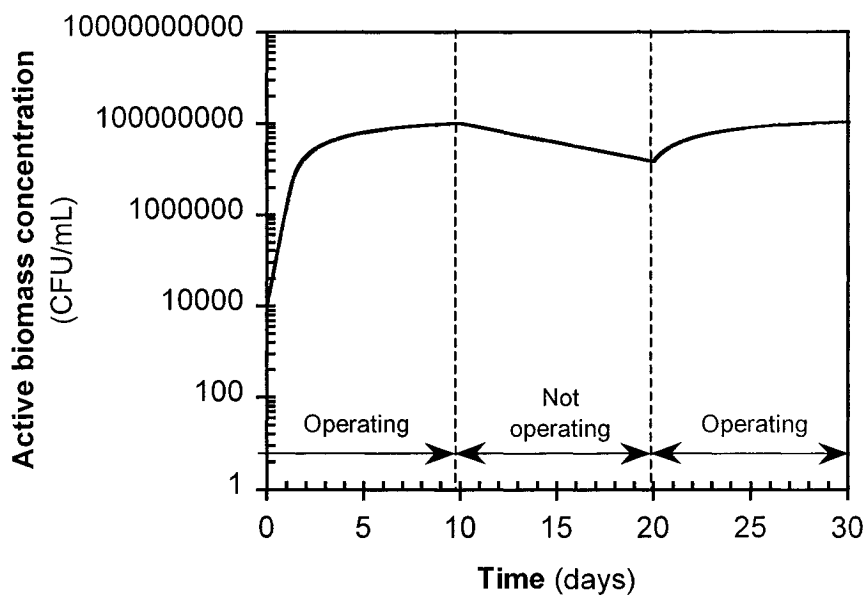


Figure 64. Biomass profile showing effects of process shutdown for a system that initially had low biomass concentrations; model predictions assumed that only the organic substrate was limiting, and not mineral nutrients or oxygen



## Changes in Substrate Concentration

Increases in substrate concentration may occur from seasonal water quality changes, varying applied ozone doses, or a combination of both. Model runs used stepped influent substrate increases to assess process response to increased substrate loading. Although substrate changes in a real system would not occur as abruptly, this provides a worst-case condition and gives insight into process robustness. Lower-bound substrate loadings represented the average values measured in this work, and upper-bound values were well above concentrations found in most waters (Bradford et al., 1994; Kaplan et al., 1994).

Simulations assessed process response from increases in total aldehydes, BDOC, and AOC. Figure 65 shows process response to a stepped increase in total aldehyde influent concentration over a range from 25  $\mu\text{g/L}$  to 150  $\mu\text{g/L}$ . Generally, total aldehyde removal initially decreased and then re-established steady state after several days; although steady-state removal decreased as substrate loading increased. In the last step (Figure 65), the total aldehyde feed concentration was increased from 100  $\mu\text{g/L}$  to 150  $\mu\text{g/L}$  and there was a substantially longer stabilization period (approximately 10 days) and lower steady-state removal (75 percent).

Increasing influent BDOC by an order of magnitude (from 0.2 to 2.0  $\text{mg/L}$ ) had a much smaller impact on removal efficiency (Figure 66). In all cases, steady-state operation was re-established within 2-3 days after substrate loading was increased, and BDOC removal remained high (97 percent) at high substrate loadings. Conversely, increasing AOC loading had a more pronounced effect (Figure 67). Influent AOC concentrations were increased from a 50- $\mu\text{g/L}$  initial concentration to a 1500- $\mu\text{g/L}$  upper bound—a

range that is not unreasonable in a system treating high-DOC water that would intermittently use ozone<sup>7</sup>, producing high AOC as a result. Relatively long stabilization periods (approximately 10 days) were needed to reach equilibrium. In the last step, where influent AOC more than doubled, nearly 20 days was need to reach steady state, and removal efficiency dropped to 60 percent. In this case, longer residence times would be needed to produce a biologically stable water.

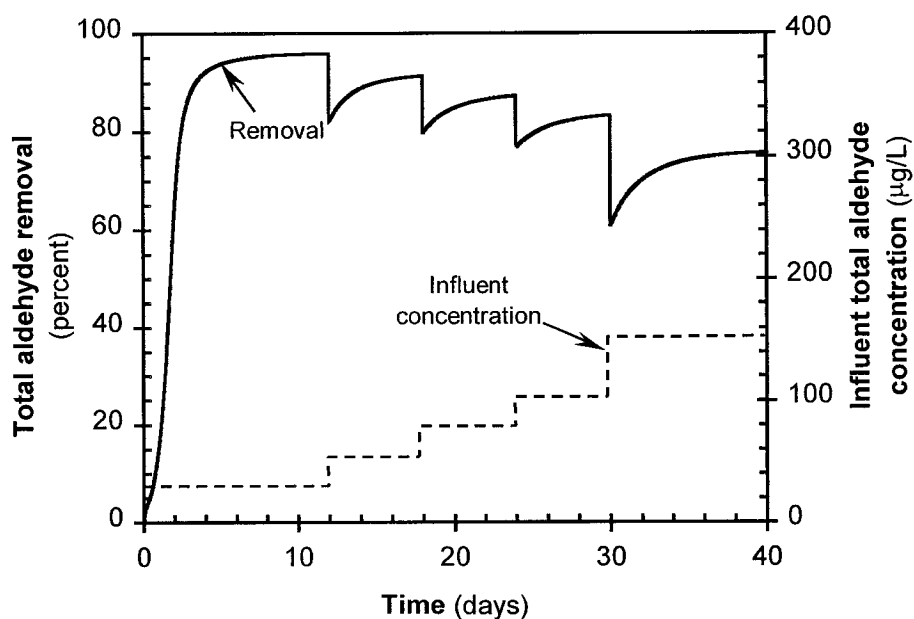


Figure 65. Effect of increasing influent concentration on total aldehyde removal

---

7. Ozone may be intermittently used for oxidizing micro-pollutants or taste and odor compounds. Alternately, a utility may use ozone oxidation intermittently for THM control or disinfection, however, it would most likely be used continuously for these applications.

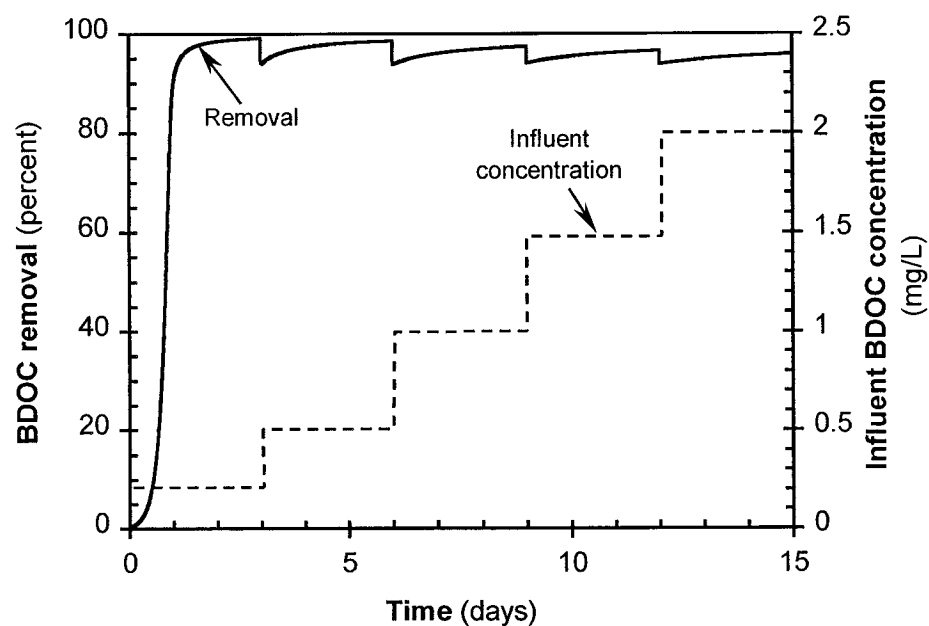


Figure 66. Effect of increasing influent concentration on BDOC removal

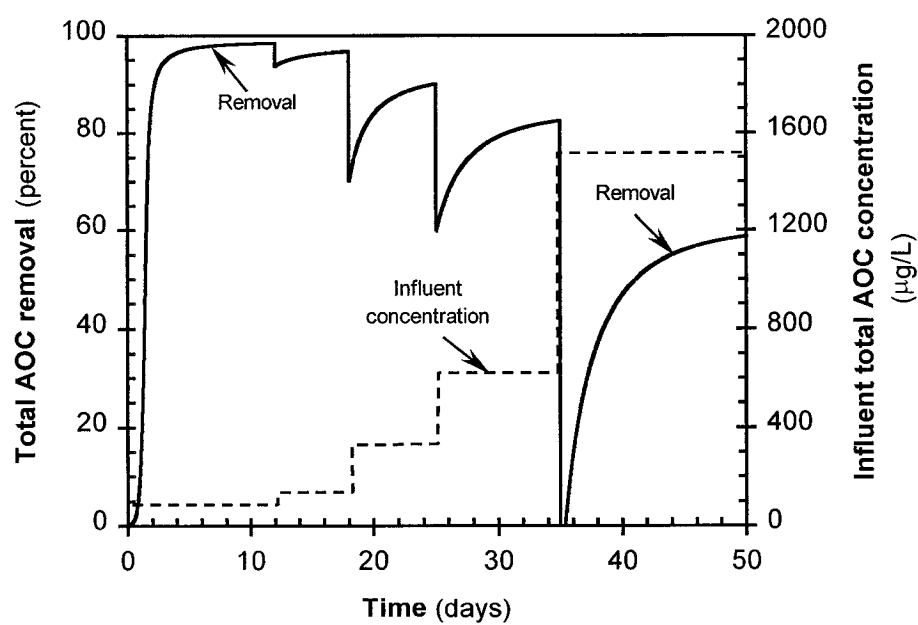


Figure 67. Effect of increasing influent concentration on AOC removal

## **Effects of Varying Hydraulic Residence Time**

Hydraulic residence time in the MBR process is governed by membrane flux.

Membranes may be operated under constant flux conditions, by increasing TMP over time, or using a constant TMP where flux decreases over time. Operating using constant TMP is most common and has been used by others for pilot- and full-scale MBRs (Muller et al., 1995; Urbain et al., 1996). Figure 68 shows the effect of operating under constant-TMP conditions, on HRT. At the beginning of the run, flux was high and as the run continued, HRT increased as a function of flux decline. The HRT profiles shown in Figure 68 were empirically established based on the membrane flux data measured in mini-pilot studies. Figure 68 shows that, over the course of a cleaning cycle, HRT varied over an order of magnitude. When the cleaning interval increased, HRT variation was even greater.

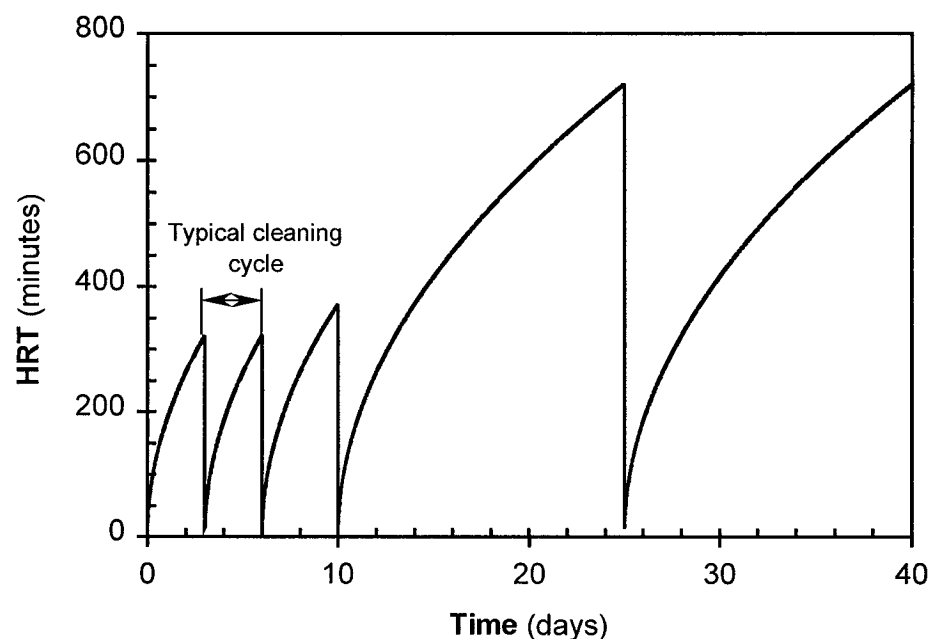


Figure 68. Effect of membrane cleaning on reactor HRT when operating at constant trans-membrane pressure

Varying HRT impacts substrate removal by changing substrate loading. Figure 69 and Figure 70 show the model-predicted total aldehyde and BDOC removals, respectively, when operating using a variable HRT (Figure 68). As expected, substrate removal decreased at low HRTs (immediately after membrane cleaning), however, to a much greater extent with total aldehydes than BDOC. At 3-day cleaning intervals, total aldehyde removal efficiency decreased by approximately 60 percent during the transitory startup period, and by over 60 percent once the process had reached steady state.

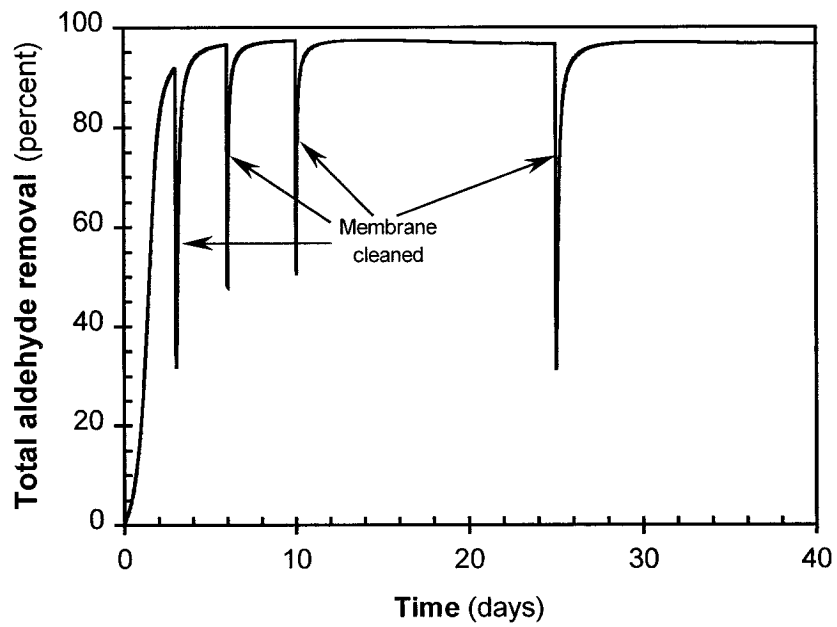


Figure 69. Effect of membrane cleaning and varying reactor HRT on total aldehyde removal

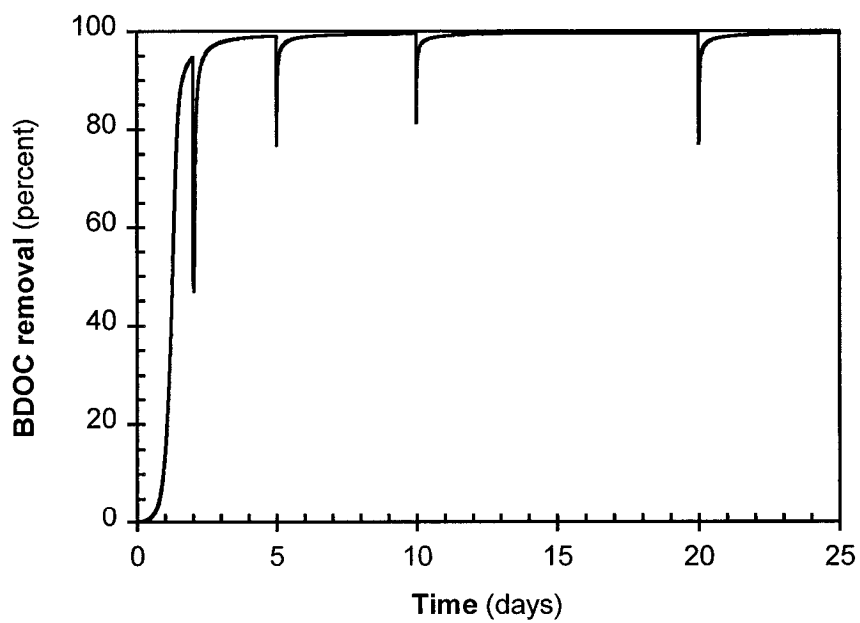


Figure 70. Effect of membrane cleaning and varying reactor HRT on BDOC removal

Increasing cleaning intervals to 15 days magnified this effect and model-predicted substrate removal decreased by approximately 70 percent immediately after cleaning. BDOC removal showed less sensitivity to HRT. During startup, membrane cleaning may reduce BDOC removal by as much as 50 percent; under steady-state conditions, perturbations decreased to approximately 20 percent. Moreover, the length of cleaning interval appears to have no effect on spikes in BDOC removal immediately after membrane cleaning.

## **SUMMARY AND CONCLUSIONS**

Hypothetical predictions were made using an MBR model calibrated to mini-pilot scale operating data. Predictions sought to assess the effects of three likely real-world operating conditions: first, the process would likely be taken off line for extended periods; second, influent substrate may vary seasonally and as a function of ozone dose; and third, changes in HRT as a function of membrane flux decline and sudden decreases in HRT after membrane cleaning. The findings of this chapter are summarized as follows:

1. Model-predictions generally showed that BDOC removal was less affected by process upsets than total aldehydes or AOC removal.

2. Taking the process off-line for 10 days resulted in biomass decrease, however, this decrease was less than an order of magnitude. After startup, the process reached equilibrium within a day for BDOC removal and within 5 days for total aldehydes.
3. Increasing substrate concentration affected total aldehyde and AOC removal efficiency to a much greater extent than BDOC removal efficiency. At high substrate loading, removal decreased by 20 percent and 40 percent for total aldehydes and AOC, respectively. Conversely, steady-state BDOC removal efficiency marginally decreased at high substrate loading.
4. When operating membranes under constant trans-membrane pressure, permeate flux substantially decreased over the first several days of operation (with a concomitant increase in HRT). This affected substrate removal by varying HRT where substrate removal decreased at low HRT values after membrane cleaning. Total aldehyde removal efficiency was impacted to a much greater extent by HRT than BDOC.



## **Chapter 9 - SUMMARY, CONCLUSIONS, AND FUTURE WORK**

### **SUMMARY AND CONCLUSIONS**

This research evaluated an MBR process combined with pre-ozonation for removing DOC and lowering halogenated by-product formation in potable water. Ozonation studies were first conducted to determine the magnitude of ozone by-product formation and to evaluate suitable BOM surrogates for mathematical modeling. A comprehensive series of tests were conducted using a bench-scale and mini-pilot-scale MBR process treating pre-ozonated water that exhibited high AOC formation potential and high THM formation potential. These tests evaluated the MBR process efficiency for removing total aldehydes, DOC, AOC, and THM precursors at different PAC doses, varying HRTs, and at different pH levels. A mathematical model was developed that predicted substrate removal in the MBR process. The combined adsorption/biofilm model was calibrated using parameter constants measured in adsorption isotherm, adsorption rate, and biokinetic studies. The calibrated model was then verified for predicting total aldehyde, DOC, and AOC removal using data measured in MBR experiments. The calibrated model was then used to predict MBR process performance under a wide range of hypothetical large-scale operating conditions.

## **MBR Studies**

The MBR experiments involved: (1) conducting semi-batch ozone studies to measure ozone by-product formation; (2) conducting bench-scale MBR studies under controlled conditions to determine suitable ranges of operating variables; and (3) conducting extensive mini-pilot-scale MBR studies to evaluate process performance over a range of operating variables.

Semi-batch ozone studies were first conducted to evaluate the effect of ozone oxidation on organic constituents, and to assess the magnitude of ozone byproduct formation.

Semi-batch tests measured ozone byproduct formation as a function of ozone exposure.

Constituents measured included: total aldehydes, THMs, DOC, and AOC. Bench-scale MBR tests were then conducted to assess suitable ranges of operating variables (e.g., HRT and rates of membrane fouling), and to conduct control experiments (e.g., tests using a sterilized, non-biologically active apparatus) not possible on a larger scale.

Bench-scale testing used ozonated water and synthetic water spiked with high aldehyde concentrations. Based on these initial laboratory MBR tests, a mini-pilot MBR was designed, constructed, and operated under pilot conditions.

Extensive mini-pilot testing was conducted using ozonated feed water to evaluate effects of the pertinent MBR operating variables including: the role of PAC in the reactor, effects of HRT, sensitivity to influent substrate concentration, and effects of

reactor wasting. These tests were used to both evaluate the MBR process and to provide an independent data set that would later be used as basis for numerical model validation. The major conclusions from MBR testing were:

- Based on extensive mini-pilot-scale testing, MBRs can achieve very high removals of biodegradable organic carbon and ozone by-products (as measured by total aldehydes, BDOC, and AOC); PAC doses may be adjusted, as needed, to enhance THM precursor removal. Membrane fouling is highly dependent on operating conditions. Adding activated carbon lowered flux-decline rates, however when reactor solids were not wasted, fouling rates increased precipitously. When operated without PAC addition, the MF membrane rapidly fouled. Continuously adding low PAC doses (5 mg/L) combined with a low reactor wasting rate drastically reduced fouling. Continuous PAC addition likely sequesters suspended solids, including biomass, that would otherwise foul the membranes.
- Pre-ozonation did not remove DOC, however pre-ozonation did increase BDOC, AOC, and aldehyde concentrations. THMFP was marginally lowered at high ozone exposures.
- When acclimated biomass was added to the MBR at startup, relatively low acclimation times were needed and steady-state operation was generally achieved within several days. DOC was removed through biodegradation and PAC adsorption. There was a direct correlation between DOC removal by PAC and

THM precursor removal. When PAC was not continually added, exhaustion occurred very rapidly, and the predominant removal mechanism was biodegradation. Nearly 50 percent of the DOC was degradable in some cases, however, removal varied as source water and ozone doses changed.

- Aldehydes, including formaldehyde, acetaldehyde, glyoxal, and methyl glyoxal, were ubiquitous ozone by-products and were removed to levels consistently near or below detection limits. Acclimation periods for aldehyde removal were short, generally less than a day. Thus, aldehydes were found to be a good surrogate for BOM. Furthermore, aldehyde analysis is faster, and has a higher precision than bioassays (AOC and BDOC).
- Pre-ozonation enhanced permeate flux through either NOM oxidation or enhancing micro-flocculation.

### **MBR Model Development**

A mathematical model of the MBR process was developed to predict process efficiency for biodegradable and adsorbable substrate removal. Process hydrodynamics, including the membrane-recycle loop, were modeled as an ideal CSTR, and the MF membrane was assumed to completely retain suspended solids within the process, including biomass and PAC. Biodegradation was modeled using single-component Monod kinetics, and the Freundlich and HSDM adsorption models were coupled to describe adsorption onto PAC. A series of governing equations was developed and

solved using finite-difference numerical methods. A model code was implemented using Mathematica<sup>®</sup> software. The major conclusions of the model development section were:

- In biological drinking water treatment processes, organic substrate loading is several orders of magnitude lower than in domestic wastewater processes and, consequently, biomass production would be low. The concept of  $S_{min}$ , or the minimum substrate concentration, has been used to model biofilm processes in low-substrate waters, however, would not likely limit biodegradation in an MBR to the same extent as in a conventional fixed-film biological process.
- Due to the relatively high-energy environment, biofilm shear rates would be high, and coupled with low biomass levels, dense biofilms are not likely to develop on PAC. Additionally, sheared biomass is retained within the system and is considered as part of the active biomass. Based on this, mass transport is limited by biokinetic reaction and surface diffusion within PAC, and not by diffusion through biofilms. With this assumption, the total biomass may be distributed in any proportion between the PAC and bulk fluid.

### **Biokinetic and Adsorption Parameter Estimation**

MBR model calibration constants were measured in a series of adsorption isotherm, adsorption rate, and biokinetic experiments. Batch adsorption equilibrium tests were

used to calculate the Freundlich isotherm constants ( $K_f$  and  $n$ ) and experimental data from adsorption rate studies were used to estimate the surface diffusivity constant ( $D_s$ ). Batch biokinetic studies estimated the Monod kinetic parameters ( $\mu_m$ ,  $K_s$ ,  $Y$ , and  $k_d$ ) for substrates in natural and synthetic waters. The main conclusions of these studies were:

- Ozone substantially lowered DOC and THM precursor adsorbitivity when compared to non-ozonated water. Ozone oxidation lowered NOM adsorbitivity by oxidizing organics to lower molecular weight, hydrophilic end products. When modeling the adsorbitivity of non-specific parameters such as DOC, THM precursors, and AOC, the effect of ozone dose, and possibly seasonal changes that affect NOM composition and character, on adsorbitivity must be considered. Thus, depending on the modeling objective, a single calibration value for adsorption parameters should not be relied upon for modeling processes subject to large variations in ozone dose or for processes, which experience drastic seasonal variations in source water NOM composition.
- Formaldehyde and acetaldehyde had no adsorption affinity for the PAC used, whereas glyoxal and methyl glyoxal showed weak adsorbability when measured in carbonate-buffered synthetic water and at high concentration. In ozonated water, AOC isotherms exhibited heterogeneity, where a portion of the AOC adsorbed at low carbon doses and the remaining AOC did not adsorb. Though, over the wide

range of PAC doses used, AOC was effectively non-adsorbable. Similarly, BDOC did not appreciably adsorb. This result simplifies DOC modeling, as the BDOC fraction can then be modeled separately from the adsorbable DOC fraction.

- Adsorption rate studies, which used the HSDM to predict adsorption kinetics, yielded similar  $D_s$  values ( $2 \times 10^{-10}$  cm<sup>2</sup>/sec) for both DOC and THM precursors. Both DOC and THM precursor rapidly adsorbed to PAC, where 90 percent of the equilibrium value was reached within 5 min.
- Replicate biokinetic tests (measured in different waters) showed reproducibility for most BDOC biokinetic constants, however microbial yields measured in low-DOC water were higher than high-DOC water. AOC levels were nearly as high as BDOC levels in the waters tested and microbial yields for AOC and BDOC were similar. Maximum growth rates and biomass yields were lower for aldehydes when compared to values measured for BDOC.
- During batch biokinetic studies, only a marginal decrease in THM precursors was observed and accurate calculation of Monod kinetic parameters was not possible. However, THM precursor degradation was measured in the MBR. Degradation of THM precursors during biological filtration is crucial for many utilities to meet strict regulations. As a result, additional effort should be invested in this area to develop other techniques for modeling THM precursor degradation.
- Finally, while adsorption and biodegradation constants measured for non-specific parameters (i.e., DOC, BDOC, and AOC) may vary, these constants are not likely

to vary substantially for specific parameters (e.g., total aldehydes). For this reason, and because of the higher analytical precision, total aldehydes (or other specific BOM components such as carboxylic acids or aldoketo acids) are a better choice as a surrogate parameter for modeling filter-removable BOM.

### **Model Verification and Sensitivity Analysis**

The MBR model was calibrated using constants measured in adsorption and biokinetic studies. Model verification comparisons were made for total aldehydes and DOC using data measured in the mini-pilot-scale MBR. A model parameter sensitivity analyses provided an estimate of the needed precision for model calibration constants.

Additionally, by identifying which parameters had the greatest influence on substrate removal, the model parameter sensitivity analysis provided insight into strategies for MBR process optimization. Adsorption and biokinetic constants were varied by +/- 50 percent from baseline values, and in some cases an order-of-magnitude variation was used. The following conclusions are based on the model verification and parameter sensitivity analysis:

- The model accurately predicted total aldehyde transient and steady state removals for all conditions tested. While values for the Monod parameters  $\mu_m$ ,  $K_s$ ,  $Y$ , and  $k_d$  were not changed, values for initial biomass were estimated in some cases.



Accurate measurement of the initial, active biomass is essential to accurately predict transient behavior, but does not influence steady-state values.

- Ozonated DOC was modeled by first establishing the biodegradable fraction, or BDOC. Model-predicted DOC removal showed good agreement with experimental data. Verification results qualitatively predicted the rapid initial AOC uptake, although the measured steady-state values were generally lower than model predictions. AOC and BDOC heterogeneity may influence modeling accuracy when there is a large difference in either adsorbitivity or biodegradability among the various fractions.
- Process efficiency was greatly influenced by changes in the Monod growth-rate parameters  $\mu_m$  and  $K_s$ , and to a much lesser extent by changes in  $k_d$  and  $Y$ . Total aldehydes showed greater sensitivity to changes in biokinetic constants than BDOC or AOC. Because MBR process efficiency is principally limited by  $\mu_m$ , the process may be optimized by using a more efficient reactor (i.e. plug flow) or by possibly seeding with biomass having a higher  $\mu_m$  value.
- Initial biomass concentration ( $X_0$ ) influenced transient times at startup; however, steady-state efficiency was not influenced by changing  $X_0$ . The model showed higher sensitivity when  $X_0$  values were lowered. Higher values did not influence removal to the same extent suggesting that there is an initial biomass threshold (approximately  $1 \times 10^7$  CFU/mL), beyond which there is a negligible effect on model predictions. This is relevant to modeling processes with high initial

biomass; suggesting accurate initial biomass measurements may not be needed for accurate predictions. From a practical perspective, it is also important to understand that biomass seeding has a limited influence on the transitory period required to reach steady-state and that seeding will not influence the ultimate steady-state removal efficiency.

- Only slight changes were observed when the Freundlich equilibrium capacity constant ( $K_f$ ) was increased, and variation in Freundlich adsorption intensity coefficient ( $1/n$ ) and the surface diffusion coefficient ( $D_s$ ) had a small effect on process efficiency. Adsorption influenced DOC removal only at startup, and due to weak DOC adsorbability, the influence was relatively small. When modeling DOC adsorption, changes in DOC adsorbability should be given equal consideration in addition to accurate parameter estimation.

### **MBR Model Simulations**

Model predictions were used to assess the effects of hypothetical operating conditions on MBR process performance. The operating factors assessed were: (1) effects of extended periods of inoperation, (2) effects of changing influent substrate concentration, and (3) changes in HRT as a function of membrane flux decline and sudden decreases in HRT after membrane cleaning. The principal conclusions were:

- Taking the process off-line for 10 days resulted in a biomass decrease, however this decrease was less than an order of magnitude. After startup, model-predictions showed that the process reached equilibrium within a day for BDOC removal, and within 5 days for total aldehydes.
- Model predictions showed that increasing substrate concentration affected total aldehyde and AOC removal efficiency to a much greater extent than BDOC removal efficiency. At high substrate loading, model-predicted removal decreased by 20 percent and 40 percent for total aldehydes and AOC, respectively. Conversely, steady-state BDOC removal decreased by 3 percent at high substrate loading. At low HRTs after membrane cleaning, substrate removal was lowered. Total aldehyde removal was impacted to a much greater extent by HRT than was BDOC removal.

## **FUTURE WORK**

The MBR process is a promising technology for treating potable water sources having high THM formation or with high BDOC levels. The scale of studies conducted in this work provided a proof of concept and a preliminary assessment of operating strategies to minimize membrane fouling and maximize BOM removal. The recommendations for subsequent investigations are:

- Additional refinement of the MBR model should include membrane flux modeling.

As demonstrated in this study, flux is highly dependant on operating conditions and due to the heterogeneous nature of the filtered solids, long-range predictive modeling may not be feasible as the resistance of the membrane fouling layer may drastically change. Accurate membrane flux models would likely need re-calibration to specific operating conditions. The effects of filtration cakes and condensed organics on the membrane surface should be examined as these factors may also influence removal. Modeling also provides a powerful tool for evaluating a wide range of operating conditions as well as process scale up. Future MBR model refinements should also address MBR scale-up issues, in particular, the effects of large-scale bioreactor configurations on mass transport and process.

- Nonspecific BOM parameters (AOC and BDOC) can not be modeled as accurately as specific BOM surrogates (total aldehydes). Although AOC and BDOC provide a broader measure of BOM, these parameters may be overly influenced by operational (e.g., ozone dose) and seasonal changes. Moreover, analytical precision of the AOC and BDOC methods is generally lower than for specific surrogates. Future investigations should also consider other specific BOM constituents (e.g., carboxylic acids) for use as a BOM surrogate and indicator of MBR efficiency.
- Additional effort should be invested to accurately model THM precursor degradation. Degradation of THM precursors during biological filtration is crucial for many utilities to meet strict regulations and the capability to predict removal

would benefit MBR optimization. Furthermore, removal of HAA precursors and other DPBs (e.g., bromate) should be investigated.

- Ultimately, economics will dictate the viability of MBRs for municipal water treatment. Additional research is needed at larger (pilot or demonstration) scales to thoroughly evaluate operating efficiencies and economics. Further testing is needed to evaluate effects of membrane type (i.e., polymeric vs. ceramic), membrane configuration (i.e., hollow fiber vs. tubular), and optimal strategies for in-situ membrane cleaning including frequent hydraulic back pulsing. Additional studies should also examine process efficiency at varying temperatures. This study has demonstrated that operating strategy has a substantial impact on membrane flux and, ultimately, on process economics and viability. The ranges of process recoveries and PAC addition strategies used in this work should be used as a baseline for further refinement in subsequent optimization studies.

## REFERENCES

- Adham, S., J.G. Jacangelo, and J. Laine. 1996. Characteristics and Costs of MF and UF Plants. *Journal AWWA*, **88**(5):22-31.
- Adham, S., V.L. Snoeyink, M.M. Clark, and C. Anselme. 1993. Predicting and Verifying TOC Removal by PAC in Pilot-Scale UF Systems. *Journal AWWA*, **85**(12):58-68.
- Amy, G., J.A. Thompson, L.Tan, M.K. Davis, and S.W. Krasner. 1990a. Evaluation of THM precursor contributions from agricultural drains. *Journal AWWA*, **82**(1):57-64.
- Amy, G.L., B.C. Alleman, and C.B. Cluff. 1990b. Removal of Dissolved Organic Matter by Nanofiltration. *Journal of Environmental Engineering*, **116**:200-205.
- Amy, G., L. Tan, and M.K. Davis. 1991. The effects of ozonation and activated carbon adsorption on trihalomethane speciation. *Water Research*, **25**:191-202.
- Anderson, L.J., J.D.Johnson, and R.F. Christman. 1986. Extent of Ozone's Reaction with Aquatic Fulvic Acid. *Environmental Science & Technology*, **20**:739-742.
- Andrews, G.F. and C. Tien. 1981. Bacterial Film Growth in Adsorbent Surfaces. *AIChE Journal*, **27**:396-403.
- Andrews, S.A. 1993. Organic By-Product Formation From the Ozonation of Aquatic Natural Organic Matter. Ph. D. dissertation, University of Alberta, Edmonton, Alberta, Canada
- Andrews, S.A. and P.M. Huck. 1994. Using Fractionated Natural Organic Matter To Quantitate Organic Byproducts Of Ozonation. *Ozone Science & Engineering*, **16**:1-12.
- APHA, AWWA, and WEF (American Public Health Association, American Water Works Association, and Water Environment Federation). 1998. *Standard Methods For The Examination of Water and Wastewater*. 20th ed. Washington, D.C.: APHA.
- Atlas, R.M. and R. Bartha. 1993. *Microbial Ecology*. 3rd ed. Redwood City, CA: Benjamin/Cummings Publishing Company, Inc.
- AWWARF (American Water Works Association Research Foundation). 1996. *Water Treatment, Membrane Processes*. 1st ed. New York, N.Y: McGraw Hill.

- Bader, H. and J. Hoigne. 1981. Determination of Ozone in Water By the Indigo Method. *Water Research*, **15**:449-456.
- Beaubien, A., M. Baty, F. Jeannot, Fracoeur, and J. Manem. 1996. Design and Operation of Anaerobic Membrane Bioreactors: Development of a Filtration Testing Strategy. *Journal of Membrane Science*, **109**:173-184.
- Block, J.C., L. Mathieu, P. Servais, D. Fontevieille, and P. Werner. 1992. Indigenous Bacterial Inocula for Measuring the Biodegradable Dissolved Organic Carbon (BDOC) in Waters. *Water Research*, **26**:481-486.
- Bradford, S.M., C.J. Palmer, and B.H. Olson. 1994. Assimilable Organic Carbon Concentrations in Southern California Surface and Groundwater. *Water Research*, **28**:427-435.
- Camper, A.K., M.W. LeChevallier, S.C. Broadaway, and G.A. McFeters. 1985. Evaluation of procedures to desorb bacteria from granular activated carbon. *Journal of Microbiological Methods*, **3**:187-198.
- Carlson, K., G. Amy, G. Blaise, and S. MacMillan. 1996. The formation of filter-removable BOM during ozonation. In *Proc. of the Fourth International BOM Conference*. Waterloo, Canada: University of Waterloo.
- Carroll, T., S. King, S.R. Gray, B.A. Bolto, and N.A. Booker. 2000. The Fouling of Microfiltration Membranes by NOM After Coagulation Treatment. *Water Research*, **34**:2861-2868.
- Cavanagh, J.E., H.S. Weinbergh, A. Gold, R. Sangalah, D. Marbury, W.H. Glaze, T.W. Collette, S.D. Richardson, and A.D. Thruston. 1992. Ozonation By-Products: Identification of Bromohydrins from the Ozonation of Natural Waters with Enhanced Bromide Levels. *Environmental Science & Technology*, **26**:1658-1662.
- Chang, H.T. and B.E. Rittmann. 1987a. Mathematical Modeling of Biofilm on Activated Carbon. *Environmental Science & Technology*, **21**:273-280.
- Chang, H.T. and B.E. Rittmann. 1987b. Verification of the Model of Biofilm on Activated Carbon. *Environmental Science & Technology*, **21**:273-280.
- Chang, Y., K.H. Choo, M.M. Benjamin, and S. Reiber. 1998. Combined Adsorption-UF Process Increases TOC Removal. *Journal AWWA*, **90**(5):90-102.
- Choo, K.H. and C.H. Lee. 1996. Membrane Fouling Mechanisms in the Membrane-Coupled Anaerobic Bioreactor. *Water Research*, **30**:1771-1780.

- Cicek, N., J.P. Franco, M.T. Suidan, and V. Urbain. 1998a. Using a Membrane Bioreactor to Reclaim Wastewater. *Journal AWWA*, **90**(11):105-113.
- Cicek, N., H. Winnen, M.T. Suidan, B.E. Wrenn, V. Urbain, and J. Manem. 1998b. Effectiveness of the Membrane Bioreactor in Biodegradation of High Molecular Weight Compounds. *Water Research*, **32**:1553-1563.
- Coffey, B.M., S.W. Krasner, M.J. Schlimenti, P.A. Hacker, J.T. Gramith. 1995. A Comparison of Biologically Active Filters for the Removal of Ozone By-Products, Turbidity, and Particles. *In Proc. of the 1995 AWWA Water Quality Technology Conference*. New Orleans, LA: AWWA
- Coleman, W.E., J.W. Munch, H.P. Ringhand, W.H. Kaylor, and D.E. Mitchell. 1992. Ozonation/Post-Chlorination of Humic Acid: A Model for Predicting Drinking Water Disinfection By-Products. *Ozone Science & Engineering*, **14**:51-69.
- Crank, J. 1956. *The Mathematics of Diffusion*. 1st ed. London: Oxford University Press.
- Crittenden, J.C. 1976. Mathematical Modeling of Fixed Bed Adsorber Dynamics-Single and Multicomponents. Ph.D. dissertation, University of Michigan, Ann Arbor, Mi.
- Crittenden, J.C., P. Luft, D.W. Hand, J.L. Oravitz, S.W. Loper, and M. Ari. 1985. Prediction of Multicomponent Adsorption Equilibria Using Ideal Adsorbed Solution Theory. *Environmental Science & Technology*, **19**:1037-1043.
- Finch, G.R. 1994. *Ozone disinfection of Giardia and Cryptosporidium*. Denver, Colo.: AWWA Research Foundation and AWWA.
- Fransolet, G., A. Depelchin, G. Villers, R. Goossens, and W.J. Masschelein. 1988. The Role of Bicarbonate in Bacterial Growth in Oligotrophic Waters. *Journal AWWA*, **80**(11):57-61.
- Frias, J., F. Ribas, and F. Lucena. 1995. Comparison of methods for the measurement of biodegradable organic carbon and assimilable organic carbon in water. *Water Research*, **29**:2785-2788.
- Gagnon, G.A., R.M. Slawson and P.M. Huck. 2000. Effect of easily biodegradable organic compounds on bacterial growth in a bench-scale drinking water distribution system. *Can. J. Civil Eng.* **27**(3): 412-420.



- Garcia-Araya, J.F., J.P. Croue, F.J. Beltran, and B. Legube. 1995. Origins and Conditions of Ketoacid Formation During Ozonation of Natural Organic Matter in Water. *Ozone Science & Engineering*, **17**:647-656.
- Garside, J., G. Amy, G. Blais, J. Debroux, and K. Carlson. 1996. Integrated ozone-biofiltration for removing disinfection by-product precursors from a highly colored ground water. In *Proc. of the Fourth International BOM Conference*. Waterloo, Canada: University of Waterloo.
- Glaze, W.H. 1986. Reaction Products of Ozone: A Review. *Environmental Health Perspectives*, **69**:151-157.
- Glaze, W.H. 1987. Drinking Water Treatment with Ozone. *Environmental Science & Technology*, **21**:224-230.
- Gracia, R., J.L. Aragues, and J.L. Ovelleiro. 1996. Study of the Catalytic Ozonation of Humic Substances in Water and Their Ozonation Byproducts. *Ozone Science & Engineering*, **18**:195-208.
- Grasso, D. and W.J. Weber. 1998. Ozone-Induced Particle Destabilization. *Journal AWWA*, **80**(8):73-81.
- Hacker, P.A., C.M. Paszko-Kolva, M.H. Stewart, R.L. Wolfe, and E.G. Means. 1994. Production and Removal Assimilable Organic Carbon Under Pilot-Plant Conditions Through the Use of Ozone and PEROXONE. *Ozone Science & Engineering*, **16**:197-210.
- Hashino, M., Y. Mori, Y. Fujii, N. Motoyama, N. Kadokawa, H. Hoshikawa, W. Nishijima, and M. Okada. 2000. Pilot plant evaluation of an ozone-microfiltration system for drinking water treatment. *Water Science & Technology*, **41**:17-23.
- Heath, M.S., S.A. Wirtel, and B.E. Rittmann. 1990. Simplified design of biofilm processes using normalized loading curves. *Water Environment Research*, **62**:185-192.
- Heesu, P., K.H. Choo, and C.H. Lee. 1999. Flux Enhancement with Powdered Activated Carbon Addition in the Membrane Anaerobic Bioreactor. *Separation Science and Technology*, **34**(14):2781-2792.
- Hoigne, J. and H. Bader. 1976. The Role of Hydroxyl Radical Reactions in Ozonation Processes in Aqueous Solutions. *Water Research*, **10**:377-386.

- Hoigne, J. 1984. Mechanisms, Rates and Selectivities of oxidations of organic compounds initiated by ozonation of water. *Handbook of ozone technology and applications*. Ann Arbor, Mich.: Ann Arbor Science.
- Hoigne, J. 1998. Chemistry of aqueous ozone and transformation of pollutants by ozonation and advanced oxidation processes. In: *The handbook of environmental chemistry*. Berlin: Springer-Verlag.
- Hozalski, R.M. 1996. Removal of Biodegradable Organic Matter in Drinking Water Biofilters: Experimental Studies and Model Development. Ph.D. dissertation, the Johns Hopkins University, Baltimore, Md.
- Huck, P.M. 1990. Measurement of biodegradable organic matter and bacterial growth potential in drinking water. *Journal AWWA*, **82**(7):78-86.
- Huck, P.M., P.M. Fedorak, and W.B. Anderson. 1991. Formation and Removal of Assimilable Organic Carbon During Biological Treatment. *Journal AWWA*, **83**(12):69-80.
- Huck, P.M., S. Zhang, and M.L. Price. 1994. BOM Removal During Biological Treatment: A First-Order Model. *Journal AWWA*, **86**(6):61-71.
- Jack, A.M. and M.M. Clark. 1998. Using PAC-UF to treat a low-quality surface water. *Journal AWWA*, **90**(11):83-95.
- Kaplan, L.A., D.J. Reasoner, and E.W. Rice. 1994. A Survey of BOM in U.S. Drinking Waters. *Journal AWWA*, **86**(2):121-132.
- Killops, S.D. 1986. Volatile Ozonation Products of Aqueous Humic Material. *Water Research*, **20**:153-165.
- Kim, S. 1987. Mathematical Modeling of Integrated Biological and Physico-Chemical Treatment Processes for Industrial Wastewater. Ph.D. dissertation, the University of Southern California, Los Angeles, Ca.
- Kim, S. and M. Pirbazari. 1989. Bioactive Adsorber Model for Industrial Wastewater Treatment. *Journal of Environmental Engineering*, **115**:1235-1256.
- Kornaros, M., C. Zafiri, and G. Lyberatos. 1996. Kinetics of Denitrification by *Pseudomonas denitrificans* Under Growth Conditions Limited by Carbon and/or Nitrate or Nitrite. *Water Environment Research*, **68**:934

- Krasner, S.W., W.H. Glaze, H.S. Weinberg, P.A. Daniel, and I.N. Najm. 1993a. Formation and Control of Bromate During Ozonation of Waters Containing Bromide. *Journal AWWA*, **85**(5):73-81.
- Krasner, S.W., M.J. Scilimenti, and B.M. Coffey. 1993b. Testing Biologically Active Filters for Removing Aldehydes Formed During Ozonation. *Journal AWWA*, **85**(5):62-71.
- Krasner, S.W. 1996a. The effects of ozonation, biofiltration, and secondary disinfection on DBP formation. In *Proc. of the American Water Works Association Water Quality Technology Conference*. Boston, Ma.: AWWA.
- Krasner, S.W., B.M. Coffey, P.A. Hacker, C.J. Hwang, K. Ching-Yuan, A.A. Mofidi, M.J. Scilimenti, 1996b. Characterization of the Components of BOM. In *Proc. of the Fourth International BOM Conference*. Waterloo, Canada: University of Waterloo.
- Kusakabe, K., S. Aso, J.I. Hayashi, K. Isomura, and S. Morooka. 1990. Decomposition of Humic Acid and Reduction of Trihalomethane Formation Potential in Water by Ozone with U.V. Irradiation. *Water Research*, **24**:781-785.
- Langlais, B., D.A. Reckhow, and D.R. Brink. 1991. *Ozone in Water Treatment*. Chelsea, Mi: Lewis Publishers, Inc.
- LeChevallier, M.W., C.D. Cawthon, and R.G. Lee. 1988. Factors Promoting Survival of Bacteria in Chlorinated Water Supplies. *Applied and Environmental Microbiology*, **54**:649-654.
- LeChevallier, M.W. 1990. Coliform Regrowth in Drinking Water: A Review. *Journal AWWA*, **82**(11):74-86.
- LeChevallier, M.W., W.C. Becker, P. Schorr, and R.G. Lee. 1992. Evaluating the Performance of Biologically Active Rapid Filters. *Journal AWWA*, **84**(4):136-146.
- LeChevallier, M.W., C. Volk, and N. Welch. 1996. Nutrient control during conventional treatment. In *Proc. of the Fourth International BOM Conference*. Waterloo, Canada: University of Waterloo.
- McGuire, M.J., M.K. Davis, S. Liang, C.H. Tate, E.M. Aieta, I.E. Wallace, D.R. Wilkes, J.C. Crittenden, and K. Vaith. 1989. Optimization and Economic Evaluation of Granular Activated Carbon for Organic Removal. Denver, Co.: American Water Works Association Research Foundation.

Miltner, R.J., H.M. Shukairy, and R.S. Summers. 1992. Disinfection By-product Formation and Control by Ozonation and Biotreatment. *Journal AWWA*, **84**(11):53-62.

Moll, D.M. and R.S. Summers. 1996. Assessment of the impact of operational parameters on drinking water filter microbial communities using taxonomic and metabolic profiles. In *Proc. of the Fourth International BOM Conference*. Waterloo, Canada: University of Waterloo.

Monod, J. 1949. The Growth of Bacterial Culture. *Ann. Rev. Microbiology*, **3**:371

Muller, E.B., A.H. Stouthamer, H.W. van Verseveld, and D.H. Eikelboom. 1995. Aerobic Domestic Waste Water Treatment in a Pilot Plant with Complete Sludge Retention by Cross-Flow Filtration. *Water Research*, **29**:1179-1189.

Oppenheimer, J.A., E.M. Aieta, J.G. Jacangelo, and I.N. Najm. 1997. CT requirements for disinfection of *Cryptosporidium* in natural waters. In *Proc. of the AWWA Water Quality Technology Conf.* Denver, Colo.: AWWA

Oppenheimer, J.A., E.M. Aieta, R.R. Trussell, J.G. Jacangelo, and I.N. Najm. 2000. *Evaluation of Cryptosporidium Inactivation in Natural Waters*. Denver, Colo.: AWWA Research Foundation and AWWA.

Peel, R. and A. Benedek. 1976. The Modeling of Activated Carbon Adsorbers in the Presence of Bio-Oxidation. *AIChE. Symposium Series*, **73**:25-35.

Pirbazari, M., B.N. Badriyha, and V. Ravindran. 1992. MF-PAC for Treating Waters Contaminated with Natural and Synthetic Organics. *Journal AWWA*, **84**(2):95-103.

Pirbazari, M., V. Ravindran, B. Badriyha, and S. Kim. 1996. Hybrid Membrane Filtration Process for Leachate Treatment. *Water Research*, **30**:2691-2706.

Prevost, M. 1996. Recent developments of various BDOC measurement techniques. In *Proc. of the Fourth International BOM Conference*. Waterloo, Canada: University of Waterloo.

Price, M.L., R.W. Bailey, A.K. Enos, M. Hook, and S.W. Hermanowicz. 1993. Evaluation of Ozone/Biological Treatment For Disinfection ByProducts Control and Biologically Stable Water. *Ozone Science & Engineering*, **15**:95-130.

Ravindran, V., B. Badriyha, M.D. Williams, S.C. Tu, and M. Pirbazari. 1995. A Hybrid Membrane Filtration Process for the Treatment of Water Contaminated With Petroleum Hydrocarbons. In *Proc. of the AWWA Water Quality Technology Conf.* New Orleans, La.: AWWA

- Reckhow, D.A. and P.C. Singer. 1984. The Removal of Organic Halide Precursors by Preozonation and Alum Coagulation. *Journal AWWA*, **76**(4):151-157.
- Rice, R.G. and M. Gomez-Taylor. 1986. Occurrence of By-Products of Strong Oxidants Reacting with Drinking Water Contaminants--Scope of the Problem. *Environmental Health Perspectives*, **69**:31-44.
- Rittmann, B.E. and P.L. McCarty. 1980a. Evaluation of Steady-State-Biofilm Kinetics. *Biotechnology and Bioengineering*, **22**:2359-2373.
- Rittmann, B.E. and P.L. McCarty. 1980b. Model of Steady-State-Biofilm Kinetics. *Biotechnology and Bioengineering*, **22**:2343-2357.
- Rittmann, B.E. 1982. The effect of shear stress on biofilm loss rate. *Biotechnology and Bioengineering*, **24**:501-506.
- Rittmann, B.E., L. Crawford, C.K. Tuck, and E. Namkung. 1986. In Situ determination of kinetic parameters for biofilms: isolation and characterization of oligotrophic biofilms. *Biotechnology and Bioengineering*, **28**:1753-1760.
- Rittmann, B.E. 1989. Detachment of Biofilms. In: *Structure and Function of Biofilms*. New York: Wiley Interscience.
- Rittmann, B.E. and J.E. Wooschlager. 1996. Fundamental components for modeling BOM and regrowth. In *Proc. of the Fourth International BOM Conference*. Waterloo, Canada: University of Waterloo.
- Robert, C. 1992. Analyse de Sensibilite du Modele PRZM. *Revue des Sciences de L'eau*, **5**:207-224.
- Robinson, J.A. 1985. Determining Microbial Kinetic Parameters Using Nonlinear Regression Analysis. In *Advances in Microbial Ecology*. 8<sup>th</sup> ed. New York: Plenum Press.
- Rook, J. J. 1974. Formation of Haloforms During Chlorination of Natural Waters. *Water Treat.Exam*, **23**:234.
- Rosenbeger, S., R.Witzig, W. Manz, U. Szewzyk, and M. Kraume. 2000. Operation of different membrane bioreactors: experimental results and physiological state of the microorganisms. *Water Science & Technology*, **41**:269-277.

- Schafer, A.I., A.G. Fane, and T.D. Waite. 2000. Fouling effects on rejection in the membrane filtration of natural waters. *Desalination*, **131**:215-224.
- Schechter, D.S. and P. Singer. 1995. Formation of Aldehydes During Ozonation. *Ozone Science & Engineering*, **17**:53-69.
- Servais, P., G. Billen, C. Ventrsque, and G.P. Bablon. 1991. Microbial Activity in GAC Filters at the Choisy-le-Roi Treatment Plant. *Journal AWWA*, **83**(2):62-68.
- Shukairy, H.M. and R.S. Summers. 1992. The Impact of Pre-Ozonation and Biodegradation on Disinfection By-Product Formation. *Water Research*, **26**:1217
- Siddiqui, M.S. and G.L. Amy. 1993. Factors Affecting DBP Formation During Ozone-Bromide Reactions. *Journal AWWA*, **85**(1):63-72.
- Smith, E.H. and W.J. Weber. 1988. Modeling Activated Carbon Adsorption of Targeted Organic Compounds From Leachate-Contaminated Groundwaters. *Environmental Science & Technology*, **22**:313-321.
- Speitel, G.E. and F.A. DiGiano. 1987a. Biofilm Shearing Under Dynamic Conditions. *Journal of Environmental Engineering*, **113**:464-475.
- Speitel, G.E., K. Dovantzis, and F.A. DiGiano. 1987b. Mathematical Modeling of Bioregeneration in GAC Columns. *Journal of Environmental Engineering*, **113**:32-48.
- Speitel, G.E., C.J. Lu, X.J. Zhu, and M.H. Turakhia. 1989. Biodegradation and Adsorption of a Bislute Mixture in GAC Columns. *Journal Water Pollution Control Federation*, **61**:221-229.
- Speitel, G.E. and X.J. Zhu. 1990. Sensitivity Analyses of Biodegradation/Adsorption Models. *Journal of Environmental Engineering*, **116**:32-48.
- Speitel, G.E., J.M. Symons, A.C. Diehl, H.W. Sorenson, and L.A. Cipparone. 1993. Effect of Ozone Dosage and Subsequent Biodegradation on Removal of DBP Precursors. *Journal AWWA*, **85**(5):86-95.
- Urbain, V., R. Benoit, and J. Manem. 1996. Membrane Bioreactor: A New Treatment Tool. *Journal AWWA*, **88**(5):75-86.
- Urfer, D., P.M. Huck, S.D. Booth, and B.M. Coffey. 1997. Biological Filtration for BOM and Particle Removal: A Critical Review. *Journal AWWA*, **89**(12):83-98.

- U.S. Environmental Protection Agency. 1994. National Primary Drinking Water Regulations; Disinfectants and Disinfection Byproducts; Proposed Rule. *Fed. Reg.*, **59**(145):38668.
- US Environmental Protection Agency. 1998a. National Primary Drinking Water Regulations; Disinfectants and Disinfection Byproducts; Final Rule. *Fed. Reg.*, **63**(241):69390.
- US Environmental Protection Agency. 1998b. M/DBP Federal Advisory Committee. (Draft) Stage 2 M/DBP Agreement in Principle.
- US Environmental Protection Agency. 1998c. National Primary Drinking Water Regulations; Interim Enhanced Surface Water Treatment; Final Rule. *Fed. Reg.*, **63**(241):69478.
- van der Kooij, D. 1979. Characterization and Classification of Fluorescent Pseudomonads Isolated from Tap Water and Surface Water. *Antonie van Leeuwenhoek*, **45**:225-240.
- van der Kooij, D., A. Visser, and W.A. Hijnen. 1982a. Determining the Concentration of Easily Assimilable Organic Carbon in Drinking Water. *Journal AWWA*, **74**(10):540-545.
- van der Kooij, D., A. Visser, and J.P. Oranje. 1982b. Multiplication of Fluorescent Pseudomonads at Low Substrate Concentrations in Tap Water. *Antonie van Leeuwenhoek*, **48**:229-243.
- van der Kooij, D., W.A. Hijnen, and J.C. Kruithof. 1989. The Effects Of Ozonation, Biological Filtration And Distribution On The Concentration Of Easily Assimilable Organic Carbon (AOC) In Drinking Water. *Ozone Science & Engineering*, **11**:297-310.
- van der Kooij, D. 1992. Assimilable Organic Carbon as an Indicator of Bacterial Regrowth. *Journal AWWA*, **84**(2):57-65.
- Watts, C.D. 1985. Organic By-Products of Ozonation of Humic and Fulvic Acid. In *Proc.Intl.Conf., Role.of.Ozone.in Water.and.Wastewater.Treatment*.
- Weber, W.J. and F.A. DiGiano. 1996. *Process Dynamics in Environmental Systems*. New York: Wiley Interscience.
- Weinberg, H.S., W.H. Glaze, S.W. Krasner, and M. Sclimenti. 1993. Formation and Removal of Aldehydes in Plants That Use Ozonation. *Journal AWWA*, **85**(5):72-85.

Williams, M.D., B.M. Coffey, S.W. Krasner. 2000. Scaling Up Ozone Systems from Bench- to Full-Scale: Implications for Ozone Dose, Disinfection, and Bromate Formation. In *Proc. IOA Pan American Group Conference*, Orlando, FL: International Ozone Association.

Xing, C.-H., E. Tardieu, Y. Qian, and X.-H. Wen. 2000. Ultrafiltration membrane bioreactor for urban wastewater reclamation. *Journal of Membrane Science*, **177**:73-82.

Yamada, H. and I. Somiya. 1989. The Determination of Carbonyl Compounds In Ozonated Water By the PFBOA Method. *Ozone Science & Engineering*, **11**:127-141.

Ying, W. (1978) Investigation and Modeling of Bio-Physicochemical Processes in Activated Carbon Columns. Ph.D. dissertation. the University of Michigan, Ann Arbor, Mi.

Ying, W. and W.J. Weber. 1979. Bio-physicochemical Adsorption Model Systems for Wastewater Treatment. *Journal Water Pollution Control Federation*, **51**:2661-2677.

Zhang, S. and P.M. Huck. 1996. Removal of AOC in biological water treatment processes: A kinetic modeling approach. *Water Research*, **30**:1196-1207.